



UNIVERSIDAD DE CHILE

FACULTAD DE CIENCIAS FÍSICAS Y MATEMÁTICAS
DEPARTAMENTO DE GEOLOGÍA

**GROUNDWATER RESOURCES OF THE WESTERN ANDEAN
FRONT: INSIGHTS FROM THE ACONCAGUA BASIN, CENTRAL
CHILE**

**TESIS PARA OPTAR AL GRADO DE DOCTOR EN CIENCIAS
MENCIÓN GEOLOGÍA**

MATÍAS NICOLÁS TAUCARE TORO

PROFESORA GUÍA:
DRA. LINDA DANIELE

PROFESORA CO-GUÍA:
DRA. GLORIA ARANCIBIA HERNÁNDEZ

MIEMBROS DE LA COMISIÓN:
DR. JORGE JÓDAR BERMÚDEZ
DR. JAMES MCPHEE TORRES
DR. DIEGO MORATA CÉSPEDES

SANTIAGO DE CHILE
2020

RESUMEN DE LA TESIS PARA OPTAR AL

GRADO DE: Doctor en Ciencias, Mención Geología

Por: Matías Nicolás Taucare Toro

Fecha:

Prof. Guía: Linda Daniele

Prof. Co-Guía: Gloria Arancibia

AGUA SUBTERRÁNEA EN EL FRENTE OCCIDENTAL ANDINO: PERSPECTIVAS DESDE LA CUENCA DEL ACONCAGUA, CHILE CENTRAL

El poco conocimiento de los procesos hidrogeológicos, junto a una simplificación excesiva de los modelos conceptuales de los acuíferos dan lugar a una imprecisa gestión de los recursos hídricos. A pesar de que Chile es un país montañoso, los estudios hidrogeológicos se han centrado exclusivamente en los depósitos aluviales (aprox. 15% del área total) y las zonas de frente de montaña son consideradas arbitrariamente como impermeables. Dado que en zonas áridas (y semiáridas) un componente importante de la recarga de acuíferos aluviales se produce a lo largo del frente de montaña, el objetivo general de esta tesis es desarrollar un modelo conceptual que explique el funcionamiento hidrogeológico del Frente Occidental Andino y su relación con los acuíferos aluviales. Se eligió analizar la cuenca del Aconcagua, una zona donde la presencia varios manantiales de caudal permanente evidencian la circulación de agua subterránea en el Frente Occidental Andino. Los manantiales más importantes afloran a lo largo de la Zona de Falla Pocuro (ZFP) que separa a las rocas volcánicas de la Cordillera Principal del relleno aluvial de la Depresión Central. La metodología empleada considera la integración de técnicas y herramientas de: i) hidrogeoquímica e isótopos estables del agua, ii) geología estructural y, iii) topología y análisis de fracturas. El estudio se llevó a cabo en

La circulación de agua subterránea y los procesos de recarga que ocurren en el Frente Occidental Andino se abordaron usando hidrogeoquímica e isótopos estables del agua de 23 manantiales, 10 pozos, 5 colectores de lluvia y 5 muestras de rocas lixiviadas. En general el agua subterránea es $\text{HCO}_3\text{-Ca}$, resultante de interacción con Ca-silicatos. El análisis de clúster jerárquico agrupa las muestras respecto a su cota a lo largo del Frente Occidental Andino sugiriendo que existe una relación entre el aumento de la mineralización ($31\text{-}1188 \mu\text{S/cm}$) y el tiempo de residencia del agua subterránea. Mientras que, el análisis factorial indica que las concentraciones de Cl, NO₃, Sr y Ba parecen estar relacionadas a la actividad agrícola que ocurre en la Depresión Central. Luego de definir la línea meteórica regional a los 33°S, los isótopos del agua muestran la participación de la lluvia y de la nieve que cae a ~2000 m s.n.m. en la recarga de los acuíferos de la Depresión Central. Además, los canales de regadío son responsables de las composiciones isotópicas de alta cota en el acuífero aluvial.

El mapeo de fracturas a diferentes escalas (de regional a escala de afloramiento) se llevó a cabo en la ZFP, donde se reconocieron tres rasgos tectónicos principales no coetáneos dentro de la ZFP: i) fallas NS normal-sinestral con fracturas selladas por laumontita, cuarzo y calcita, ii) fallas NS inversas consistentes en bandas de cizalle (salvanda) de 30 a 60 cm, y iii) fallas NW inversas consistentes en planos discretos abiertos. Luego, a través de la topología se cuantificó la densidad de fracturas conectadas dentro de la ZFP, identificando dos zonas de alta densidad de fracturas conectadas ($>2.4 \text{ km/km}^2$). Ambas zonas coinciden con los manantiales principales de la ZFP: Termas de Jahuel (~14.0 m^3/h at 22 °C) y Termas El Corazón (~7.2 m^3/h at 20 °C). A escala de afloramiento se observa que el agua subterránea de estos manantiales circula por las fallas NW inversas, lo cual es consistente con la orientación preferencial de la red de fracturas dentro de la ZFP (N30-60W). Así, mientras que las fallas NS forman barreras las fallas NW son ejes de alta permeabilidad para la circulación de agua.

Finalmente, se propone un modelo conceptual original que puede considerarse válido para todo Chile Central. El agua que se origina a ~2000 m s.n.m. alimenta la circulación de agua subterránea en la roca fracturada, que es transmitida hasta por las quebradas ubicadas en la parte media de la montaña. Hacia la parte baja, las fallas NW permitirían la recarga de bloque de montaña de los acuíferos aluviales aprovechando la alta densidad de fracturas conectadas en la ZFP. También ocurren procesos de frente de montaña que recargan los acuíferos aluviales en el piedemonte a través de la infiltración focalizada de escorrentías permanentes y transitorias.

GROUNDWATER RESOURCES OF THE WESTERN ANDEAN FRONT: INSIGHTS FROM THE ACONCAGUA BASIN, CENTRAL CHILE

The misunderstanding of hydrogeological processes together with the oversimplification of aquifer conceptual models result in numerous inaccuracies in the management of groundwater resources. Despite that Chile is a mountainous country, hydrogeological studies have exclusively focused to alluvial deposits in valleys (~15 % of total area of Chile) and mountain front zones are considered arbitrarily impermeable. Given that in arid zones (and semiarid) a significant component of the alluvial aquifers recharge occurs along the mountain front zone, this PhD thesis aims to develop a reliable conceptual mode that explains the Western Andean Front hydrogeological functioning. The Aconcagua Basin was selected because there several perennial springs show evidence of groundwater flows in the Western Andean Front. The major springs outflow along the NS-oriented Pocuro Fault Zone (PFZ), which separates the volcanic rocks of the Principal Cordillera from the alluvial deposits of the Central Depression. Thus, the study was addressed by means of: i) hydrogeochemistry and water stable isotope; ii) structural geology; and iii) a topological approach and fracture analysis.

The groundwater circulation and recharge processes occurring at the Western Andean Front were addressed using hydrogeochemical and water stable isotope analyses of 23 perennial springs, 10 boreholes, 5 rain-collectors and 5 leaching-rocks samples. Most groundwater in the Western Andean Front is $\text{HCO}_3\text{-Ca}$ and results from the interaction with Ca-silicate. The Hierarchical Cluster Analysis groups the samples according to its elevation along the Western Andean Front and supports a clear correlation between the increasing groundwater mineralization (31-1188 $\mu\text{S}/\text{cm}$) and residence time. Whereas, the Factorial Analysis point that Cl^- , NO_3^- , Sr and Ba concentrations seems to be related to agriculture practices in the Central Depression. After defining the regional meteoric water line at 33°S in Chile, water isotopes demonstrate the role of rain and snowmelt above ~2000 m asl in the recharge of groundwater. Also, irrigation canals contribute to the high-altitude isotopic signature in the alluvial aquifer of Central Depression.

The multi-scale mapping of fractures (from regional to the outcrop scale) was conducted in the PFZ. Three non-coetaneous major tectonic features were recognized within PFZ: i) NS-oriented normal-sinistral faults with sealed fractures presence (laumontite, quartz and calcite), ii) NS-oriented reverse faults consisting in shear bands (gouge) of 30-60 cm thick, and iii) NW-oriented reverse faults consisting in open fractures plane. Then, topology allows for quantification of the density of connected fractures within the PFZ and its relationship with groundwater circulation. The study results identify two areas of high density of connected fractures that are related to the main springs of the PFZ: Termas de Jahuel (discharge ~14.0 m^3/h at 22 °C) and Termas El Corazón (discharge ~7.2 m^3/h at 20 °C). Outcrop-scale mapping reveals that groundwater outflows from NW-reverse faults, which is consistent with the preferential orientation of the fracture network (N30-60W) within the PFZ. Thus, while NS-oriented faults act as a hydraulic barrier, the NW-oriented faults are high-permeability axes for groundwater circulation.

Finally, an original conceptual model applicable to the entire Central Chile is proposed. The water releases from high-elevation areas infiltrate in mid-mountain gullies feeding groundwater circulation in the fractured rocks of Western Andean Front. To the downstream, mountain-block recharge occurs through NW-reverse faults taking advantage of the high density of connected fractures of the PFZ. Likewise, mountain-front processes recharge the alluvial aquifers in the piedmont zones through the focused infiltration of perennial and ephemeral streams.

*“La legislación chilena dice que los derechos de agua son perpetuos
y lo que nosotros sabemos es que hay disminución de las precipitaciones
y disminución de la escorrentía.
Entonces entregan derechos de algo que está disminuyendo...
la gente tiene derechos sobre agua que no existe”.*

Roberto Rondanelli (CR²-U de Chile)
en “El negocio del agua”

AGRADECIMIENTOS

Agradezco a la Agencia Nacional de Investigación y Desarrollo de Chile (ANID), ya que mi doctorado fue financiado por la Beca Doctorado Nacional n° 21160325. De igual forma, mi proyecto de tesis fue financiado exclusivamente por fondos públicos a través de los programas de ANID: FONDECYT n° 1170569 (*Decoding springs, groundwater and fractured rocks connections at the San Felipe-Los Andes área - Aconcagua basin, Central Chile*), FONDAP n° 15090013 (Centro de Excelencia en Geotermia de los Andes, CEGA) y FONDEQUIP EQM120098 (Laboratorio de espectrometría de masas con plasma acoplado por inducción de tipo cuadrupolo). Las pasantías a la *Université de Montpellier* y a la *Université de Rennes* fueron financiadas por el programa ECOS-ANID n° 180055/C18U03 y por el beneficio de pasantía doctoral en el extranjero, respectivamente. Además, gracias al beneficio de los gastos operacionales pude realizar una estancia corta en la Universidad de Almería. Quiero agradecer también al programa UNESCO IGCP636 (*Unifying international research forces to unlock and strengthen geothermal exploitation of the Americas and Europe*) que me permitió participar de enriquecedoras discusiones sobre metodologías innovadoras de trabajo en terreno y técnicas de modelización vinculadas a los recursos geotérmicos.

Quiero agradecer especialmente a mi profesora guía Linda Daniele quien confió en mí para acompañarla en este hermoso proyecto de exploración hidrogeológica en las rocas fracturadas de la Cordillera de Los Andes. A lo largo de estos cuatro años Linda ha dedicado su tiempo en formarme éticamente como investigador, en enseñarme valores y en ser un apoyo tanto en lo académico como en lo emocional. Como dicen por ahí, un buen profesor hace el papel de un padre, de un guía y de un amigo... Gracias Linda por tanto. Agradezco también a mi profesora co-guía Gloria Arancibia quien desde los primeros días de esta travesía ha sabido guiarme activamente en mi desarrollo académico. Durante su curso de Tópicos de Geociencias me enseño las bases de la redacción científica, y las discusiones con Gloria me brindaban la seguridad para hacer las cosas aún mejor. Agradezco a Diego Morata quien es el pilar principal del CEGA, un centro de investigación de clase mundial del que me siento orgulloso ser parte y que ha permitido formar numerosos profesionales de excelencia. Durante mi desarrollo académico, tuve la suerte de trabajar con el profesor Benoît Viguier. A pesar de que él no reconoce que el vino chileno es mejor que el francés, fue la persona que me ayudo a aterrizar a la realidad todo lo teórico. Es un excelente compañero tanto de terreno como de redacción y, además, un gran amigo. Quiero agradecer también a los profesores Jorge Jodar y James McPhee por su tiempo dedicado y por las excelentes sugerencias que ayudaron a mejorar esta tesis. Por otro lado, durante mis pasantías pude conocer a grandes profesores, con quienes tuve discusiones bastante enriquecedoras y pude observar lo genial del trabajo interdisciplinario. Así, agradezco de la *Université de Montpellier* a Hervé Jourde y Veronique Leonardi; de la *Université de Rennes* a Tanguy Le Borgne, Aditya Bandopadhyay, Virginie Vergnaud, Philippe Davy y Laurent Longuevergne; y, por último, de la Universidad de Almería a Angela Vallejos.

Este doctorado no hubiese sido nada sin las largas campañas de terreno y mucho menos si no hubiese tenido los accesos a los recintos privados. Por lo mismo, agradezco infinitamente a Franz Röber del Hotel San Estebán una muy buena persona y bastante preocupada por el bienestar de uno. Don Franz, no solo me hospedaba, con él tenía largas conversaciones de política, historia y de los recursos hídricos de su región, además me daba los contactos para poder tomar mis muestras y me permitió instalar un recolector de lluvia en sus dependencias. Agradezco también por la buena voluntad y los accesos permitidos a Diego Boris de Termas El Corazón, Carlos Bordones de Termas de Jahuel, Antón Estévez de Fundo El Barro, Jorge Pino de la Quebrada El Carrizo, Ariel González de la APR de Santa Filomena, Rodrigo Fernández de Agrícola El Triunfo, Anton Sponar de Sky El Arpa y Segundo Pereira del Estero Pocuro. También agradecer a Génesis Abarca con quien compartí bastante en San Estebán, y al igual que don Franz, me permitió instalar un recolector de lluvia en su casa. De igual forma, las muestras de agua no eran útiles sin sus respectivos análisis químicos. Por eso agradezco enormemente a Erika Rojas y a Samuel Lepe, y en especial a Verónica Rodríguez por su buena disposición y apoyo durante el trabajo en el Laboratorio de Geoquímica de Fluidos del CEGA. También a Antonio Delgado del Instituto Andaluz de Ciencias de la Tierra (CSIC-Universidad de Granada), por el análisis de isótopos estables de las aguas.

Doy las gracias a mis compañeros de la Universidad de Chile, a Antonia Genot, Giselle Placencia, Angello Negri, Diego Aravena, Pablo Valdenegro, Nicolás Pérez, Daniele Tardani, Francisco Ramírez, Daniel Balzan, Sebastián Herrera, Huber Rivera, Christian Pizarro, Marcelo Cortés, Luna Pérez y Vanessa Treskow. Agradecer también a mis compañeros de la Pontificia Universidad Católica, a Ronny Figueroa, Tomás Roquer, Gert Heuser, Josefa Sepúlveda y Eduardo Molina. A mis amigos Francisco Trujillo, Jessica Saavedra, Eduardo Díaz, Antonio Simon y Carlo Divasto por los buenos momentos junto a ellos. También agradezco a mis amigos de Iquique, a Catalina Hernández, Iván Ortiz, Ignacio Dunstan, Daniel Tellez, César Huechucoy, Juan Guerrero y Felipe Cortés. Además, quiero mencionar a quienes hicieron mis pasantías más gratas y entretenidas, a los de la *Université de Montpellier*, en especial a Tamara Andueza, Jessica Bouby y Julie Gontier, a los de la *Université de Rennes* a Justine Molron, Leonardo Machado, Marta Cosma, Quentin Courtois, Diane Dolag, Alexandre Coche, Etienne Philipson, Charlotte Le Traon, Maxime Bernard, Thomas Bernard, Eliot Chatton, Madelein Nicolas y Olivier Bochet. No puedo olvidar mencionar a Eszter Dúdas, AlineBaudry y Marine Noblanc, y mucho menos a los chilenos en *Rennes* a Mixsy Igor, Camila Silva, Camilo Silva y Ximena Ortiz.

Para finalizar, quiero dar las gracias a mis papás por su amor constante, por los valores que hoy definen mi vida y como si fuera poco, por haberme dado la oportunidad de estudiar sin quedar endeudado. Quiero agradecer a mi tía Ximena y a mi tío Francisco por su apoyo incondicional y todo el cariño que siempre me entregan, y a mis primos por las risas que hemos compartido. Y bueno, estoy profundamente agradecido de mi compañera de vida, con quien he crecido y he reído, porque siempre está junto a mí... mi gordita.

TABLE OF CONTENTS

PART I: THE STATE OF THE ART

Chapter 1: Introduction

1.1. Theoretical background	1
1.2. Research problem	4
1.3. Hypothesis and objectives	7
1.3.1. Research questions and hypothesis	7
1.3.2. Objectives	7
1.4. Scientific production	8
1.4.1. Publications and conference abstracts resulting from this thesis	8
1.4.1.1. Research papers	8
1.4.1.2. Conference abstracts	8
1.4.2. Publications and conference abstracts resulting from side-studies	9
1.4.2.1. Research papers	9
1.4.2.2. Conference abstracts	9
References	11

Chapter 2: Study area: The Aconcagua Basin

2.1. Geological setting	18
2.2. Hydro(geo)logical setting	23
2.2.1 Hydroclimatic variability	23
2.2.2. Groundwater resources	25
References	26

PART II: BUILDING THE CONCEPTUAL MODEL OF THE WESTERN ANDEAN FRONT

Chapter 3: Methodology

3.1. Hydrogeochemical and isotopic methods	36
3.1.1. Sampling and analysis	36
3.1.2. Ionic extraction by leaching test	38
3.1.3. Multivariate Statistical Analysis	38
3.1.4. Local meteoric water line construction	39
3.2. Structural and fracture network analyses	40
3.2.1. Multi-scale structural mapping	40
3.2.2. Topological approach	42
References	44

Chapter 4: Groundwater circulation and recharge processes in the Western Andean Front

Abstract	48
4.1. Hydrogeochemical patterns in the Western Andean Front	49
4.2. Hydrogeochemical processes in the Western Andean Front	53
4.2.1. Groundwater evolution along flow paths	53
4.2.2. Source of dissolved ions: water-rock interactions and anthropogenic influences	57
4.3. Water stable isotopes and groundwater origins	59
4.3.1. The 33°S Chile Meteoric Water Line	59
4.3.2. Areas contributing to recharge groundwater	59
4.4. Groundwater circulation and recharge processes	63
References	67

Chapter 5: Architecture and fracture connectivity of the Pocuro Fault Zone

Abstract	71
5.1. Architecture of the Pocuro Fault zone	72
5.1.1. Tectonics features at regional scale	72
5.1.2. Fracture patterns and relative timing from outcrop scale mapping	74
5.2. Fracture analysis and connectivity of the Pocuro Fault Zone	79
5.3. The Oblique Basement Faults	82
References	84

Chapter 6: Conclusion

6.1. The conceptual model of the Western Andean Front	87
6.2. Summary and future insights	92
References	93

Bibliography	96
---------------------	----

APPENDIX

Appendix A: Water samples

A.1. Location of sampling points (Datum: UTM WGS84-19S)	116
A.2. Piper diagram showing the hydrogeochemical facies of water samples	117

Appendix B: Structural geology

B.1. Location of structural sites	118
B.2. Measured fractures from each structural site within the Pocuro Fault Zone	118
B.3. Histogram of measured fractures within the Pocuro Fault Zone	119
B.4. Fracture orientations plotted in pole contour diagrams	120
B.5. Microstructural analysis	121
B.6. Diffractograms of the fracture minerals filling	123
B.7. Fracture data inversion	124
B.8. Total of hydrothermal tensional fractures from each structural site	125
B.9. Stress field estimation from veins data	126
B.10. Stress and strain field estimation from fault slip data	129
B.11. Cartoon diagrams summarizing the crosscutting relationship	131

LIST OF FIGURES

- Fig. 1.1:** Diagram showing the processes that may contribute to the aquifer functioning. As example, there are several elements considered, such as the groundwater inflow (Gi), precipitation recharge (Pr), surface recharge (Sr), borehole withdrawals (Bw), evapotranspiration (Er) and groundwater outflow (Go). 1
- Fig. 1.2:** Diagram showing the recharge processes in mountain front zones: Mountain-front recharge (MFR) and Mountain-block recharge (MBR). Illustration based on Wilson and Guan (2004). 2
- Fig. 1.3:** Diagram showing the fault-contact between the mountain-block and the adjacent alluvial aquifer. The fault zone illustration is based on Choi *et al.* (2016). 3
- Fig. 1.4:** a) Chilean population by region (data from INE); b) and c) annual mean air temperature and annual mean precipitation distribution, respectively (spatially interpolated gridded climate data from Fick and Hijmans, 2017); d) and e) morphotectonic features (based on Cembrano *et al.* 2007) and crustal fault (based on Arancibia, 2004; Cembrano *et al.* 2005; Farias *et al.* 2005; Melnick and Echter, 2006; Charrier *et al.* 2007; Allmendinger and González, 2010; Poblete *et al.* 2014; Betka *et al.* 2016; Martínez *et al.* 2016; Pérez-Flores *et al.* 2017; Piquer *et al.* 2019; Santibáñez *et al.* 2019; Veloso *et al.* 2019; Yáñez and Rivera, 2019) of the Chilean Andes, respectively. 5
- Fig. 1.5:** a) Current and simplistic conceptual model for the Chilean alluvial aquifers and, b) hypothetical conceptual model considering the hydraulic connection between the alluvial aquifers and the mountain front. 6
- Fig. 2.1:** Chronostratigraphic chart of the Central Chile (at 32.8°S) showing the main stratigraphic units and the dominant tectonic event (based on Godoy *et al.* 1999; Jordan *et al.* 2001; Yáñez *et al.* 2001; Charrier *et al.* 2002; Fuentes *et al.* 2002; Nyström *et al.* 2003; Arancibia, 2004; Muñoz *et al.* 2006; Charrier *et al.* 2007; Jara and Charrier, 2014; Piquer *et al.* 2017; Horton, 2018; Riesner *et al.* 2019; Boyce *et al.* 2020). 19
- Fig. 2.2:** Morphotectonic features of the Central Chile Andes (based on Cembrano *et al.* 2007). It illustrates the major lineaments (based on Yáñez and Rivera, 2019) and the contour of the Nazca plate shape beneath the South American plate (Cahill and Isacks, 1992). Relative convergence vector of the Nazca plate from Angermann *et al.* (1999). WVTF: West vergent thrust faults. 20
- Fig. 2.3:** Geological map of the study area (1:200.000), datum WGS84-19S. The lithological information is based on Rivano *et al.* 1993, Fuentes (2004), Jara and Charrier (2014) and Boyce *et al.* (2020). 21

Fig. 2.4: Hydro(geo)logical context in the Aconcagua Basin. Hydroclimatic time series since 1980 to the present: a) Oceanic Niño Index (NOAA/National Weather Service, 2019); b) monthly mean air temperature at “*Vilcuya*” meteorological station; c) monthly precipitation at “*San Felipe*” meteorological station; d) daily river flow at “*Río Aconcagua en San Felipe*” gauging station; e) water table depth (meters below ground surface) at the “*Perfil San Felipe*” observation borehole; f) authorized groundwater extraction in the San Felipe Aquifer and respective uses during the historic time-period (1980-2009) and the megadrought (2010-2018). In pink is highlighted the “Megadrought” of Central Chile. b), c), d) and e) available data at DGA web site (DGA, 2019).

24

Fig. 2.5: Springs located in the Western Andean Front and boreholes in the San Felipe Aquifer. Major springs are highlighted: *Termas de Jahuel* (Jh) and *Termas El Corazón* (TEC).

25

Fig. 3.1: Location of the sampling points and isotopic information. a) Central Chile and the main Andean morphotectonic domains: Coastal Cordillera (CC), Central Depression (CD) and Principal Cordillera (PC). The Western Andean Front (WAF) and the Aconcagua Basin are shown by red diagonal lines and delineated red area, respectively. b) The Aconcagua Basin. c) Geological map of the study area (from Taucare *et al.* 2020).

37

Fig. 3.2: a) Map of the study area showing each structural site: b) *Potrerillos* (PT), c) *Termas El Corazón* (TEC), d) *Bypass* (BP), and e) *Esteros Pocuro* (EP).

41

Fig. 3.3: Topological nomenclature for fracture network characterization (Sanderson and Nixon, 2015). a) Fracture network map, and b) its topological characterization.

42

Fig. 3.4: High-resolution photomosaic utilized for the topological approach. The major springs of the study area are highlighted: *Termas de Jahuel* (Jh) and *Termas El Corazón* (TEC).

43

Fig. 4.1: a) Location of groundwater samples at the study area. b) Electrical conductivity and c) temperature vs. elevation (m asl) of groundwater samples.

49

Fig. 4.2: Stiff diagrams of groundwater samples at the study area.

50

Fig. 4.3: Dissolved elements concentration vs. elevation (m asl) of springs (sky-blue) and boreholes (black and white) water samples.

53

Fig. 4.4: Hierarchical cluster analysis. a) Dendrogram shows the three main clusters. b) Stiff diagrams represent the average concentration of major ions in meq/l.

54

Fig. 4.5: Logarithmic ionic ratios calculated for water and rock samples vs. Cl ($r = \text{meq/L}$).

55

Fig. 4.6: Molar relationships of a) Na vs. HCO₃ and b) Ca vs. HCO₃ showing the plagioclase dissolution (stoichiometry ratios): albite (1:1), anorthite (1:2) and labradorite (1:3).

57

Fig. 4.7: Factorial analysis. a) Weight of variables for Factor 1 and 2. b) Projection of samples factorial scores.

58

Fig. 4.8: Water stable isotopes. a) Relationship between δD vs. $\delta^{18}\text{O}$ and 33°S Chile MWL. b) Orographic-continental effect on $\delta^{18}\text{O}$ values at 33°S. The vertical content of the isotopic content in groundwater ($\nabla_z \delta^{18}\text{O}_{\text{GW-spring}}$) along the Western Andean Front was calculated considering only the springs (no. 1 has not been included because it is very heavy related to the corresponding elevation).	60
Fig. 4.9: Hydrogeological conceptual model of the Western Andean Front. Colours of the springs are related to the HCA clusters.	64
Fig. 4.10: Drinking water quality limits according with national (NCh409/1) and international (WHO) drinking water limits, and mineral bottling water (Decree no. 106) for a) NO ₃ and b) As.	66
Fig. 5.1: a) Structural map for the study area and for each structural site: b) <i>Potrerillos</i> (PT), c) <i>Termas El Corazón</i> (TEC), d) <i>Bypass</i> (BP), and e) <i>Estero Pocuro</i> (EP). In blue the NS-oriented normal-sinistral faults, in red the NS-oriented reverse faults, and in white the NW-oriented reverse faults.	73
Fig. 5.2: Field photos showing the outcrops at metric-scale within the PFZ: a) N40-60E/30E normal faults cross-cutting a microdiorite dyke with an offset up to 80 cm; b) veins filled by hydrothermal minerals with no preferential orientations; c) N09S/60E reverse fault cross-cutting the Abanico Formation with an offset up to 3 m; and d) N70-80W/60E reverse faults (black triangles remark the fault trace).	74
Fig. 5.3: Rose diagrams showing the orientation of fractures grouped according with the failure mode for each structural site. Size of the bars in the rose diagrams is the percentage of the fracture orientation in the structural site. The histograms show the proportion of each fracture type.	75
Fig. 5.4: Rose diagrams showing the orientation of the hydrothermal veins for each structural site: a) laumontite-quartz, b) calcite, and c) composite veins (laumontite-quartz edge and calcite centre). Size of the bars in the rose diagrams is the sum of the vein orientation in the structural site (N/P: No present).	76
Fig. 5.5: Photographs of the outcrops and relative timing of the different fractures in the study area (Cal, calcite; Gth, goethite; Hem, Hematite; Lmt, laumontite; Qz, quartz).	78
Fig. 5.6: Morphostructural lineaments map of the PFZ. The major springs of the study area are highlighted: <i>Termas de Jahuel</i> (Jh) and <i>Termas El Corazón</i> (TEC).	80
Fig. 5.7: Topological analysis of the fracture network in the Pocuro Fault Zone. a) Orientations of the fracture network. Rose diagram shows the orientation of mapped lineaments with bin size 10°. b) Topological characterization of the fracture network. c) Contour map shows the density of connected branches (C-I and C-C branch). Rose diagrams (bin size 10°) show the orientation of fractures mapped from representative areas at <i>Termas El Corazón</i> (TEC) and to the east of <i>Termas de Jahuel</i> (Jh). d) Contour map shows the density of connected nodes (Nc = Y-node + X-node).	81

Fig. 5.8: Western Andean Front hydrogeological cartoon highlighting the role of the Oblique Basement Faults on groundwater circulation and the recharge of adjacent alluvial aquifers. The size of the springs reflects its flow rate (large springs have a high flow while the little ones have a lower flow).	83
Fig. 6.1: a) Location of groundwater samples at the study area (colours of the samples are related to the HCA clusters). b) electrical conductivity vs. elevation (m asl) of groundwater samples, and c) Schoeller-Berkaloff diagram from selected samples.	88
Fig. 6.2: Recharge processes along the Western Andean Front. The average of groundwater composition according to the location is represented by the Stiff diagrams (colours are related to the HCA clusters).	89
Fig. 6.3: a) Summary of the main faults identified within the PFZ. b) and c) geoelectrical profiles transversal to the mountain front and to a perched valley in the mountain block, respectively (from Figueroa, 2020).	90
Fig. 6.4: Hydrogeological conceptual model of the Western Andean Front at Central Chile (surficial flow comprises both perennial and ephemeral streams).	91

LIST OF TABLES

Table 3.1: Dataset of annual weight-mean in precipitation and average in snowpack.	40
Table 4.1: Chemical analysis of spring, borehole, and meteoric water samples (<i>bdl</i> : below detection limit).	51
Table 4.2: Average values of chemical composition for each water cluster identified by the HCA.	56
Table 4.3: Chemical composition of the leaching-rock samples.	56
Table 4.4: Isotopic analysis of spring, borehole, and meteoric water samples.	61
Table 5.1: Summary of the major tectonic features and its intern fracture patterns. Mineral recognition from the X-ray diffraction.	77

PART I:

THE STATE OF THE ART

This page intentionally left blank

Introduction

1.1. THEOREICAL BACKGROUND

In arid and semiarid regions groundwater resources play a crucial role for water supply due to the scarcity or absence of surface water (Simmers, 2003). However, the increasing anthropogenic and climatic pressures critically impact the availability of traditional groundwater resources in shallow alluvial aquifers. The implementation of sustainable aquifer management policies fundamentally depends on a good understanding of the aquifer functioning and the related recharge processes (Fig. 1.1) (Simmers, 1997; de Vries and Simmers, 2002; Scanlon *et al.* 2006; Healy, 2010). Indeed, the hydrogeological inaccuracies or the oversimplification of the hydrogeological conceptual models lead to unsuitable management policies, strengthening the risk to overexploit the groundwater resources (Huggenberger and Aigner, 1999; Scanlon *et al.* 2006; Kresic and Mikszewski, 2012).

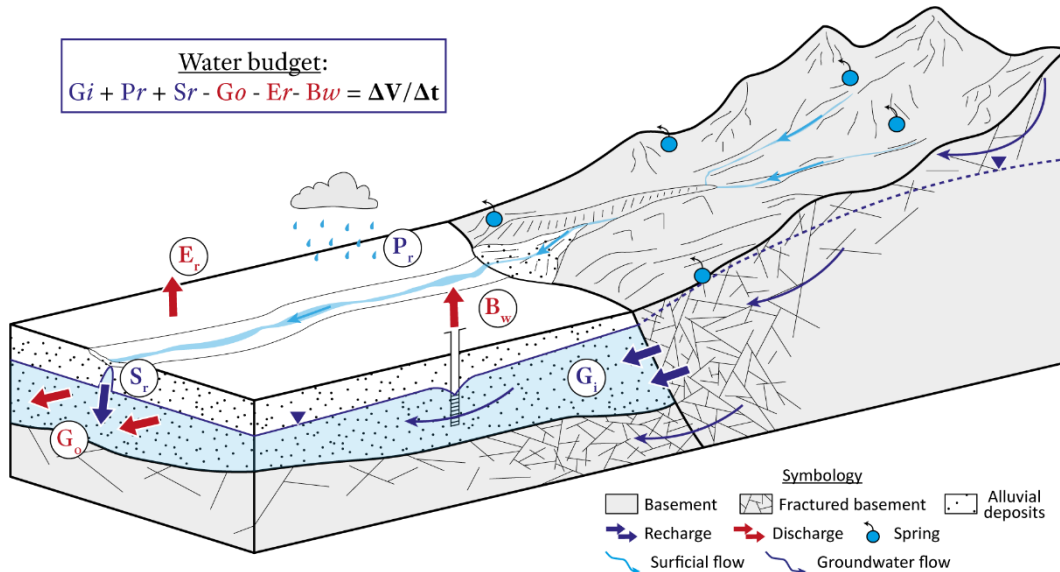


Fig. 1.1: Diagram showing the processes that may contribute to the aquifer functioning. As example, there are several elements considered, such as the groundwater inflow (Gi), precipitation recharge (Pr), surface recharge (Sr), borehole withdrawals (Bw), evapotranspiration (Er) and groundwater outflow (Go).

Recharge is defined as the downward flow of water that reaches the water table, adding to groundwater storage (Healy, 2010). The recharge occurs through two mechanisms: diffuse and focused. Diffuse recharge is the direct infiltration into soil surface of precipitation distributed over large areas and percolating through the vadose zone to the water table. Focused recharge is the movement of water concentrated from surface-water bodies (*e.g.* streams, canals) to an underlying aquifer. Generally, diffuse recharge dominates in humid regions and focused recharge in arid regions (Simmers, 1997).

In semiarid mountainous zones, a significant fraction of adjacent alluvial aquifer recharge originates on high parts because they (Wilson and Guan, 2004): i) receive more precipitation (both rain and snow) than the alluvial basins; ii) snowpack and glaciers support the streamflow and shallow groundwater circulation during the driest periods; and iii) the fast infiltration that occurs along host-rock fractures allows reducing the potential evapotranspiration losses. To the downstream, two fundamentals hydrogeological processes may recharge the adjacent alluvial aquifers (Fig. 1.2) (Wilson and Guan, 2004; Aishlin and McNamara, 2011; Bresciani *et al.* 2018; Markovich *et al.* 2019): the mountain-front recharge (MFR) and the mountain-block recharge (MBR). The MFR consists in the runoff infiltration along the piedmont zone from perennial and ephemeral streams originated on high areas, due the coarsest sediments occur at the margin of the mountain block (*e.g.* alluvial fans). The MBR is the groundwater flow derived from the mountain block to the basin (sometimes is referred as interaquifer flow), which is normally transmitted by diffuse flows along the mountain front as well as by focused flows through oblique faults crossing the mountain front.

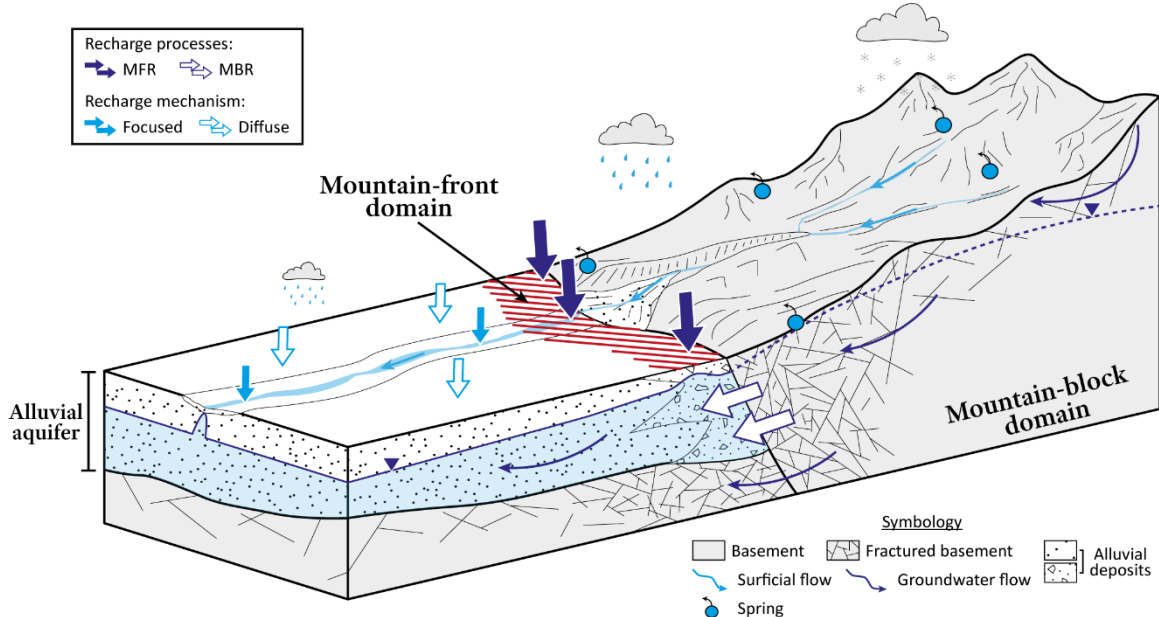


Fig. 1.2: Diagram showing the recharge processes in mountain front zones: Mountain-front recharge (MFR) and Mountain-block recharge (MBR). Illustration based on Wilson and Guan (2004).

Typically, mountain front zones are shaped by fault zones which separate the mountain domain from the alluvial basins (Fig. 1.3) (e.g. Campagna and Aydin, 1994; Armijo *et al.* 2010; Saylor *et al.* 2010; Salcher *et al.* 2012; Chapman *et al.* 2019; Laborde *et al.* 2019). As Bense *et al.* (2013) pointed out, a fault zone is the volume of rock where permeability has been altered by fault-related deformation. Fault zones commonly include a fault core surrounded by a damage zone (Caine *et al.* 1996; Kim *et al.* 2004; Faulkner *et al.* 2010; Choi *et al.* 2016). The fault core is the zone of the most intense strain and accommodates most of the displacement within the fault zone. Generally, it is found in the centre of the fault zone and develops as shear bands (gouge, fault breccia, cataclasite) or slip-surfaces. The damage zone is characterized by a relatively low strain compared to the fault core, and generally exhibit secondary structures such as minor faults, joints, and veins.

Since a hydrogeological point of view, the fault core shows generally a lower permeability than the damage zone, thus damage zone can be significantly more permeable than the fault core (Fig. 1.3) (e.g. Ogilvie and Glover, 2001; Balsamo *et al.* 2010; Agosta *et al.* 2012; Mitchell and Faulkner, 2012). In addition, fault zones can result from the interaction with other faults (Peacock *et al.* 2017), triggering a complex fracture network that impacts the groundwater circulation pathways, and hence the MBR processes. However, the circulation of groundwater in the mountain block (*i.e.* fractured media) requires more than only fractures. In this sense, a critical factor that determines the preferential flowpaths within a fracture media is the connectivity, because if the fractures are not connected the groundwater will not flow (Berkowitz, 2002; Manzocchi, 2002; Makel, 2007; Maillot *et al.* 2016; Viswanathan *et al.* 2018).

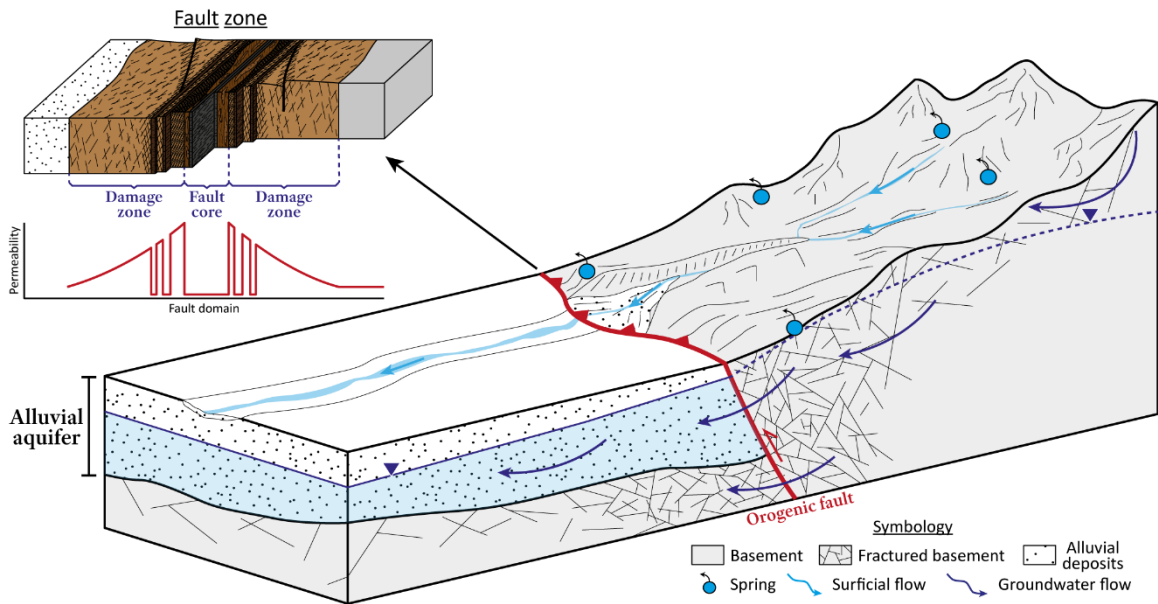


Fig. 1.3: Diagram showing the fault-contact between the mountain-block and the adjacent alluvial aquifer. The fault zone illustration is based on Choi *et al.* (2016).

1.2. RESEARCH PROBLEM

Chile is a long and narrow country extending 4300 km long and averages 180 km wide. The total population reported is 17,574,003 (data from *Instituto Nacional de Estadísticas de Chile*, INE), and despite being such a long country, ~70 % of the inhabitants lives in Central Chile (Fig. 1.4a), where the main socio-economic activities are also concentrated (*i.e.* agriculture, mining, forestry and hydropower plants). Consistent with its vast length, Chile provides an extraordinary variety of climatic conditions (Sarricolea *et al.* 2016), as demonstrated by the spatial variations of the air temperature and precipitations (Fig. 1.4b, c). The Chilean landscape is characterized by a narrow central valley filled with alluvial deposits (Central Depression) bordered by two cordilleras (Fig. 1.4d): the Coastal Cordillera, to the west, and the Principal Cordillera, to the east (Cembrano *et al.* 2007). This landscape is the result of a complex geological history recorded in cortical faults throughout Chile (Fig. 1.4e; See Sect. 2.1) (Mpodozis and Ramos, 1989).

Even though Chile is a mountainous country, the hydrogeological studies have been focused on alluvial deposits (Fig. 1.5a) filling valley bottoms and basin floors in the Central Depression (Muñoz *et al.* 2003; Rojas and Dassargues, 2007; Oyarzún *et al.* 2014; Jordan *et al.* 2015; Ribeiro *et al.* 2015; Muñoz *et al.* 2016; Oyarzún *et al.* 2016; Salas *et al.* 2016; Fernández *et al.* 2017; Urrutia *et al.* 2018; Viguier *et al.* 2018, 2019; Valois *et al.* 2020). Whilst such lithologies solely cover ~15% of the total area of Chile (Fig. 1.4d) (SERNAGEOMIN, 2003), the hydrogeological relations between alluvial deposits and surrounding cordilleras have remained unstudied. As a result, the recharge from fractured rocks of the mountain front has not been considered in hydrogeological conceptual models leading to an oversimplification of the aquifers functioning and boundary conditions (Fig. 1.5a). Indeed, according to Water Management Authority (*Dirección General de Aguas*, DGA), the renewal of Central Depression alluvial aquifers results from the focused recharge of river infiltration and from diffuse recharge of precipitation (Fig. 1.5a). However, such hydrogeological view omits potential groundwater resources in adjacent fractured rocks as well as the existence of mountain block recharge processes originating from the Principal Cordillera.

In Central (32.0°-36.0°S), the western flank of the Principal Cordillera (*i.e.* Western Andean Front) is in contact with the Central Depression aquifers by NS-oriented crustal faults (Armijo *et al.* 2010). In the Western Andean Front the precipitation rate is around two times higher than in the Central Depression (data provided by DGA) and, moreover, there are several perennial springs (Hauser, 1997; Benavente *et al.* 2016) that evidence the groundwater circulation within the mountain block (Fig. 1.5b). Thus, such context invites to explore the hydrogeological system in the Western Andean Front, where groundwater circulation may play an important role in the recharge of the adjacent Central Depression alluvial aquifers through the fractured rocks (Fig. 1.5b).

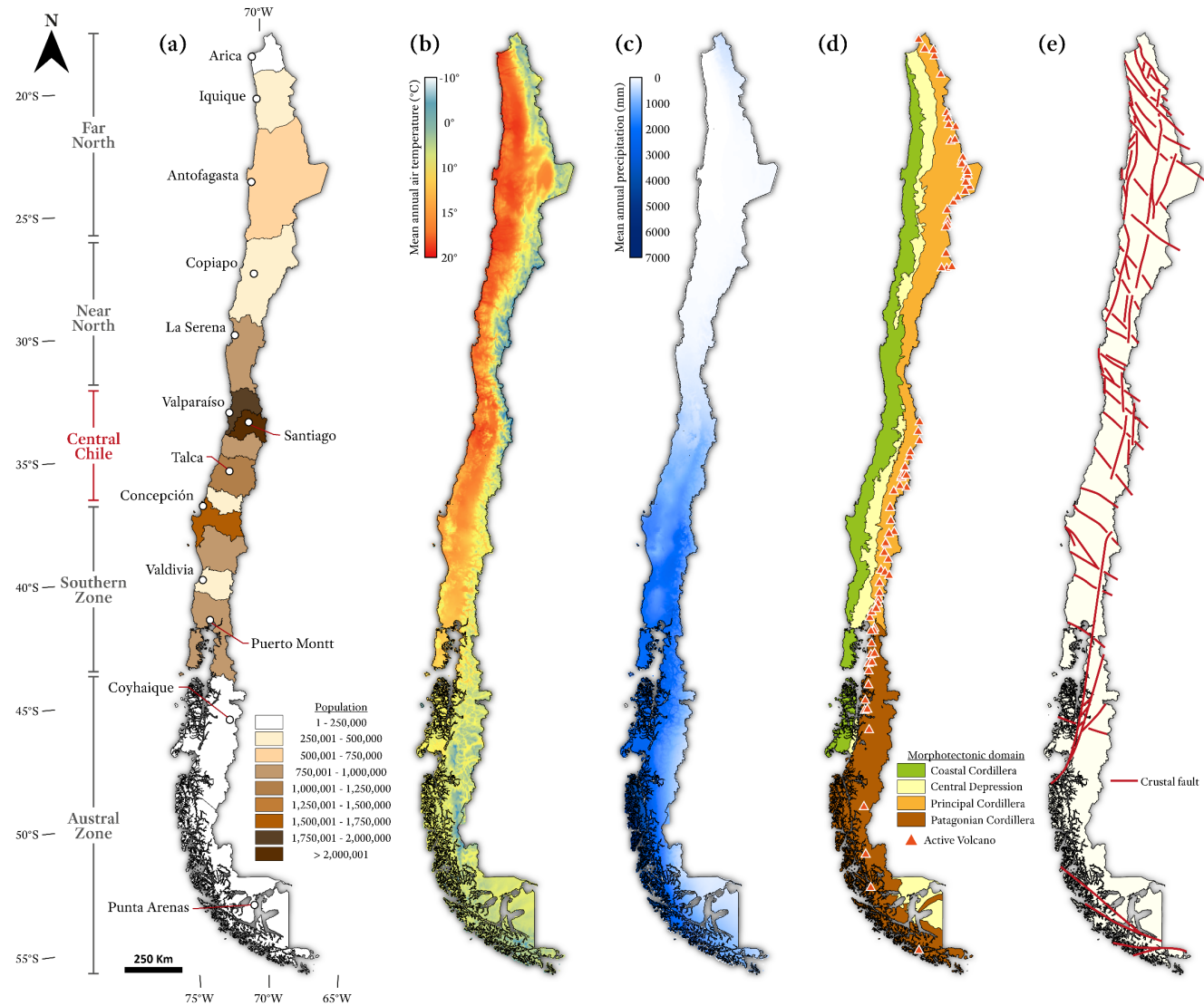


Fig. 1.4: a) Chilean population by region (data from INE); b) and c) annual mean air temperature and annual mean precipitation distribution, respectively (spatially interpolated gridded climate data from Fick and Hijmans, 2017); d) and e) morphotectonic features (based on Cembrano *et al.* 2007) and crustal fault (based on Arancibia, 2004; Cembrano *et al.* 2005; Farias *et al.* 2005; Melnick and Echter, 2006; Charrier *et al.* 2007; Allmendinger and González, 2010; Poblete *et al.* 2014; Betka *et al.* 2016; Martínez *et al.* 2016; Pérez-Flores *et al.* 2017; Piquer *et al.* 2019; Santibáñez *et al.* 2019; Veloso *et al.* 2019; Yáñez and Rivera, 2019) of the Chilean Andes, respectively.

In addition, Central Chile has undergone an uninterrupted sequence of dry years since 2010, known as “Megadrought” (Garreaud *et al.* 2017, 2019), with rainfall deficits between 20 % and 40 %. The combined effects of continuous dry years and increasing withdrawals (essentially for agriculture activities; Valdés-Pineda *et al.* 2014) have led to overexploit shallow alluvial aquifers and drying the rivers fed by the groundwater. Nowadays, social tensions are emerging between water resource stakeholders, especially since water management is based on the principle of private water rights that limit the equity of water resource repartition (Galaz, 2007; Valdés-Pineda *et al.* 2014; Costumero *et al.* 2016; Rivera *et al.* 2016; Tamayo and Carmona, 2019). Considering the alarming state of water resources in Central Chile, regional hydrogeological conceptual models must be improved to reach better management policies.

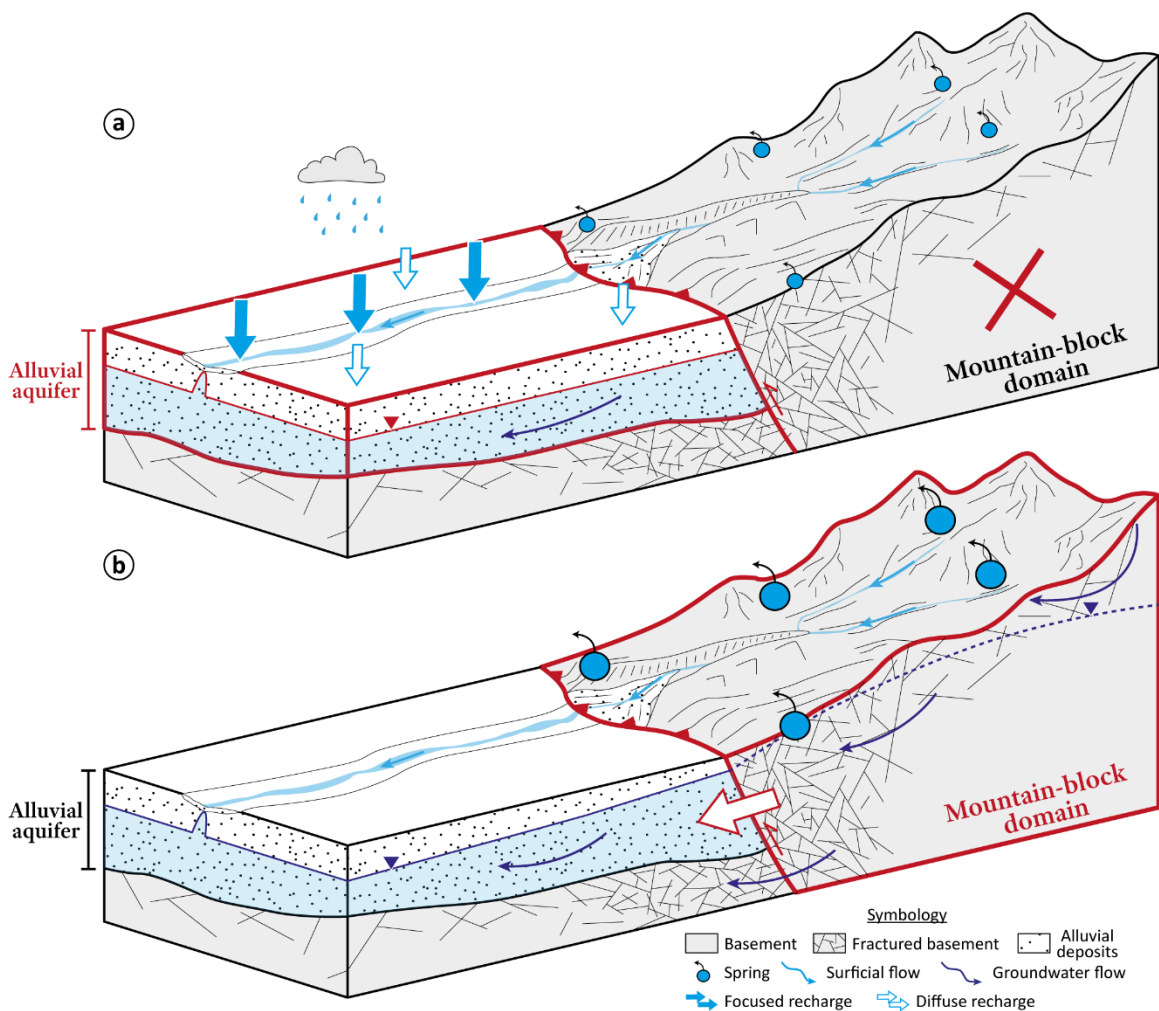


Fig. 1.5: a) Current and simplistic conceptual model for the Chilean alluvial aquifers and, b) hypothetical conceptual model considering the hydraulic connection between the alluvial aquifers and the mountain front.

1.3. HYPOTHESIS AND OBJECTIVES

1.3.1. Research questions and hypothesis

From the above background, the following research questions arise:

- What is the origin of the springs? Where does the recharge of those springs occur?
- Is there a hydrogeological connection between the Western Andean Front and the Central Depression alluvial aquifers?
- If a hydrogeological connection exists there, how is this connection possible? Do the crustal faults have any role in this connection? Which recharge process(es) occur(s)?

The hypothesis is that the springs result from a groundwater flow originated in high parts of the Principal Cordillera. The presence of the cortical faults along the Western Andean Front provide flow paths leading the mountain-block recharge processes. Thus, groundwater circulating in fractured rocks of the Western Andean Front is contributing to recharge the alluvial aquifers in the Central Depression, and consequently a hydrogeologic connection exists between both domains (Fig. 1.5b).

1.3.2. Objectives

This PhD thesis aims to develop a reliable conceptual model of groundwater circulation and related recharge processes taking place in the Western Andean Front as well as to unravel the role of the cortical faults in the recharge of Central Depression aquifers. The study was carried out in the Aconcagua Basin since there several perennial springs evidence groundwater flows in the Western Andean Front. The major springs outflow along the NS-oriented Pocuro Fault Zone (PFZ), which separates the volcanic rocks of the Principal Cordillera from the alluvial deposits of the Central Depression. Furthermore, the Aconcagua Basin is an emblematic area which gathers all water resources concerns of Central Chile. To answer the previous questions, the study was conducted through:

- A hydrogeochemical and isotopic analysis to assess the groundwater circulation and related recharge processes. It is expected to determine if there is a hydrogeological connection between the Western Andean Front and the Central Depression.
- A detailed structural geology exploration to unravel the fault zone architecture and how is the connection between the Western Andean Front and the Central Depression. It is expected to establish the role of the cortical faults in the groundwater circulation.
- A topological approach to quantify the connectivity degree of the fractured rocks along the Western Andean Front. It is expected to identify where the connection between the Western Andean Front and the Central Depression occurs.

1.4. SCIENTIFIC PRODUCTION

1.4.1. Publication and conference abstracts resulting from this thesis

1.4.1.1. Research papers

Taucare M., Daniele L., Viguier B., Vallejos A & Arancibia G. 2020. Groundwater resources and recharge processes in the Western Andean Front of Central Chile. *Science of The Total Environment* 722, 137824. <https://doi.org/10.1016/j.scitotenv.2020.137824>

Taucare M., Viguier B., Daniele L., Heuser G., Arancibia G. & Leonardi V. 2020. Connectivity of fractures and groundwater flows analyses into the Western Andean Front by means of a topological approach (Aconcagua Basin, Central Chile). *Hydrogeology Journal*.

Taucare M., Roquer T., Heuser G., Arancibia G., Veloso E., Viguier B., Daniele L. & Morata D. 2020. Fluid circulation during the Andean Cenozoic orogeny: Insights from the Pocuro Fault Zone. (In preparation).

1.4.1.2. Conference abstracts

Taucare M., Daniele L., Viguier B., Treskow V., Arancibia G. & Morata D. 2019. Insight the Western Andean Front Hydrogeology using springs geochemistry: the case of Aconcagua Basin (Central Chile). In: 46th IAH Congress. Málaga, España. Oral presentation.

Treskow V., Daniele L., Taucare M. & Viguier B. 2019. Hydrogeochemistry of low-pH springs at El Arpa Valley (Central Chile). In: 46th IAH Congress. Málaga, España. See the poster in ResearchGate: <https://doi.org/10.13140/RG.2.2.29317.29922>

Taucare M., Daniele L., Arancibia G., Heuser G., Roquer T. & Morata D. 2018. Structural control in the evolution of an Andean hydrothermal system: The case of Pocuro fault zone (32°35'S – 33°00'S). In: XV Congreso Geológico Chileno. Concepción, Chile. See the poster in ResearchGate: <https://doi.org/10.13140/RG.2.2.20870.42562>

Taucare M., Daniele L., Arancibia G., Viguier B. & Morata D. 2018. Conceptual model for sustainable direct use of geothermal resources: The case of Los Andes – San Felipe basin (central Chile). In: VI European Geothermal Workshop (EGW). Strasbourg, France. See the poster in ResearchGate: <https://doi.org/10.13140/RG.2.2.22967.57765>

Jara M., Daniele L., Taucare M., Arancibia G. & Morata D. 2018. Using reactive transport model to simulate a hydrothermal system in the Pocuro fault zone (central Chile). In: XXII Computational

Methods in Water Resources (CMWR). Saint Malo, France. See the poster in ResearchGate: <https://doi.org/10.13140/RG.2.2.19612.13445>

Taucare M., Daniele L., Arancibia G. & Morata D. 2017. Hydrogeochemical and isotopical data to assess recharge processes and hydrothermal evolution in hydrogeological fault zone setting of central Chile. In: IGCP636 Annual Meeting 2017. Santiago, Chile. Oral presentation.

Taucare M., Daniele L., Arancibia G. & Morata D. 2016. Descifrando las conexiones entre agua, rocas y fracturas en San Felipe – Los Andes (Cuenca del Río Aconcagua), Chile Central. In: IX Congreso Argentino de Hidrogeología. San Fernando de Catamarca, Argentina. See the poster in ResearchGate: <https://doi.org/10.13140/RG.2.2.13243.57128>

1.4.2. Publications and conference abstracts resulting from sides-studies

1.4.2.1. Research papers

Figueroa R., Viguier B., Taucare M., Yáñez G., Arancibia G., Sanhueza J. & Daniele L. 2020. Advances in the characterization of Western Andean Front recharge processes by a multidisciplinary analysis (Central Chile). Journal of Hydrology (Under review).

Daniele L., Taucare M., Viguier B., Arancibia G., Aravena D., Roquer T., Sepúlveda., Molina E., Muñoz M., Delgado A. & Morata D. 2020. Exploring the shallow geothermal resources in the Chilean Southern Volcanic Zone: insight from the Liquiñe thermal springs. Journal of Geochemical Exploration (Submitted).

1.4.2.2. Conference abstracts

Daniele L., Viguier B., Taucare M., Jourde H. & Leonardi V. 2019. Groundwater resources in Chile: the required revision of conceptual models to cope with anthropogenic and climate pressure changes. In: 46th IAH Congress. Málaga, España. Poster.

Figueroa R.J., Taucare M., Viguier B., Yáñez G., Arancibia G., Sanhueza J., Treskow V. & Daniele L. 2019. Assessing hydrogeological system in piedmont fault zone by gravimetric and electrical surveys, Central Andes (32°50'S). In: 46th IAH Congress. Málaga, España. Poster.

Placencia-Marin G., Daniele L., Viguier B., Taucare M. & Morata D. 2019. Hydrogeochemical evidences of multi-layered groundwater circulation and anthropogenic pollution in Atacama Desert Hillslopes (Oasis de Pica, Northern Chile). In: 46th IAH Congress. Málaga, España. Poster.

Ruiz B., Méndez C., Placencia-Marin G., Daniele L., Fuentes M.J., Genot A., Quiroga I. & Taucare M. 2019. Facing the water scarcity in Chile: creation of the Early Carrer Hydrogeologist' Network (ECHN) Chile. In: 46th IAH Congress. Málaga, España. Poster.

Daniele L., Arancibia G., Morata D., Taucare M., Roquer T., Molina E. & Sepúlveda J. 2018. Aguas termales y control estructural: Caso de la zona Liquiñe, sur de Chile (39°S). In: XV Congreso Geológico Chileno. Concepción, Chile.

Figueroa R.J., Taucare M., Yáñez G., Arancibia G. & Daniele L. 2018. Caracterización geofísica de un sistema hidrogeológico en medio fracturado: Caso de estudio de la zona de Falla Pocuro, Chile Central. In: XV Congreso Geológico Chileno. Concepción, Chile.

Treskow V., Taucare M., Daniele L. & Morata D. 2018. Análisis hidrogeoquímico de las aguas ácidas en Campos de Ahumada, Chile Central (32°35'S – 32°45'S). In: XV Congreso Geológico Chileno. Concepción, Chile.

REFERENCES

- Agosta F., Ruano P., Rustichelli A., Tondi E., Galindo-Zaldívar J. & Sanz de Galdeano C. 2012. Inner structure and deformation mechanisms of normal faults in conglomerates and carbonate grainstones (Granada Basin, Betic Cordillera, Spain): Inferences on fault permeability. *Journal of Structural Geology* 45, 4-20. <https://doi.org/10.1016/j.jsg.2012.04.003>
- Aishlin P. & McNamara J.P. 2011. Bedrock infiltration and mountain block recharge accounting using chloride mass balance. *Hydrological Processes* 25 (12), 1934-1948. <https://doi.org/10.1002/hyp.7950>
- Allmendinger R.W. & González G. 2010. Invited review paper: Neogene to Quaternary tectonics of the coastal Cordillera, northern Chile. *Tectonophysics* 495 (1-2), 93-110. <https://doi.org/10.1016/j.tecto.2009.04.019>
- Arancibia G. 2004. Mid-cretaceous crustal shortening: Evidence from a regional-scale ductile shear zone in the Coastal Range of central Chile (32° S). *Journal of South American Earth Sciences* 17 (3), 209–226. <https://doi.org/10.1016/j.jsames.2004.06.001>
- Armijo R., Rauld R., Thiele R., Vargas G., Campos J., Lacassin R. & Kausel E. 2010. The West Andean Thrust, the San Ramón Fault, and the seismic hazard for Santiago, Chile. *Tectonics* 29 (2), TC2007. <https://doi.org/10.1029/2008TC002427>
- Balsamo F., Storti F., Salvini F., Silva A.T. & Lima C.C. 2010. Structural and petrophysical evolution of extensional fault zones in low-porosity, poorly lithified sandstones of the Barreiras Formation, NE Brazil. *Journal of Structural Geology* 32 (11), 1806-1826. <https://doi.org/10.1016/j.jsg.2009.10.010>
- Benavente O., Tassi F., Reich M., Aguilera F., Capecchiacci F., Gutiérrez F., Vaselli O. & Rizzo A. 2016. Chemical and isotopic features of cold and thermal fluids discharged in the Southern Volcanic Zone between 32.5°S and 36°S: Insights into the physical and chemical processes controlling fluid geochemistry in geothermal systems of Central Chile. *Chemical Geology* 420, 97–113. <https://doi.org/10.1016/J.CHEMGEO.2015.11.010>
- Bense V.F., Gleeson T., Loveless S.E., Bour O. & Scibek. 2013. Fault zone hydrogeology. *Earth-Science Reviews* 127, 171-192. <https://doi.org/10.1016/j.earscirev.2013.09.008>
- Berkowitz B. 2002. Characterizing flow and transport in fractured geological media: A review. *Advances in Water Resources* 25 (8-12), 861-884. [https://doi.org/10.1016/S0309-1708\(02\)00042-8](https://doi.org/10.1016/S0309-1708(02)00042-8)
- Betka P., Klepeis K. & Mosher S. 2016. Fault kinematics of the Magallanes-Fagnano fault system, southern Chile; an example of diffuse strain and sinistral transtension along a continental transform margin. *Journal of Structural Geology* 85, 130-153. <https://doi.org/10.1016/j.jsg.2016.02.001>
- Bresciani E., Cranswick R.H., Banks E.W., Batlle-Aguilar J., Cook P.G. & Batelaan O. 2018. Using hydraulic head, chloride and electrical conductivity data to distinguish between mountain-front and mountain-block recharge to basin aquifers. *Hydrology and Earth System Sciences* 22, 1629-1648. <https://doi.org/10.5194/hess-22-1629-2018>

- Caine J.S., Evans J.P. & Forster C.B. 1996. Fault zone architecture and permeability structure. *Geology* 24 (11), 1025-1028. [https://doi.org/10.1130/0091-7613\(1996\)024<1025:FZAAPS>2.3.CO;2](https://doi.org/10.1130/0091-7613(1996)024<1025:FZAAPS>2.3.CO;2)
- Campagna D.J. & Aydin A. 1994. Basin genesis associated with strike-slip faulting in the Basin and Range, southeastern Nevada. *Tectonics* 13 (2), 327-341. <https://doi.org/10.1029/93TC02723>
- Cembrano J., González G., Arancibia G., Ahumada I., Olivares V. & Herrera V. 2005. Fault zone development and strain partitioning in an extensional strike-slip duplex: A case study from the Mesozoic Atacama fault system, Northern Chile. *Tectonophysics* 400 (1-4), 105-125. <https://doi.org/10.1016/j.tecto.2005.02.012>
- Cembrano J., Laveno A., Yáñez G., Riquelme R., García M., González G. & Héral G. 2007. Neotectonics. In: Moreno T. & Gibbons W. (Eds.), *The Geology of Chile*. Geological Society of London, 21-114. <https://doi.org/10.1144/GOCH.9>
- Chapman J.B., Carrapa B., DeCelles P., Wothonington J., Mancin N., Cobianchi M., Stoica M., Wang X., Gadoev M. & Oimahmadov I. 2019. The Tajik Basin: A composite record of sedimentary basin evolution in response to tectonics in the Pamir. *Basin Research*, 1-21. <https://doi.org/10.1111/bre.12381>
- Charrier R., Pinto L. & Rodríguez M.P. 2007. Tectonostratigraphic evolution of the Andean Orogen in Chile. In: Moreno T. & Gibbons W. (Eds.), *The Geology of Chile*. Geological Society of London, 21-114. <https://doi.org/10.1144/GOCH.3>
- Choi J-H., Edwards P., Ko K. & Kim Y-S. 2016. Definition and classification of fault damage zones: A review and a new methodological approach. *Earth-Science Reviews* 152, 70-87. <https://doi.org/10.1016/j.earscirev.2015.11.006>
- Costumero R., Sánchez J., García-Pedrero A., Rivera D., Lillo M., Gonzalo-Martín C. & Menasalvas E. 2016. Geography of legal water disputes in Chile. *Journal of Maps* 13 (1), 7-13. <https://doi.org/10.1080/17445647.2016.1252803>
- de Vries J.J. & Simmers I. 2002. Groundwater recharge: an overview of processes and challenges. *Hydrogeology Journal* 10 (1), 5-17. <https://doi.org/10.1007/s10040-001-0171-7>
- Farías M., Charrier R., Comte D., Martinod J. & Héral G. 2005. Late Cenozoic deformation and uplift of the western flank of the Altiplano: Evidence from the depositional, tectonic, and geomorphologic evolution and shallow seismic activity (northern Chile at 19°30'S). *Tectonics* 24 (4), TC4001. <https://doi.org/10.1029/2004TC001667>
- Faulkner D.R., Jackson C.A.L., Lunn R.J., Schlische R.W., Shipton Z.K., Wibberley C.A.J. & Withjack M.O. 2010. A review of recent developments concerning the structure, mechanics and fluid flow properties of fault zones. *Journal of Structural Geology* 32 (11), 1557-1575. <https://doi.org/10.1016/j.jsg.2010.06.009>
- Fernández E., Grilli A., Alvarez D. & Aravena R. 2017. Evaluation of nitrate levels in groundwater under agricultural fields in two pilot areas in central Chile: A hydrogeological and geochemical approach. *Hydrological Processes* 31 (1), 1206-1224. <https://doi.org/10.1002/hyp.11103>

Fick S.E. & Hijmans R.J. 2017. WorldClim 2: new 1-km spatial resolution climate surfaces for global land areas.

International Journal of Climatology 37 (12), 4302-4315. <https://doi.org/10.1002/joc.5086>

Galaz V. 2007. Stealing from the poor? Game theory and the politics of water markets in Chile. Environmental Politics 13 (2), 414-437. <https://doi.org/10.1080/0964401042000209649>

Garreaud R.D., Alvarez-Garreton C., Barichivich J., Boisier J.P., Christie D., Galleguillos M., LeQuesne C., McPhee J. & Zambrano-Bigiarini M. 2017. The 2010–2015 megadrought in central Chile: impacts on regional hydroclimate and vegetation. Hydrology and Earth System Sciences 21 (12), 6307–6327. <https://doi.org/10.5194/hess-21-6307-2017>

Garreaud R.D., Boisier J.P., Rondanelli R., Montecinos A., Sepúlveda H.H. & Veloso-Aguila D. 2019. The Central Chile Mega Drought (2010–2018): A climate dynamics perspective. International Journal of Climatology, 1-19. <https://doi.org/10.1002/joc.6219>

Hauser A. 1997. Catastro y caracterización de las fuentes de aguas minerales y termales de Chile. Servicio Nacional de Geología y Minería (SERNAGEOMIN), Santiago, Chile.

Healy R. 2010. Estimating Groundwater Recharge. Cambridge University Press, 256 pp. <https://doi.org/10.1017/CBO9780511780745.002>

Huggenberger P. & Aigner T. 1999. Introduction to the special issue on aquifer-sedimentology: problems, perspectives and modern approaches. Sedimentary Geology 129 (3-4), 179-186. [https://doi.org/10.1016/S0037-0738\(99\)00101-3](https://doi.org/10.1016/S0037-0738(99)00101-3)

Jordan T., Herrera C., Kirk-Lawlor N. & Godfrey L. 2015. Architecture of the aquifers of the Calama Basin, Loa catchment basin, northern Chile. Geosphere 11 (5), 1438-1474. <https://doi.org/10.1130/GES01176.1>

Kim Y-S., Peacock D.C.P. & Sanderson D.J. 2004. Fault damage zones. Journal of Structural Geology 26 (3), 503-517. <https://doi.org/10.1016/j.jsg.2003.08.002>

Kresic N. & Mikszewski A. 2012. Hydrogeological conceptual site models: Data analysis and visualization (1st ed.). CRC Press, 600 pp. <https://doi.org/10.1201/b12151>

Laborde A., Barrier L., Simoes M., Li H., Coudroy T., Van der Woerd J. & Tapponnier P. 2019. Cenozoic deformation of the Tarim Basin and surrounding ranges (Xinjiang, China): A regional overview. Earth-Science Reviews 197, 102891. <https://doi.org/10.1016/j.earscirev.2019.102891>

Maillot J., Davy P., Le Goc R., Darcel C. & de Dreuzy J.R. 2016. Connectivity, permeability and channeling in randomly-distributed and kinematically-defined discrete fracture network models. Water Resources Research 613–615. <https://doi.org/10.1002/2016WR018973>

Makel G.H. 2007. The modelling of fractured reservoirs: constraints and potential for fracture network geometry and hydraulics analysis. Geological Society of London 292, 375-403. <https://doi.org/10.1144/SP292.21>

Manzocchi T. 2002. The connectivity of two-dimensional networks of spatially correlated fractures. Water Resources Research 38 (9), 1-1-1-20. <https://doi.org/10.1029/2000WR000180>

- Markovich K.H., Manning A.H., Condon L.E. & McIntosh J.C. 2019. Mountain-block Recharge: A review of Current Understanding. *Water Resources Research*, 55. <https://doi.org/10.1029/2019WR025676>
- Martínez F., Arriagada C., Peña M., Deckart K. & Charrier R. 2016. Tectonic styles and crustal shortening of the Central Andes “Pampean” flat-slab segment in northern Chile (27–29°S). *Tectonophysics* 667, 144-162. <https://doi.org/10.1016/j.tecto.2015.11.019>
- Melnick D. & Echtler H.P. 2006. Morphotectonic and Geologic Digital Map Compilations of the South-Central Andes (36°–42°S). In: Oncken O., Chong G., Franz G., Giese P., Götze H-J., Ramos V.A., Strecker M.R. & Wigger P. (Eds.), *The Andes*. Springer, 565-568. https://doi.org/10.1007/978-3-540-48684-8_30
- Mitchell T.M. & Faulkner D.R. 2012. Towards quantifying the matrix permeability of fault damage zones in low porosity rocks. *Earth and Planetary Science Letters* 339-340, 24-31. <https://doi.org/10.1016/j.epsl.2012.05.014>
- Mpodozis C. & Ramos V. 1989. The Andes of Chile and Argentina. In: Erickson G.E., Cañas-Pinochet M.T. & Reinemund J. (Eds.), *Geology of the Andes and its relation to hydrocarbon and mineral resources*. Circum-Pacific Council for Energy and Mineral Resources, 59–90.
- Muñoz J.F., Fernández B. & Escauriaza C. 2003. Evaluation of groundwater availability and sustainable extraction rate for the Upper Santiago Valley Aquifer, Chile. *Hydrogeology Journal* 11 (6), 687-700. <https://doi.org/10.1007/s10040-003-0292-2>
- Muñoz E., Arumí J.L., Wagener T., Oyarzún R. & Parra V. 2016. Unraveling complex hydrogeological processes in Andean basins in south-central Chile: An integrated assessment to understand hydrological dissimilarity. *Hydrological Processes* 30 (26), 4934-4943. <https://doi.org/10.1002/hyp.11032>
- Ogilvie S.R. & Glover P.W.J. 2001. The petrophysical properties of deformation bands in relation to their microstructure. *Earth and Planetary Science Letters* 139 (1-2), 129-142. [https://doi.org/10.1016/S0012-821X\(01\)00492-7](https://doi.org/10.1016/S0012-821X(01)00492-7)
- Oyarzún R., Barrera F., Salazar P., Maturana H., Oyarzún J., Aguirre E., Alvarez P., Jourde H. & Kretschmer N. 2014. Multi-method assessment of connectivity between surface water and shallow groundwater: the case of Limarí River basin, north-central Chile. *Hydrogeology Journal* 22 (8), 1857-1873. <https://doi.org/10.1007/s10040-014-1170-9>
- Oyarzún R., Zambra S., Maturana H., Oyarzún J., Aguirre E. & Kretschmer N. 2016. Chemical and isotopic assessment of surface water–shallow groundwater interaction in the arid Grande river basin, North-Central Chile. *Hydrological Sciences Journal* 61 (12), 2193-2204. <https://doi.org/10.1080/02626667.2015.1093635>
- Peacock D.C.P., Nixon C.W., Rotevatn A., Sanderson D.J. & Zuluaga L.F. 2017. Interacting faults. *Journal of Structural Geology* 97, 1-22. <https://doi.org/10.1016/j.jsg.2017.02.008>
- Pérez-Flores P., Wang G., Mitchell T.M., Meredith P.G., Nara Y., Sarkar V. & Cembrano J. 2017b. The effect of offset on fracture permeability of rocks from the Southern Andes Volcanic Zone, Chile. *Journal of Structural Geology* 104, 142-158. <https://doi.org/10.1016/j.jsg.2017.09.015>

- Piquer J., Yañez G., Rivera O. & Cooke D.R. 2019. Long-lived crustal damage zones associated with fault intersections in the high Andes of Central Chile. *Andean Geology* 46, 223-239. <https://doi.org/10.5027/andgeoV46n2-3106>
- Poblete F., Roperch P., Hervé F., Diraison M., Espinoza M. & Arriagada C. 2014. The curved Magallanes fold and thrust belt: Tectonic insights from a paleomagnetic and anisotropy of magnetic susceptibility study. *Tectonics* 33 (12), 2526-2551. <https://doi.org/10.1002/2014TC003555>
- Ribeiro L., Kretschmer N., Nascimiento J., Buxo A., Rötting T., Soto G., Señoret M., Oyarzún J., Maturana H. & Oyarzún R. 2015. Evaluating piezometric trends using the Mann-Kendall test on the alluvial aquifers of the Elqui River basin, Chile. *Hydrological Sciences Journal* 60 (10), 1840-1852. <https://doi.org/10.1080/02626667.2014.945936>
- Rivera D., Godoy-Faúndez A., Lillo M., Alvez A., Delgado V., Gonzalo-Martín C., Menasalvas E., Costumero R. & García-Pedrero A. 2016. Legal disputes as a proxy for regional conflicts over water rights in Chile. *Journal of Hydrology* 535, 36-45. <https://doi.org/10.1016/j.jhydrol.2016.01.057>
- Rojas R. & Dassargues A. 2007. Groundwater flow modelling of the regional aquifer of the Pampa del Tamarugal, northern Chile. *Hydrogeology Journal* 15 (3), 537-551. <https://doi.org/10.1007/s10040-006-0084-6>
- Salas I., Herrera C., Luque J.A., Delgado J., Urrutia J. & Jordan T. 2016. Recent climatic events controlling the hydrological and the aquifer dynamics at arid areas: The case of Huasco River watershed, northern Chile. *Science of The Total Environment* 571, 178-194. <https://doi.org/10.1016/j.scitotenv.2016.07.132>
- Salcher B.C., Meurers B., Smit J., Decker K., Hölszel M. & Wagreich M. 2012. Strike-slip tectonics and Quaternary basin formation along the Vienna Basin fault system inferred from Bouguer gravity derivatives. *Tectonics* 31 (3), TC3004. <https://doi.org/10.1029/2011TC002979>
- Santibáñez I., Cembrano J., García-Pérez T., Costa C., Yáñez G., Marquardt C., Arancibia G. & González G. 2019. Crustal faults in the Chilean Andes: geological constraints and seismic potential. *Andean Geology* 46 (1), 32-65. <http://dx.doi.org/10.5027/andgeoV46n1-3067>
- Sarricolea P., Herrera-Ossandon M. & Meseguer-Ruiz Ó. 2016. Climatic regionalisation of continental Chile. *Journal of Maps* 13 (2), 66-73. <https://doi.org/10.1080/17445647.2016.1259592>
- Saylor J., DeCelles P., Gehrels G., Murphy M., Zhang R. & Kapp P. 2010. Basin formation in the High Himalaya by arc-parallel extension and tectonic damming: Zhada basin, southwestern Tibet. *Tectonics* 29 (1), TC1004. <https://doi.org/10.1029/2008TC002390>
- Scanlon B.R., Keese K.E., Flint A.L., Flint L.E., Gaye C.B., Edmunds W.M. & Simmers I. 2006. Global synthesis of groundwater recharge in semiarid and arid regions. *Hydrological Processes* 20 (15), 3335-3370. <https://doi.org/10.1002/hyp.6335>
- SERNAGEOMIN. 2003. Mapa geológico de Chile 1:1,000,000. Servicio Nacional de Geología y Minería (SERNAGEOMIN), Santiago, Chile.

- Simmers I. 1997. Groundwater recharge principles, problems and developments. In: Simmers I. (Ed.), Recharge of phreatic aquifers in (semi-)arid areas. CRC Press, 1-18.
- Simmers I. 2003. Hydrological Processes and Water Resources Management. In: Simmers I. (Ed.), Understanding Water in a Dry Environment: Hydrological Processes in Arid and Semi-Arid Zones. CRC Press, 1-14.
- Tamayo T. & Carmona A. 2019. El negocio del agua: cómo Chile se convirtió en tierra seca. Ediciones B, 232 pp.
- Urrutia J., Jódar J., Medina A., Herrera C., Chong G., Urqueta H. & Luque J.A. 2018. Hydrogeology and sustainable future groundwater abstraction from the Agua Verde aquifer in the Atacama Desert, northern Chile. *Hydrogeology Journal* 26 (6), 1989-2007. <https://doi.org/10.1007/s10040-018-1740-3>
- Valdés-Pineda R., Pizarro R., García-Chevesich P., Valdés J.B., Olivares C., Vera M., Balocchi F., Pérez F., Vallejos C., Fuentes R., Abarza A. & Helwig B. 2014. Water governance in Chile: Availability, management and climate change. *Journal of Hydrology* 519 (Part C), 2538-2567. <https://doi.org/10.1016/j.jhydrol.2014.04.016>
- Valois R., MacDonell S., Núñez J.H. & Maureira-Cortés H. 2020. Groundwater level trends and recharge event characterization using historical observed data in semi-arid Chile. *Hydrological Sciences Journal*, 20 pp. <https://doi.org/10.1080/02626667.2020.1711912>
- Veloso E., Tardani D., Elizalde D., Godoy B., Sánchez-Alfaro P., Aron F., Reich M. & Morata D. 2019. A review of the geodynamic constraints on the development and evolution of geothermal systems in the Central Andean Volcanic Zone (18–28°Lat.S). *International Geology Review*, 1-25. [10.1080/00206814.2019.1644678](https://doi.org/10.1080/00206814.2019.1644678)
- Viguier B., Jourde H., Yáñez G., Lira E.S., Leonardi V., Moya C.E., García-Pérez T., Maringue J. & Lictevout E. 2018. Multidisciplinary study for the assessment of the geometry, boundaries and preferential recharge zones of an overexploited aquifer in the Atacama Desert (Pampa del Tamarugal, Northern Chile). *Journal of South American Earth Sciences* 86, 366-383. <https://doi.org/10.1016/J.JSAMES.2018.05.018>
- Viguier B., Daniele L., Jourde H., Leonardi V. & Yáñez G. 2019. Changes in the conceptual model of the Pampa del Tamarugal Aquifer: Implications for Central Depression water resources. *Journal of South American Earth Sciences* 94, 102217. <https://doi.org/10.1016/j.jsames.2019.102217>
- Viswanathan H.S., Hyman J.D., Karra S., O’Malley D., Srinivasan S., Hagberg A. & Srinivasan G. 2018. Advancing Graph-Based Algorithms for Predicting Flow and Transport in Fractured Rock. *Water Resources Research* 54 (9), 6085-6099. <https://doi.org/10.1029/2017WR022368>
- Wilson J.L. & Guan H. 2004. Mountain-block hydrology and mountain-front recharge. In: Hogan J.F., Phillips F.M. & Scanlon B.R. (Eds.), *Groundwater Recharge in a Desert Environment: The Southwestern United States*. American Geophysical Union 9, 113–137.
- Yáñez G. & Rivera O. 2019. Crustal dense blocks in the fore-arc and arc region of Chilean ranges and their role in the magma ascent and composition: Breaking paradigms in the Andean metallogeny. *Journal of South American Earth Sciences* 93, 51-66. <https://doi.org/10.1016/j.jsames.2019.04.006>

This page intentionally left blank

2

Study area: The Aconcagua Basin

2.1. GEOLOGICAL SETTING

The Andes extends along the western margin of South America. This orogen resulted from the continental crust shortening and magmatic activity in response to ongoing subduction since the Jurassic (Coira *et al.* 1982; Mpodozis and Ramos, 1989; DeCelles *et al.* 2009; Schellart, 2017). Subsequently, the Andean orogeny began since the Late Cretaceous through several compressive phases alternated with extensional ones in combination with the eastward migration of the magmatic arc (Fig. 2.1) (Parada *et al.* 1988; Arancibia, 2004; Kay *et al.* 2005; Charrier *et al.* 2007). These tectonics phases have been developed through several NS oriented crustal faults, which were controlled by inherited pre-Andean oblique-to-the-orogen faults (Giambiagi *et al.* 2003; Cembrano and Lara, 2009; Piquer *et al.* 2017; Riesner *et al.* 2018; Veloso *et al.* 2019; Yáñez and Rivera, 2019).

As a consequence, the Andean region of Central Chile (32.0°-36.0°S) is segmented into three major NS-oriented morphotectonic domains (Jordan *et al.* 1983), identified from west to east as (Fig. 2.2): i) the Coastal Cordillera (up to 2000 m above sea level (asl)), ii) the Central Depression (~570 m asl) and iii) the Principal Cordillera (up to 5000-6000 m asl). At 32.5°S the subduction of the Juan Fernandez ridge beneath the South American plate triggered changes in the subduction angle (Yáñez *et al.* 2001, 2002; Yáñez and Cembrano, 2004; Tassara *et al.* 2006; Martinod *et al.* 2010), observed in the remarkable variations of the morphotectonic setting (Fig. 2.2): between 28.0°S and 32.5°S there is an absence of Central Depression as well as volcanism, while between 32.5°S and 42.0°S the Central Depression and the volcanism are present.

The western flank of the Principal Cordillera (referred hereafter as “Western Andean Front”) is a first-order morphological feature associated with a topographical difference of more than 2000 m relative to the Central Depression (Fig. 2.2) (Rauld, 2011). Along Central Chile, the Western Andean Front is shaped by west vergent thrust faults (Armijo *et al.* 2010; Fariñas *et al.* 2010; Vargas *et al.* 2014).

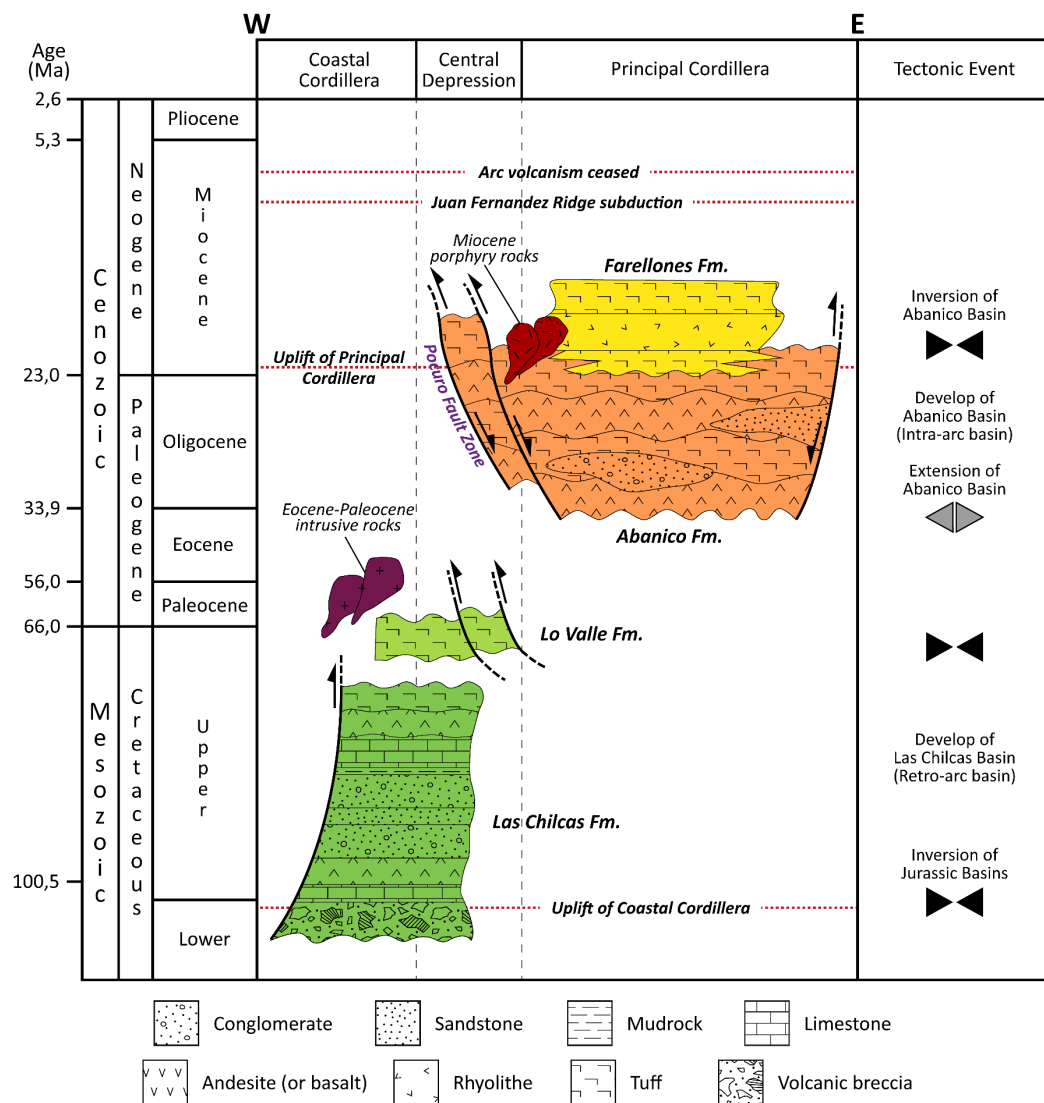


Fig. 2.1: Chronostratigraphic chart of the Central Chile (at 32.8°S) showing the main stratigraphic units and the dominant tectonic event (based on Godoy *et al.* 1999; Jordan *et al.* 2001; Yañez *et al.* 2001; Charrier *et al.* 2002; Fuentes *et al.* 2002; Nyström *et al.* 2003; Arancibia, 2004; Muñoz *et al.* 2006; Charrier *et al.* 2007; Jara and Charrier, 2014; Piquer *et al.* 2017; Horton, 2018; Riesner *et al.* 2019; Boyce *et al.* 2020).

Such structures acted as normal faults during the extension of the Abanico Basin (late Eocene-Oligocene; Fig. 2.1), and then were reactivated as reverse faults during the inversion of the Abanico Basin (late Miocene-early Pliocene; Fig. 2.1) (Godoy *et al.* 1999; Jordan *et al.* 2001; Charrier *et al.* 2002). The beginning of the inversion event coincides with a major shortening episode within the entire Andes with cumulative shortening of 1.7 mm/year and convergence rate of ~150 mm/year at ~20 Ma in Central Chile (Cembrano *et al.* 2007; Riesner *et al.* 2017). Then the cumulative shortening and convergence rate progressively decreases until currently values of 0.1 mm/year and 66 mm/year, respectively. The Western Andean Front reached the maximum uplift during the inversion event, after that the deformation migrated towards the eastern part of the Principal Cordillera (Farias *et al.* 2008).

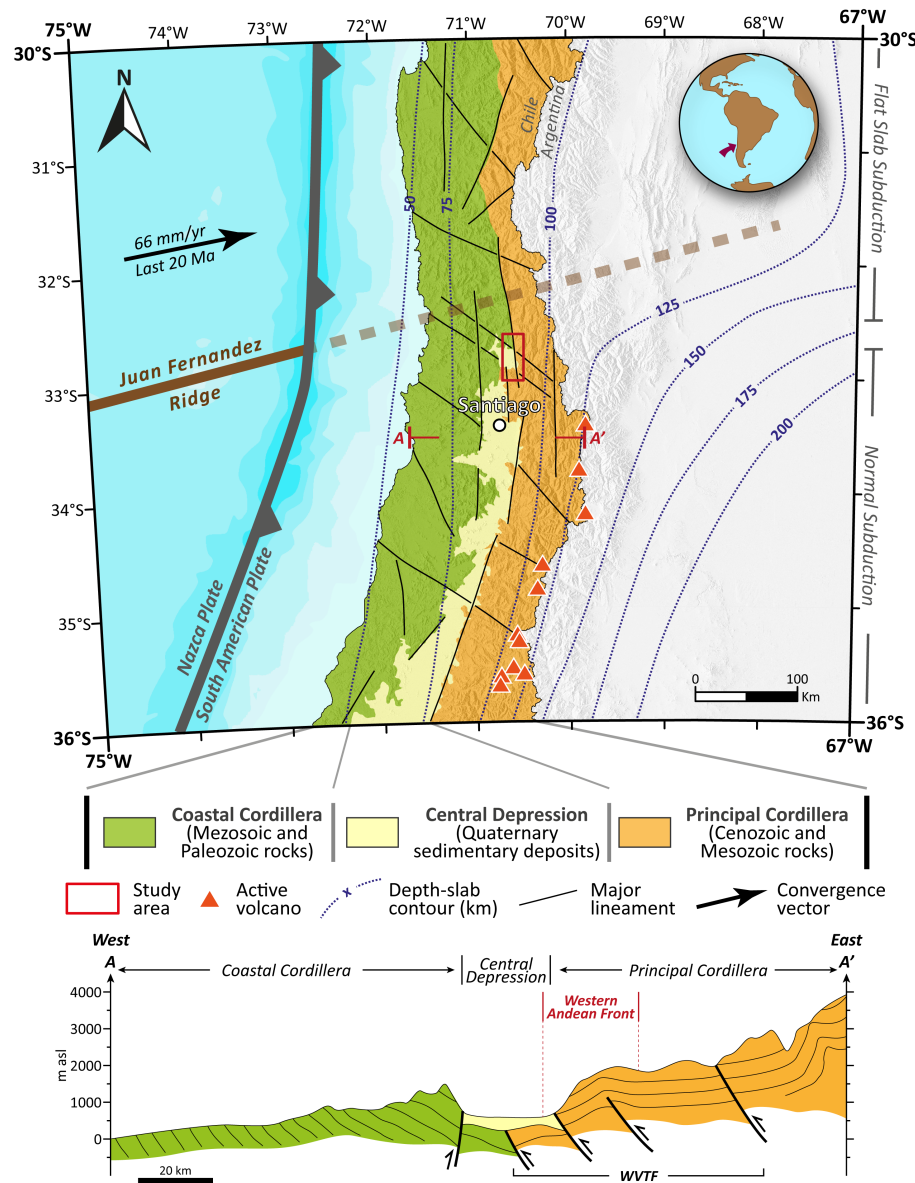


Fig. 2.2: Morphotectonic features of the Central Chile Andes (based on Cembrano *et al.* 2007). It illustrates the major lineaments (based on Yañez and Rivera, 2019) and the contour of the Nazca plate shape beneath the South American plate (Cahill and Isacks, 1992). Relative convergence vector of the Nazca plate from Angermann *et al.* (1999). WVTF: West vergent thrust faults.

In the Aconcagua Basin (32.8° ; Fig. 2.3), the Western Andean Front is shaped by the Pocuro Fault Zone (PFZ). The PFZ is a NS oriented brittle deformation zone spanning over 150 km long and 4 km wide, which record the previous described tectonic events (Fig. 2.1). Accordingly, the PFZ has been described as a normal fault inverted and reactivated as reverse fault during the Andean Cenozoic orogeny (Carter and Aguirre, 1965; Rivano *et al.* 1993; Jara and Charrier, 2014). The PFZ exhibits a hydrothermal alteration zone characterized by veins filled with minerals resulting from fluids at 100–310°C (Fuentes *et al.* 2004). The PFZ channelled such fluids from depths in an active geothermal system developed during the Miocene (Padilla and Vergara, 1985; Fuentes *et al.* 2004).

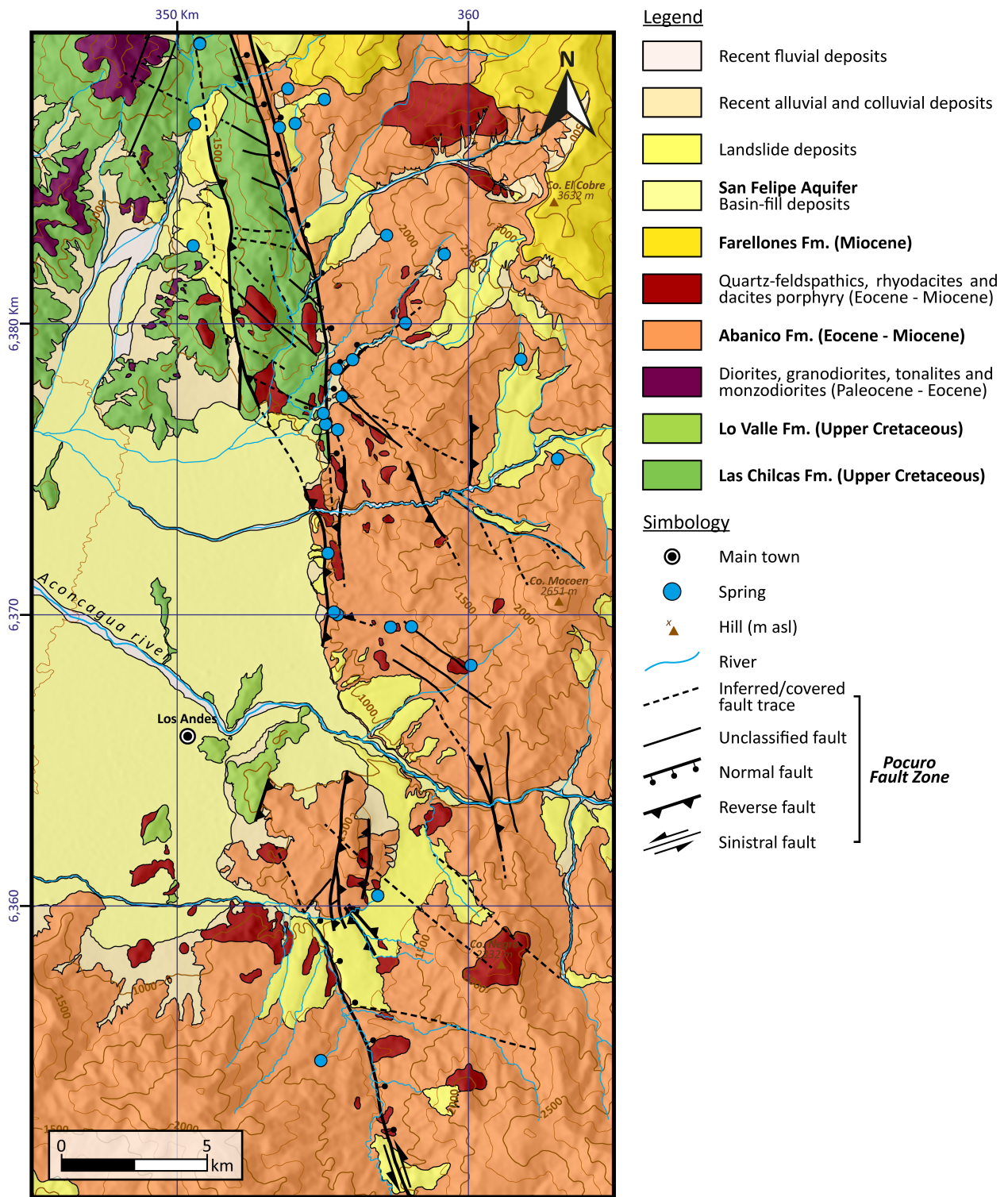


Fig. 2.3: Geological map of the study area (1:200.000), datum WGS84-19S. The lithological information is based on Rivano *et al.* 1993, Fuentes (2004), Jara and Charrier (2014) and Boyce *et al.* (2020).

The exposed rocks in the study area (Fig. 2.3) consist of a stratified sequence deposited in continental environment during the Cretaceous and the middle Miocene (Fig. 2.1):

- Las Chilcas Formation (late Cretaceous) located in the Coastal Cordillera, comprises ~6000 m of basalts, andesites and pyroclastic rocks intercalated by sedimentary layers, and limestones as subordinated layers (Thomas, 1958; Wall *et al.* 1999; Boyce *et al.* 2020). This formation is dated between 105.7 ± 3.3 Ma and 82.7 ± 5.7 Ma by U-Pb on detrital-zircon (Boyce, 2015).
- Lo Valle Formation (late Cretaceous) outcrops as *inselberg* into the Central Depression and it is constituted by 700-1800 m of dacitic tuff with intercalations of porphyritic andesites (Thomas, 1958; Gana and Wall, 1997; Boyce *et al.* 2020). This formation is dated between 73.3 ± 0.5 Ma and 65.0 ± 2.0 Ma by $^{40}\text{Ar}/^{39}\text{Ar}$ on plagioclase (Gana and Wall, 1997) and U-Pb on detrital-zircon (Boyce, 2015). Lo Valle Fm. overlies in angular unconformity on Las Chilcas Fm. (Rivano *et al.* 1993; Boyce *et al.* 2020).
- Abanico Formation (late Eocene to early Miocene) located in the Principal Cordillera is made up by ~3000 m of andesites, basalts and pyroclastic rocks intercalated with conglomerates, sandstones and mudrocks (Fuentes *et al.* 2002; Nyström *et al.* 2003; Muñoz *et al.* 2006; Jara and Charrier, 2014; Piquer *et al.* 2017). This formation is dated between 37.0 ± 0.0 Ma and 20.9 ± 0.3 Ma by $^{40}\text{Ar}/^{39}\text{Ar}$ and K/Ar on whole rock, plagioclase, biotite and hornblende (Gana and Wall, 1997; Fuentes *et al.* 2002; Muñoz *et al.* 2006), U-Pb on detrital-zircon (Jara and Charrier, 2014; Piquer *et al.* 2017) and U-Th/He in zircon and apatite (Piquer *et al.* 2017). The Abanico Fm. is in fault-contact with Las Chilcas Fm. by the PFZ (Jara and Charrier, 2014)
- Farellones Formation (early to middle Miocene) outcrops in the highest part of the Principal Cordillera and it is a 1000-2500 m thick sequence of dacitic-rhyolitic tuff, andesites and rhyolites (Rivano *et al.* 1990; Fuentes *et al.* 2002; Nyström *et al.* 2003; Jara and Charrier, 2014; Piquer *et al.* 2017). This formation is dated between 21.4 ± 0.4 Ma and 16.7 ± 0.2 Ma by K/Ar on whole rock, plagioclase and biotite (Vergara *et al.* 1988), $^{40}\text{Ar}/^{39}\text{Ar}$ on whole rock, biotite and hornblende (Fuentes *et al.* 2002), U-Pb on detrital-zircon (Deckart *et al.* 2005; Jara and Charrier, 2014; Piquer *et al.* 2017) and U-Th/He in zircon and apatite (Piquer *et al.* 2017). The Farellones Fm. overlies in progressive unconformity on the Abanico Fm (Fuentes *et al.* 2002; Jara and Charrier, 2014).

Subsequent erosional processes (post Pliocene) in the Principal Cordillera, originated detrital materials which were transported along EW-oriented fluvio-glacial valleys (*e.g.* Aconcagua River). Then, the transport of detrital materials allowed the filling of the Central Depression basin floor, with an average thickness of ~300 m (Yañez *et al.* 2015).

2.2. HYDRO(GEO)LOGICAL SETTING

2.2.1. Hydroclimatic variability

Central Chile is characterized by a semi-arid climate where moisture fluxes originate from the Pacific Ocean and cold fronts associated with low pressure systems (Barret *et al.* 2009). The Principal Cordillera acts as an orographic barrier isolating the western flank of the Chilean Andes from the Atlantic influence (Barret *et al.* 2009). During the historic time-period (1980-2010), annual precipitation averaged 520 mm/year in the Coastal Cordillera, 280 mm/year in the Central Depression and 620 mm/year in the Principal Cordillera according to the database of *Dirección General de Aguas* (DGA) (DGA, 2019). Typically, most of precipitation (~65 %) occurs during the austral winter. The interannual variability is typically related to El Niño Southern Oscillation (ENSO) (Montecinos and Aceituno, 2003) showing wet and dry years during El Niño and la Niña phases, respectively (Fig. 2.4a). In the interface between the Central Depression and the Principal Cordillera, the Western Andean Front is a hydroclimate transition area where the 0 °C isotherm line oscillates around 2000 m asl. In the mountain front zone, air temperature averages 15 °C at 1100 m asl and ranges from -5 °C during the austral winter to 38 °C during the austral summer (Fig. 2.4b) (DGA, 2019).

On mountain flanks, several temporary streams occur after anomalous rainy events (Garreaud, 2013; Viale and Garreaud, 2014) unlike major exoreic perennial streams originating from the Principal Cordillera (*e.g.* Aconcagua River). Perennial streams are fed by precipitation during wet time periods whereas groundwater and snowmelt on highs areas support the river base-flow during dry time periods (Waylen and Caviedes, 1990; Cortés *et al.* 2011, Ohlanders *et al.* 2013). However, since 2010 the “Megadrought”, characterized by an uninterrupted sequence of dry years uncorrelated from the ENSO variations (Fig. 2.4a, c), has led to an alarming rainfall deficit from 25 to 45 % in Central Chile relative to the historic period (1980-2010) (Boisier *et al.* 2016; Garreaud *et al.* 2017). Although snow and glacier melt on highs support the river discharges (Ohlanders *et al.* 2013; Rodriguez *et al.* 2016; Janke *et al.* 2017; Schaffer *et al.* 2019), surface water resources have rapidly declined up to 90 % (Garreaud *et al.* 2017) leading the drought of many rivers (Fig. 2.4d).

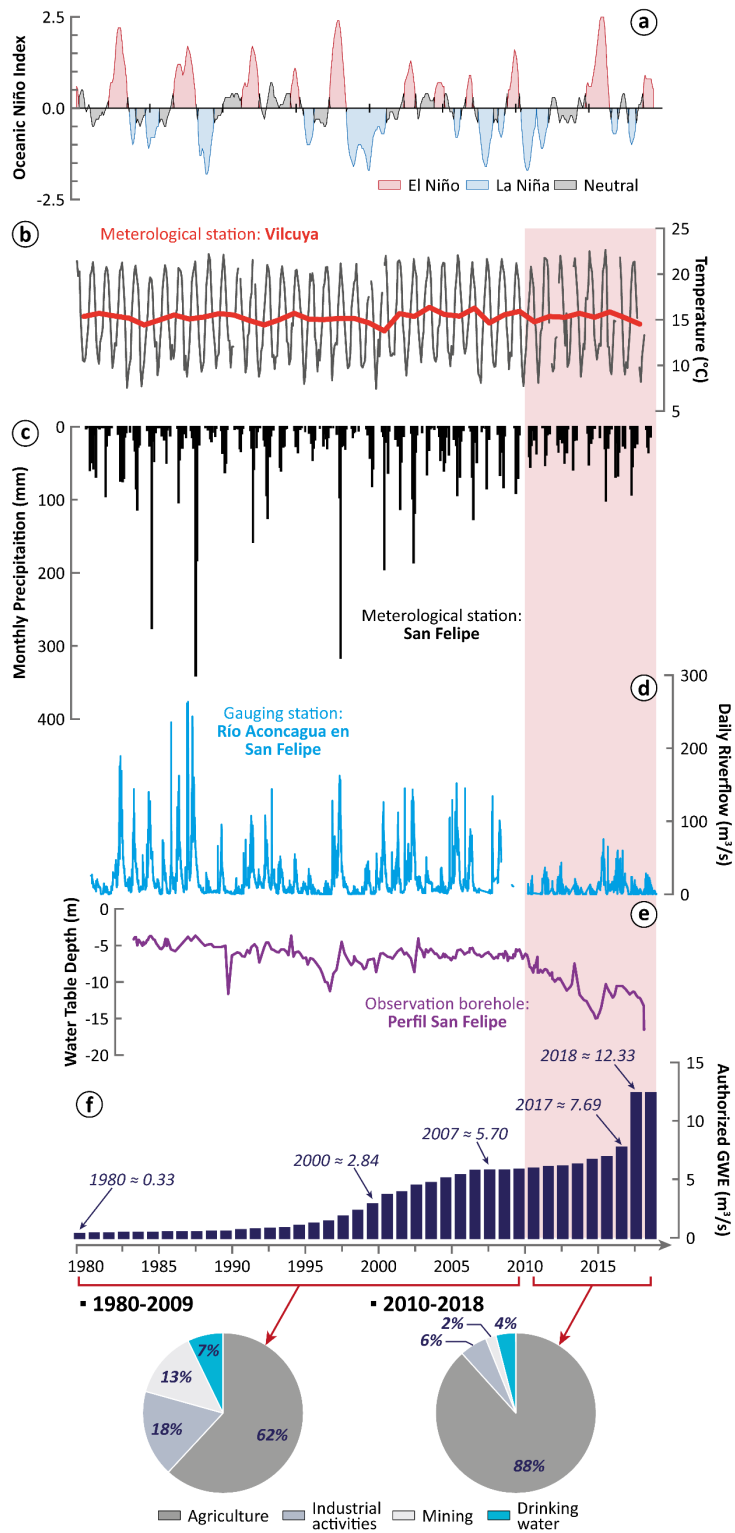


Fig. 2.4: Hydro(geo)logical context in the Aconcagua Basin. Hydroclimatic time series since 1980 to the present: a) Oceanic Niño Index (NOAA/National Weather Service, 2019); b) monthly mean air temperature at “Vilcuya” meteorological station; c) monthly precipitation at “San Felipe” meteorological station; d) daily river flow at “Río Aconcagua en San Felipe” gauging station; e) water table depth (meters below ground surface) at the “Perfil San Felipe” observation borehole; f) authorized groundwater extraction in the San Felipe Aquifer (*i.e.* groundwater rights) and respective uses during the historic time-period (1980-2009) and the megadrought (2010-2018). In pink is highlighted the “Megadrought” of Central Chile. b), c), d) and e) available data at DGA web site (DGA, 2019).

2.2.2. Groundwater resources

Along the Western Andean Front at least 23 perennial springs outflow at different elevations from fractured rocks (Fig. 2.5). In this zone, Darwin (1839) described the two major springs of the study area (Fig. 2.5): *Termas de Jahuel* (22 °C; Jh) and *Termas El Corazón* (20 °C; TEC). The mean spring discharges are $\sim 14.0 \text{ m}^3/\text{h}$ and $\sim 7.2 \text{ m}^3/\text{h}$, respectively. Due to the stability in physico-chemical parameters and geochemical composition over time (Darapsky, 1890; Hauser, 1997; Bustamante *et al.* 2012; Benavente *et al.* 2016), those springs have been used for thermal-bath activities and mineral water bottling over decades (Daniele *et al.* 2019).

To the west, in the Central Depression, the San Felipe Aquifer is contained into the Quaternary alluvial sediments (200-360 m thick) filling the Aconcagua Basin (Fig. 2.5) (DGA, 2015, 2016). According to DGA (2016), the San Felipe aquifer is limited by the PFZ and the volcano-sedimentary sequences that are considered as no-flow boundary conditions. Groundwater recharge is exclusively related to diffuse recharge from precipitation as well as to focused recharge from Aconcagua River. Historically, surface-water coming from Principal Cordillera and distributed by canals has permitted the development of small farming activities in the Central Depression. But since the late 1980s, groundwater is mainly extracted by deep boreholes (200-300 m depth) for supplying intensive agriculture practices, especially avocado and grapevine cultivation, which has led to a water footprint increment (*e.g.* Novoa *et al.* 2019). Consequently, the authorized groundwater extraction from the San Felipe alluvial aquifer has significantly increased leading to a progressive water table decline (Fig. 2.4e, f). In fact, withdrawals from the San Felipe aquifer have increased further during the “Megadrought” (Fig. 2.4e). It results in an alarming and sharp water table drop up to 40 m (provided by Dirección General de Aguas, DGA, 2019). Nowadays, groundwater resources in the Central Depression are overexploited.

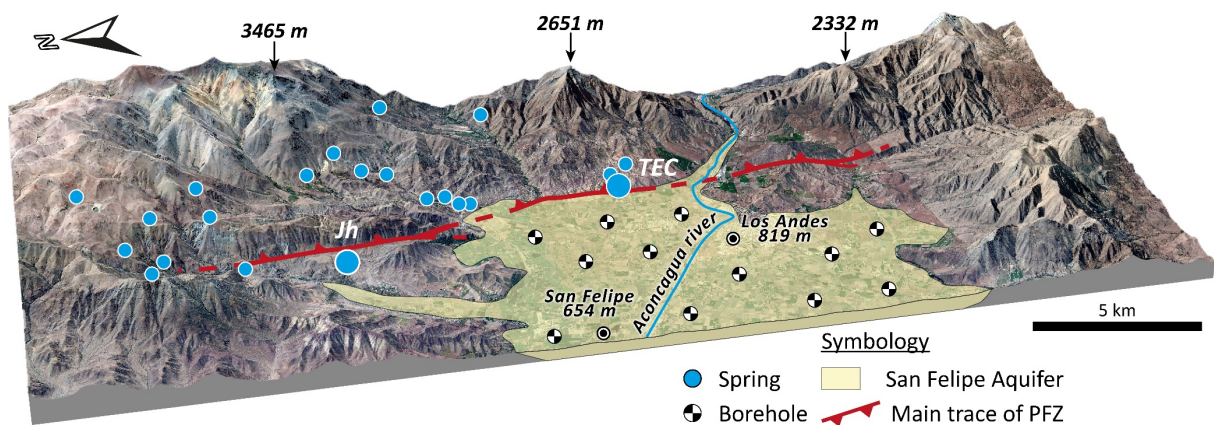


Fig. 2.5: Springs located in the Western Andean Front and boreholes in the San Felipe Aquifer. Major springs are highlighted: *Termas de Jahuel* (Jh) and *Termas El Corazón* (TEC).

REFERENCES

- Angermann D., Klotz J. & Reigber C. 1999. Space-geodetic estimation of the nazca-south america euler vector. Earth and Planetary Science Letters 171 (3), 329-334. [https://doi.org/10.1016/S0012-821X\(99\)00173-9](https://doi.org/10.1016/S0012-821X(99)00173-9)
- Arancibia G. 2004. Mid-cretaceous crustal shortening: Evidence from a regional-scale ductile shear zone in the Coastal Range of central Chile (32° S). Journal of South American Earth Sciences 17 (3), 209–226. <https://doi.org/10.1016/j.jsames.2004.06.001>
- Armijo R., Rauld R., Thiele R., Vargas G., Campos J., Lacassin R. & Kausel E. 2010. The West Andean Thrust, the San Ramón Fault, and the seismic hazard for Santiago, Chile. Tectonics 29 (2), TC2007. <https://doi.org/10.1029/2008TC002427>
- Barrett B.S., Garreaud R.D. & Falvey M. 2009. Effect of the Andes Cordillera on precipitation from a midlatitude cold front. Monthly Weather Review 137, 3092–3109. <https://doi.org/10.1175/2009MWR2881.1>
- Benavente O., Tassi F., Reich M., Aguilera F., Capecchiacci F., Gutiérrez F., Vaselli O. & Rizzo A. 2016. Chemical and isotopic features of cold and thermal fluids discharged in the Southern Volcanic Zone between 32.5°S and 36°S: Insights into the physical and chemical processes controlling fluid geochemistry in geothermal systems of Central Chile. Chemical Geology 420, 97–113. <https://doi.org/10.1016/J.CHEMGEO.2015.11.010>
- Boisier J.P., Rondanelli R., Garreaud R.D. & Muñoz F. 2016. Anthropogenic and natural contributions to the Southeast Pacific precipitation decline and recent megadrought in central Chile. Geophysical Research Letters 43 (1), 413–421. <https://doi.org/10.1002/2015GL067265>
- Boyce D. 2015. Modelo de evolución tectónica y paleogeográfica del margen andino en Chile Central durante el cretácico medio - tardío: El registro estructural y sedimentario en la formación Las Chilcas (MSc Thesis). Universidad de Chile, Santiago, Chile.
- Boyce D., Charrier R. & Farias M. 2020. The first Andean compressive tectonic phase. Sedimentologic and structural analysis of mid-Cretaceous deposits in the Coastal Cordillera, Central Chile (32°50'S). Tectonics 39 (2), e2019TC005825. <https://doi.org/10.1029/2019TC005825>
- Bustamante M., Lemus M., Cortés R., Vivallos J., Cáceres D. & Wall R. 2012. Exploración geológica para el fomento de la energía geotérmica: Área de Jahuel, Región de Valparaíso. Servicio Nacional de Geología y Minería (SERNAGEOMIN), Santiago, Chile.
- Cahill T. & Isacks B.L. 1992. Seismicity and shape of the subducted Nazca Plate. Journal of Geophysical Research: Solid Earth 91 (B12), 17503-17529. <https://doi.org/10.1029/92JB00493>
- Carter W.D. & Aguirre L. 1965. Structural Geology of Aconcagua Province and its Relationship to the Central Valley Graben, Chile. Geological Society of America Bulletin 76 (6), 651-664. [https://doi.org/10.1130/0016-7606\(1965\)76\[651:SGOAPA\]2.0.CO;2](https://doi.org/10.1130/0016-7606(1965)76[651:SGOAPA]2.0.CO;2)

- Cembrano J., Lavenu A., Yáñez G., Riquelme R., Garcia M., González G. & Héral G. 2007. Neotectonics. In: Moreno T. & Gibbons W. (Eds.), The Geology of Chile. Geological Society of London, 21-114. <https://doi.org/10.1144/GOCH.9>
- Cembrano J. & Lara L. 2009. The link between volcanism and tectonics in the southern volcanic zone of the Chilean Andes: A review. *Tectonophysics* 471 (1-2). 96-113. <https://doi.org/10.1016/j.tecto.2009.02.038>
- Charrier R., Baeza O., Elgueta S., Flynn J.J., Gans P., Ka S.M., Muñoz N., Wyss A.R. & Zurita E. 2002. Evidence for Cenozoic extensional basin development and tectonic inversion south of the flat-slab segment, southern Central Andes, Chile (33°-36°S.L.). *Journal of South American Earth Sciences* 15 (1), 117-139. [https://doi.org/10.1016/S0895-9811\(02\)00009-3](https://doi.org/10.1016/S0895-9811(02)00009-3)
- Charrier R., Pinto L. & Rodríguez M.P. 2007. Tectonostratigraphic evolution of the Andean Orogen in Chile. In: Moreno T. & Gibbons W. (Eds.), The Geology of Chile. Geological Society of London, 21-114. <https://doi.org/10.1144/GOCH.3>
- Coira B., Davidson J., Mpodozis C. & Ramos V. 1982. Tectonic and magmatic evolution of the Andes of northern Argentina and Chile. *Earth-Science Reviews* 18 (3-4), 303-332. [https://doi.org/10.1016/0012-8252\(82\)90042-3](https://doi.org/10.1016/0012-8252(82)90042-3)
- Cortés G., Vargas X. & McPhee J. 2011. Climatic sensitivity of streamflow timing in the extratropical western Andes Cordillera. *Journal of Hydrology* 405 (1-2), 93-109. <https://doi.org/10.1016/j.jhydrol.2011.05.013>
- Darwin C. 1839. The voyage of the Beagle. Wordsworth, 733 pp.
- Daniele L., Cannatelli C., Buscher J.T. & Bonatici G. 2019. Chemical composition of Chilean bottled waters: Anomalous values and possible effects on human health. *Science of The Total Environment* 689, 526-533. <https://doi.org/10.1016/j.scitotenv.2019.06.165>
- Darapsky L. 1890. Las aguas minerales en Chile. Imprenta del Universo de Guillermo Helfmann, 196 p.
- DeCelles P.G., Ducea M.N., Kapp P. & Zandt G. 2009. Cyclicity in Cordilleran orogenic systems. *Nature Geoscience* 2, 251-257. <https://doi.org/10.1038/ngeo469>
- Deckart K., Clark A.H., Aguilar A.C., Vargas R.R., Bertens A.N., Mortensen J.K. & Fanning M. 2005. Magmatic and hydrothermal chronology of the Giant Río Blanco porphyry copper deposit, central Chile: Implications of an integrated U-Pb and 40Ar/ 39Ar database. *Economic Geology* 100, 905-934. <https://doi.org/10.2113/gsecongeo.100.5.905>
- DGA. 2015. Determinación de la Disponibilidad de Aguas Subterráneas en el Valle del Río Aconcagua. Dirección General de Aguas (DGA), Santiago, Chile.
- DGA. 2016. Disponibilidad de Recursos Hídricos para el Otorgamiento de Derechos de Aprovechamiento de Aguas Subterráneas en el Valle del Aconcagua: Sectores hidrogeológicos de San Felipe, Putaendo, Panquehue, Catemu y Llay Llay. Dirección General de Aguas (DGA), Santiago, Chile.
- DGA. 2019. Inventario Público de Información Hidrológica y Meteorológica. Dirección General de Aguas (DGA),

Santiago, Chile. <http://snia.dga.cl/BNAConsultas/reportes>

- Farías M., Charrier R., Carretier S., Martinod J., Fock A., Campbell D., Cáceres J. & Comte D. 2008. Late Miocene high and rapid surface uplift and its erosional response in the Andes of central Chile (33°–35°S). *Tectonics* 27 (1), TC1005. <https://doi.org/10.1029/2006TC002046>
- Farías M., Comte D., Charrier R., Martinod J., David C., Tassara A., Tapia F. & Fock A. 2010. Crustal-scale structural architecture in central Chile based on seismicity and surface geology: Implications for Andean mountain building. *Tectonics* 29 (3), TC3006. <https://doi.org/10.1029/2009TC002480>
- Fuentes F., Vergara M., Aguirre L. & Féraud G. 2002. Contact relationships of Tertiary volcanic units from the Andes of Central Chile (33°S): a reinterpretation based on $^{40}\text{Ar}/^{39}\text{Ar}$ dating. *Revista Geológica de Chile* 29 (2), 151-165.
- Fuentes F. 2004. Petrología y metamorfismo de muy bajo grado de unidades volcánicas oligoceno-miocenas en la ladera occidental de Los Andes de Chile Central (33°S) (PhD Thesis). Universidad de Chile, Santiago, Chile.
- Fuentes F., Aguirre L., Vergara M., Valdebenito L. & Fonseca E. 2004. Miocene fossil hydrothermal system associated with a volcanic complex in the Andes of central Chile. *Journal of Volcanology and Geothermal Research* 138 (1–2), 139-161. <https://doi.org/10.1016/j.jvolgeores.2004.07.001>
- Gana P. & Wall R. 1997. Evidencias geocronológicas $^{40}\text{Ar}/^{39}\text{Ar}$ y K-Ar de un hiatus cretácico superior-eoceno en Chile central (33-33° 30'S). *Revista Geológica de Chile* 24 (2), 145–163.
- Garreaud R.D. 2013. Warm Winter Storms in Central Chile. *Journal of Hydrometeorology* 14, 1515-1534. <https://doi.org/10.1175/JHM-D-12-0135.1>
- Garreaud R.D., Alvarez-Garreton C., Barichivich J., Boisier J.P., Christie D., Galleguillos M., LeQuesne C., McPhee J. & Zambrano-Bigiarini M. 2017. The 2010–2015 megadrought in central Chile: impacts on regional hydroclimate and vegetation. *Hydrology and Earth System Sciences* 21 (12), 6307–6327. <https://doi.org/10.5194/hess-21-6307-2017>
- Giambiagi L.B., Ramos V.A., Godoy E., Alvarez P.P. & Orts S. 2003. Cenozoic deformation and tectonic style of the Andes, between 33° and 34° south latitude. *Tectonics* 22 (4), 1041. <https://doi.org/10.1029/2001TC001354>
- Godoy E., Yañez G. & Vera E. 1999. Inversion of an Oligocene volcano-tectonic basin and uplifting of its superimposed Miocene magmatic arc in the Chilean Central Andes: first seismic and gravity evidences. *Tectonophysics* 306 (2), 217–236. [https://doi.org/10.1016/S0040-1951\(99\)00046-3](https://doi.org/10.1016/S0040-1951(99)00046-3)
- Hauser A. 1997. Catastro y caracterización de las fuentes de aguas minerales y termales de Chile. Servicio Nacional de Geología y Minería (SERNAGEOMIN), Santiago, Chile.
- Horton B.K. 2018. Tectonic Regimes of the Central and Southern Andes: Responses to Variations in Plate Coupling During Subduction. *Tectonics* 37 (2), 402-429. <https://doi.org/10.1002/2017TC004624>

- Janke J.R., Ng S. & Bellisario A. 2017. An inventory and estimate of water stored in firn fields, glaciers, debris-covered glaciers, and rock glaciers in the Aconcagua River Basin, Chile. *Geomorphology* 296, 142-152. <https://doi.org/10.1016/j.geomorph.2017.09.002>
- Jara P. & Charrier R. 2014. New stratigraphical and geochronological constraints for the Mezo-Cenozoic deposits in the High Andes of central Chile between 32° and 32°30'S: Structural and palaeogeographic implications. *Andean Geology* 41 (1), 174–209. <https://doi.org/10.5027/andgeoV41n1-a07>
- Jordan T.E., Isacks B., Allmendinger R., Brewer J., Ramos V. & Aando C. 1983. Andean tectonics related to geometry of subducted Nazca plate. *GSA Bulletin* 94 (3), 341–361. [https://doi.org/10.1130/0016-7606\(1983\)94<341:ATRTGO>2.0.CO;2](https://doi.org/10.1130/0016-7606(1983)94<341:ATRTGO>2.0.CO;2)
- Jordan T.E., Burns W.M., Veiga R., Pángaro F., Copeland P., Kelley S. & Mpodozis C. 2001. Extension and basin formation in the southern Andes caused by increased convergence rate: A mid-Cenozoic trigger for the Andes. *Tectonics* 20 (3), 308–324. <https://doi.org/10.1029/1999TC001181>
- Kay S.M., Godoy E. & Kurtz A. 2005. Episodic arc migration, crustal thickening, subduction erosion, and magmatism in the south-central Andes. *Bulletin of the Geological Society of America* 117 (1-2), 67–88. <https://doi.org/10.1130/B25431.1>
- Martinod J., Husson L., Roperch P., Guillaume B. & Espurt N. 2010. Horizontal subduction zones, convergence velocity and the building of the Andes. *Earth and Planetary Science Letters* 299 (3-4), 299-309. <https://doi.org/10.1016/j.epsl.2010.09.010>
- Montecinos A. & Aceituno P. 2003. Seasonality of the ENSO-related rainfall variability in central Chile and associated circulation anomalies. *Journal of Climate* 16, 281–296. [https://doi.org/10.1175/1520-0442\(2003\)016<0281:SOTERR>2.0.CO;2](https://doi.org/10.1175/1520-0442(2003)016<0281:SOTERR>2.0.CO;2)
- Mpodozis C. & Ramos V. 1989. The Andes of Chile and Argentina. In: Erickson G.E., Cañas-Pinochet M.T. & Reinemund J. (Eds.), *Geology of the Andes and its relation to hydrocarbon and mineral resources*. Circum-Pacific Council for Energy and Mineral Resources, 59–90.
- Muñoz M., Fuentes F., Vergara M., Aguirre L., Nyström J., Féraud G. & Demant A. 2006. Abanico East Formation: petrology and geochemistry of volcanic rocks behind the Cenozoic arc front in the Andean Cordillera, central Chile (33°50'S), *Revista Geológica de Chile* 33 (1), 109-140. <http://dx.doi.org/10.5027/andgeoV33n1-a05>
- NOAA/National Weather Service. 2019. El Niño Southern Oscillation (ENSO): Historical El Niño/La Niña episodes (1950-present). https://origin.cpc.ncep.noaa.gov/products/analysis_monitoring/ensostuff/ONI_v5.php
- Novoa V., Ahumada-Rudolph R., Rojas O., Sáez K., de la Barrera F. & Arumí J.L. 2019. Understanding agricultural water footprint variability to improve water management in Chile. *Science of The Total Environment* 670, 188-199. <https://doi.org/10.1016/j.scitotenv.2019.03.127>
- Nyström J., Vergara M., Morata D. & Levi B. 2003. Tertiary volcanism during extension in the Andean foothills of

central Chile ($33^{\circ}15'$ – $33^{\circ}45'$ S). Geological Society of America Bulletin 115 (12), 1523-15237.
<https://doi.org/10.1130/B25099.1>

Ohlanders N., Rodriguez M. & McPhee J. 2013. Stable water isotope variation in a Central Andean watershed dominated by glacier and snowmelt. Hydrology and Earth System Sciences 17, 1035–1050.
<https://doi.org/10.5194/hess-17-1035-2013>

Padilla H. & Vergara M. 1985. Control estructural y alteración tipo campo geotérmico en los intrusivos subvolcánicos miocénicos del área Cuesta de Chacabuco-Baños El Corazón, Chile Central. Revista Geológica de Chile 24, 3-17.

Parada M.A., Rivano S., Sepulveda P., Herve M., Herve F., Puig A., Munizaga F., Brook M., Pankhurst R. & Snelling N. 1988. Mesozoic and cenozoic plutonic development in the Andes of central Chile ($30^{\circ}30'$ – $32^{\circ}30'$ S). Journal of South American Earth Sciences 1 (3), 249–260. [https://doi.org/10.1016/0895-9811\(88\)90003-X](https://doi.org/10.1016/0895-9811(88)90003-X)

Piquer J., Berry R.F., Scott R.J. & Cooke D.R. 2016. Arc-oblique fault systems: their role in the Cenozoic structural evolution and metallogenesis of the Andes of central Chile. Journal of Structural Geology 89, 101-117.
<https://doi.org/10.1016/j.jsg.2016.05.008>

Piquer J., Hollings P., Rivera O., Cooke D.R., Baker M. & Testa F. 2017. Along-strike segmentation of the Abanico Basin, central Chile: New chronological, geochemical and structural constraints. Lithos 268–271, 174–197.
<https://doi.org/10.1016/j.lithos.2016.10.025>

Rauld R. 2011. Deformación cortical y peligro sísmico asociado a la falla San Ramón en el frente cordillerano de Santiago, Chile Central (33° S) (PhD Thesis). Universidad de Chile, Santiago, Chile.

Riesner M., Lacassin R., Simoes M., Armijo R., Rauld R. & Vargas G. 2017. Kinematics of the active West Andean fold-and-thrust belt (central Chile): Structure and long-term shortening rate. Tectonics 36 (2), 287-303.
<https://doi.org/10.1002/2016TC004269>

Riesner M., Lacassin R., Simoes M., Carrizo D. & Armijo R. 2018. Revisiting the Crustal Structure and Kinematics of the Central Andes at 33.5° S: Implications for the Mechanics of Andean Mountain Building. Tectonics 37 (5), 1347-1375. <https://doi.org/10.1002/2017TC004513>

Riesner M., Simoes M., Carrizo D. & Lacassin R. 2019. Early exhumation of the Frontal Cordillera (Southern Central Andes) and implications for Andean mountain-building at $\sim 33.5^{\circ}$ S. Scientific Reports 9, 7972.
<https://doi.org/10.1038/s41598-019-44320-1>

Rivano S., Godoy E., Vergara M. & Villarroel R. 1990. Redefinición de la formación farellones en la Cordillera de los Andes de Chile central (32 - 34° S). Revista Geológica de Chile 17 (2), 205–214.

Rivano S., Sepúlveda P., Boric R. & Espíneira D. 1993. Hojas Quillota y Portillo, Escala 1:250.000. Servicio Nacional de Geología y Minería (SERNAGEOMIN), Santiago, Chile.

Rodriguez M., Ohlanders N., Pellicciotti F., Williams M.K. & McPhee J. 2016. Estimating runoff from a glacierized

- catchment using natural tracers in the semi-arid Andes cordillera. *Hydrological Processes* 30 (20), 3609-3626. <https://doi.org/10.1002/hyp.10973>
- Schaffer N., MacDonell S., Réveillet S., Réveillet M., Yáñez E. & Valois R. 2019. Rock glaciers as a water resource in a changing climate in the semiarid Chilean Andes. *Regional Environmental Change* 19 (5), 1263-1279. <https://doi.org/10.1007/s10113-018-01459-3>
- Schellart W.P. 2017. Andean mountain building and magmatic arc migration driven by subduction- induced whole mantle flow. *Nature Communications* 8, 2010. <https://doi.org/10.1038/s41467-017-01847-z>
- Tassara A., Götze H.J., Schmidt S. & Hackney R. 2006. Three-dimensional density model of the Nazca plate and the Andean continental margin. *Journal of Geophysical Research* 111 (B9), B09404. <https://doi.org/10.1029/2005JB003976>
- Thomas H. 1958. Geología de la cordillera de la costa entre el Valle de La Ligua y la Cuesta de Barriga. Servicio Nacional de Geología y Minería (SERNAGEOMIN), Santiago, Chile.
- Vargas G., Klinger Y., Rockwell T.K., Forman S.L., Rebollo S., Baize S., Lacassin R. & Armijo R. 2014. Probing large intraplate earthquakes at the west flank of the Andes. *Geology* 42 (12), 1083-1086. <https://doi.org/10.1130/G35741.1>
- Veloso E., Tardani D., Elizalde D., Godoy B., Sánchez-Alfaro P., Aron F., Reich M. & Morata D. 2019. A review of the geodynamic constraints on the development and evolution of geothermal systems in the Central Andean Volcanic Zone (18–28°Lat.S). *International Geology Review*, 1-25. [10.1080/00206814.2019.1644678](https://doi.org/10.1080/00206814.2019.1644678)
- Vergara M., Charrier R., Munizaga F., Rivano S., Sepulveda P., Thiele R. & Drake R. 1988. Miocene volcanism in the central Chilean Andes (31°30'S–34°35'S). *Journal of South American Earth Sciences* 1 (2), 199-209. [https://doi.org/10.1016/0895-9811\(88\)90038-7](https://doi.org/10.1016/0895-9811(88)90038-7)
- Viale M. & Garreaud R.D. 2014. Summer Precipitation Events over the Western Slope of the Subtropical Andes. *Monthly Weather Review* 142, 1074-1092. <https://doi.org/10.1175/MWR-D-13-00259.1>
- Wall R., Sellés D. & Gana P. 1999. Área Tilit-Santiago, región Metropolitana, Escala 1:100.000. Servicio Nacional de Geología y Minería (SERNAGEOMIN), Santiago, Chile.
- Waylen P.R. & Caviedes C.N. 1990. Annual and seasonal fluctuations of precipitation and streamflow in the Aconcagua River basin, Chile. *Journal of Hydrology* 120 (1-4), 79-102. [https://doi.org/10.1016/0022-1694\(90\)90143-L](https://doi.org/10.1016/0022-1694(90)90143-L)
- Yáñez G., Ranero C., von Huene R. & Díaz J. 2001. Magnetic anomaly interpretation across the southern central Andes (32°-34°S): The role of the Juan Fernandez Ridge in the late Tertiary evolution of the margin. *Journal of Geophysical Research* 106 (B4), 6325-6345. <https://doi.org/10.1029/2000JB900337>
- Yáñez G., Cembrano J., Pardo M., Ranero C. & Selles D. 2002. The Challenger–Juan Fernández–Maipo major tectonic transition of the Nazca–Andean subduction system at 33–34°S: geodynamic evidence and implications. *Journal of South American Earth Sciences* 15 (1), 23-38. <https://doi.org/10.1016/S0895->

9811(02)00004-4

- Yáñez G. & Cembrano J. 2004. Role of viscous plate coupling in the late Tertiary Andean tectonics. *Journal of Geophysical Research: Solid Earth* 109 (B2), B02407. <https://doi.org/10.1029/2003jb002494>
- Yáñez G., Muñoz M., Flores-Aqueveque V. & Bosch A. 2015. Gravity depth to basement in Santiago Basin, Chile: implications for its geological evolution, hydrogeology, low enthalpy geothermal, soil characterization and geo-hazards. *Andean Geology* 42 (2), 147–172. <https://doi.org/10.5027/andgeoV42n2-a01>
- Yáñez G. & Rivera O. 2019. Crustal dense blocks in the fore-arc and arc region of Chilean ranges and their role in the magma ascent and composition: Breaking paradigms in the Andean metallogeny. *Journal of South American Earth Sciences* 93, 51-66. <https://doi.org/10.1016/j.jsames.2019.04.006>

This page intentionally left blank

PART II:

**BUILDING THE CONCEPTUAL MODEL
OF THE WESTERN ANDEAN FRONT**

This page intentionally left blank

3

Methodology

3.1. HYDROGEOCHEMICAL AND ISOTOPIC METHODS

3.1.1. Sampling and analysis

Between February 2017 and September 2018, a total of 33 groundwater points was sampled for geochemical and isotopic analyses: 23 springs and 10 boreholes (Fig. 3.1). Additionally, 5 rain collectors were installed between 830 and 2715 m asl. A paraffin oil layer was inserted into each collector to avoid any evaporation and isotope fractioning process (IAEA/GNIP, 2014). Electrical conductivity, temperature and pH were measured *in situ*. Water samples were filtered using 0.45 µm Millipore filters. Unacidified samples were collected for anion analysis, and acidified samples (Suprapur® Nitric acid) for cations and trace elements analysis. Unfiltered samples were collected for stable isotope analysis. All samples were stored in pre-cleaned polyethylene bottles at 4 °C.

Major, minor and trace elements were analysed at *Centro de Excelencia en Geotermia de los Andes* (CEGA) of the *Departamento de Geología (Universidad de Chile)*. Cl, SO₄ and NO₃ contents were determined by Ion Chromatography (IC, 861 Compact IC Metrohm) with a detection limit of 0.030, 0.070 and 0.100 ppm, respectively. SiO₂, Na, K, Ca and Mg were measured by Atomic Absorption Spectrophotometry (F-AAS, Perkin-Elmer PinAAcle 900F) with detection limits of 0.1, 0.094, 0.044, 0.014 and 0.010 ppm, respectively. Li, B, As, Sr and Ba contents were determined by Inductively Coupled Plasma Mass Spectrometry (ICP-MS, Thermo iCAP Q) with detection limits of 0.020, 0.070, 0.020, 0.001 and 0.010 ppb, respectively. Alkalinity (as HCO₃) was determined by titration at the sampling time to prevent precipitation of carbonates, by using HCl (0.1 N) as limiting reagent. δ¹⁸O and δD (water stable isotopes) were analyzed by Finnigan Delta Plus XL mass spectrometer at *Estación Experimental de Zaidín* (CSIC, Spain) with an analytical uncertainty of ±0.1 ‰ and ±1.1 ‰ VSMOW, respectively.

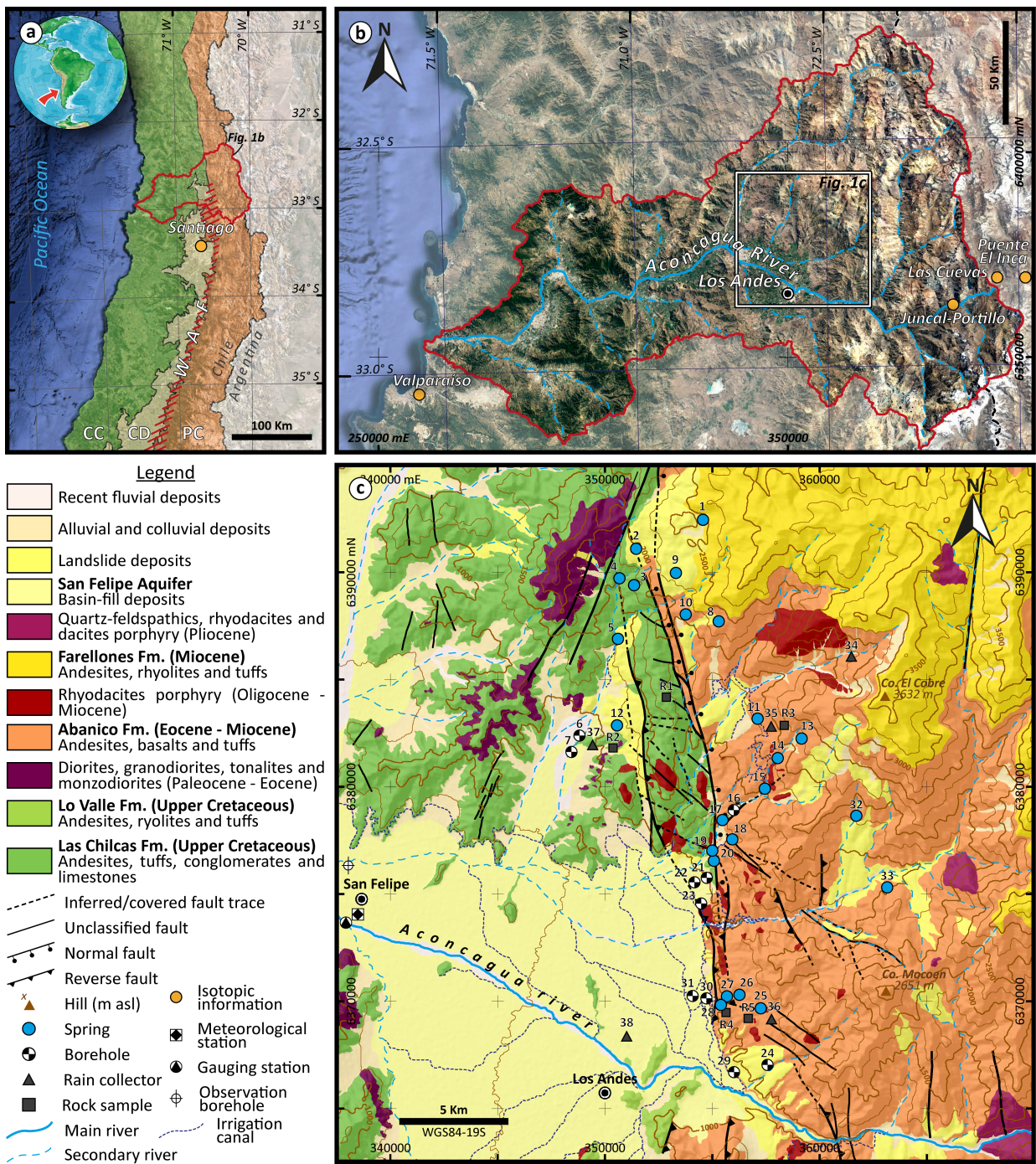


Fig. 3.1: Location of the sampling points and isotopic information. a) Central Chile and the Andean morphotectonic domains: in green the Coastal Cordillera (CC), in pale-yellow the Central Depression (CD) and in orange the Principal Cordillera (PC). The Western Andean Front (WAF) is remarked in the red hatched area and the Aconcagua Basin are shown by the delineated area. b) The Aconcagua Basin. c) Geological map of the study area (from Taucare *et al.* 2020).

3.1.2. Ionic extraction by leaching test

One way to get information about the source of dissolved solids in groundwater is comparing them with the composition of rocks where groundwater circulation occurs (Kaasalainen and Stefánsson, 2012). Five fresh rock samples were collected from representative outcrops of Las Chilcas and Abanico Formation in the Western Andean Front. All rocks were pulverized using a tungsten mortar and sieved to obtain a fine particle size (<39 µm). Cl, SO₄ and NO₃ were extracted using 2 g of rock sample in 100 ml of Milli-Q Water by ultrasound-assisted leaching with a 50 Hz frequency (*e.g.* Güngör and Elik, 2007). At end of leaching, the separation of the final solution from the solid residue was accomplished by centrifugation at 3000 rpm during 10 min. Samples obtained were collected and filtered through a 0.45 µm Millipore filters and analysed. Na, K, Ca, Mg, Li, B, As, Sr and Ba were extracted by acid digestion bomb method (Matusiewicz, 2003; Wang *et al.* 2019) using 0.1 g of sample that was dissolved in a mixture of 1.2 ml of HNO₃ and 1.0 ml of HF at 135 °C during 24 hours on a hot plate. After cooling at 25 °C, 2 ml of the solution were dissolved with a mixture of 1 ml HCl and 3 ml HNO₃ and heated again at 135 °C for 24 hours. In both cases, the resulting solutions have been analysed at the CEGA laboratories. Note that HCO₃ concentrations have not been obtained from the leaching test because the anion extraction was carried out using Mili-Q Water in laboratory without the presence of CO₂.

3.1.3. Multivariate Statistical Analysis

The data handling was performed using a Multivariate Statistical Analysis to classify the water samples by hydrogeochemical similarities and to study the correlations between the geochemical variables. In this study, two multivariate methods were applied using the IBM SPSS Statistics Software V26: the hierarchical cluster analysis (HCA) and the factorial analysis (FA). Both methods are useful for hydrogeological studies (Moya *et al.* 2015; Moeck *et al.* 2016; Negri *et al.* 2018). The preprocessing stage consists to discard (Cloutier *et al.* 2008): i) additive characteristics (such as electrical conductivity that is directly related to ion contents), ii) variables with an elevated number of samples below the detection limit, iii) variables that were not analyzed in all samples (*e.g.* δ¹⁸O and δD), and iv) the variables with insignificant regional variations (*e.g.* temperature, pH and K). Concentration values that are lower than the detection limits were replaced by half of the detection limit value. Then, to minimize or eliminate the presence of outliers and the high biased, typical for compositional data (Filzmoser *et al.* 2009), log-transformation was applied on raw data prior to multivariate analysis. Finally, all statistical analyses were performed using the Cl, SO₄, HCO₃, NO₃, Na, Ca, Mg, SiO₂, Li, B, As, Sr and Ba as geochemical variables.

HCA was performed to determine the relationships between the samples using the Euclidian distance as linkage rule (Moeck *et al.* 2016). The use of HCA allows highlighting the most distinctive geochemical clusters (Güler *et al.* 2002). The similarity between clusters is expressed by the Euclidean linkage distance in a dendrogram. FA allows identifying the relationships between the geochemical variables by a small number of uncorrelated factors (Giménez-Forcada *et al.* 2017; Negri *et al.* 2018). The KMO test was used to determine the factors that explain the variance of the geochemical variables (Kayser, 1960). To an accurate analysis, these factors must have eigenvalues higher than one. The factors were rotated using varimax method to maximize the variance of the squared loading for each factor. Finally, the variable weights in each factor is relevant if it is greater than 0.50.

3.1.4. Local meteoric water line construction

The analyzed stable water isotopes were compared to those contained in precipitation to characterize the hydrological processes in the study area and identify the areas contributing to the groundwater recharge. Sánchez-Murillo *et al.* (2018) have recently proposed a Chilean meteoric water line ($\delta D = 7.47\delta^{18}O + 3.42$) considering hydrological stations along Chile as a whole. But this latter is not completely representative for the study area. Indeed, due to the origin and temporal variations of the moisture fluxes, the meteoric $\delta^{18}O$ and δD are mainly enriched to the North and depleted to the South (Aravena *et al.*, 1999; Garreaud, 2009; Garreaud *et al.*, 2013). Moreover, in Central Chile, the orographic-continental effect is the dominant factor that controls the meteoric $\delta^{18}O$ and δD variations across EW-transect (Jorquera *et al.* 2015).

Hence, for an accurate characterization of the hydrological processes in the study area, it was necessary to define a reliable local meteoric water line at 33°S in Chile, hereafter “33°S Chile MWL”. The available data of $\delta^{18}O$ and δD annual weight means in precipitation were employed (Hoke *et al.* 2013; IAEA/WMO, 2019) from the Coastal Cordillera, the Central Depression and the Principal Cordillera (Fig. 3.1a, b and Table 3.1). Available $\delta^{18}O$ and δD averages in snowpack, collected between 2200-2600 and 2600-3000 m asl in the Principal Cordillera by Ohlanders *et al.* (2013) were also used to attempt characterizing the role of snow in the recharge of groundwater. Analyzed $\delta^{18}O$ and δD in collected rainwater (no. 35, 36, 37) during this study were also compared to those from regional literature.

Precipitation							
Station	Reference	Spanning Period	Number of w-mean	Lat. (°South)	Long. (°West)	Altitude (m asl)	Morphostructural domain
Valparaiso	IAEA/WMO (2019)	1988-1991	4	33.06	71.60	74	Coastal Cordillera
		1972-1975					
Santiago	IAEA/WMO (2019)	1989-1999	20	33.45	70.70	520	Central Depression
		2011-2015					
Puente el Inca	Hoke <i>et al.</i> (2013)	2008-2009	2	32.82	69.92	2750	Principal Cordillera
Las Cuevas	Hoke <i>et al.</i> (2013)	2008-2009	2	32.81	70.05	3200	Principal Cordillera
Snow							
Station	Reference	Spanning Period	Number of averages	Lat. (°South)	Long. (°West)	Altitude (m asl)	Morphostructural domain
Juncal-Portillo	Ohlanders <i>et al.</i> (2013)	August 2011	1	32.86	70.14	2200-2600 2600-3000	Principal Cordillera
			1				

Table 3.1: Dataset of annual weight-mean in precipitation and average in snowpack.

3.2. STRUCTURAL AND FRACTURE NETWORK ANALYSES

3.2.1. Multi-scale structural mapping

The field work was conducted describing the major tectonic and geomorphological features through multi-scale mapping, from regional scale (1:50,000) to local scale (1:250). Then, in order to describe the fracture patterns, a detailed outcrop-scale mapping (1:10) was performed in four representative areas into PFZ (referred hereafter as structural sites; Fig. 3.2): *Potrerillos*, *Termas El Corazón*, *Bypass* and *Estero Pocuro*. The structural sites were selected based on their well-preserved outcrops in both cross section and in plan-view. For the fracture description the following parameters have been considered: geometry, failure mode, filling mineral, fracture arrangements, kinematic and cross-cutting relationships. The field work was complemented with X-Ray Diffraction for mineral recognition of the veins infill, the matrix of hydrothermal breccias and the slickensides at the *Laboratorio de Cristalografía* of the *Universidad de Chile*.

The term fracture is used to refer any planar/tabular mechanical break or discontinuity that separates a rock body into two or more parts, disrupting the original physical properties of a rock regardless of the failure mode (Gudmundsson, 2011; Peacock *et al.* 2016). In addition, as Veloso *et al.* (2017) pointed out, a fracture may contain an infill material such as hydrothermal crystallized, magmatic, cataclastic, brecciated (sheared and broken) or comminuted deformed materials.

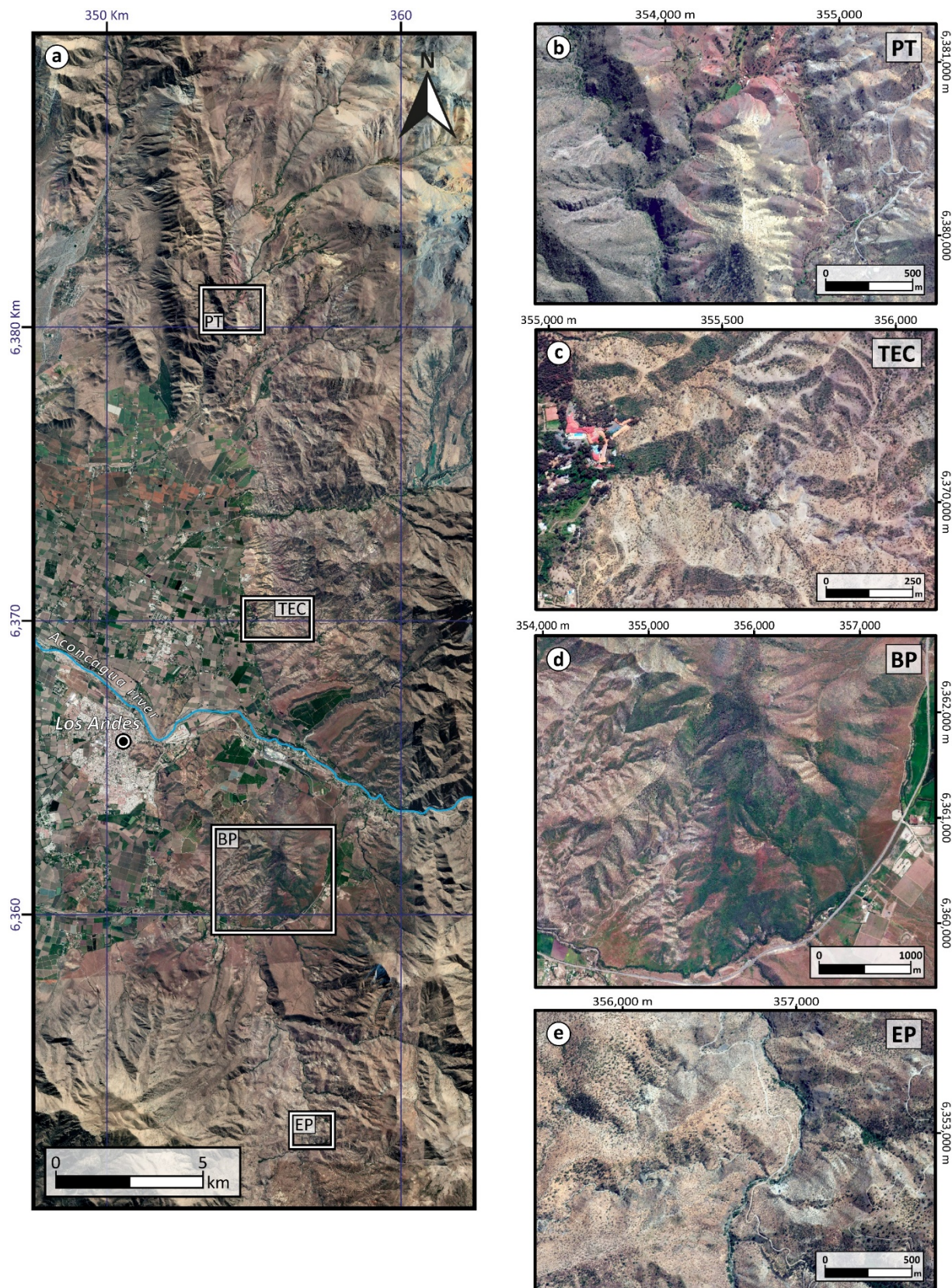


Fig. 3.2: a) Map of the study area showing each structural site: b) *Potrerillos* (PT), c) *Termas El Corazón* (TEC), d) *Bypass* (BP), and e) *Estero Pocuro* (EP).

3.2.2. Topological approach

The topological approach uses components, such as “nodes” and “branches” (Jing and Stephansson, 1997; Sanderson and Nixon, 2015, 2018): A “node” is a point where a line ends or intersects another line (Fig. 3.3). A “node” can be classified as isolated (I-node), abutting (Y-node), or as crossing nodes (X-node). A “branch” is a line bounded by an isolated node (I-) or a connecting node (Y- or X-) (Fig. 3.3), and it can be classified as an isolated (I-I), partially connected (C-I), fully connected (C-C) branch, but also as an unknown branch (Unk) when this latter intersects the limits of the study area.

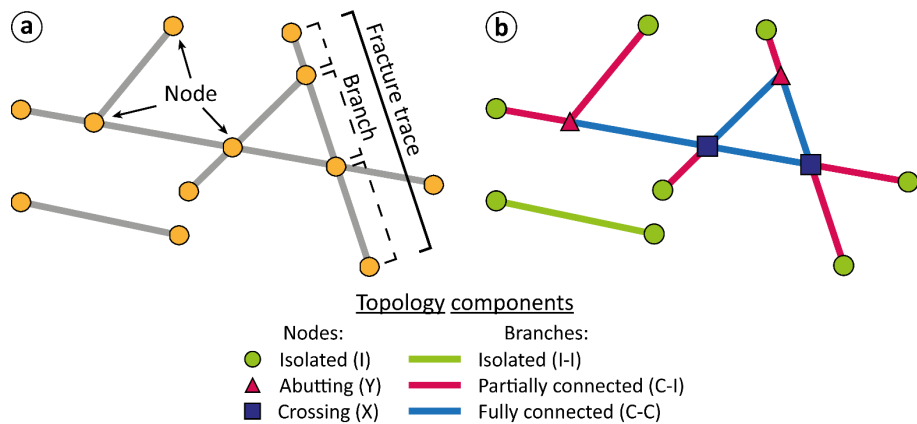


Fig. 3.3: Topological nomenclature for fracture network characterization (Sanderson and Nixon, 2015). a) Fracture network map, and b) its topological characterization.

At the scale of the study area ($\sim 650 \text{ km}^2$; Fig. 3.4), the topological approach was conducted by the digitalization of morphostructural lineaments from high-resolution photomosaic extracted from a Google Earth (pixel size $\approx 2.5 \text{ m}$) and supported by the structural field mapping. The spatial distribution of the fracture network topological parameters was processed by a geographic information system (GIS), using the NetworkGT tool developed by Nyberg *et al.* (2018). Because groundwater circulates in connected fractures (Makel, 2007), only connected branches (C-I and C-C) and connecting nodes (Y- and X-) were further considered. Using a Kernel density tool (e.g. Dimmen *et al.* 2017), the spatial distribution is shown for the following parameters in the PFZ are shown: i) the density of fractures, which involves the total branch length per surface unit (km/km^2), and ii) the density of connected nodes, which illustrates the number of connected nodes ($N_c = Y\text{-node} + X\text{-node}$) per surface unit (N_c/km^2). In addition, fracture analyses were carried out at the outcrop scale in two areas within the PFZ (Fig. 3.2b, c), at *Termas El Corazón* (TEC) in the Abanico Fm and at 5 km to the east of *Termas de Jahuel* (Jh; Potrerillos structural site) in the Las Chilcas Fm. Both areas ($\sim 200 \text{ m}^2$) have well-preserved outcrops and contain galleries (7-30 m long) that enable a three-dimensional view (cross section and plan-view) of the fracture network.

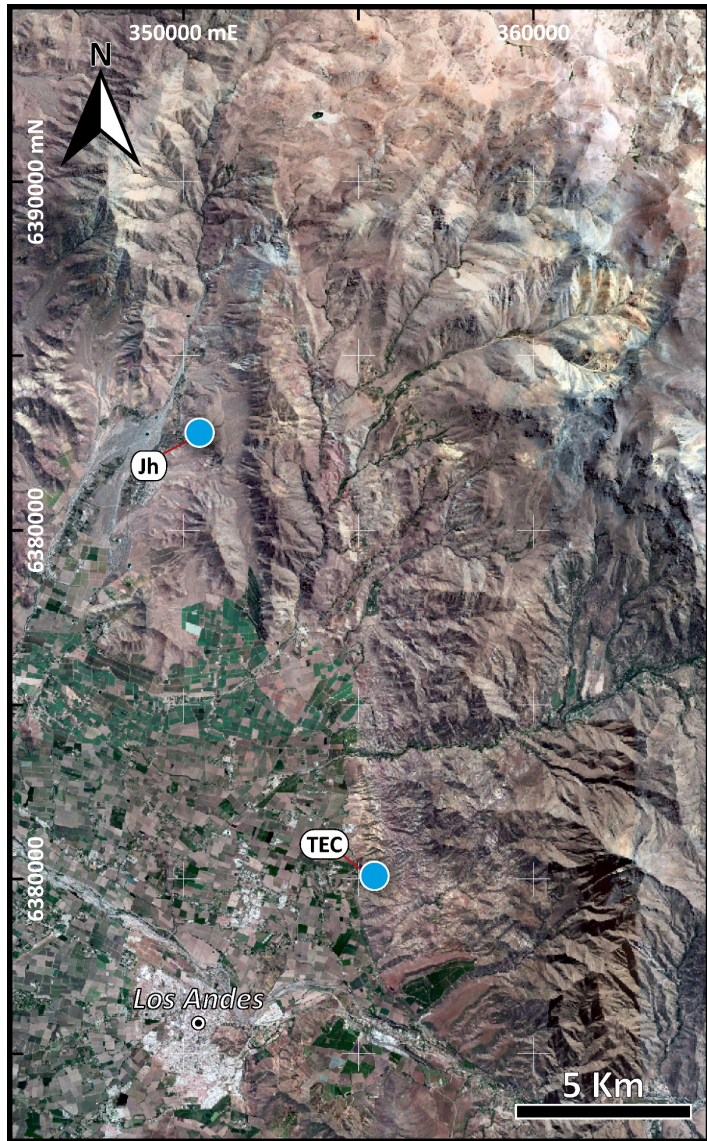


Fig. 3.4: High-resolution photomosaic utilized for the topological approach. The major springs of the study area are highlighted: *Termas de Jahuel* (Jh) and *Termas El Corazón* (TEC).

REFERENCES

- Aravena R., Suzuki O., Peña H., Pollastri A., Fuenzalida H. & Grilli A. 1999. Isotopic composition and origin of the precipitation in Northern Chile. *Applied Geochemistry* 14 (4), 411-422. [https://doi.org/10.1016/S0883-2927\(98\)00067-5](https://doi.org/10.1016/S0883-2927(98)00067-5)
- Cloutier V., Lefebvre R., Therrien R. & Savard M.M. 2008. Multivariate statistical analysis of geochemical data as indicative of the hydrogeochemical evolution of groundwater in a sedimentary rock aquifer system. *Journal of Hydrology* 353 (3-4), 294–313. <https://doi.org/10.1016/j.jhydrol.2008.02.015>
- Dimmen V., Rotevatn A., Peacock D.C.P., Nixon C.W. & Nærland K. 2017. Quantifying structural controls on fluid flow: Insights from carbonate-hosted fault damage zones on the Maltese Islands. *Journal of Structural Geology* 101, 43-57. <https://doi.org/10.1016/j.jsg.2017.05.012>
- Filzmoser P., Hron K. & Reimann C. 2009. Univariate statistical analysis of environmental (compositional) data: Problems and possibilities. *Science of The Total Environment* 407 (23), 6100–6108. <https://doi.org/10.1016/J.SCITOTENV.2009.08.008>
- Garreaud R.D. 2009. The Andes climate and weather. *Advances in Geosciences* 22, 3–11. <https://doi.org/10.5194/adgeo-22-3-2009>
- Garreaud R.D., Lopez P., Minvielle M. & Rojas M. 2013. Large-Scale Control on the Patagonian Climate. *Journal of Climate* 26, 215-230. <https://doi.org/10.1175/JCLI-D-12-00001.1>
- Giménez-Forcada E., Vega-Alegre M. & Timón-Sánchez S. 2017. Characterization of regional cold-hydrothermal inflows enriched in arsenic and associated trace-elements in the southern part of the Duero Basin (Spain), by multivariate statistical analysis. *Science of The Total Environment* 593-594, 211-226. <https://doi.org/10.1016/j.scitotenv.2017.03.071>
- Gudmundsson A. 2011. Rock fractures in geological processes. Cambridge University Press, 592. <https://doi.org/10.1017/CBO9780511975684>
- Güler C., Thyne G.D., McCray J.E. & Turner A.K. 2002. Evaluation of graphical and multivariate statistical methods for classification of water chemistry data. *Hydrogeology Journal* 10 (4), 455–474. <https://doi.org/10.1007/s10040-002-0196-6>
- Güngör H. & Elik A. 2007. Comparison of ultrasound-assisted leaching with conventional and acid bomb digestion for determination of metals in sediment samples. *Microchemical Journal* 86 (1), 65–70. <https://doi.org/10.1016/J.MICROC.2006.10.006>
- Hoke G.D., Aranibar J.N., Viale M., Araneo D.C. & Llano C. 2013. Seasonal moisture sources and the isotopic composition of precipitation, rivers, and carbonates across the Andes at 32.5-35.5°S. *Geochemistry, Geophysics, Geosystems* 14 (4), 962–978. <https://doi.org/10.1002/ggge.20045>
- IAEA/GNIP. 2014. Precipitation sampling guide.

IAEA/WMO. 2019. Global Network of Isotopes in Precipitation. The GNIP Database. <http://nucleus.iaea.org/wiser>

Jing L. & Stephansson O. 1997. Network Topology and Homogenization of Fractured Rocks. In: Jamtveit B. & Yardley B.W.D. (Eds), Fluid Flow and Transport in Rocks. Springer, 191-202. https://doi.org/10.1007/978-94-009-1533-6_11

Jorquera C.O., Oates C.J., Plant J.A., Kyser K., Ihlenfeld C. & Voulvoulis N. 2015. Regional hydrogeochemical mapping in Central Chile: natural and anthropogenic sources of elements and compounds. Geochemistry: Exploration, Environment, Analysis 15 (1), 72–96. <https://doi.org/10.1144/geochem2013-220>

Kaasalainen H. & Stefánsson A. 2012. The chemistry of trace elements in surface geothermal waters and steam, Iceland. Chemical Geology 330–331, 60–85. <https://doi.org/10.1016/j.chemgeo.2012.08.019>

Kayser H.F. 1960. The application of electronic computers to factor analysis. Educational and Physchological Measurement 20 (1), 141-151. <https://doi.org/10.1177/001316446002000116>

Makel G.H. 2007. The modelling of fractured reservoirs: constraints and potential for fracture network geometry and hydraulics analysis. Geological Society of London 292, 375-403. <https://doi.org/10.1144/SP292.21>

Matusiewicz H. 2003. Wet digestion methods. In: Mester Z.M. & Sturgeon R. (Eds.), Sample Preparation for Trace Element Analysis. Elsevier 41, 193–233. [https://doi.org/10.1016/S0166-526X\(03\)41006-4](https://doi.org/10.1016/S0166-526X(03)41006-4)

Moeck C., Radny D., Borer P., Rothardt J., Auckenthaler A., Berg M. & Schirmer M. 2016. Multicomponent statistical analysis to identify flow and transport processes in a highly-complex environment. Journal of Hydrology 542, 437–449. <https://doi.org/10.1016/j.jhydrol.2016.09.023>

Moya C.E., Raiber M., Taulis M. & Cox M.E. 2015. Hydrochemical evolution and groundwater flow processes in the Galilee and Eromanga basins, Great Artesian Basin, Australia: A multivariate statistical approach. Science of The Total Environment 508, 411–426. <https://doi.org/10.1016/J.SCITOTENV.2014.11.099>

Negri A., Daniele L., Aravena D., Muñoz M., Delgado A. & Morata D. 2018. Decoding fjord water contribution and geochemical processes in the Aysen thermal springs (Southern Patagonia, Chile). Journal of Geochemical Exploration 185, 1–13. <https://doi.org/10.1016/J.GEXPLO.2017.10.026>

Nyberg B., Nixon C.W. & Sanderson D.J. 2018. NetworkGT: A GIS tool for geometric and topological analysis of two-dimensional fracture networks. Geosphere 14 (4), 1618-1634. <https://doi.org/10.1130/GES01595.1>

Ohlanders N., Rodriguez M. & McPhee J. 2013. Stable water isotope variation in a Central Andean watershed dominated by glacier and snowmelt. Hydrology and Earth System Sciences 17, 1035–1050. <https://doi.org/10.5194/hess-17-1035-2013>

Peacock D.C.P., Nixon C.W., Rotevatn A., Sanderson D.J. & Zuluaga L.F. 2016. Glossary of fault and other fracture networks. Journal of Structural Geology 92, 12-92. <https://doi.org/10.1016/j.jsg.2016.09.008>

Sánchez-Murillo R., Aguirre-Dueñas E., Gallardo-Amestica M., Moya-Vega P., Birkel C., Esquivel-Hernández G. & Boll J. 2018. Isotopic characterization of waters across chile. In: Rivera D.A., Godoy-Faundez A. & Lillo-

- Saavedra M. (Eds.), Andean Hydrology. CRC Press, 205–230. <https://doi.org/10.1201/9781315155982-9>
- Sanderson D.J. & Nixon C.W. 2015. The use of topology in fracture network characterization. *Journal of Structural Geology* 72, 56-66. <https://doi.org/10.1016/j.jsg.2015.01.005>
- Sanderson D.J. & Nixon C.W. 2018. Topology, connectivity and percolation in fracture networks. *Journal of Structural Geology* 115, 167-177. <https://doi.org/10.1016/j.jsg.2018.07.011>
- Taucare M., Daniele L., Viguier B., Vallejos A & Arancibia G. 2020. Groundwater resources and recharge processes in the Western Andean Front of Central Chile. *Science of The Total Environment* 722, 137824. <https://doi.org/10.1016/j.scitotenv.2020.137824>
- Veloso E., Cembrano J., Arancibia G., Heuser G., Neira S., Siña A., Garrido I., Vermeesch P. & Selby D. 2017. Tectono-metallogenetic evolution of the Fe–Cu deposit of Dominga, northern Chile. *Mineralium Deposita* 52, 595-620. <https://doi.org/10.1007/s00126-016-0682-8>
- Wang P., Sun Z., Hu Y. & Cheng H. 2019. Leaching of heavy metals from abandoned mine tailings brought by precipitation and the associated environmental impact. *Science of The Total Environment* 695, 133893. <https://doi.org/10.1016/j.scitotenv.2019.133893>

This page intentionally left blank

4

Groundwater circulation and recharge processes in the Western Andean Front

Abstract

In Central Chile, the increment of withdrawals together with drought conditions has exposed the poor understanding of the regional hydrogeological system. In this study, the Western Andean Front hydrogeology is addressed by hydrogeochemical and water stable isotope analyses of 23 springs, 10 boreholes, 5 rain-collectors and 5 leaching-rocks samples at Aconcagua Basin. From the upstream to the downstream parts of the Western Andean Front, most groundwater is $\text{HCO}_3\text{-Ca}$ and results from the dissolution of anorthite, labradorite and other silicate minerals. The Hierarchical Cluster Analysis groups the samples according to its position along the Western Andean Front and supports a clear correlation between the increasing groundwater mineralization (31-1188 $\mu\text{S}/\text{cm}$) and residence time. Through Factorial Analysis, was found that Cl, NO_3 , Sr and Ba concentrations are related to agriculture practices in the Central Depression. After defining the regional meteoric water line at 33°S in Chile, water isotopes demonstrate the role of rain and snowmelt above ~2000 m asl in the recharge of groundwater. Finally, an original conceptual model applicable to the entire Central Chile is propose. During dry periods, water releases from high-elevation areas infiltrate in mid-mountain gullies feeding groundwater circulation in the fractured rocks of Western Andean Front. To the downstream, mountain-block and -front processes recharge the alluvial aquifers. Irrigation canals, conducting water from Principal Cordillera, play a significant role in the recharge of Central Depression aquifers. While groundwater in the Western Andean Front has a high-quality according to different water uses, intensive agriculture practices in the Central Depression cause an increment of hazardous elements for human-health in groundwater.

Keywords Groundwater • Fractured aquifer • Mountain front zone • Hydrogeochemistry • Water stable isotopes • Aconcagua Basin

4.1. HYDROGEOCHEMICAL PATTERNS IN THE WESTERN ANDEAN FRONT

In the study area (Fig. 4.1a), the groundwater electrical conductivity (EC) ranges from 31 to 1188 $\mu\text{S}/\text{cm}$ and increases as elevation decreases (Table 4.1 and Fig. 4.1b). High-elevation springs (>2000 m asl) have EC values between 31 and 168 $\mu\text{S}/\text{cm}$ (Fig. 4.1b). Springs and boreholes at lower elevation into the Western Andean Front (<2000 m asl) have EC values between 143 and 647 $\mu\text{S}/\text{cm}$ (Fig. 4.1b). Finally, in the alluvial San Felipe aquifer, the boreholes display EC values between 519 and 1188 $\mu\text{S}/\text{cm}$ (Fig. 4.1b). Groundwater temperature in spring mainly agrees with the local mean annual air temperature (15 °C; Fig. 4.1c). But daily fluctuations can be observed in the outflowing water, especially in high-elevation areas. This is visible in the spring no. 1 (located at 2465 m asl), where the measured temperature is 27 °C during the afternoon, while during the morning may reach 5 °C. Some springs in the PFZ (*e.g.* no. 12, 19, 28) have a permanent low-thermal component (21 to 24 °C) with respect to the local mean annual air temperature (Fig. 4.1c), which highlights the presence of deeper groundwater circulation in the Western Andean Front. Boreholes groundwater temperature ranges from 18.6° (no. 30) to 23.2 °C (no. 7, 22) (Fig. 4.1c). The pH values, ranging between 6.9 (no. 29) and 8.5 (no. 15), do not show a significant spatial variation.

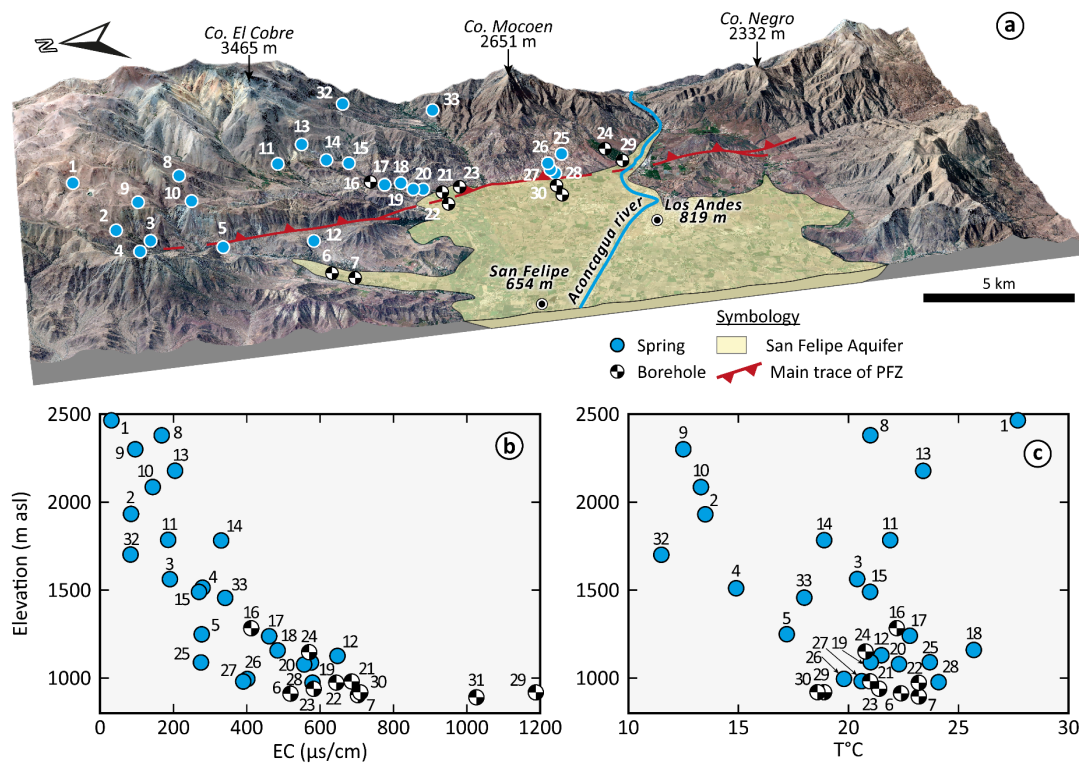


Fig. 4.1: a) Location of groundwater samples at the study area. b) Electrical conductivity and c) temperature *vs.* elevation (m asl) of groundwater samples.

The hydrogeochemical facies of groundwater along the Western Andean Front is mainly $\text{HCO}_3\text{-Ca}$ (Fig. 4.2). That facies results from the dissolution of Ca-silicate minerals containing into the volcano-sedimentary rocks of the study area (see Sect. 4.2.2). In addition, two sample points (no. 12, 29) located at the downstream of PFZ are $\text{SO}_4\text{-Ca}$, which may suggest a higher residence time of groundwater. The spring no. 3 is $\text{HCO}_3\text{-Na}$ likely due to the dissolution of Na-silicate minerals into dykes (field observation). The relation between EC and elevation is also visible in the variation of elements concentrations in groundwater (Fig. 4.3), where the concentrations are lowest in high-elevation areas and progressively increase down to the San Felipe aquifer. Note that samples located in the basin have a significant increase in the concentrations of Cl , NO_3 , Sr and Ba instead of the samples located into the fractured rock (Fig. 4.3a, g, h, i).

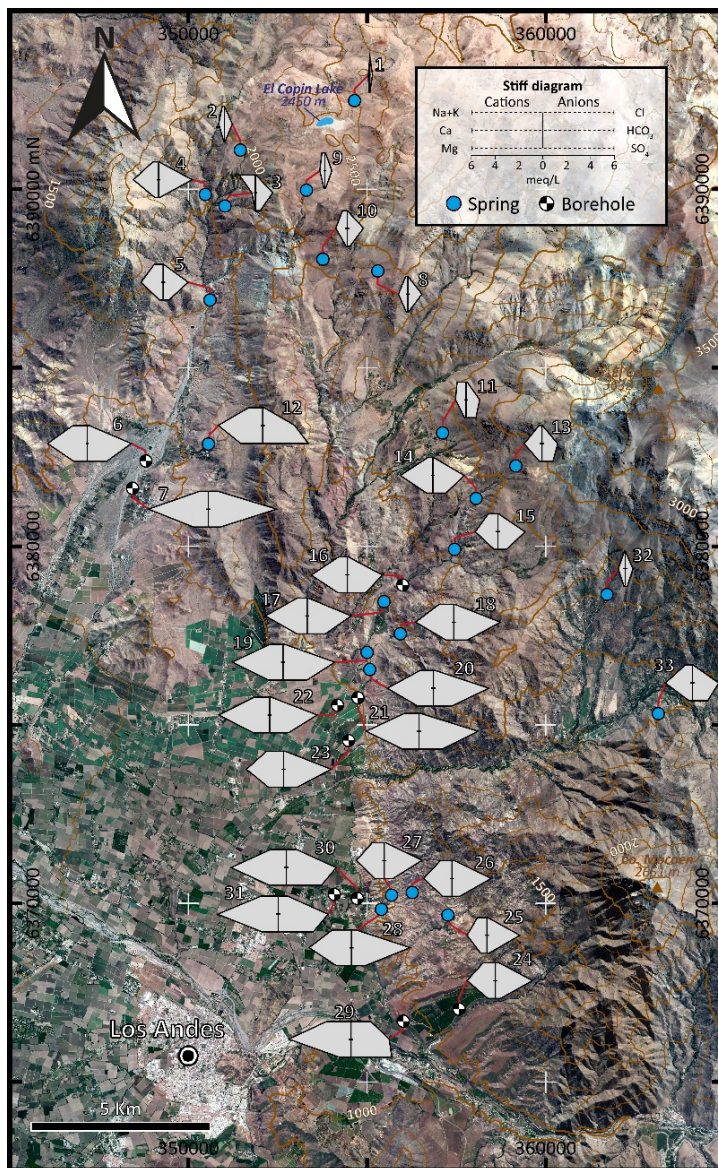


Fig. 4.2: Stiff diagrams of groundwater samples at the study area.

Id	Source	Altitude (m asl)	T°C	pH	EC (µS/cm)	Major Elements (ppm)							Trace Elements (ppb)					Ionic Ratios (meq/L)					
						SiO ₂	Cl	SO ₄	HCO ₃	NO ₃	Na	K	Ca	Mg	Li	B	As	Sr	Ba	rNa/rCa	rMg/rCa	rLi/rCl	rB/rCl
1	Spring	2465	27.7	8.17	31	11.0	0.08	0.9	15.1	0.21	0.42	bdl	3.08	0.40	bdl	3.30	0.40	17.50	2.19	0.364	0.346	0.0017	0.183
2	Spring	1933	13.5	7.38	84	20.9	0.44	2.9	44.1	2.45	4.66	0.13	10.45	0.83	bdl	8.38	0.86	18.02	0.62	0.173	0.276	0.0011	0.024
3	Spring	1562	20.4	8.40	190	15.8	1.07	18.7	89.8	0.34	31.88	0.51	7.09	0.23	1.36	20.11	1.40	5.54	0.62	0.311	0.500	0.0053	0.184
4	Spring	1515	14.9	7.82	278	22.2	0.92	4.2	174.6	0.43	11.88	bdl	42.68	4.30	0.83	49.98	2.72	77.13	4.19	0.283	0.311	0.0028	0.207
5	Spring	1246	17.2	8.47	277	23.1	1.63	24.3	131.4	5.64	17.28	0.37	36.78	4.11	2.89	78.69	8.35	176.64	5.49	0.295	0.327	0.0033	0.199
6	Borehole	938	22.4	7.16	519	32.6	7.91	78.5	225.8	12.87	28.08	1.47	67.22	14.11	2.56	147.19	3.71	309.07	23.76	0.453	0.411	0.0039	0.141
7	Borehole	895	23.2	7.48	703	33.9	23.34	41.5	338.6	34.97	20.92	1.67	105.36	17.63	5.08	56.64	0.97	439.92	48.00	0.410	0.360	0.0008	0.059
8	Spring	2380	21.0	7.09	168	18.0	0.50	2.4	73.2	0.34	5.00	bdl	16.38	1.57	bdl	6.28	0.62	54.08	1.39	0.399	0.189	0.0050	0.034
9	Spring	2301	12.5	7.95	96	26.0	0.96	2.5	37.6	2.29	6.88	0.49	9.16	1.05	bdl	6.54	1.17	24.87	1.73	0.287	0.310	0.0024	0.018
10	Spring	2085	13.3	7.90	144	18.0	0.24	11.5	85.4	2.70	9.10	bdl	20.16	1.39	0.25	13.12	1.51	49.79	1.86	0.272	0.278	0.0026	0.026
11	Spring	1784	21.9	7.13	186	20.1	2.75	39.6	70.2	0.11	17.10	0.40	18.32	1.86	2.33	186.69	3.29	118.91	0.84	0.410	0.184	0.0091	0.475
12	Spring	1128	21.5	7.43	647	29.5	5.92	185.6	164.7	9.90	26.68	2.35	74.88	22.70	6.18	110.45	12.27	287.32	15.80	0.145	0.210	0.0041	1.506
13	Spring	2179	23.4	6.97	204	20.1	1.68	44.8	82.4	1.01	6.13	1.38	29.80	2.91	1.43	176.80	12.51	58.28	0.69	0.246	0.257	0.0022	0.405
14	Spring	1783	18.9	7.41	330	21.7	1.21	52.7	161.7	2.43	9.11	0.54	54.76	6.98	0.98	185.46	1.59	104.05	1.92	0.239	0.254	0.0029	0.339
15	Spring	1490	21.0	8.52	272	25.0	2.10	34.9	140.3	2.89	17.55	1.04	38.30	4.12	1.27	130.16	7.80	81.64	1.24	0.387	0.216	0.0041	0.217
16	Borehole	1283	22.2	7.36	412	24.9	2.89	73.4	180.0	5.67	17.19	0.63	60.86	9.50	1.26	118.95	9.28	142.56	6.33	0.251	0.292	0.0034	0.247
17	Spring	1239	22.8	7.14	461	26.2	3.41	74.7	225.8	5.42	19.55	0.38	71.22	10.95	1.91	117.23	1.69	67.90	4.31	0.279	0.349	0.0052	0.240
18	Spring	1157	25.7	8.19	484	27.0	4.03	56.0	241.0	5.17	29.10	0.04	65.59	8.60	3.27	88.69	2.99	253.80	5.33	0.435	0.273	0.0006	0.020
19	Spring	1088	21.0	7.10	575	28.1	4.89	97.7	265.4	9.47	24.80	0.27	86.22	15.29	3.25	122.95	2.84	125.17	0.58	0.443	0.316	0.0069	0.086
20	Spring	1077	22.3	7.22	557	29.9	4.55	73.6	286.8	11.78	24.96	0.69	78.14	16.55	4.65	111.04	12.74	332.71	1.92	0.384	0.343	0.0048	0.071
21	Borehole	980	21.0	7.54	686	32.0	5.86	93.6	305.1	9.48	28.80	0.65	88.80	16.77	3.22	123.07	5.06	381.86	61.06	0.430	0.350	0.0072	0.108
22	Borehole	973	23.2	7.55	644	37.0	6.01	77.5	244.1	16.43	29.10	0.63	85.88	17.01	3.85	121.06	5.73	399.18	67.20	3.921	0.053	0.0065	0.185
23	Borehole	939	21.4	7.77	581	34.0	7.18	56.4	244.1	37.50	32.70	0.53	62.96	15.69	5.48	102.67	6.78	379.10	8.63	0.243	0.166	0.0046	0.536
24	Borehole	1146	20.8	7.43	570	31.0	12.21	22.3	192.3	11.90	24.15	0.51	48.43	8.01	1.46	25.15	2.69	290.66	2.51	0.394	0.113	0.0053	0.545
25	Spring	1088	23.7	7.45	275	31.6	2.48	10.1	170.8	9.02	17.54	0.64	34.50	6.62	3.34	21.71	3.24	136.20	2.21	0.814	0.167	0.0043	0.669
Detection limits:						0.1	0.03	0.07	0.0	0.10	0.09	0.04	0.014	0.001	0.02	0.07	0.02	0.01	0.01	0.01	0.01	0.01	0.01

Table 4.1: Chemical analysis of spring, borehole, and meteoric water samples (bdl: below detection limit).

Id	Source	Altitude (m asl)	T°C	pH	EC (µS/cm)	Major Elements (ppm)								Trace Elements (ppb)					Ionic Ratios (meq/L)				
						SiO ₂	Cl	SO ₄	HCO ₃	NO ₃	Na	K	Ca	Mg	Li	B	As	Sr	Ba	rNa/rCa	rMg/rCa	rLi/rCl	rB/rCl
26	Spring	993	19.8	7.37	402	26.8	8.67	33.4	201.4	7.27	21.12	3.91	47.92	9.98	8.23	62.69	9.13	341.36	3.11	0.179	0.161	0.0043	1.037
27	Spring	981	20.6	7.66	390	26.0	6.19	36.3	195.3	6.92	23.20	0.73	47.00	9.97	8.73	68.05	8.87	345.97	3.27	0.400	0.177	0.0031	0.610
28	Spring	975	24.1	7.95	579	24.8	14.26	55.4	302.0	4.39	33.82	6.47	71.88	15.69	2.30	85.81	5.06	421.58	14.84	0.292	0.155	0.0029	0.493
29	Borehole	919	18.9	6.99	1188	25.8	60.17	166.4	197.1	10.29	48.20	0.90	105.35	12.10	58.66	209.41	22.05	927.64	11.48	0.119	0.214	0.0012	0.396
30	Borehole	918	18.6	7.59	710	27.0	30.01	140.9	256.3	9.66	30.90	0.93	93.95	17.66	14.30	53.77	3.98	715.44	14.52	0.389	0.131	0.0002	0.189
31	Borehole	889	-	7.68	1026	25.8	28.04	141.6	256.3	9.35	32.00	1.42	102.65	17.30	14.12	73.70	3.00	753.15	24.57	0.266	0.158	0.0002	0.123
32	Spring	1701	11.5	7.96	83	17.6	0.50	10.2	42.7	0.83	1.03	0.24	12.13	1.32	bdl	16.07	1.40	19.97	1.04	0.655	0.190	0.0001	0.067
33	Spring	1456	18.0	7.72	341	22.9	1.697	62.6	134.2	bdl	15.46	bdl	46.20	4.34	0.97	84.95	2.84	125.17	0.58	0.074	0.179	0.0002	0.319
34	Meteoric	2715	15.7	5.87	14	bdl	1.01	0.7	1.0	1.59	0.30	0.73	1.79	0.00	bdl	bdl	0.21	3.66	4.05	0.146	0.001	0.0001	0.001
35	Meteoric	1965	15.6	6.17	45	0.3	0.53	2.1	16.9	bdl	0.45	1.16	6.89	0.22	0.54	24.30	1.73	11.36	2.32	0.057	0.053	0.0052	0.452
36	Meteoric	1132	14.2	5.70	28	bdl	1.19	1.9	7.6	bdl	0.48	2.92	2.24	0.29	bdl	4.15	1.30	12.13	4.08	0.186	0.215	0.0001	0.034
37	Meteoric	970	14.5	6.70	50	bdl	1.95	2.5	15.7	bdl	1.22	8.74	3.01	0.66	bdl	13.08	0.94	8.24	4.84	0.353	0.361	0.0001	0.066
38	Meteoric	830	15.0	6.68	56	1.5	0.56	3.4	22.0	bdl	0.19	0.57	11.77	0.22	bdl	6.75	1.03	19.27	10.14	0.014	0.031	0.0002	0.119
Detection limits:						0.1	0.03	0.07	0.0	0.10	0.09	0.04	0.014	0.001	0.02	0.07	0.02	0.001	0.01				

(Continuation of Table 4.1)

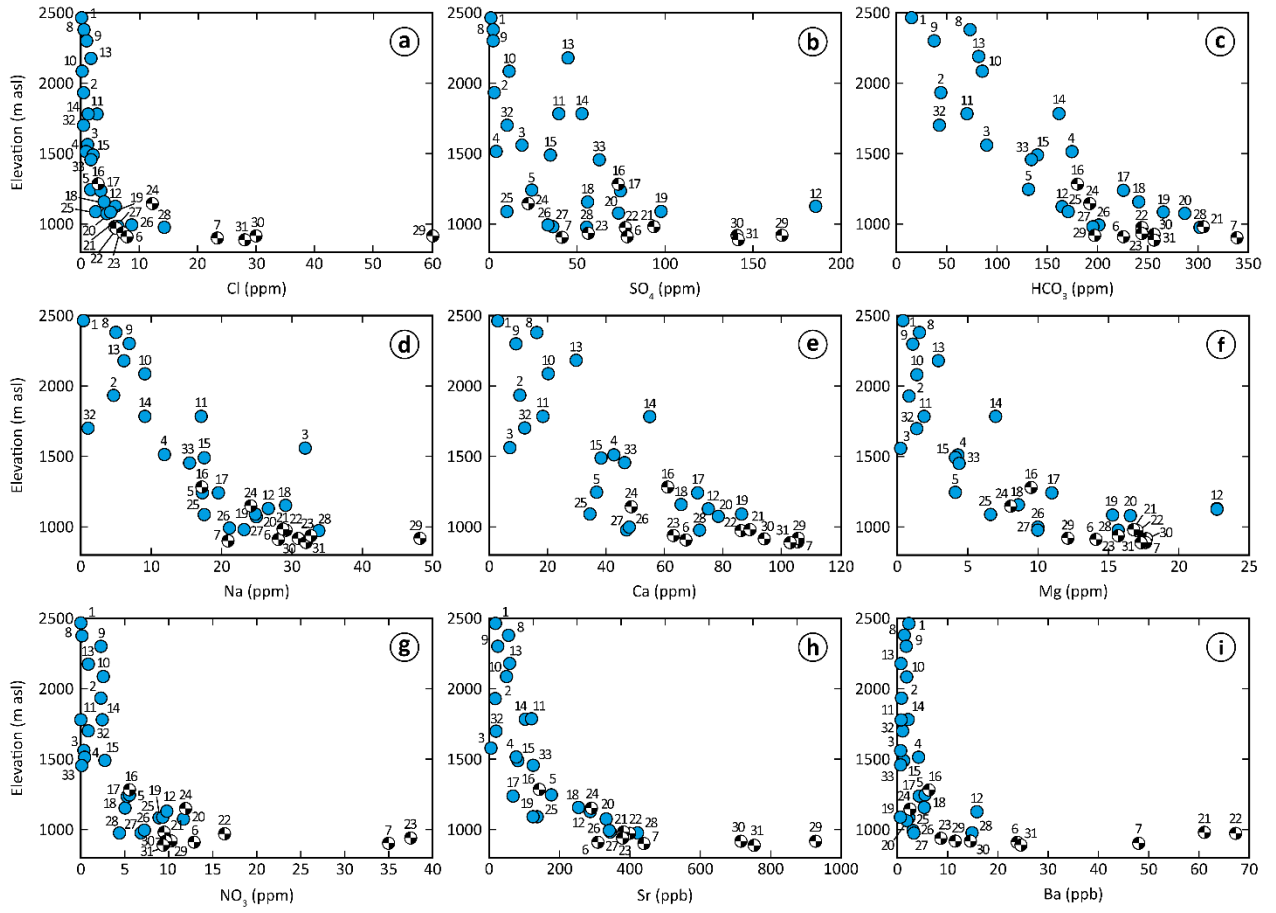


Fig. 4.3: Dissolved elements concentration *vs.* elevation (m asl) of springs (sky-blue) and boreholes (black/white) samples.

4.2. HYDROGEOCHEMICAL PROCESSES IN THE WESTERN ANDEAN FRONT

4.2.1. Groundwater evolution along flow paths

The hierarchical cluster analysis (HCA) reveals three main clusters (C1, C2 and C3; Fig. 4.4a), whose average properties are summarized in the Table 4.2 and Fig. 4.4b. C1 includes all boreholes of the San Felipe aquifer (no. 6, 7, 21, 22, 23, 29, 30, 31) and springs with the highest electrical conductivity values (no. 12, 28). C2 includes the springs and boreholes located in the lowest and middle part of the Western Andean Front. C2 can be subdivided in two sub-groups (C2.1 and C2.2) composed of (i) springs outflowing from fractured rocks within the PFZ (no. 5, 14, 17, 18, 19, 20, 25, 26, 27) and boreholes into Quaternary colluvium deposits in PFZ (no. 16, 24); and (ii) springs outflowing in the middle part of the Western Andean Front from fractured rocks (no. 3, 4, 10, 11, 13, 15, 33). C3 includes the springs in highest elevations of the Western Andean Front (C3.1: no. 1, 2, 8, 9, 32) and meteoric waters (C3.2: no. 34, 35, 36, 37, 38).

The Euclidian distance between C1 and C2 is lower than between C1-C2 and C3 (Fig. 4.4a). This reveals that C1 and C2 are geochemically more similar respect with C3. In addition, average properties inferred from HCA (Table 4.2) highlight that element concentrations (electrical conductivity) increase with decreasing elevation (Fig. 4.4b). However, the proportion of major elements is preserved from the upstream parts of the Western Andean Front up to the basin at the downstream. Those results seem to indicate that the variation of mineralization is due to an increase of the residence time rather than changes of geochemical reactions.

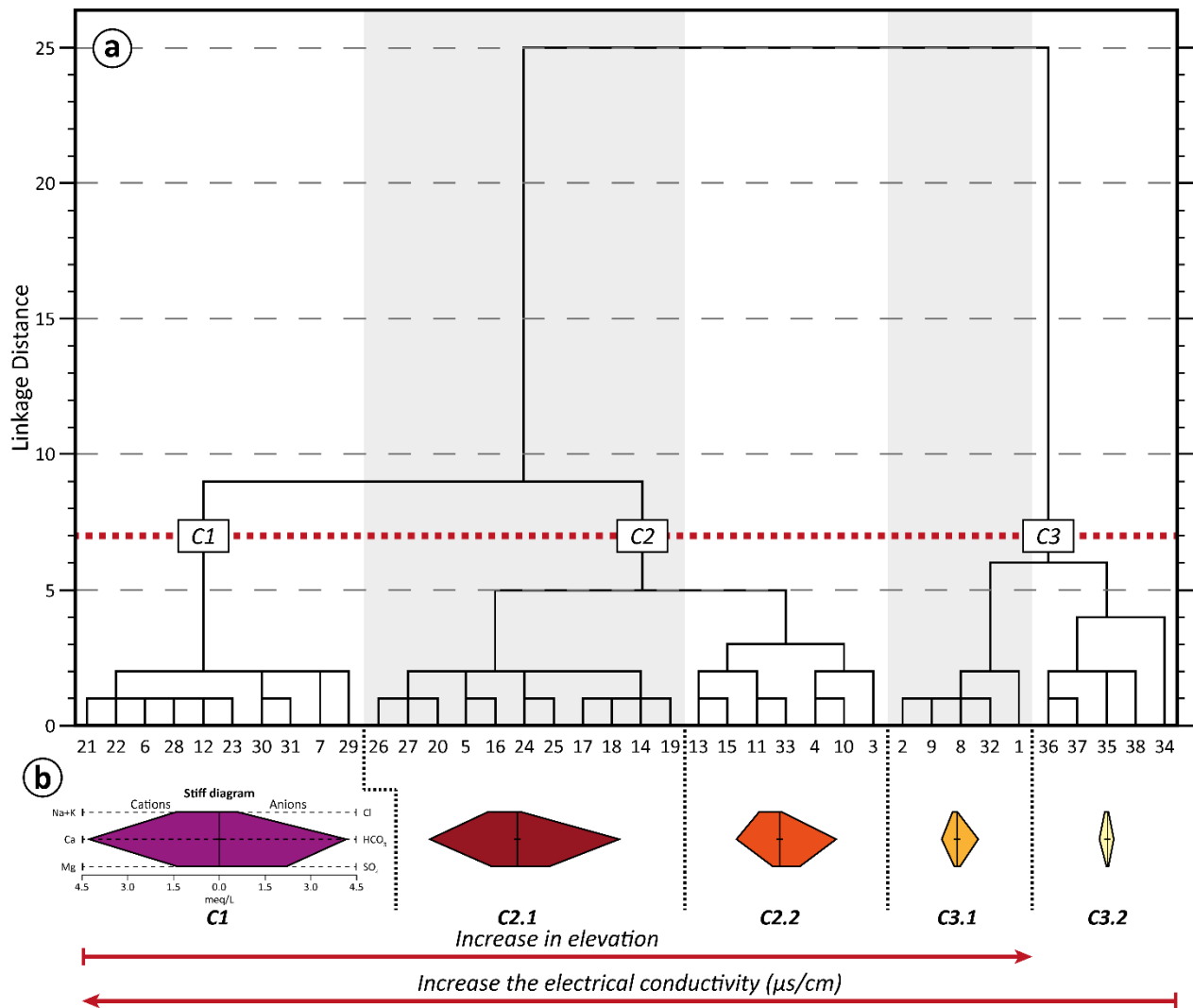


Fig. 4.4: Hierarchical cluster analysis. a) Dendrogram shows the three main clusters. b) Stiff diagrams represent the average concentration of major ions in meq/l.

To test the previous assumption, concentrations were compared in both groundwater and meteoric water with data of leaching-rocks sampled in the study area (Table 4.3). Considering the regional mineral proportions (Fuentes *et al.* 2004), dominated by Ca-plagioclase (anorthite) and in lower proportions by Na-plagioclase (albite) and CaMg-Pyroxenes, the ionic ratios Na/Ca and Mg/Ca against the Cl were examined (Fig. 4.5a, b). These plots reveal a well-defined gradual evolution of the groundwater concentrations from C3 up to C1 samples and tend to reach the composition of the host-rocks. Li and B are useful to characterise common sources of dissolved ions in waters (Nicholson, 1993). Li/Cl (Fig. 4.5c) and B/Cl (Fig. 4.5d) reveal that the source of dissolved ions in high-elevation springs (C3) is due to meteoric water input, while most of groundwater in the Western Andean Front (C1 and C2) originates from the dissolution of the host-rocks. Hence, the increase of groundwater mineralization is due to the residence time of groundwater that circulates in the Western Andean Front.

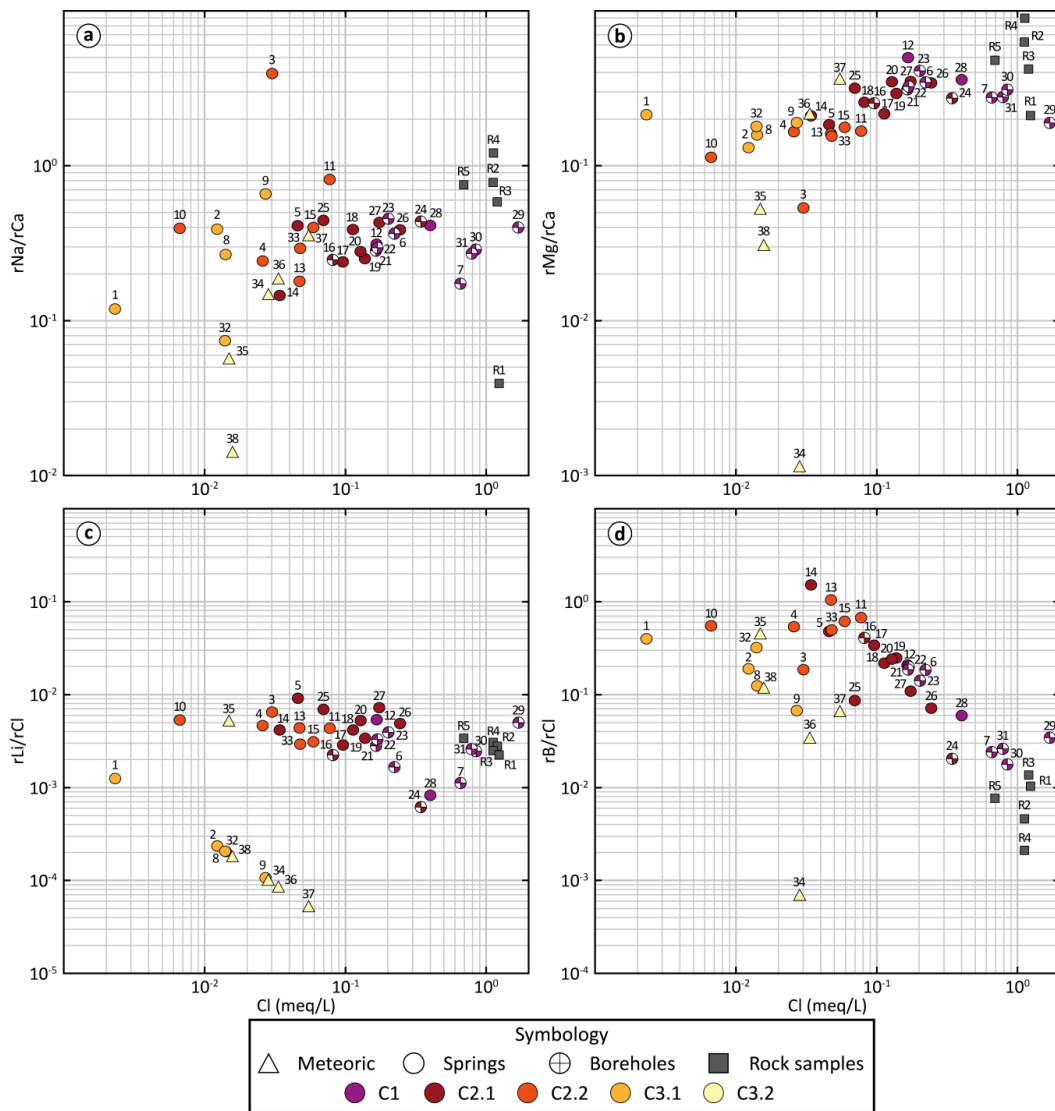


Fig. 4.5: Logarithmic ionic ratios calculated for water and rock samples *vs.* Cl ($r = \text{meq/L}$).

HCA Clusters	Samples	Altitude (m asl)	Water Type	EC (µS/cm)	T°C	Major Elements (ppm)							Trace Elements (ppb)					
						SiO ₂	Cl	SO ₄	HCO ₃	NO ₃	Na	Ca	Mg	Li	B	As	Sr	Ba
C1	6, 7, 12, 21, 22, 23, 28, 29, 30, 31	953	HCO ₃ -Ca	728	22	30.2	18.9	103.7	253.4	15.5	31.1	85.9	16.7	11.6	108.4	6.9	501.4	29.0
C2	5, 14, 16, 17, 18, 19, 20, 24, 25, 26, 27	1189	HCO ₃ -Ca	430	21	26.9	4.7	50.4	204.7	7.3	20.7	57.4	9.7	3.6	91.0	5.8	210.6	3.4
	3, 4, 10, 11, 13, 15, 33	1724	HCO ₃ -Ca	231	19	20.6	1.5	30.9	111.0	1.1	15.6	28.9	2.7	1.2	94.5	4.6	73.8	1.4
C3	1, 2, 8, 9, 32	2156	HCO ₃ -Ca	92	17	18.7	0.5	3.8	42.5	1.2	3.6	10.2	1.0	0.0	8.1	0.9	26.9	1.4
	34, 35, 36, 37, 38	-	HCO ₃ -Ca	39	15	0.4	1.0	2.1	12.6	0.4	0.5	5.1	0.3	0.1	9.7	1.0	10.9	5.1

Table 4.2: Average values of chemical composition for each water cluster identified by the HCA.

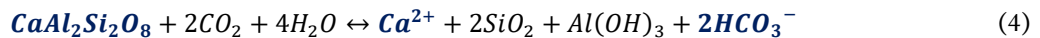
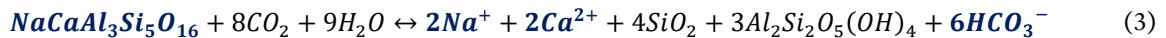
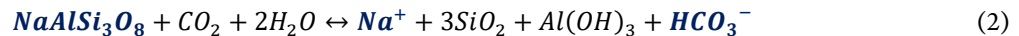
Id	Lithology	Geological Formation	Major Elements (ppm)							Trace Elements (ppb)					Ionic Ratios (meq/L)			
			Cl	SO ₄	NO ₃	Na	K	Ca	Mg	Li	B	As	Sr	Ba	rNa/rCa	rMg/rCa	rLi/rCl	rB/rCl
R1	Lithic-rich andesitic lapilli-tuff	Las Chilcas	43.88	12.68	8.36	4087	7486	90807	11638	19	46	68	402	220	0.039	0.211	0.0022	0.010
R2	Arkose	Las Chilcas	39.79	226.08	5.30	34793	14393	39053	14911	19	19	74	883	1854	0.777	0.630	0.0025	0.005
R3	Lithic-rich andesitic lapilli-tuff	Abanico	42.61	9.36	8.94	22171	11399	33147	8450	23	59	37	648	448	0.583	0.420	0.0028	0.014
R4	Hydorthermally altered crystal-rich andesitic tuff	Abanico	39.95	17.19	8.21	40924	14122	29661	16754	24	9	8	555	474	1.203	0.931	0.0030	0.002
R5	Lithic-rich andesitic agglomerate	Abanico	24.59	83.09	4.53	28262	10500	32748	9519	16	19	18	431	282	0.753	0.479	0.0034	0.008

Table 4.3: Chemical composition of the leaching-rock samples.

4.2.2. Source of dissolved ions: water-rock interactions and anthropogenic influences

Regarding previous findings, in this section the geochemical reactions and processes that occur along the Western Andean Front flow paths were defined.

In the study area, the volcano-sedimentary rocks are compositionally andesitic (Table 4.3) and the principal minerals are plagioclases. In the Andes of Central Chile there is the whole family of plagioclases, ranging from Na-plagioclase (albite) to Ca-plagioclase (anorthite), with labradorite as an intermediate plagioclase (Fuentes *et al.* 2004). The dissolution of plagioclase occurs in presence of carbonic acid, derived from soil CO₂ dissolution (Eq. 1). Albite, labradorite and anorthite release a ratio of 1:1 of Na/HCO₃ (Eq. 2), 1:3 of Na and Ca/HCO₃ (Eq. 3), and 1:2 of Ca/HCO₃ (Eq. 4), respectively (Fig. 4.6) (Elango and Kannan, 2007; Frengstad *et al.* 2007; Lerman and Wu, 2008).



There is a positive correlation of Na and Ca with respect to HCO₃ (Fig. 4.6). Na *vs.* HCO₃ (Fig. 4.6a) shows that most samples fit to the 1:3-trend showing a main dissolution of labradorite. In turn, Ca *vs.* HCO₃ (Fig. 4.6b) shows that most samples plot between 1:3 and 1:2 stoichiometric lines but tend to the 1:2-trend. These observations indicate the main role of anorthite dissolution in groundwater composition, even though labradorite dissolution occurs in a minor proportion. The results agree with the proportion of plagioclase minerals in the study area, where anorthite is dominant (Fuentes *et al.* 2004). Thus, the plagioclase dissolution explained the amounts of Na, Ca and HCO₃.

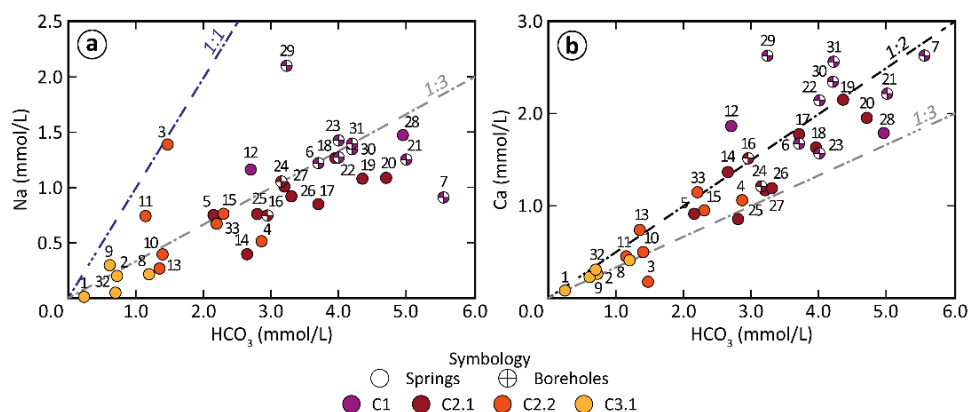


Fig. 4.6: Molar relationships of a) Na *vs.* HCO₃ and b) Ca *vs.* HCO₃ showing the plagioclase dissolution (stoichiometry ratios): albite (1:1), anorthite (1:2) and labradorite (1:3).

The factorial analysis (FA) results in two factors (F1 and F2), which explain 82.6 % of the total variance. The KMO value of 0.84 ensures the quality of the FA. The two factors suggest different sources of the analysed variables (Fig. 4.7a). F1 (58.25 %) shows the association of SO_4 , HCO_3 , Na, Ca, Mg, SiO_2 , Li, B, As and Sr. Given that the source of Na, Ca and HCO_3 is the dissolution of plagioclases, F1 reflects the water-rock interaction. F2 (24.37 %) shows the association of Cl, NO_3 , Sr and Ba. In the study area, the agriculture practices release in soils: (i) fertilizers containing NO_3 and Sr (*e.g.* Fernández *et al.* 2017; Biddau *et al.* 2019); (ii) rodenticides with compounds of Ba (field observation); and iii) organochlorine pesticides (Cl) (*e.g.* Pozo *et al.* 2017; Climent *et al.* 2019). Thus, F2 is related to anthropogenic influence. However, the weight of Cl and NO_3 (Fig. 4.7a) suggests that water-rock interaction may also contribute to the Cl and NO_3 concentrations in groundwater as supported by rock composition (Table 4.2).

The distribution of each sample relative to the F1 and F2 (Fig. 4.7b) shows that C3 has negative scores in both factors. C3.2 (meteoric water) reveals that neither water-rock interaction (F1) nor anthropogenic activities (F2) influence its composition. Despite that C3.1 shows negatives scores in F1, it reveals a minor influence of water-rock interactions in the groundwater of high-elevation springs. C2 shows positive values of F1 (up to ~1), which evidences the main role of water-rock interaction in the groundwater composition of samples located at mid- and low-elevation in the Western Andean Front (C2.1 and C2.2). Finally, C1 has positive values in both factors, reflecting the gradual influence of the anthropogenic activities into groundwater composition (F1 reaches ~0.8, while F2 reaches ~2.0). For samples with F2 values higher than F1 values, the anthropogenic activity is assumed predominant rather than the water-rock interaction, such as visible in the boreholes no. 6, 7, 21, 22, 29, 30 and 31.

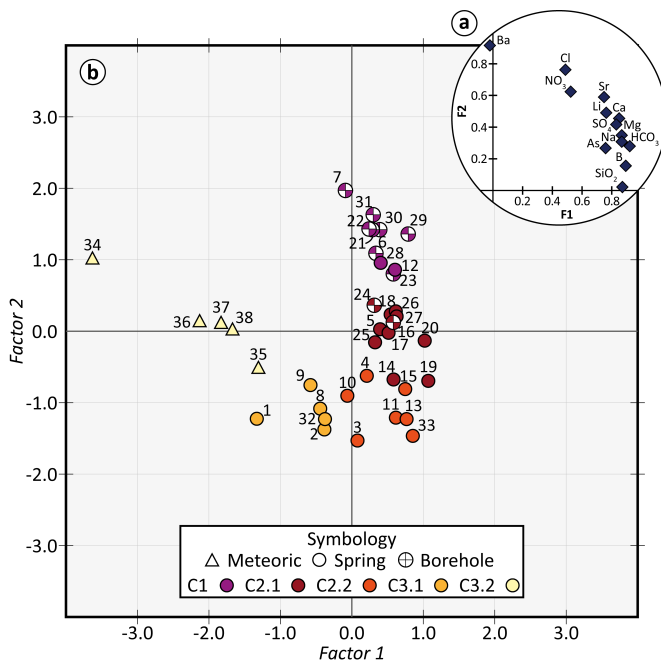


Fig. 4.7: Factorial analysis. a) Weight of variables for Factor 1 and 2. b) Projection of samples factorial scores.

4.3. WATER STABLE ISOTOPES AND GROUNDWATER ORIGINS

4.3.1. The 33°S Chile Meteoric Water Line

Inferred from regional annual precipitation weight means, the “33°S Chile MWL” is $\delta D = 8.07\delta^{18}O + 11.42$ ($R^2=0.97$) (Fig. 4.8a), and shows a similarity with the global meteoric water line GMWL ($\delta D = 8\delta^{18}O + 10$; Craig, 1961). The regional influence of the orographic-continental effect is expressed by a gradient with elevation ($\nabla_z \delta^{18}O_p$) of -0.30 ‰ per 100 m asl (Fig. 4.8b) like one estimated by Sánchez-Murillo *et al.* (2018) for entire Chile (-0.347 ‰ per 100 m). For collected meteoric samples (no. 35, 36, 37), $\delta^{18}O$ and δD analyses agree with “33°S Chile MWL” strengthening the representativeness for studying local hydrological processes. In addition, snowpack isotope compositions in the Principal Cordillera (Ohlanders *et al.* 2013) perfectly match with “33°S Chile MWL” (Fig. 4.8a) although a deviation is observed with the regional elevation gradient (Fig. 4.8b). This deviation results from the role played by the abrupt topographic variations along the sub-catchments of the Principal Cordillera (narrow valleys with abrupt flanks) in the snow depositional effects. Consequently, snowpack isotope compositions correspond to elevations above 3000 m asl (Fig. 4.8b). Therefore, the provided “33°S Chile MWL” is robust for characterizing both the origin of groundwater and the related recharge processes in the study area, but also in other catchments of Central Chile.

4.3.2. Areas contributing to recharge groundwater

The contents of $\delta^{18}O$ and δD of springs range from -13.15 ‰ to -6.31 ‰ and from -92.56 ‰ to -69.52 ‰, respectively; and $\delta^{18}O$ and δD at boreholes range from -15.38 ‰ to -9.41 ‰ and -107.92 ‰ to -78.30 ‰, respectively (Table 4.4). The comparison between groundwater and “33°S Chile MWL” shows that the groundwater originates from precipitation which took place under hydroclimatic conditions similar to the current ones (Fig. 4.8a). Most samples show an enrichment trend ($\delta D = 3.54\delta^{18}O - 45.42$; $R^2=0.80$) indicating a partial evaporation of the meteoritic water. The slope of this enrichment trend (3.54) is typical of evaporation processes under dry conditions (Clark, 2015), which agrees with the semiarid conditions of the Aconcagua Basin. By the position of samples on this evaporation trend, an absence of negative relationship between partial evaporation rate (Fig. 4.5a) and the elevation of sampling points is observed (Fig. 4.5b). This indicates that fractioning due to evaporation processes occurs locally during the water infiltration rather than along the flow paths in the Western Andean Front. Such a statement is also supported by the isotopic composition of borehole samples (no. 6 and 7) that lie on the evaporation trend (Fig. 4.8a), even though the groundwater level is ~75 m below ground surface where evapotranspiration has no further impact (e.g. Shah *et al.* 2007).

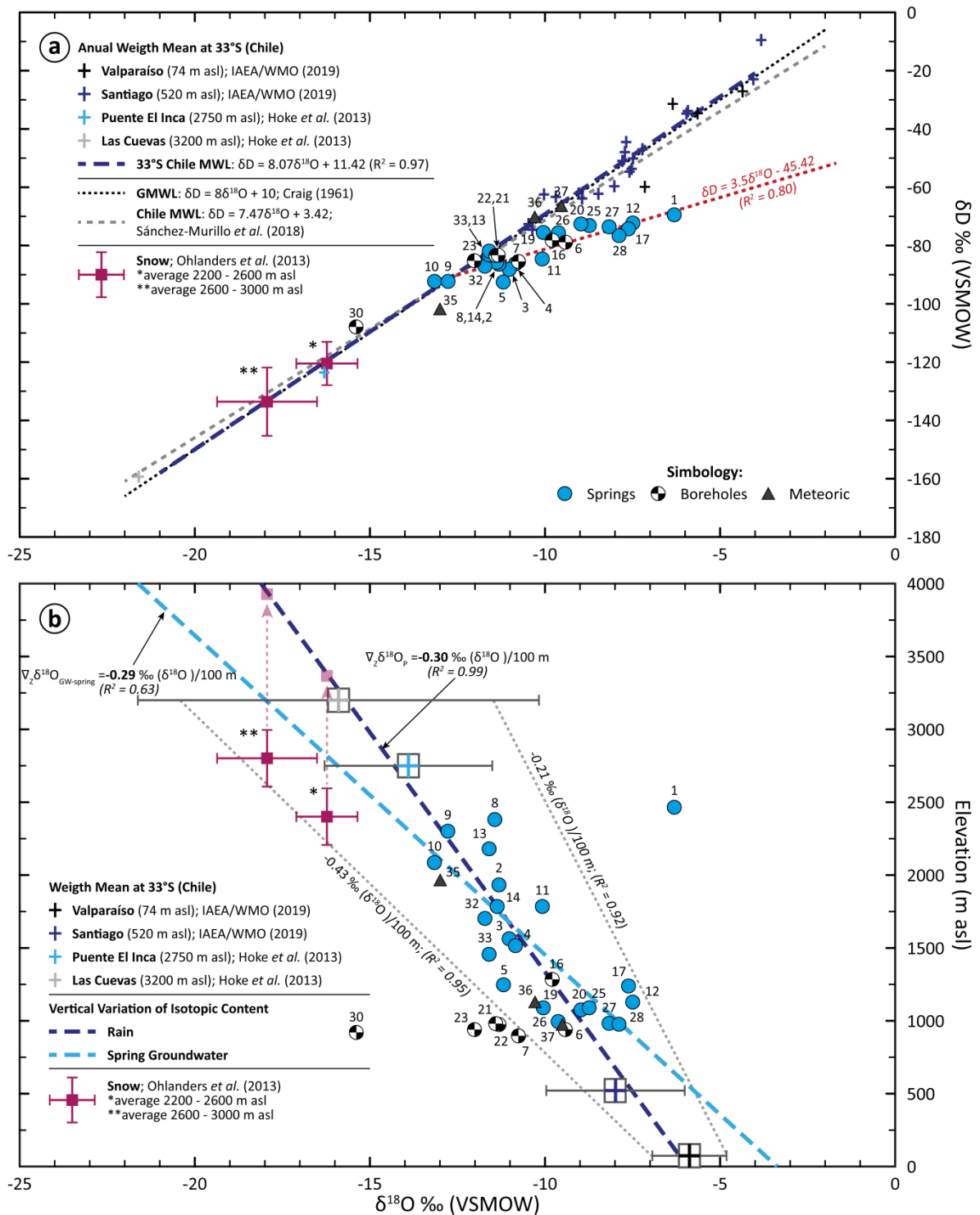


Fig. 4.8: Water stable isotopes. a) Relationship between δD vs. $\delta^{18}\text{O}$ and 33°S Chile MWL. b) Orographic-continental effect on $\delta^{18}\text{O}$ values at 33°S. The vertical content of the isotopic content in groundwater ($\nabla_z \delta^{18}\text{O}_{\text{GW-spring}}$) along the Western Andean Front was calculated considering only the springs (no. 1 has not been included because it is very heavy related to the corresponding elevation).

Id	Source	Altitude (m asl)	Stable Isotopes	
			δD (VSMOW)	$\delta^{18}O$ (VSMOW)
1	Spring	2465	-69.52	-6.31
2	Spring	1933	-86.24	-11.31
3	Spring	1562	-88.17	-11.02
4	Spring	1515	-86.262	-10.840
5	Spring	1246	-92.56	-11.18
6	Borehole	938	-78.94	-9.41
7	Borehole	895	-85.54	-10.76
8	Spring	2380	-83.67	-11.43
9	Spring	2301	-92.34	-12.77
10	Spring	2085	-92.33	-13.15
11	Spring	1784	-84.60	-10.07
12	Spring	1128	-72.33	-7.49
13	Spring	2179	-81.92	-11.59
14	Spring	1783	-85.76	-11.36
15	Spring	1490	-	-
16	Borehole	1283	-78.30	-9.79
17	Spring	1239	-74.10	-7.61
18	Spring	1157	-	-
19	Spring	1088	-75.50	-10.05
20	Spring	1077	-72.63	-8.97
21	Borehole	980	-83.48	-11.40
22	Borehole	973	-83.42	-11.31
23	Borehole	939	-85.33	-12.01
24	Borehole	1146	-	-
25	Spring	1088	-73.15	-8.73
26	Spring	993	-75.68	-9.62
27	Spring	981	-73.59	-8.17
28	Spring	975	-76.60	-7.89
29	Borehole	919	-	-
30	Borehole	918	-107.92	-15.38
31	Borehole	889	-	-
32	Spring	1701	-87.18	-11.71
33	Spring	1456	-83.35	-11.59
34	Meteoric	2715	-	-
35	Meteoric	1965	-101.80	-12.99
36	Meteoric	1132	-70.34	-10.29
37	Meteoric	970	-66.43	-9.53
38	Meteoric	830	-	-

Table 4.4: Isotopic analysis of spring, borehole, and meteoric water samples.

At the interception between evaporation line and “33°S Chile MWL” (Fig. 4.8a), the value of $\delta^{18}\text{O}$ is -12.55 ‰. Regarding that, the precipitation contributing to recharge groundwater takes place at around 2200 m asl (Fig. 4.8b). Involved recharge processes can be diffuse (direct process) in precipitation areas, but also focused (indirect process) into geomorphological structures (*e.g.* gullies) where runoff infiltrates. Nevertheless, some springs (no. 1, 8, 9), related to precipitation at 2200 m asl (see above), are located between 2300 and 2500 m asl (Table 4.4). This altitude deviation is due to the wide range of meteoric isotope composition in high elevation sub-catchments and to the fractioning processes resulting of the evaporation and elution of snowpack (Ohlanders *et al.* 2013). Some samples (no. 21, 22, 23, 32, 33) could be also considered as not impacted by the evaporation (Fig. 4.8a). Regarding this uncertainty, precipitation at lower elevations (1800 and 2000 m asl; Fig. 4.8b) can also contribute to recharge the groundwater. Given that the isotopic composition in rain and snow are similar, is difficult to distinguish if groundwater originates from residual rain (after evaporation) or snowmelt. Both origins are highly likely.

The similarity of the vertical gradient (per 100 m a.s.l) of isotopic content in precipitation ($\nabla_z \delta^{18}\text{O}_P = -0.30\text{ ‰}$) and in springs groundwater ($\nabla_z \delta^{18}\text{O}_{\text{GW-spring}} = -0.29\text{ ‰}$) (Fig. 4.8b) indicates that groundwater of springs originates from local recharge processes rather than from a diffuse process along the slope of the mountain (Custodio and Jódar, 2016). In this latter case, the expected variation of the isotopic content in groundwater of springs with the elevation would be not linear as well, but with a higher vertical gradient, given that groundwater samples would be a mixture of water originating from the upstream recharge areas and local infiltration (*i.e.* “slope effect”; Custodio and Jódar, 2016). Therefore, groundwater recharge occurs locally by focused indirect recharge processes through geomorphological structures such as fractures and gullies. The isotopic content of groundwater of springs can also be used to characterize the local precipitation altitudinal line for Central Chile.

To the downstream of PFZ in Quaternary alluvial deposits, groundwater at the borehole no. 30 shows an isotopic inconsistency with respect to previous observation. The contents of $\delta^{18}\text{O}$ and δD are depleted and equivalent to the precipitation at ~3000 m asl (Fig. 4.8a, b) whereas the borehole no. 30 is located at 918 m asl. In addition, it does not show an enrichment process caused by the evaporation (Fig. 4.8a). To explain that, two assumptions must be cited: (i) A rapid and deep infiltration of rainy events at 3000 m asl through fractures without influence of evaporation. However, to the east of this borehole (no. 30), the maximum elevation in the Western Andean Front is 2651 m asl (*Co. Mocoen*; Fig. 4.1a). This latter would imply a deep groundwater circulation originating from highs at about ten kilometres further east. But borehole no. 30 groundwater does not show a significant thermal property (18.8 °C). (ii) A rapid transfer of surface water, from high-elevation areas in the Principal Cordillera

(~3000 m asl) up to permeable alluvial deposits at downstream where surface water infiltrates. Indeed, a major irrigation canal is located at less than ~50 m of the borehole no. 30. This canal is devoid of impervious layer (field observation) and conducts water from the high parts of the Principal Cordillera up to the Central Depression.

Regarding previous information, canal-losses permit to recharge the groundwater of borehole no. 30 rather than supposed deep groundwater circulation coming from distant high-elevation areas. The $\delta^{18}\text{O}$ and δD analyses allow demonstrating the role of anthropogenic activities (irrigation canals) in the recharge of San Felipe aquifer.

4.4. GROUNDWATER CIRCULATION AND RECHARGE PROCESSES

In the high-elevation sub-catchments (>2200 m asl), the rapid infiltration of snowmelt and rainstorms in fractures is relevant regarding the storage of groundwater in high-elevation areas (Fig. 4.9a, b). There, groundwater composition is poorly influenced by water-rock interactions. During dry years, the release of groundwater stored in high-elevation areas supports the shallow groundwater circulation (Staudinger *et al.* 2017; Foks *et al.* 2018; Jódar *et al.* 2017; Glas *et al.* 2019). It is a primary source of the groundwater recharge for Western Andean Front hydrogeological systems. The occurrence of such process is relevant considering the current and future hydroclimatic conditions of Central Chile (*i.e.* “Megadrought”; Garreaud *et al.* 2017, 2019). Nevertheless, climate predictions show a decrease in precipitation together with a decline of the snow cover area (Garreaud *et al.* 2017; Stehr and Aguayo, 2017). As a result, the contribution of high-elevation areas to the Western Andean Front groundwater recharge is expected to decline.

At lower elevations, below 2200 m asl (Fig. 4.9a), runoff and sub-surface circulation coming from higher-elevation areas are concentrated in mid-mountain gullies and infiltrate at depth in fractures and colluvial deposits (Fig. 4.9b). Focused recharge feeds springs located in the Western Andean Front. Local observers report a rapid and short increment of the spring discharge, located at the downstream in the PFZ (Fig. 4.9c), after rainy events and fast melting periods of the snow cover. Although this study does not address hydrodynamic changes, this information must be considered. It indicates that groundwater circulation in fractured rocks is governed by piston flows. In the Western Andean Front the contents of HCO_3 , Na, Ca, Mg and SiO_2 result from the dissolution of labradorite, anorthite and CaMg-pyroxenes. Other dissolved ions, such as SO_4 , Li, B, As and Sr, originate from water-rock interactions despite that involved mineral reactions were not identified. The absence of different sources of dissolved ions as well as evapoconcentration processes along the flow paths lead to assume that the increment of the mineralization toward the downstream is due to an increase of the residence time.

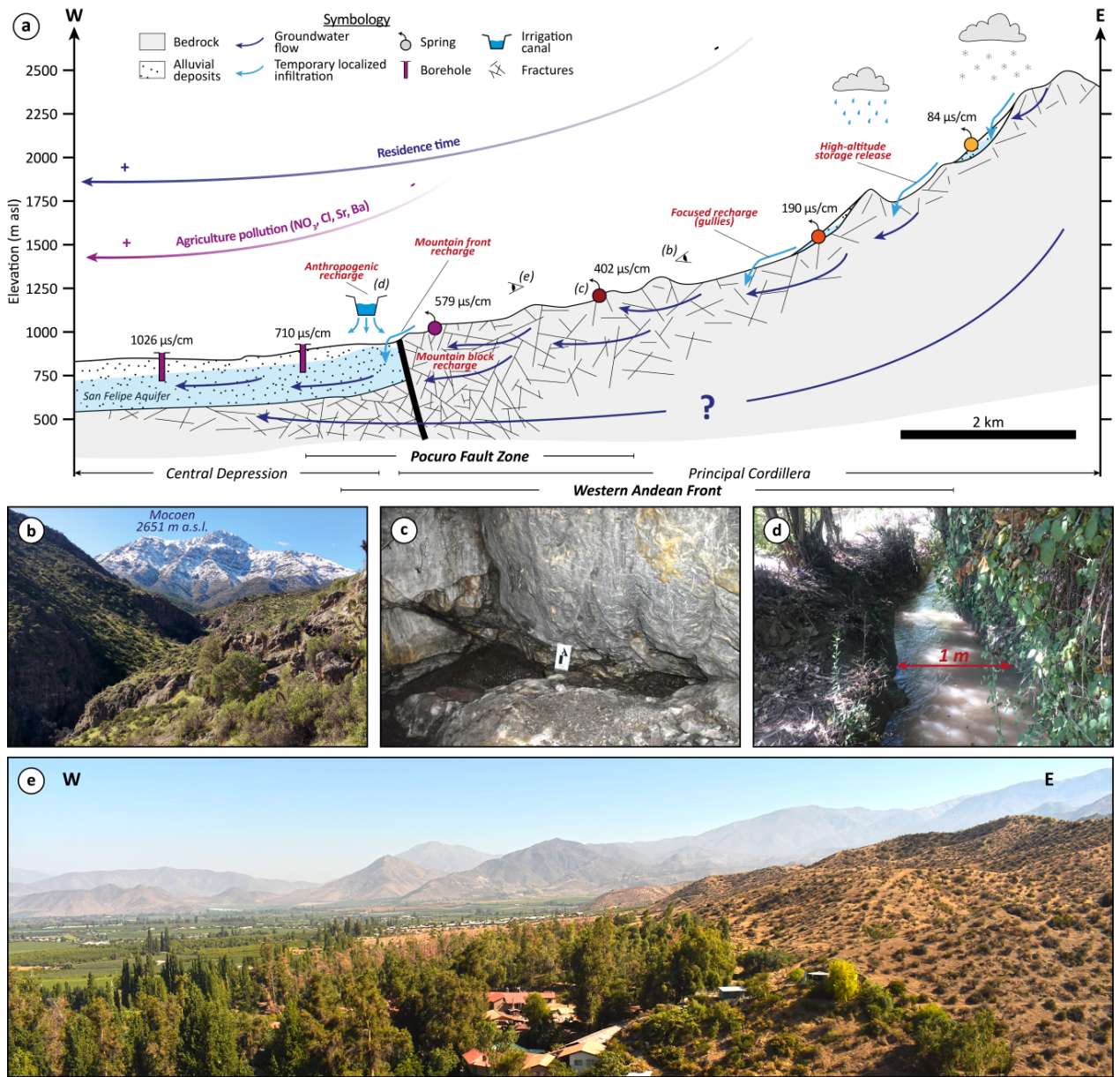


Fig. 4.9: Hydrogeological conceptual model of the Western Andean Front. Colours of the springs and boreholes are related to the HCA clusters.

The analyses of NO_3 and As in groundwater (Fig. 4.10), hazardous elements for human health, reveal that the Western Andean Front groundwater is relatively good quality, without anthropogenic pollution. All samples show NO_3 concentrations below the Chilean (NCh409/1) and international (WHO) drinking water limits (Fig. 4.10a). Regarding As concentrations (Fig. 4.10b), some samples (no. 12, 13, 20) exceed the established limits for drinking water. However, those points are not used for drinking water purposes, although they can be used for mineral bottling water (Daniele *et al.* 2019). Indeed, these samples are below the Chilean Decree 106 (Fig. 4.10b).

In the downstream part of the Western Andean Front (Fig. 4.9a, e), the occurrence of low-thermal groundwater circulation (up to 9 °C above the local mean annual air temperature) indicates that deep flows contribute to recharge the San Felipe Aquifer. The mountain-block recharge process (Wilson and Guan, 2004) is related to groundwater flows coming from recharge areas in the Western Andean Front and circulating by interconnected fractures (PFZ) up to the downstream adjacent alluvial basin (focused recharge). Oblique basement faults crossing the mountain front zone are typically considered as high-permeability axes allowing a focused recharge of adjacent alluvial aquifers (Wilson and Guan, 2004; Kebede *et al.* 2008; Taillefer *et al.* 2018; Walter *et al.* 2019). Despite an absence of direct evidence, a spatial relation has been observed between oblique basement faults and major groundwater circulation in Central Chile (Oyarzún *et al.* 2017; Piquer *et al.* 2019). Such a process would permit a permanent recharge of the San Felipe Aquifer, between 5 and 50 % of the total alluvial aquifer recharge according to recent estimations in other mountain-front zones (Markovich *et al.* 2019). At the downstream of the mountain front zone shaped by PFZ (Fig. 4.9e), the focused and rapid infiltration of streams in coarse alluvial deposits also contributes to recharge the San Felipe Aquifer (Fig. 4.9a). This process originates from the perennial infiltration of secondary rivers fed by high-elevation springs as well as the infiltration of ephemeral streams (triggered by rainstorms on dry soils of the Western Andean Front).

In addition to previous natural processes, there is another process related to agriculture activities (Fig. 4.9a, d). Water originating from high elevation areas is rapidly transferred down to irrigation canals localized in the Central Depression (Fig. 3.1c). The absence of impervious layer at canal bottoms (Fig. 4.9d) promotes a permanent focused infiltration (Barberá *et al.* 2018; Martos-Rosillo *et al.* 2019) and therefore an artificial groundwater recharge, historically used in the Andes (Ochoa-Tocachi *et al.* 2019). Subsequently, the groundwater in the alluvial aquifer has an isotopic composition similar to high-elevation precipitation (Fig. 4.8).

In Central Depression, the infiltration from agriculture practices (fertilizers) impacted the groundwater quality by an increase of NO₃ concentration. Moreover, the increase of Cl, Sr, and Ba concentrations in groundwater is statically related to the agriculture (organochlorine pesticides, fertilizers, and rodenticides inputs). Given that groundwater coming from the Western Andean Front has a good quality, a change of agriculture practices will help for diminishing the presence of human-origin hazardous components in the San Felipe Aquifer. About a quantitative aspect, current dry years have promoted the implementation of impermeable infrastructures for diminishing “water losses” from canal-infiltration. The findings reveal that the implementation of an impervious layer at canal bottoms will dramatically impact the renewal of the San Felipe Aquifer.

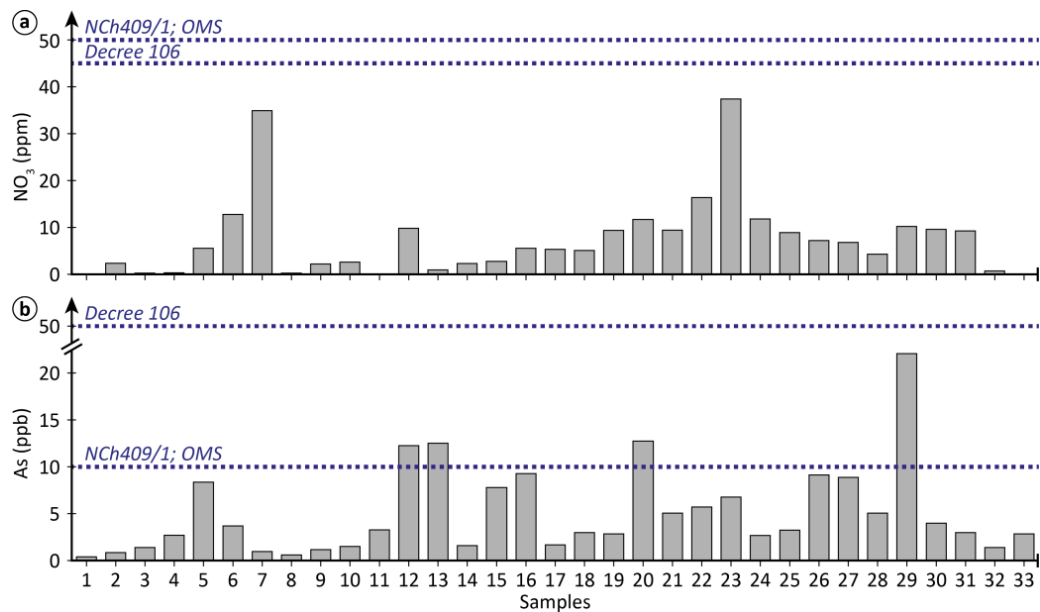


Fig. 4.10: Drinking water quality limits according with national (NCh409/1) and international (WHO) drinking water limits, and mineral bottling water (Decree no. 106) for a) NO_3 and b) As.

REFERENCES

- Barberá J.A., Jódar J., Custodio E., González-Ramón A., Jiménez-Gavilán P., Vadillo I., Pedrera A. & Martos-Rosillo S. 2018. Groundwater dynamics in a hydrologically-modified alpine watershed from an ancient managed recharge system (Sierra Nevada National Park, Southern Spain): Insights from hydrogeochemical and isotopic information. *Science of The Total Environment* 640-641, 874-893. <https://doi.org/10.1016/j.scitotenv.2018.05.305>
- Biddau R., Cidu R., Da Pelo S., Carletti A., Ghiglieri G. & Pittalis D. 2019. Source and fate of nitrate in contaminated groundwater systems: Assessing spatial and temporal variations by hydrogeochemistry and multiple stable isotope tools. *Science of The Total Environment* 647, 1121-1136. <https://doi.org/10.1016/j.scitotenv.2018.08.007>
- Clark I. 2015. *Groundwater geochemistry and isotopes* (1st ed.). CRC Press, 456 pp. <https://doi.org/10.1201/b18347>
- Climent M.J., Coscollà C., López A., Barra R. & Urrutia R. 2019. Legacy and current-use pesticides (CUPs) in the atmosphere of a rural area in central Chile, using passive air samplers. *Science of The Total Environment* 662, 646-654. <https://doi.org/10.1016/j.scitotenv.2019.01.302>
- Craig H. 1961. Isotopic Variations in Meteoric Waters. *Science* 133 (3465), 1702-1703. <https://doi.org/10.1126/science.133.3465.1702>
- Custodio E. & Jódar J. 2016. Simple solutions for steady-state diffuse recharge evaluation in sloping homogeneous unconfined aquifers by means of atmospheric tracers. *Journal of Hydrology* 540, 287-305. <https://doi.org/10.1016/j.jhydrol.2016.06.035>
- Daniele L., Cannatelli C., Buscher J.T. & Bonatici G. 2019. Chemical composition of Chilean bottled waters: Anomalous values and possible effects on human health. *Science of The Total Environment* 689, 526-533. <https://doi.org/10.1016/j.scitotenv.2019.06.165>
- Elango L. & Kannan R. 2007. Rock–water interaction and its control on chemical composition of groundwater. In: Sarkar D., Datta R. & Hannigan R. (Eds.), *Concepts and Applications in Environmental Geochemistry*. Elsevier 5, 229–243. [https://doi.org/10.1016/S1474-8177\(07\)05011-5](https://doi.org/10.1016/S1474-8177(07)05011-5)
- Fernández E., Grilli A., Alvarez D. & Aravena R. 2017. Evaluation of nitrate levels in groundwater under agricultural fields in two pilot areas in central Chile: A hydrogeological and geochemical approach. *Hydrological Processes* 31 (6), 1206-1224. <https://doi.org/10.1002/hyp.11103>
- Foks S.S., Stets E.G., Singha K. & Clow D.W. 2018. Influence of climate on alpine stream chemistry and water sources. *Hydrological Processes* 32 (13), 1993–2008. <https://doi.org/10.1002/hyp.13124>
- Frengstad B. & Banks D. 2007. Universal controls on the evolution of groundwater chemistry in shallow crystalline rock aquifers: the evidence from empirical and theoretical studies. In: Krásný J. & Sharp J.M. (Eds.), *Groundwater in Fractured Rocks: IAH Selected Paper Series*. CRC Press, 275–289.

- Fuentes F., Aguirre L., Vergara M., Valdebenito L. & Fonseca E. 2004. Miocene fossil hydrothermal system associated with a volcanic complex in the Andes of central Chile. *Journal of Volcanology and Geothermal Research* 138 (1–2), 139–161. <https://doi.org/10.1016/j.jvolgeores.2004.07.001>
- Garreaud R.D., Alvarez-Garreton C., Barichivich J., Boisier J.P., Christie D., Galleguillos M., LeQuesne C., McPhee J. & Zambrano-Bigiarini M. 2017. The 2010–2015 megadrought in central Chile: impacts on regional hydroclimate and vegetation. *Hydrology and Earth System Sciences* 21 (12), 6307–6327. <https://doi.org/10.5194/hess-21-6307-2017>
- Garreaud R.D., Boisier J.P., Rondanelli R., Montecinos A., Sepúlveda H.H. & Veloso-Aguila D. 2019. The Central Chile Mega Drought (2010–2018): A climate dynamics perspective. *International Journal of Climatology*, 1–19. <https://doi.org/10.1002/joc.6219>
- Glas R., Lautz L., McKenzie J., Moucha R., Chavez D., Mark B. & Lane Jr J.W. 2019. Hydrogeology of an alpine talus aquifer: Cordillera Blanca, Peru. *Hydrogeology Journal* 27 (6), 2137–2154. <https://doi.org/10.1007/s10040-019-01982-5>
- Hoke G.D., Aranibar J.N., Viale M., Araneo D.C. & Llano C. 2013. Seasonal moisture sources and the isotopic composition of precipitation, rivers, and carbonates across the Andes at 32.5–35.5°S. *Geochemistry, Geophysics, Geosystems* 14 (4), 962–978. <https://doi.org/10.1002/ggge.20045>
- IAEA/WMO. 2019. Global Network of Isotopes in Precipitation. The GNIP Database. <http://nucleus.iaea.org/wiser>
- Jódar J., Cabrera J.A., Martos-Rosillo S., Ruiz-Constán A., González-Ramón A., Lambán L.J., Herrera C. & Custodio E. 2017. Groundwater discharge in high-mountain watersheds: A valuable resource for downstream semi-arid zones. The case of the Bérrchules River in Sierra Nevada (Southern Spain). *Science of The Total Environment* 593–594, 760–772. <https://doi.org/10.1016/j.scitotenv.2017.03.190>
- Kebede S., Travi Y., Asrat A., Alemayehu T., Ayenew T. & Tessema Z. 2008. Groundwater water origin and flow along selected transects in Ethiopian rift volcanic aquifers. *Hydrogeology Journal* 16 (1), 55–73. <https://doi.org/10.1007/s10040-007-0210-0>
- Lerman A. & Wu L. 2008. Kinetics of Global Geochemical Cycles. In: Brantley S., Kubicki J. & White A. (Eds.), *Kinetics of Water-Rock Interaction*. Springer, 655–736. https://doi.org/10.1007/978-0-387-73563-4_13
- Markovich K.H., Manning A.H., Condon L.E. & McIntosh J.C. 2019. Mountain-block Recharge: A review of Current Understanding. *Water Resources Research*, 55. <https://doi.org/10.1029/2019WR025676>
- Martos-Rosillo S., Ruiz-Constán A., González-Ramón A., Mediavilla R., Martín-Civantos J.M., Martínez-Moreno F.J., Jódar J., Marín-Lechado C., Medialdea A., Galindo-Zaldívar J., Pedrera A. & Durán J.J. 2019. The oldest managed aquifer recharge system in Europe: New insights from the Espino recharge channel (Sierra Nevada, southern Spain). *Journal of Hydrology* 578, 124047. <https://doi.org/10.1016/j.jhydrol.2019.124047>
- Ochoa-Tocachi B.F., Bardales J.D., Antiporta J., Pérez K., Acosta L., Mao F., Zulkafli Z., Gil-Ríos J., Angulo O., Grainger S., Gammie G., De Bièvre B. & buytaert W. 2019. Potential contributions of pre-Inca infiltration

infrastructure to Andean water security. *Nature Sustainability* 2, 584–593. <https://doi.org/10.1038/s41893-019-0307-1>

Ohlanders N., Rodriguez M. & McPhee J. 2013. Stable water isotope variation in a Central Andean watershed dominated by glacier and snowmelt. *Hydrology and Earth System Sciences* 17, 1035–1050. <https://doi.org/10.5194/hess-17-1035-2013>

Oyarzún R., Oyarzún J., Fairley J.P., Núñez J., Gómez N., Arumí J.L. & Maturana H. 2017. A simple approach for the analysis of the structural-geologic control of groundwater in an arid rural, mid-mountain, granitic and volcanic-sedimentary terrain: The case of the Coquimbo Region, North-Central Chile. *Journal of Arid Environments* 142, 31–35. <https://doi.org/10.1016/J.JARIDENV.2017.03.003>

Piquer J., Yañez G., Rivera O. & Cooke D.R. 2019. Long-lived crustal damage zones associated with fault intersections in the high Andes of Central Chile. *Andean Geology* 46, 223–239. <https://doi.org/10.5027/andgeoV46n2-3106>

Pozo K., Oyola G., Estellano V.H., Harner T., Rudolph A., Prybilova P., Kukucka P., Audi O., Klánová J., Metzdorff A. & Focardi S. 2017. Persistent Organic Pollutants (POPs) in the atmosphere of three Chilean cities using passive air samplers. *Science of The Total Environment* 586, 107–114. <https://doi.org/10.1016/j.scitotenv.2016.11.054>

Sánchez-Murillo R., Aguirre-Dueñas E., Gallardo-Amestica M., Moya-Vega P., Birkel C., Esquivel-Hernández G. & Boll J. 2018. Isotopic characterization of waters across chile. In: Rivera D.A., Godoy-Faundez A. & Lillo-Saavedra M. (Eds.), *Andean Hydrology*. CRC Press, 205–230. <https://doi.org/10.1201/9781315155982-9>

Shah N., Nachabe M. & Ross M. 2007. Extinction Depth and Evapotranspiration from Ground Water under Selected Land Covers. *Groundwater* 45 (3), 329–338. <https://doi.org/10.1111/j.1745-6584.2007.00302.x>

Staudinger M., Stoelzle M., Seeger S., Seibert J., Weiler M. & Stahl K. 2017. Catchment water storage variation with elevation. *Hydrological Processes* 31 (11), 2000–2015. <https://doi.org/10.1002/hyp.11158>

Stehr A. & Aguayo M. 2017. Snow cover dynamics in Andean watersheds of Chile (32.0–39.5° S) during the years 2000–2016. *Hydrology and Earth System Sciences* 21 (10), 5111–5126. <https://doi.org/10.5194/hess-21-5111-2017>

Taillefer A., Guillou-Frottier L., Soliva R., Magri F., Lopez S., Courrioux G., Millot R., Ladouce B. & Le Goff E. 2018. Topographic and Faults Control of Hydrothermal Circulation Along Dormant Faults in an Orogen. *Geochemistry, Geophysics, Geosystems* 19 (12), 4972–4995. <https://doi.org/10.1029/2018GC007965>

Walter B., Géraud Y., Hauteville Y., Diraison M. & Raisson F. 2019. Fluid Circulations at Structural Intersections through the Toro-Bunyoro Fault System (Albertine Rift, Uganda): A Multidisciplinary Study of a Composite Hydrogeological System. *Geofluids*, 20 pp. <https://doi.org/10.1155/2019/8161469>

Wilson J.L. & Guan H. 2004. Mountain-block hydrology and mountain-front recharge. In: Hogan J.F., Phillips F.M. & Scanlon B.R. (Eds.), *Groundwater Recharge in a Desert Environment: The Southwestern United States*. American Geophysical Union 9, 113–137.

This page intentionally left blank

Architecture and fracture connectivity of the Pocuro Fault Zone

Abstract

The misunderstanding of hydrogeological processes together with the oversimplification of aquifer conceptual models result in numerous inaccuracies in the management of groundwater resources. In Central Chile, the hydrogeological studies were exclusively focused to alluvial aquifers on valleys (~15% of total area) and mountain front zones remain considered as no-flow boundary conditions. However, the hydrogeochemistry and isotopic analyses reveal that groundwater circulation in the mountain block recharge the Central Depression aquifers. Thus, the aim is to identify how the Western Andean Front recharges those aquifers. Given that the Pocuro Fault Zone (PFZ) is the contact among both domains, through a multi-scale structural mapping and a topological approach, the architecture of the PFZ and its connectivity degree is addressed. Regional-scale mapping show that N30-60W is the preferential orientation within the PFZ and three non-coetaneous major tectonic features were recognized: i) NS-oriented normal-sinistral faults surrounded by a damage zone constituted by veins filled with hydrothermal minerals, ii) NS-oriented reverse faults constituted by shear bands, and iii) NW-oriented reverse faults consisting in discrete fault planes. The latter fault system cuts and displaces the previous ones. Outcrop-scale mapping reveals that groundwater outflows from NW-oriented fractures. Topology allows us to quantify the connectivity degree of fractures within the PFZ and its relationship with groundwater circulation. Two areas of high density of connected fractures and nodes were identified ($>2.4 \text{ km/km}^2$ and 2.5 Nc/km^2). Both areas are spatially related to the main springs of PFZ: Termas de Jahuel and Termas El Corazón. The results indicate that within PFZ, the NS-oriented faults act as hydraulic barriers for groundwater by the presence of sealed fractures and shear bands. Whereas the NW-oriented faults act as high-permeability axes allowing the conduction of groundwater taking advantage the high density of PFZ connected fractures.

Keywords Cross-cutting relationship • Topology • Groundwater exploration • Oblique Basement Faults • Pocuro Fault Zone • Western Andean Front

5.1. ARCHITECTURE OF THE POCURO FAULT ZONE

5.1.1. Tectonics features at regional scale

At the regional scale (1:50,000) three major tectonic features within PFZ were recognized in the study area (Fig. 5.1a):

- Two major *ca.* NS-oriented and subvertical normal-sinistral faults marked by a series of aligned hills and valleys extending about 10 km each one (Fig. 5.1). These faults do not expose a well-defined core zone, though are characterized by a ~4 km wide damage zone where the typical outcrops consist of low-dip normal faults (Fig. 5.2a) and a dense network of veins filled by hydrothermal minerals with no preferential orientations (Fig. 5.2b). The density of veins increases approaching to the fault trace (field observation). In addition, a major extensional duplex is observed in the northern part of the study area, defined by minor N50-70W-oriented sinistral faults that are spatially to the *ca.* NS-oriented major faults (Fig. 5.1).
- A semi-continuous NS-oriented abrupt escarp expresses the surface trace of NS-oriented west vergent reverse fault (Fig. 5.1) extending at least 25 km. This reverse fault exposes a well-defined core zone consisting mainly in clay-rich shear bands (*i.e.* gouge) of ~30 cm thick surrounded by disseminated iron oxides halo (Fig. 5.2c). In addition, spatially associated with this reverse fault appear minor NS-N25W-oriented double vergent reverse faults, which display pop-up arrangements (Fig. 5.1).
- Several N45-60W-oriented morphostructural lineaments expressed by semi-continuous rectilinear and sub-parallel valleys oblique to the mountain front (Fig. 5.1). The bottom of these rectilinear valleys exhibits sub-parallel reverse faults without hydrothermal infill (Fig. 5.2d).

In addition, at the intersection of the NS-oriented faults (both normal-sinistral and reverse faults) with the NW-oriented reverse faults there are some minor cooper deposits and several springs outflow from the fractured rocks (Fig. 5.1a).

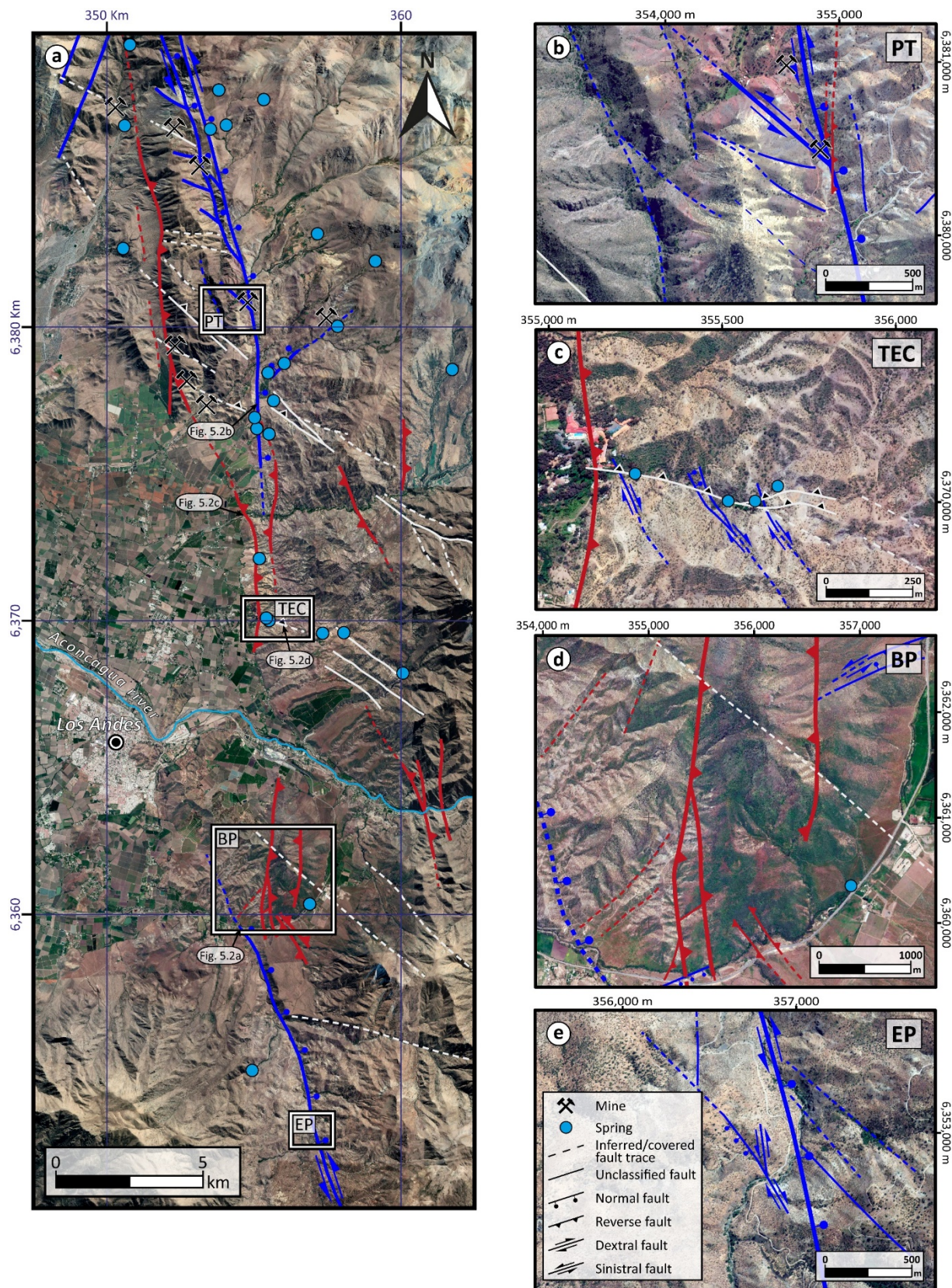


Fig. 5.1: a) Structural map for the study area and for each structural site: b) *Potrerillos* (PT), c) *Termas El Corazón* (TEC), d) *Bypass* (BP), and e) *Estero Pocuro* (EP). In blue the NS-oriented normal-sinistral faults, in red the NS-oriented reverse faults, and in white the NW-oriented reverse faults.

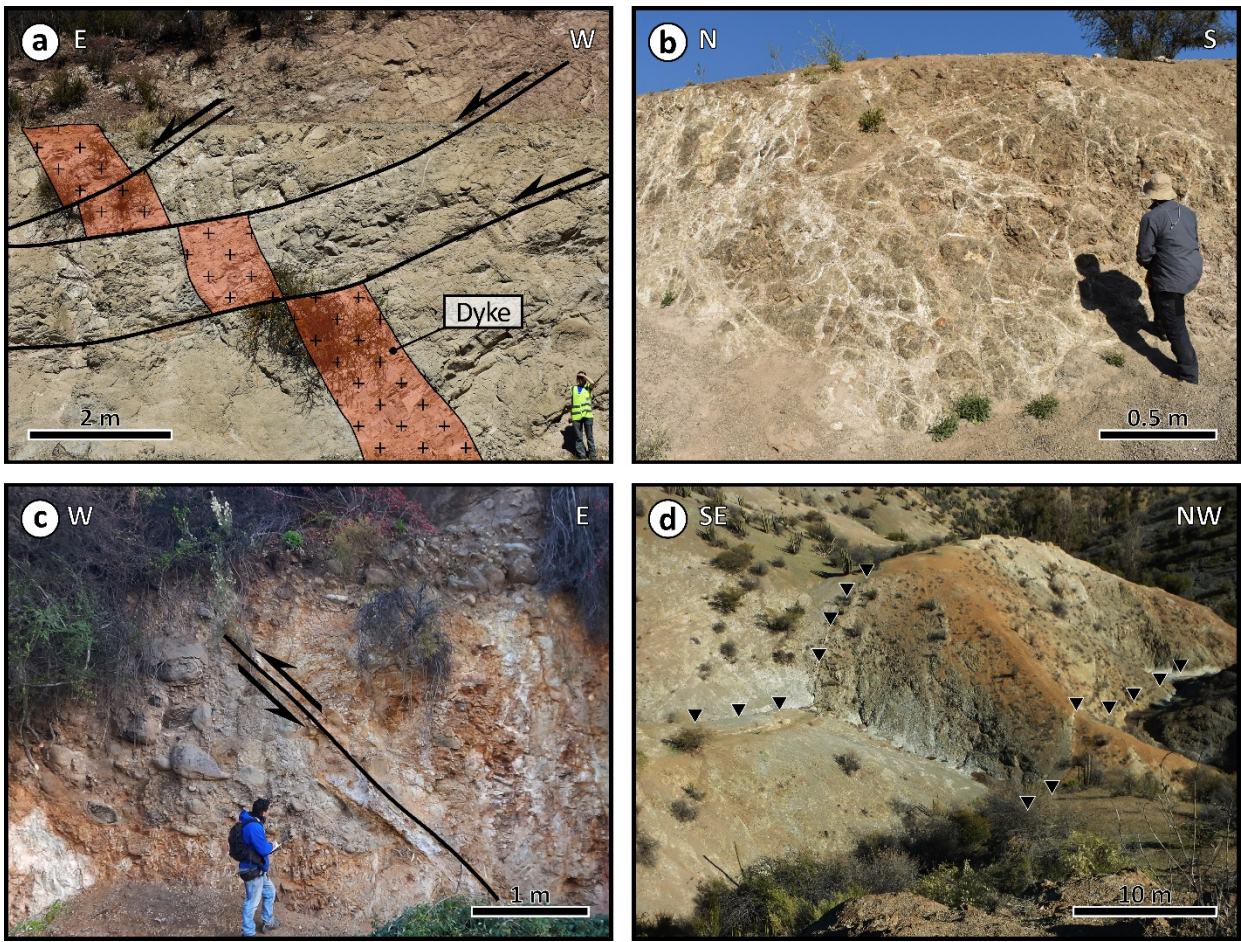


Fig. 5.2: Field photos showing the outcrops at metric-scale within the PFZ: a) N40-60E/30E normal faults cross-cutting a microdiorite dyke with an offset up to 80 cm; b) veins filled by hydrothermal minerals with no preferential orientations; c) N09S/60E reverse fault cross-cutting the Abanico Formation with an offset up to 3 m; and d) N70-80W/60E reverse faults (black triangles remark the fault trace).

5.1.2. Fracture patterns and relative timing from outcrop scale mapping

To establish the fracture patterns of the major faults, a total of 415 fractures and its interactions were described at the four structural sites (Fig. 5.3). In the study area the fractures are dominated by tensional ones ($n=283$) and a smaller number of hybrid ($n=46$) and shear fractures ($n=86$). The preferential orientation of tensional fractures (including veins and dykes) is N30-60E distributed especially in *Termas El Corazón* and *Bypass* structural sites (central sites), although in *Potrerillos* and *Esteros Pocuro* structural sites (ending sites) the preferential orientation is N20-50W (Fig. 5.3). The tensional fractures mainly comprise veins filled with clay-size hydrothermal minerals: laumontite-quartz assemblage ($n=211$), calcite ($n=40$) and composite veins ($n=9$). The latter veins are made of laumontite-quartz edge and calcite centre. The laumontite-quartz veins show a bimodal preferential orientation, N20-50W at the ending sites and N30-60E at the central sites (Fig. 5.4a). The calcite veins only appear at the central sites, and as the laumontite-quartz vein, they also show a bimodal preferential orientation

N30-60E and N60-80W (Fig. 5.4b). Finally, the composite veins do not show a preferential orientation (Fig. 5.4c). Overall, mostly veins have a dip angle between 60° and 90° and modal thickness of 2 mm (ranging from 1mm up to 35 mm). In turn, hybrid and shear fractures are more frequent in the outcrops of the central sites than in the ending ones, and do not show a preferential orientation (Fig. 5.3). The hybrid fractures are filled by laumontite-quartz assemblage or calcite, while the shear fractures typically show fault-plane and shear bands (fault breccia, cataclasite and gouge), in some cases surrounded by goethite-hematite.

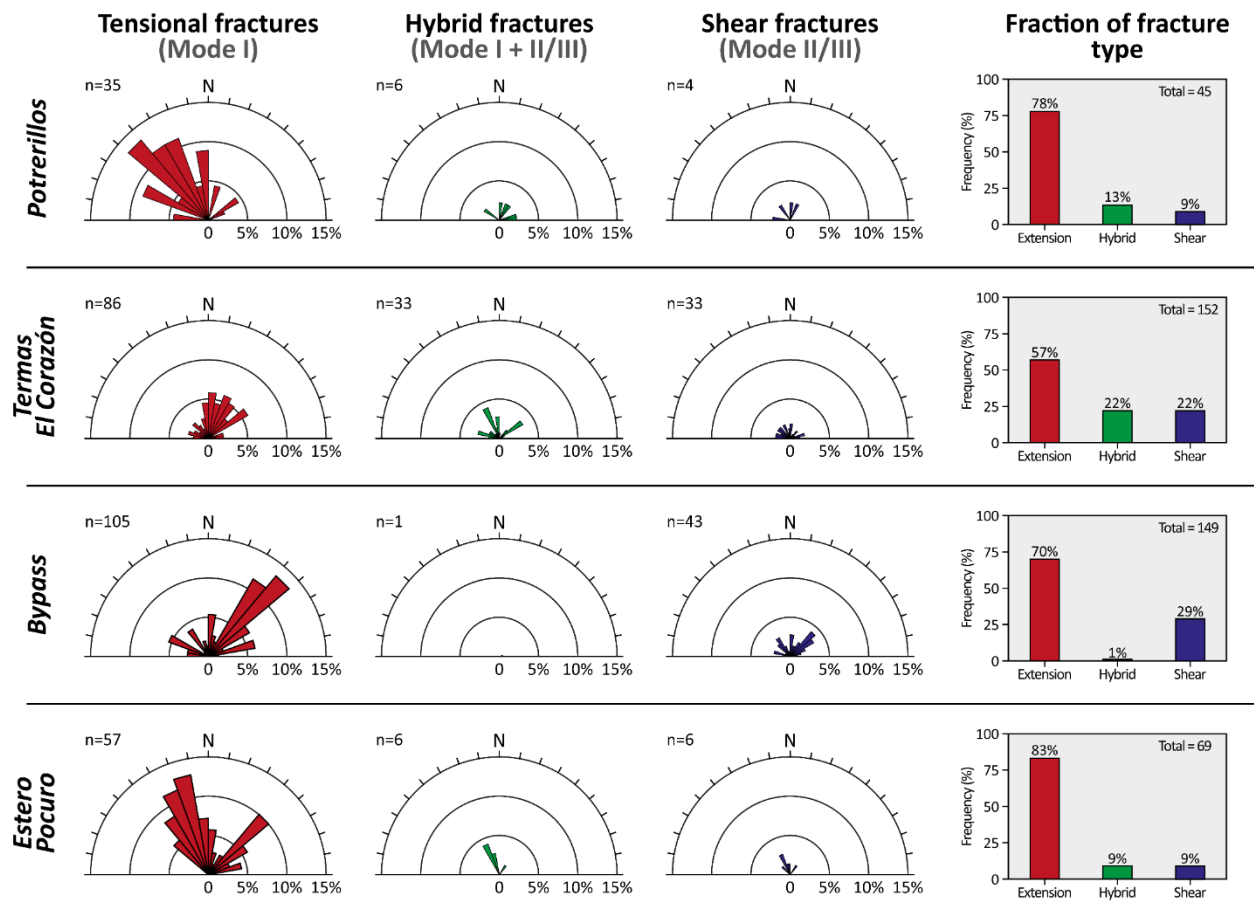


Fig. 5.3: Rose diagrams showing the orientation of fractures grouped according with the failure mode for each structural site. Size of the bars in the rose diagrams is the percentage of the fracture orientation in the structural site. The histograms show the proportion of each fracture type.

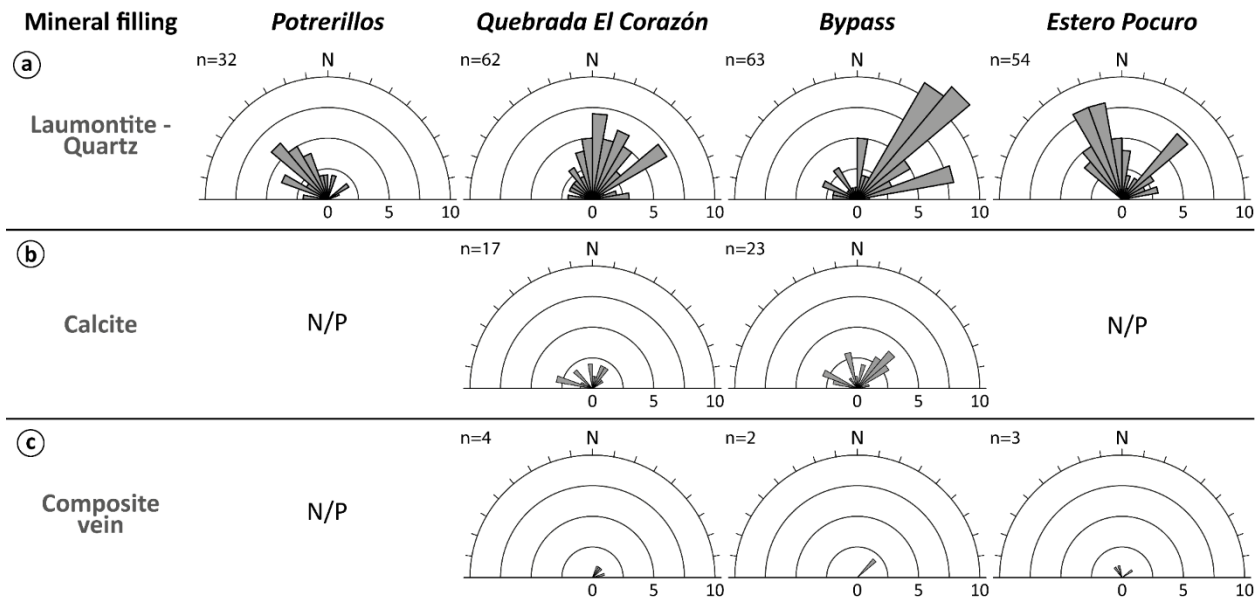


Fig. 5.4: Rose diagrams showing the orientation of the hydrothermal veins for each structural site: a) laumontite-quartz, b) calcite, and c) composite veins (laumontite-quartz edge and calcite centre). Size of the bars in the rose diagrams is the sum of the vein orientation in the structural site (N/P: No present).

Examining the fracture arrangements, kinematic and cross-cutting relationship, the fracture network within the PFZ reveals that is the result of a polyphase deformation. Indeed, the variety of fracture interactions exposed in the study area allows us to infer at least four brittle deformational stages (Table 5.1; Fig. 5.5), likely produced under different strain/stress fields:

(i) Stage I is related to the laumontite-quartz veins, usually displaying duplex arrangements (Fig. 5.5a and 5.5b). On the one hand, at the ending sites (*Potrillo*s and *Estero Pocuro*) N20-50W imbricates veins are geometrically associated with NNE- and NNW-oriented sinistral faults (or hybrid veins), resulting in sinistral duplexes. On the other hand, at the central sites (*Termas El Corazón* and *Bypass*) are common duplexes constituted by N30-60E- and N70-80W-oriented veins bounded by N10-30E dextral and EW sinistral faults, respectively. Such arrangements are also associated with N40-60E and N30-60W normal faults with an offset up to 80 cm in microdioritic dykes (Fig. 5.2a).

(ii) Stage II is related to the calcite veins that cross-cut the laumontite-quartz veins. The calcite veins rarely show geometric arrangements, but normally are spatially associated with N40-60E sinistral hybrid veins filled by calcite. These latter cut and displace the laumontite-quartz veins up to 6 cm (Fig. 5.5c). The cross-cutting relationship between laumontite-quartz and calcite veins, point that the composite veins (laumontite-quartz edge and calcite centre; Fig. 5.5d) result from the re-opening of previous formed laumontite-quartz veins, allowing the circulation of new fluids and the subsequent precipitation of calcite.

(iii) Stage III is related to NS-reverse faults with goethite-hematite slip-surface (Fig. 5.5e). Those faults cross-cut both laumontite-quartz and calcite fractures. Such faults are spatially associated with N45E-oriented sinistral-reverse and N70E-oriented dextral-reverse faults with disseminated goethite-hematite halo (Fig. 5.5f). Some of those faults display pop-up arrangements and unlike the laumontite-quartz and calcite fractures, these fractures do not show evidence of associated tensional fractures.

(iv) The Stage IV is related to N60-70W-oriented reverse faults. These faults are discrete fault planes without hydrothermal infill or shear bands, and cross-cut the previously described fractures. Topographic offset up to 60 cm in the surface is due to these faults (Fig. 5.5g). Normally appear at the bottom of valleys and based on field observation, a narrow relationship between these faults and groundwater. Specially in *Termas El Corazón* four springs occur aligned on the trace of a N70W-oriented reverse fault (Fig. 5.1c). In fact, the existence of excavated galleries exposes that groundwater is circulating today through these faults (See Sect. 5.2; Fig. 5.5h).

Then, the fractures that record different deformation stages were grouped into the major tectonic features. The laumontite-quartz and calcite fractures are typically found in the outcrops of the NS-oriented normal-sinistral faults. Therefore, these faults are characterized by tensional and sealed fractures developed during at least two deformational stages. The NS reverse faults with goethite-hematite slip-surface correspond to the outcrops of NS-oriented reverse faults, and the N60-70W and N70-80E reverse faults correspond to NW-reverse faults outcrops.

Since the hydrogeological point of view, the presence of sealed fractures in the NS-oriented normal-sinistral faults (Fig. 5.2b) and shear bands along the NS-oriented reverse faults (Fig. 5.2c) indicate that NS-oriented faults in the PFZ are very low-permeability structures (regardless the relative deformation time). Conversely, the NW-oriented reverse faults are discrete fault planes, without the presence of any hydrothermal mineral or clay-rich shear bands, and consequently, these faults are likely high-permeability structures.

Major tectonic features	Deformation stage	Fracture type	Preferential orientation	Dip angle	Mineral association	Internal structure	Fracture arrangements
NS normal-sinistral faults	i	Veins, normal faults, dextral and sinistral hybrid veins	N20-50W, N30-60E	60-90	Laumontite-quartz	Massive	Duplex
	ii	Veins, sinistral hybrid veins	N60-80W, N30-60E	60-90	Calcite	Banded vein	-
NS reverse fault	iii	Reverse fault	NS	60-90	Goethite-hematite	Shear band	Pop-up
NW reverse faults	iv	Reverse fault	N60-70W	20-60	-	-	-

Table 5.1: Summary of the major tectonic features and its intern fracture patterns. Mineral recognition from the X-ray diffraction.

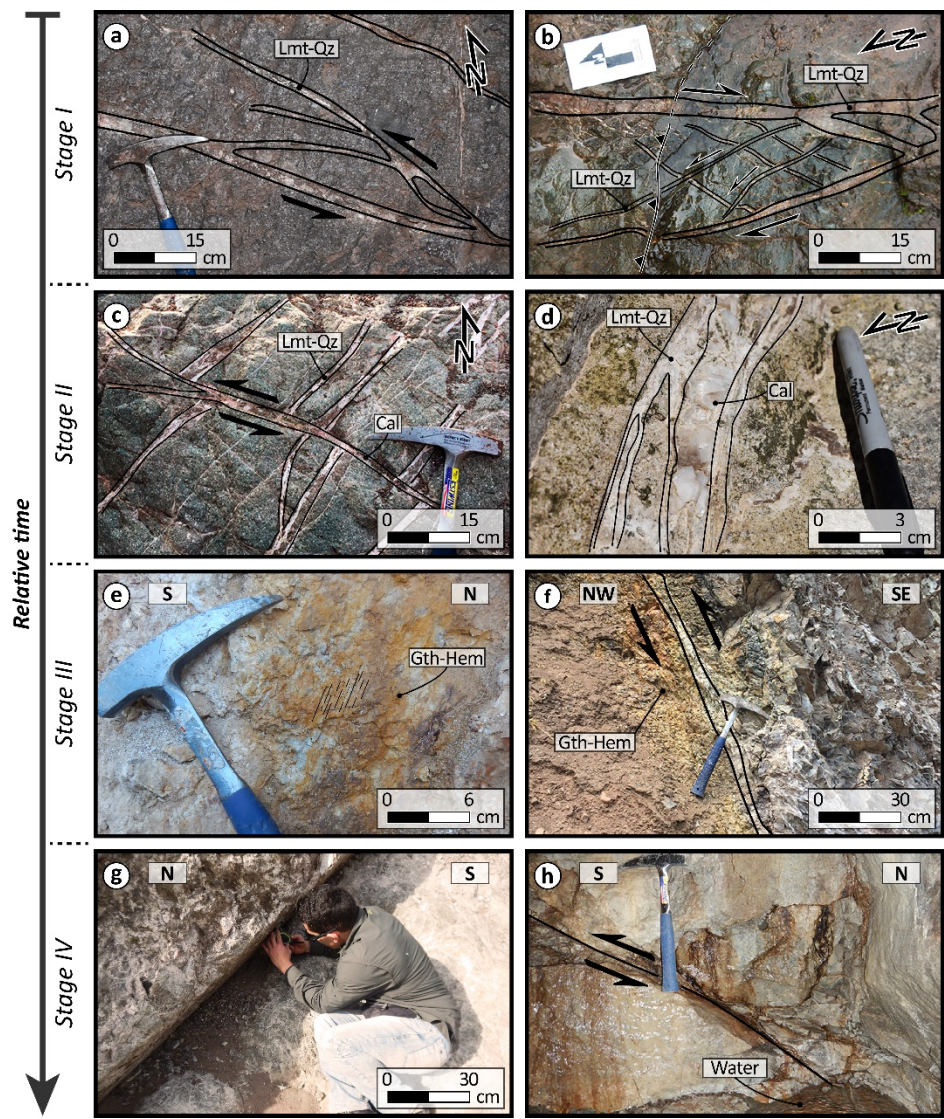


Fig. 5.5: Photographs of the outcrops and relative timing of the different fractures in the study area (Cal, calcite; Gth, goethite; Hem, hematite; Lmt, laumontite; Qz, quartz).

5.2. FRACTURE ANALYSIS AND CONNECTIVITY OF THE POCURO FAULT ZONE

Once established the internal architecture of the Pocuro Fault Zone, is necessary to evaluate the connectivity degree of this fracture network and the relation with the groundwater resources along the Western Andean Front. In order to address the connectivity degree, a total of 216 morphostructural lineaments were digitized at the scale of the study area (Fig. 5.6). In addition, at the outcrop scale a total of 152 and 45 fractures were mapped at *Termas El Corazón* and to the east of *Termas de Jahuel*, respectively.

At the scale of the study area, the analysis of the fracture network shows that the damage zone of PFZ is governed by a N30-60W preferential orientation (Fig. 5.7a). At the outcrop scale, a well-defined N30-50W preferential orientation characterizes the fracture network near *Termas de Jahuel*, while no one preferential orientation pattern is observed in *Termas El Corazón* (Fig. 5.7c). This missing preferential orientation pattern may result from the PFZ complexity related to the different tectonic events (Fig. 5.5). But, into both galleries, excavated for increasing the groundwater discharge, it was observed that groundwater outflows from N40-60W fractures (*e.g.* Fig. 5.5h). At *Termas El Corazón*, the NW-oriented fractures are associated to an NW-oriented reverse fault that controls the landscape in the gully orientation, where several springs outflow (Fig. 5.1c). At about *Termas de Jahuel*, the spring is related to buried NW-oriented reverse fault (local landslide), which outcrop to the east as visible in the structural map (Fig. 5.1a).

A total of 472 nodes and 511 branches were extracted from the fracture network (Fig. 5.7b): 228 I-nodes, 194 Y-nodes and 50 X-nodes as well as 25 I-I branches, 169 C-I branches, 305 C-C branches and 12 Unk branches. The topological analysis highlights two areas of high density of connected fractures (Fig. 5.7c) and connected nodes (Fig. 5.7d), both related to the main springs of the PFZ. The first one, related to the area in the east of *Termas de Jahuel* (<5 km), shows a density of fractures and connected nodes reaching 2.4 km/km^2 and 2.5 Nc/km^2 , respectively; while the second one, related to *Termas El Corazón*, shows a density of fractures and connected nodes reaching 3.3 km/km^2 and 5.5 Nc/km^2 , respectively.

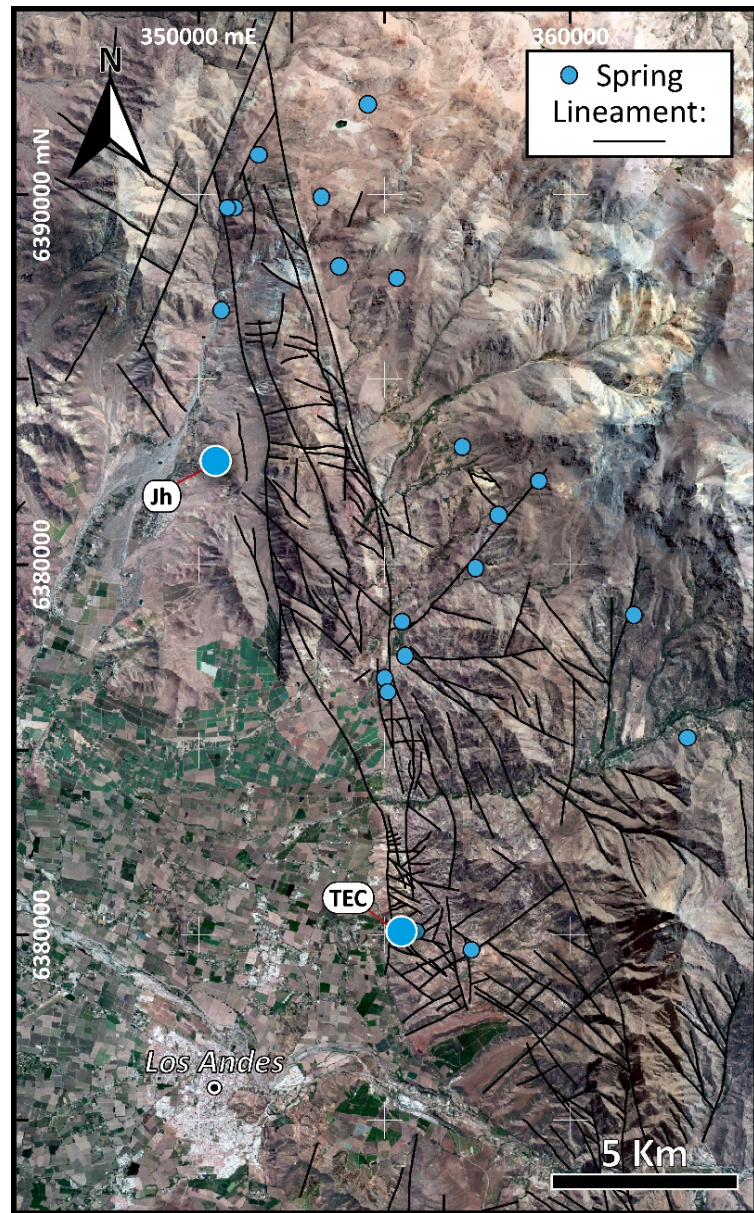


Fig. 5.6: Morphostructural lineaments map of the PFZ. The major springs of the study area are highlighted: *Termas de Jahuel* (Jh) and *Termas El Corazón* (TEC).

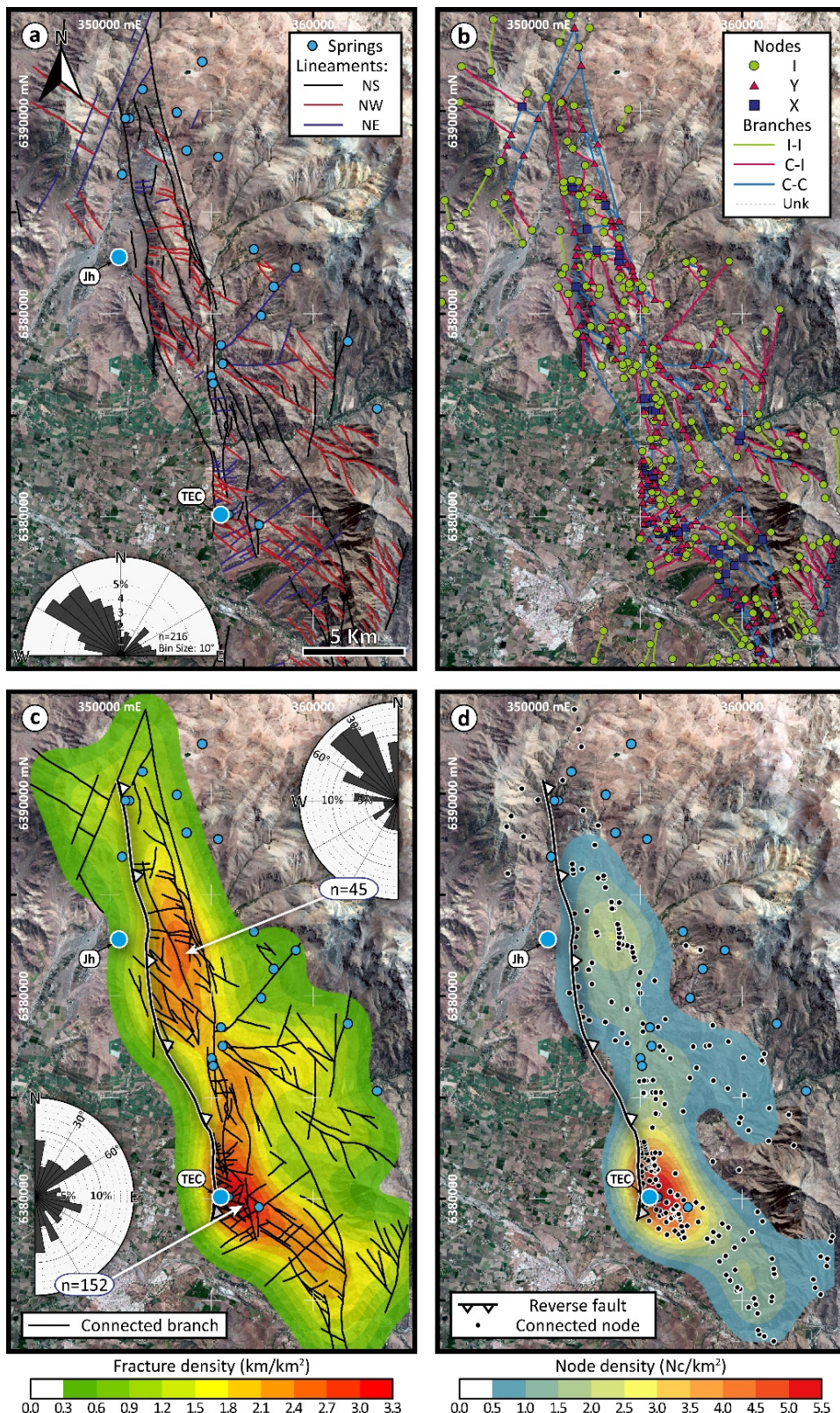


Fig. 5.7: Topological analysis of the fracture network in the Pocuro Fault Zone (PFZ). a) Orientations of the fracture network. Rose diagram shows the orientation of mapped lineaments with bin size 10°. b) Topological characterization of the fracture network. c) Contour map showing the density of connected branches (C-I and C-C branch). Rose diagrams (bin size 10°) show the orientation of fractures mapped from representative areas at *Termas El Corazón* (TEC) and to the east of *Termas de Jahuel* (Jh). d) Contour map showing the density of connected nodes ($N_c = Y\text{-node} + X\text{-node}$).

5.3. THE OBLIQUE BASEMENT FAULTS

The observed topological relation between the density of fractures, connected nodes and springs, together with the observed congruence between the orientation of fractures in both galleries and areas into the PFZ damage zone indicates that the NW orientation is a main groundwater-drainage axis. NW-fractures, oblique to the main NS-oriented fault trace of PFZ, would drain most groundwater into the PFZ damage zone, taking advantage of a higher density of connected fractures than into the Principal Cordillera (Fig. 5.7c and 5.7d). Oyarzún *et al.* (2017) and Piquer *et al.* (2019) showed that in Central Chile, the NW- and NE-oriented basement faults are spatially related to the main springs and shallow groundwater circulation in hard rocks, but also to some productive wells (some of them discharging greater than 36 m³/h; Oyarzún *et al.* 2017). Yáñez *et al.* (2015) demonstrated by geophysical exploration (gravity surveys supported by magnetic and geoelectrical surveys) that NW- and NE-oriented fractures, structurally related to basement faults and oblique to the Western Andean Front, are continued into the Central Depression below the Quaternary cover. At a regional scale, it has been determined the first-order control of both geothermal surface manifestations and active volcanism are by NW-oriented long-lived crustal faults, regionally known as Andean Transverse Faults (Cembrano and Lara, 2009; Sánchez-Alfaro *et al.* 2013; Tardani *et al.* 2016; Veloso *et al.* 2019). The preferential circulation of fluids (including hydrothermal fluids) along the oblique-to-the-arc faults is due to a NS preferential extension direction leading to the opening of interconnected fractures along these faults, with respect to the main EW compression of the Nazca plate subduction (Veloso *et al.* 2019). Therefore, the NW-faults are discrete high-permeability axes crossing the PFZ and contributing likely to recharge of the San Felipe aquifer in the Central Depression (Fig. 5.8).

This hydrogeological consideration agrees with mountain front conceptual models (Wilson and Guan, 2004; Markovich *et al.* 2019). These conceptual models highlight the role of oblique basement faults (crossing the mountain front zone) into the focused recharge of adjacent alluvial aquifers by conducting groundwater circulation flowing from the fractured mountain block (Fig. 5.8). Such a recharge process, also known as lateral groundwater transfer, was likewise observed in others mountain front zones, such as in the Basin and Range Province of USA (Wilson and Guan, 2004), East African Rift Valley (Kebede *et al.* 2008; Walter *et al.* 2019) and in the eastern part of the Pyrenean range in Europe (Taillefer *et al.* 2018). Considering the worldwide conceptual models of mountain hydrogeology, in this work the NW-oriented faults are named as Oblique Basement Faults (OBF; Fig. 5.8).

Consequently, the hydrogeological insights defined for the PFZ in the Aconcagua Basin (strengthened by results acquired at different scales) allow to extrapolate this groundwater recharge process to the whole Western Andean Front in Central Chile. Deep flows originating from the Principal

Cordillera and circulating through basement faults have probably long residence times (regional groundwater circulation) and may constitute non-renewable groundwater resources. Thus, the recharge of adjacent alluvial aquifers caused by deep flows through Oblique Basement Faults is expected to be little impacted by the current megadrought (Garreaud *et al.* 2017, 2019). However, most springs are fed by shallower flows that originate from the focused infiltration of precipitation and snowmelt taking place above 2000 m a.s.l in the Western Andean Front (Taucare *et al.* 2020). Those springs are more vulnerable to short-term hydroclimatic changes. Therefore, the decrease over the last decade in both precipitation rates (Garreaud *et al.* 2017, 2019) and snowpack in high elevation Andes (Ohlanders *et al.* 2013; Ruiz Pereira *et al.* 2019) is expected to have a dramatic impact on the availability of groundwater resources along the Western Andean Front. Consequently, the local communities dependent on this resource for drinking water supply and agricultural activities will be affected.

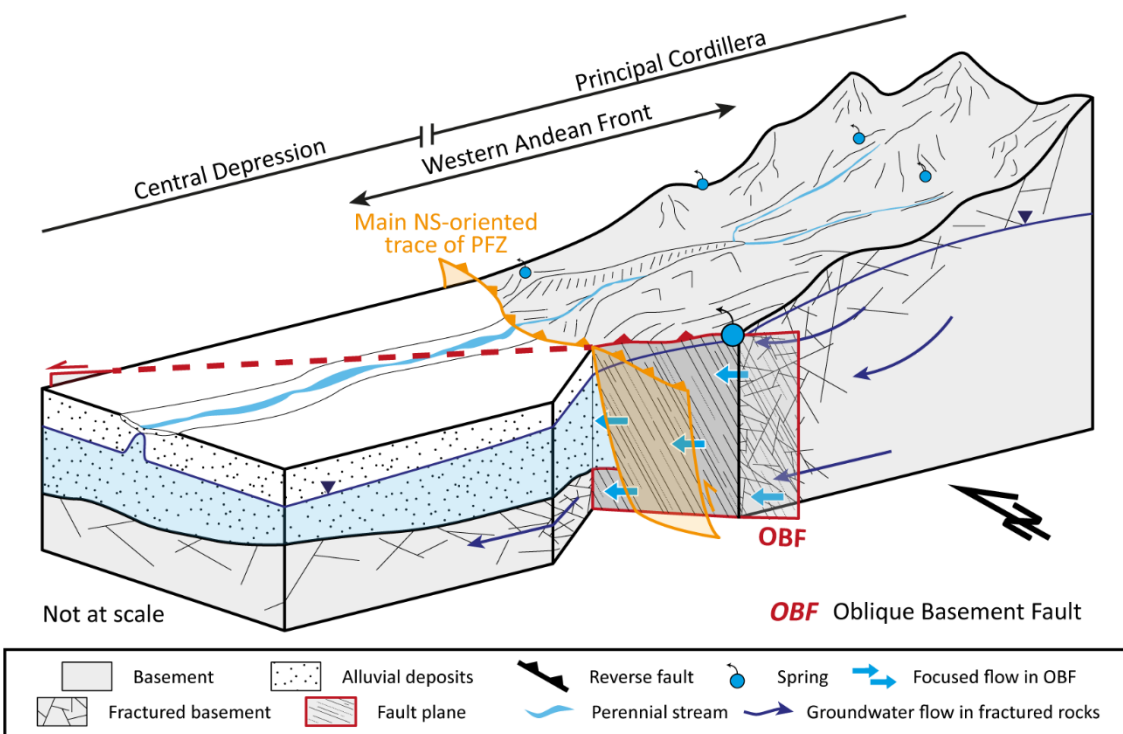


Fig. 5.8: Western Andean Front hydrogeological diagram highlighting the role of the Oblique Basement Faults with respect to groundwater circulation and the recharge of adjacent alluvial aquifers. The size of each spring symbol reflects its flow rate (large spring symbol represents a high flow while the small ones have a lower flow).

REFERENCES

- Cembrano J. & Lara L. 2009. The link between volcanism and tectonics in the southern volcanic zone of the Chilean Andes: A review. *Tectonophysics* 471 (1-2). 96-113. <https://doi.org/10.1016/j.tecto.2009.02.038>
- Garreaud R.D., Alvarez-Garreton C., Barichivich J., Boisier J.P., Christie D., Galleguillos M., LeQuesne C., McPhee J. & Zambrano-Bigiarini M. 2017. The 2010–2015 megadrought in central Chile: impacts on regional hydroclimate and vegetation. *Hydrology and Earth System Sciences* 21 (12), 6307–6327. <https://doi.org/10.5194/hess-21-6307-2017>
- Garreaud R.D., Boisier J.P., Rondanelli R., Montecinos A., Sepúlveda H.H. & Veloso-Aguila D. 2019. The Central Chile Mega Drought (2010–2018): A climate dynamics perspective. *International Journal of Climatology*, 1-19. <https://doi.org/10.1002/joc.6219>
- Kebede S., Travi Y., Asrat A., Alemayehu T., Ayenew T. & Tessema Z. 2008. Groundwater water origin and flow along selected transects in Ethiopian rift volcanic aquifers. *Hydrogeology Journal* 16 (1), 55-73. <https://doi.org/10.1007/s10040-007-0210-0>
- Markovich K.H., Manning A.H., Condon L.E. & McIntosh J.C. 2019. Mountain-block Recharge: A review of Current Understanding. *Water Resources Research*, 55. <https://doi.org/10.1029/2019WR025676>
- Ohlanders N., Rodriguez M. & McPhee J. 2013. Stable water isotope variation in a Central Andean watershed dominated by glacier and snowmelt. *Hydrology and Earth System Sciences* 17, 1035–1050. <https://doi.org/10.5194/hess-17-1035-2013>
- Oyarzún R., Oyarzún J., Fairley J.P., Núñez J., Gómez N., Arumí J.L. & Maturana H. 2017. A simple approach for the analysis of the structural-geologic control of groundwater in an arid rural, mid-mountain, granitic and volcanic-sedimentary terrain: The case of the Coquimbo Region, North-Central Chile. *Journal of Arid Environments* 142, 31–35. <https://doi.org/10.1016/J.JARIDENV.2017.03.003>
- Piquer J., Yañez G., Rivera O. & Cooke D.R. 2019. Long-lived crustal damage zones associated with fault intersections in the high Andes of Central Chile. *Andean Geology* 46, 223-239. <https://doi.org/10.5027/andgeoV46n2-3106>
- Ruiz-Pereira S.F. & Veetil B.K. 2019. Glacier decline in the Central Andes (33°S): Context and magnitude from satellite and historical data. *Journal of South American Earth Sciences* 94, 102249. <https://doi.org/10.1016/j.jsames.2019.102249>
- Sánchez-Alfaro P., Pérez-Flores P., Arancibia G., Cembrano J. & Reich M. 2013. Crustal deformation effects on the chemical evolution of geothermal systems: the intra-arc Liquiñe–Ofqui fault system, Southern Andes. *International Geology Review* 55 (11). <http://dx.doi.org/10.1080/00206814.2013.775731>
- Taillefer A., Guillou-Frottier L., Soliva R., Magri F., Lopez S., Courrioux G., Millot R., Ladouce B. & Le Goff E. 2018. Topographic and Faults Control of Hydrothermal Circulation Along Dormant Faults in an Orogen. *Geochemistry, Geophysics, Geosystems* 19 (12), 4972-4995. <https://doi.org/10.1029/2018GC007965>

- Tardani D., Reich M., Roulleau E., Takahata N., Sano Y., Pérez-Flores P., Sánchez-Alfaro P., Cembrano J. & Arancibia G. 2016. Exploring the structural controls on helium, nitrogen and carbon isotope signatures in hydrothermal fluids along an intra-arc fault system. *Geochimica et Cosmochimica Acta* 184, 193-211. <https://doi.org/10.1016/j.gca.2016.04.031>
- Taucare M., Daniele L., Viguier B., Vallejos A & Arancibia G. 2020. Groundwater resources and recharge processes in the Western Andean Front of Central Chile. *Science of The Total Environment* 722, 137824. <https://doi.org/10.1016/j.scitotenv.2020.137824>
- Veloso E., Tardani D., Elizalde D., Godoy B., Sánchez-Alfaro P., Aron F., Reich M. & Morata D. 2019. A review of the geodynamic constraints on the development and evolution of geothermal systems in the Central Andean Volcanic Zone (18–28°Lat.S). *International Geology Review*, 1-25. [10.1080/00206814.2019.1644678](https://doi.org/10.1080/00206814.2019.1644678)
- Walter B., Géraud Y., Hauteville Y., Diraison M. & Raisson F. 2019. Fluid Circulations at Structural Intersections through the Toro-Bunyoro Fault System (Albertine Rift, Uganda): A Multidisciplinary Study of a Composite Hydrogeological System. *Geofluids*, 20 pp. <https://doi.org/10.1155/2019/8161469>
- Wilson J.L. & Guan H. 2004. Mountain-block hydrology and mountain-front recharge. In: Hogan J.F., Phillips F.M. & Scanlon B.R. (Eds.), *Groundwater Recharge in a Desert Environment: The Southwestern United States*. American Geophysical Union 9, 113–137.
- Yáñez G., Muñoz M., Flores-Aqueveque V. & Bosch A. 2015. Gravity depth to basement in Santiago Basin, Chile: implications for its geological evolution, hydrogeology, low enthalpy geothermal, soil characterization and geo-hazards. *Andean Geology* 42 (2), 147–172. <https://doi.org/10.5027/andgeoV42n2-a01>

This page intentionally left blank

6

Conclusion

6.1. THE CONCEPTUAL MODEL OF THE WESTERN ANDEAN FRONT

The Western Andean Front is a morphotectonic transition zone between the Principal Cordillera and the Central Depression, and it is shaped by NS-oriented faults (Armijo *et al.* 2010; Farias *et al.* 2010; Vargas *et al.* 2014). Through this thesis, the capacity of the Western Andean Front that allows it to be able to transfer groundwater from the Principal Cordillera up to the Central Depression aquifers at the downstream was explored.

The first step required the assessment of the groundwater circulation and the recharge processes occurring in the Western Andean Front (Fig. 6.1a). From the upstream to the downstream, the samples show a clear negative correlation between the groundwater mineralization and its position along the Western Andean Font (Fig. 6.1b): the groundwater mineralization increases progressively from the low-mineralized springs on high to the groundwater of the San Felipe aquifer in lowlands. Groundwater composition at high elevation is poorly influenced by water-rock interaction, but along the Western Andean Front the groundwater composition results predominantly from this process. Considering the anorthite dissolution as the principal hydrogeochemical process, with a dissolution rate of 5.08×10^{-14} mol/m²s at 25 °C/1 atm (Brantley *et al.* 2008), the current concentration of Ca and HCO₃ in groundwater is estimated within 50 years on high and about 1500 years in the basin. Nevertheless, more accurate estimations require reactive transport models, which translate the conceptual models into the mathematics world allowing the quantification of subsurface environmental processes including coupled processes (Steefel *et al.* 2005, 2017; Li *et al.* 2017; Maher and Mayer, 2019). As the proportion of major elements is preserved along the flow path (Fig. 6.1c), the variation of mineralization in the Western Andean Front is due to an increase of the residence time.

The flow path in the Western Andean Front begins in high-elevation areas (>2200 m asl) by the storage of snowmelt and rainstorms in shallow alluvial deposits (*e.g.* talus deposits; Fig. 6.2) (Pourrier *et al.* 2014; Janke *et al.* 2017; Burger *et al.* 2018). The release of such groundwater stored is a primary source of

the groundwater recharge for Western Andean Front hydrogeological systems and ensures the shallow groundwater circulation even during dry years (Ohlanders *et al.* 2013; Rodriguez *et al.* 2016; Stehr and Aguayo, 2017; Schaffer *et al.* 2019). At lower elevations (<2200 m asl), runoff and sub-surface circulation coming from higher-elevation areas leads the focused recharge along the fractured bottom of the mid-mountain gullies (Fig. 6.2). To the downstream, the mountain-block recharge (Wilson and Guan, 2004) is due to groundwater flows coming from the Western Andean Front and circulating by well-connected fractures area (PFZ) up to the downstream adjacent alluvial basin (Fig. 6.2). In the piedmont, the focused infiltration in coarse alluvial deposits of both perennial and ephemeral streams allow the mountain front recharge (Fig. 6.2).

Once determined the hydrogeological connection between the Western Andean Front and the Central Depression, the second step is required to establish the role of the cortical faults in the groundwater circulation. In the Aconcagua Basin, the Pocuro Fault Zone (PFZ) separates the volcanic rocks of the Principal Cordillera (mountain-block domain) from the alluvial deposits of the Central Depression (alluvial domain). Thereby, unravelling the PFZ architecture will reveal how is the hydrogeological connection between both domains. Through the multi-scale structural mapping and the topological approach was determined that the PFZ is a high-connected fracture network resulting from different tectonic events (Fig. 6.3a).

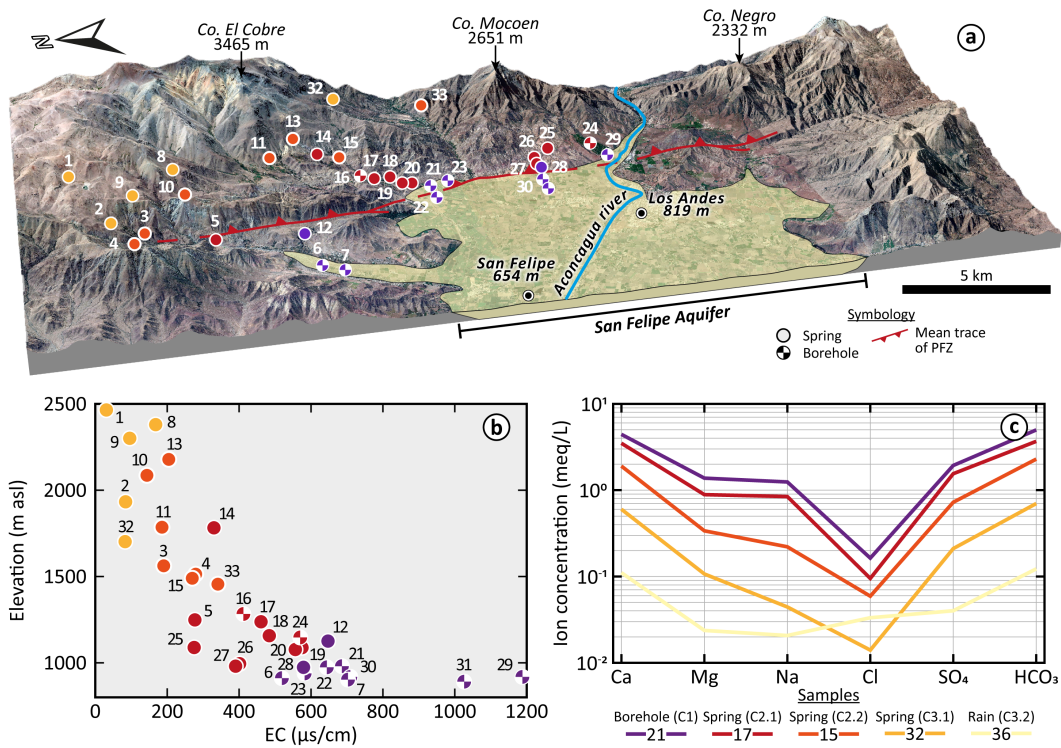


Fig. 6.1: a) Location of groundwater samples at the study area (colours of the samples are related to the HCA clusters). b) electrical conductivity *vs.* elevation (m asl) of groundwater samples, and c) Schoeller-Berkaloff diagram from selected samples.

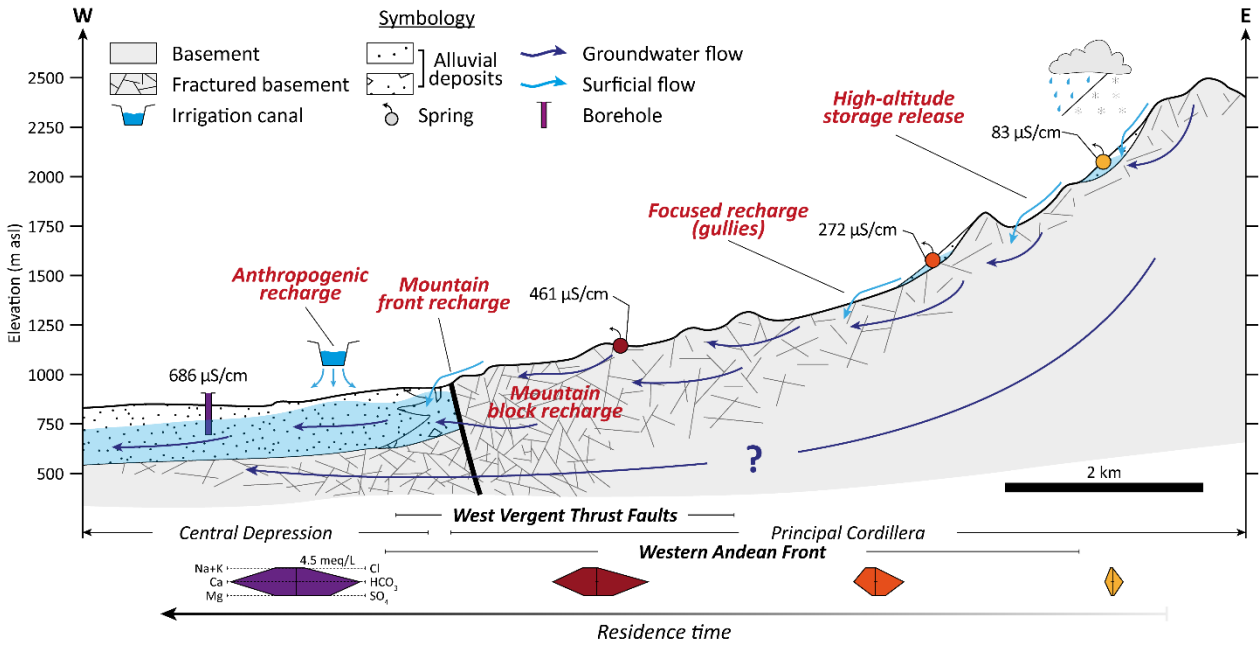


Fig. 6.2: Recharge processes along the Western Andean Front. The average of groundwater composition according to the location is represented by the Stiff diagrams (colours are related to the HCA clusters).

On one hand, the findings reveal NS-oriented faults are characterized by a clay-rich core zone: sealed fractures (clay-size hydrothermal minerals) and gouge (clay-rich shear band). A recent hydrogeophysical study in the PFZ (Figueroa, 2020), described the NS-oriented clay-rich faults on geoelectrical profiles as low resistivity subvertical bands contrasting with the surrounding domain (<60 Ω·m; Fig. 6.3b, c). The low resistivity values are typical of clay in saturated conditions (e.g. Descloretes *et al.* 2013). Also, these faults extend for at least 200 m below ground surface (Fig. 6.3b, c). Although diffuse mountain-block recharge may occur (Wilson and Guan, 2004; Markovich *et al.* 2019), the NS-oriented faults in the PFZ are very low-permeability structures and hence they act as hydraulic barriers that limit the groundwater circulation originating from the mountain block (Fig. 6.4).

On the other hand, the Oblique Basement Faults (OBF) are discrete fault planes driving groundwater, without the presence of any hydrothermal mineral or shear bands. Unlike the NS-oriented faults the resolution of geoelectrical survey does not permit to detect those discrete structures (Figueroa, 2020). The cross-cutting relationship allows establishing that the OBF represent the last deformation stage in the study area and they continue into the Central Depression basement below the alluvial deposits (Yáñez *et al.* 2015). Therefore, the OBF are high-permeability structures that contribute to recharge the Central Depression alluvial aquifers through focused flows (Fig. 6.4). Moreover, the hydrogeological connection between both domains is enhanced by the high degree of connected fractures within the PFZ (detectable up to ~80 m below the ground surface in the mountain block; Fig. 6.3b).

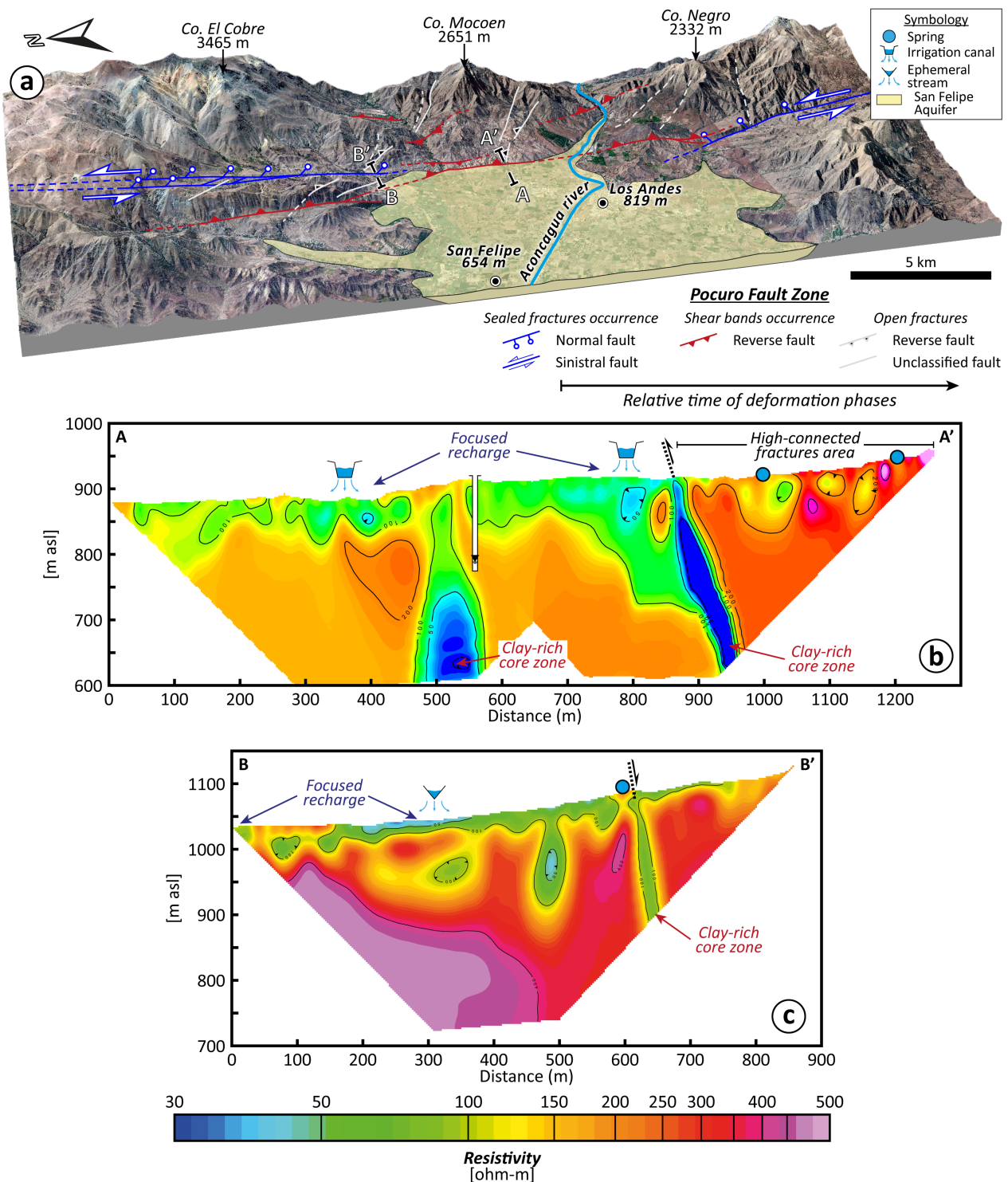


Fig. 6.3: a) Summary of the main faults identified within the PFZ. b) and c) geoelectrical profiles transversal to the mountain front and to a perched valley in the mountain block, respectively (from Figueroa, 2020).

In addition to the recharge processes related to the fractured media, both focused infiltration from ephemeral streams in perched valleys located as well as from irrigation canal excavated in the ground also contribute to recharge the Central Depression alluvial aquifer (Fig. 6.3a, b). The focused infiltration of ephemeral streams originated on high allow recharge the coarse alluvial deposits in perched valleys. These latter constitute high-permeability ($1.4 \cdot 10^{-3} \text{ m}^2/\text{s}$) alluvial corridors that enable the hydraulic continuity from the perched valley up to the Central Depression aquifers (Figueroa, 2020). In turn, perennial streams derived from high elevation areas are rapidly transferred down to irrigation canals localized in the Central Depression. Both cases support the renewal of the Central Depression aquifers during dry years (Fig. 6.4).

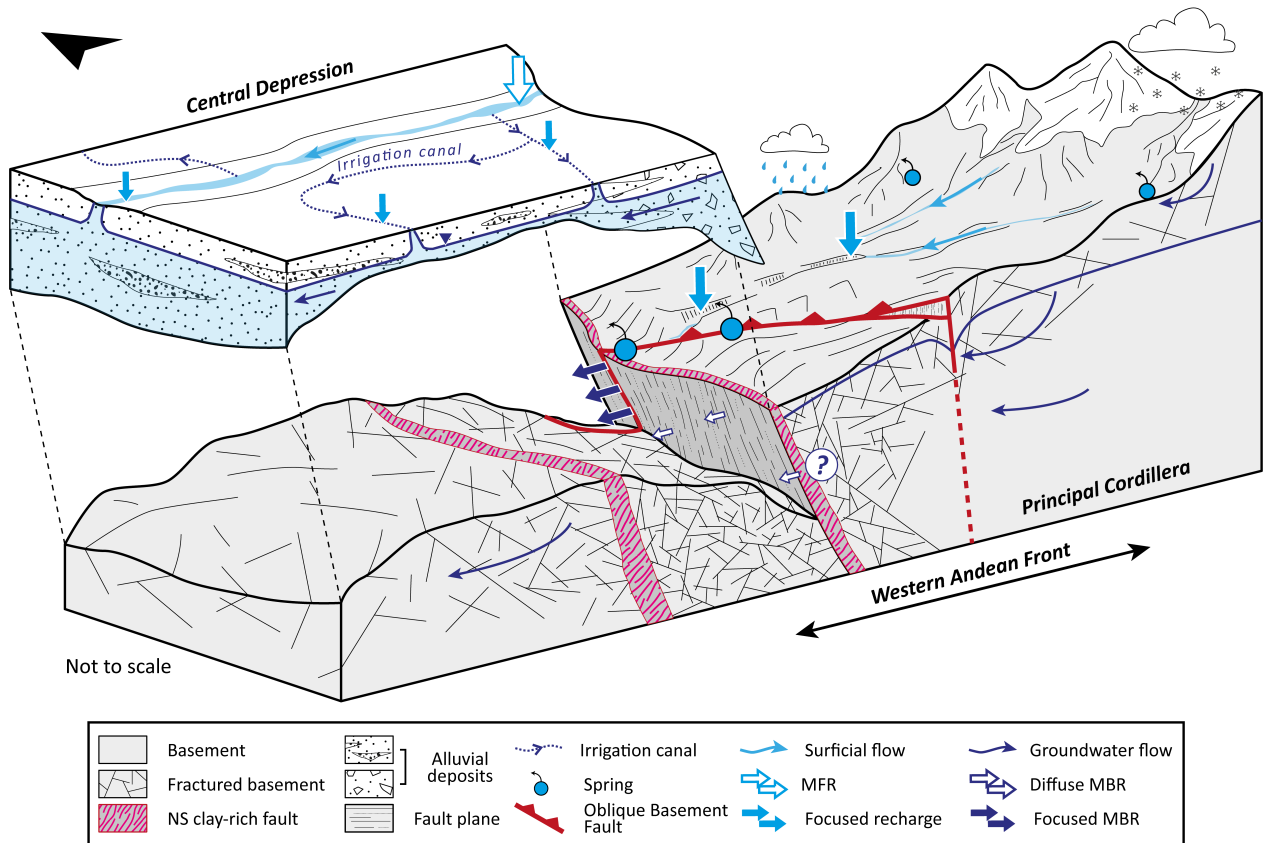


Fig. 6.4: Hydrogeological conceptual model of the Western Andean Front at Central Chile (surficial flow comprises both perennial and ephemeral streams).

6.2. SUMMARY AND FUTURE INSIGHTS

This research addresses the groundwater resources and related recharge processes in the Western Andean Front (Central Chile; Fig. 6.4) at the Aconcagua Basin by means of hydrogeochemical and water isotopes analyses, structural geology, and a topological approach. Unlike former considerations, the existence of groundwater circulation in fractured rocks originating from rain and snowmelt above ~2000 m asl was demonstrated. Groundwater recharge in the Western Andean Front occurs in gullies at mid-elevation as well as in perched valleys. The Oblique Basement Faults, crossing the main NS-oriented fault trace of PFZ, allow draining groundwater from the Principal Cordillera taking advantage of the high-density of connected fractures in the PFZ. Consequently, mountain-block recharge processes contribute to recharge the Central Depression alluvial aquifers. Both perennial and ephemeral streams originated on high areas allow the mountain-front recharge. In addition, it is demonstrating that dug irrigation canals (that conduct water from high-elevation areas) play a significant role in the recharge of Central Depression aquifers. The previous findings are in line with observations and results obtained in other mountainous zones around the world. Therefore, the current and simplistic hydrogeological view of the Western Andean Front (*i.e.* an impervious limit) is not completely right and required additional detailed studies.

Groundwater in the Western Andean Front has a high-quality according to the national (NCh409/1 and Decree 106) and international (WHO) limits of element concentrations for different water-uses (drinking water, mineral bottle water, thermal baths and irrigation). However, intensive agriculture practices in the Central Depression lead to a decline of the groundwater quality in alluvial aquifers by an increase of potentially hazardous elements for human-health.

Considering the increasing climatic and anthropogenic pressures in Central Chile, a thorough revision of the hydrogeological conceptual models is suggested. This study highlights the Western Andean Front as an interesting target for the exploration of groundwater resources and given the similar morphotectonic and hydroclimatic setting, this model is suitable for Central Chile. Thus, these new insights into hydrogeological models will help to assess the water resource management policies in Chile in a better way. However, further researches are still required to improve the groundwater recharge quantifying and to characterize its vulnerability to near future hydroclimatic changes.

REFERENCES

- Armijo R., Rauld R., Thiele R., Vargas G., Campos J., Lacassin R. & Kausel E. 2010. The West Andean Thrust, the San Ramón Fault, and the seismic hazard for Santiago, Chile. *Tectonics* 29 (2), TC2007. <https://doi.org/10.1029/2008TC002427>
- Brantley S.L., Kubicki J.D. & White A.F. 2008. Kinetics of Water-Rock Interaction. Springer, 833 pp. <https://doi.org/10.1007/978-0-387-73563-4>
- Burger F., Ayala A., Farias D., Shaw T.E., MacDonell S., Brock B., McPhee J. & Pellicciotti F. 2018. Interannual variability in glacier contribution to runoff from a high-elevation Andean catchment: understanding the role of debris cover in glacier hydrology. *Hydrological Processes* 33 (2), 214-229. <https://doi.org/10.1002/hyp.13354>
- Descloitres M., Chalikakis K., Legchenko A., Moussa A.M., Genthon P., Favreau G., Le Coz M., Boucher M. & Oï M. 2013. Investigation of groundwater resources in the Komadugu Yobe Valley (Lake Chad Basin, Niger) using MRS and TDEM methods. *Journal of African Earth Sciences* 87, 71-85. <https://doi.org/10.1016/j.jafrearsci.2013.07.006>
- Farías M., Comte D., Charrier R., Martinod J., David C., Tassara A., Tapia F. & Fock A. 2010. Crustal-scale structural architecture in central Chile based on seismicity and surface geology: Implications for Andean mountain building. *Tectonics* 29 (3), TC3006. <https://doi.org/10.1029/2009TC002480>
- Figueroa R. 2020. Advances in the Western Andean Front aquifers characterization by gravimetric and electrical surveys (Central Chile-23°50'S) (MSc Thesis). Pontificia Universidad Católica de Chile, Santiago, Chile.
- Janke J.R., Ng S. & Bellisario A. 2017. An inventory and estimate of water stored in firn fields, glaciers, debris-covered glaciers, and rock glaciers in the Aconcagua River Basin, Chile. *Geomorphology* 296, 142-152. <https://doi.org/10.1016/j.geomorph.2017.09.002>
- Li L., Maher K., Navarrete-Sitcher A., Druhan J., Meile C., Lawrence C., Moore J., Perdrial J., Sullivan P., Thompson A., Jin L., Bolton E.W., Brantley S.L., Dietrich W.E., Mayer K.U., Steefel C.I., Valocchi A., Zachara J., Kocar B., McIntosh J., Tutolo B.M., Kumar M., Sonnenthal E., Bao C. & Beisman J. 2017. Expanding the role of reactive transport models in critical zone processes. *Earth-Science Reviews* 165, 280-301. <https://doi.org/10.1016/j.earscirev.2016.09.001>
- Maher K. & Mayer K.U. 2019. The art of reactive transport model building. *Elements* 15 (2), 117-118. <https://doi.org/10.2138/gselements.15.2.117>
- Markovich K.H., Manning A.H., Condon L.E. & McIntosh J.C. 2019. Mountain-block Recharge: A review of Current Understanding. *Water Resources Research*, 55. <https://doi.org/10.1029/2019WR025676>
- Ohlanders N., Rodriguez M. & McPhee J. 2013. Stable water isotope variation in a Central Andean watershed dominated by glacier and snowmelt. *Hydrology and Earth System Sciences* 17, 1035-1050. <https://doi.org/10.5194/hess-17-1035-2013>

- Pourrier J., Jourde H., Kinnard C., Gascoin S. & Monnier S. 2014. Glacier meltwater flow paths and storage in a geomorphologically complex glacial foreland: The case of the Tapado glacier, dry Andes of Chile (30°S). *Journal of Hydrology* 519 (Part A), 1068-1083. <https://doi.org/10.1016/j.jhydrol.2014.08.023>
- Rodriguez M., Ohlanders N., Pellicciotti F., Williams M.K. & McPhee J. 2016. Estimating runoff from a glacierized catchment using natural tracers in the semi-arid Andes cordillera. *Hydrological Processes* 30 (20), 3609-3626. <https://doi.org/10.1002/hyp.10973>
- Schaffer N., MacDonell S., Réveillet S., Réveillet M., Yáñez E. & Valois R. 2019. Rock glaciers as a water resource in a changing climate in the semiarid Chilean Andes. *Regional Environmental Change* 19 (5), 1263-1279. <https://doi.org/10.1007/s10113-018-01459-3>
- Steefel C.I., DePaolo D.J. & Lichtner P.C. 2005. Reactive transport modeling: An essential tool and a new research approach for the Earth sciences. *Earth and Planetary Science Letters* 240 (3-4), 539-558. <https://doi.org/10.1016/j.epsl.2005.09.017>
- Steefel C.I., Appelo C.A.J., Arora B., Jacques D., Kalbacher T., Kolditz O., Lagneau V., Lichtner P.C., Mayer K.U., Meeussen J.C.L., Molins S., Moulton D., Shao H., Šimůnek J., Spycher N., Yabusaki S.B. & Yeh G.T. 2015. Reactive transport codes for subsurfaces environmental simulation. *Computational Geosciences* 19, 445-478. <https://doi.org/10.1007/s10596-014-9443-x>
- Stehr A. & Aguayo M. 2017. Snow cover dynamics in Andean watersheds of Chile (32.0–39.5° S) during the years 2000–2016. *Hydrology and Earth System Sciences* 21 (10), 5111-5126. <https://doi.org/10.5194/hess-21-5111-2017>
- Vargas G., Klinger Y., Rockwell T.K., Forman S.L., Rebolledo S., Baize S., Lacassin R. & Armijo R. 2014. Probing large intraplate earthquakes at the west flank of the Andes. *Geology* 42 (12), 1083–1086. <https://doi.org/10.1130/G35741.1>
- Wilson J.L. & Guan H. 2004. Mountain-block hydrology and mountain-front recharge. In: Hogan J.F., Phillips F.M. & Scanlon B.R. (Eds.), *Groundwater Recharge in a Desert Environment: The Southwestern United States*. American Geophysical Union 9, 113–137.
- Yáñez G., Muñoz M., Flores-Aqueveque V. & Bosch A. 2015. Gravity depth to basement in Santiago Basin, Chile: implications for its geological evolution, hydrogeology, low enthalpy geothermal, soil characterization and geo-hazards. *Andean Geology* 42 (2), 147–172. <https://doi.org/10.5027/andgeoV42n2-a01>

This page intentionally left blank

BIBLIOGRAPHY

- Agosta F., Ruano P., Rustichelli A., Tondi E., Galindo-Zaldívar J. & Sanz de Galdeano C. 2012. Inner structure and deformation mechanisms of normal faults in conglomerates and carbonate grainstones (Granada Basin, Betic Cordillera, Spain): Inferences on fault permeability. *Journal of Structural Geology* 45, 4-20. <https://doi.org/10.1016/j.jsg.2012.04.003>
- Aishlin P. & McNamara J.P. 2011. Bedrock infiltration and mountain block recharge accounting using chloride mass balance. *Hydrological Processes* 25 (12), 1934-1948. <https://doi.org/10.1002/hyp.7950>
- Allmendinger R.W. & González G. 2010. Invited review paper: Neogene to Quaternary tectonics of the coastal Cordillera, northern Chile. *Tectonophysics* 495 (1-2), 93-110. <https://doi.org/10.1016/j.tecto.2009.04.019>
- Allmendinger R.W., Cardozo N.C. & Fisher D. 2012. Structural geology algorithms: Vectors & Tensors. Cambridge University Press, 302 pp. <https://doi.org/10.1017/CBO9780511920202>
- Angermann D., Klotz J. & Reigber C. 1999. Space-geodetic estimation of the nazca-south america euler vector. *Earth and Planetary Science Letters* 171 (3), 329-334. [https://doi.org/10.1016/S0012-821X\(99\)00173-9](https://doi.org/10.1016/S0012-821X(99)00173-9)
- Arancibia G. 2004. Mid-cretaceous crustal shortening: Evidence from a regional-scale ductile shear zone in the Coastal Range of central Chile (32° S). *Journal of South American Earth Sciences* 17 (3), 209-226. <https://doi.org/10.1016/j.jsames.2004.06.001>
- Aravena R., Suzuki O., Peña H., Pollastri A., Fuenzalida H. & Grilli A. 1999. Isotopic composition and origin of the precipitation in Northern Chile. *Applied Geochemistry* 14 (4), 411-422. [https://doi.org/10.1016/S0883-2927\(98\)00067-5](https://doi.org/10.1016/S0883-2927(98)00067-5)
- Armijo R., Rauld R., Thiele R., Vargas G., Campos J., Lacassin R. & Kausel E. 2010. The West Andean Thrust, the San Ramón Fault, and the seismic hazard for Santiago, Chile. *Tectonics* 29 (2), TC2007. <https://doi.org/10.1029/2008TC002427>
- Balsamo F., Storti F., Salvini F., Silva A.T. & Lima C.C. 2010. Structural and petrophysical evolution of extensional fault zones in low-porosity, poorly lithified sandstones of the Barreiras Formation, NE Brazil. *Journal of Structural Geology* 32 (11), 1806-1826. <https://doi.org/10.1016/j.jsg.2009.10.010>
- Barberá J.A., Jódar J., Custodio E., González-Ramón A., Jiménez-Gavilán P., Vadillo I., Pedrera A. & Martos-Rosillo S. 2018. Groundwater dynamics in a hydrologically-modified alpine watershed from an ancient managed recharge system (Sierra Nevada National Park, Southern Spain): Insights from hydrogeochemical and isotopic information. *Science of The Total Environment* 640-641, 874-893. <https://doi.org/10.1016/j.scitotenv.2018.05.305>
- Barrett B.S., Garreaud R.D. & Falvey M. 2009. Effect of the Andes Cordillera on precipitation from a midlatitude cold front. *Monthly Weather Review* 137, 3092–3109. <https://doi.org/10.1175/2009MWR2881.1>

- Benavente O., Tassi F., Reich M., Aguilera F., Capecchiacci F., Gutiérrez F., Vaselli O. & Rizzo A. 2016. Chemical and isotopic features of cold and thermal fluids discharged in the Southern Volcanic Zone between 32.5°S and 36°S: Insights into the physical and chemical processes controlling fluid geochemistry in geothermal systems of Central Chile. *Chemical Geology* 420, 97–113. <https://doi.org/10.1016/J.CHEMGEOL.2015.11.010>
- Bense V.F., Gleeson T., Loveless S.E., Bour O. & Scibek. 2013. Fault zone hydrogeology. *Earth-Science Reviews* 127, 171–192. <https://doi.org/10.1016/j.earscirev.2013.09.008>
- Berkowitz B. 2002. Characterizing flow and transport in fractured geological media: A review. *Advances in Water Resources* 25 (8-12), 861–884. [https://doi.org/10.1016/S0309-1708\(02\)00042-8](https://doi.org/10.1016/S0309-1708(02)00042-8)
- Betka P., Klepeis K. & Mosher S. 2016. Fault kinematics of the Magallanes-Fagnano fault system, southern Chile; an example of diffuse strain and sinistral transtension along a continental transform margin. *Journal of Structural Geology* 85, 130–153. <https://doi.org/10.1016/j.jsg.2016.02.001>
- Biddau R., Cidu R., Da Pelo S., Carletti A., Ghiglieri G. & Pittalis D. 2019. Source and fate of nitrate in contaminated groundwater systems: Assessing spatial and temporal variations by hydrogeochemistry and multiple stable isotope tools. *Science of The Total Environment* 647, 1121–1136. <https://doi.org/10.1016/j.scitotenv.2018.08.007>
- Boisier J.P., Rondanelli R., Garreaud R.D. & Muñoz F. 2016. Anthropogenic and natural contributions to the Southeast Pacific precipitation decline and recent megadrought in central Chile. *Geophysical Research Letters* 43 (1), 413–421. <https://doi.org/10.1002/2015GL067265>
- Bons P.D., Elburg M.A. & Gomez-Rivas E. 2012. A review of the formation of tectonic veins and their microstructures. *Journal of Structural Geology* 43, 33–62. <https://doi.org/10.1016/j.jsg.2012.07.005>
- Boyce D. 2015. Modelo de evolución tectónica y paleogeográfica del margen andino en Chile Central durante el cretácico medio - tardío: El registro estructural y sedimentario en la formación Las Chilcas (MSc Thesis). Universidad de Chile, Santiago, Chile.
- Boyce D., Charrier R. & Farias M. 2020. The first Andean compressive tectonic phase. Sedimentologic and structural analysis of mid-Cretaceous deposits in the Coastal Cordillera, Central Chile (32°50'S). *Tectonics* 39 (2), e2019TC005825. <https://doi.org/10.1029/2019TC005825>
- Brantley S.L., Kubicki J.D. & White A.F. 2008. *Kinetics of Water-Rock Interaction*. Springer, 833 pp. <https://doi.org/10.1007/978-0-387-73563-4>
- Bresciani E., Cranswick R.H., Banks E.W., Batlle-Aguilar J., Cook P.G. & Batelaan O. 2018. Using hydraulic head, chloride and electrical conductivity data to distinguish between mountain-front and mountain-block recharge to basin aquifers. *Hydrology and Earth System Sciences* 22, 1629–1648. <https://doi.org/10.5194/hess-22-1629-2018>
- Burger F., Ayala A., Farias D., Shaw T.E., MacDonell S., Brock B., McPhee J. & Pellicciotti F. 2018. Interannual variability in glacier contribution to runoff from a high-elevation Andean catchment: understanding the role

of debris cover in glacier hydrology. *Hydrological Processes* 33 (2), 214-229.
<https://doi.org/10.1002/hyp.13354>

Bustamante M., Lemus M., Cortés R., Vivallos J., Cáceres D. & Wall R. 2012. Exploración geológica para el fomento de la energía geotérmica: Área de Jahuel, Región de Valparaíso. Servicio Nacional de Geología y Minería (SERNAGEOMIN), Santiago, Chile.

Cahill T. & Isacks B.L. 1992. Seismicity and shape of the subducted Nazca Plate. *Journal of Geophysical Research: Solid Earth* 91 (B12), 17503-17529. <https://doi.org/10.1029/92JB00493>

Caine J.S., Evans J.P. & Forster C.B. 1996. Fault zone architecture and permeability structure. *Geology* 24 (11), 1025-1028. [https://doi.org/10.1130/0091-7613\(1996\)024<1025:FZAAPS>2.3.CO;2](https://doi.org/10.1130/0091-7613(1996)024<1025:FZAAPS>2.3.CO;2)

Campagna D.J. & Aydin A. 1994. Basin genesis associated with strike-slip faulting in the Basin and Range, southeastern Nevada. *Tectonics* 13 (2), 327-341. <https://doi.org/10.1029/93TC02723>

Carter W.D. & Aguirre L. 1965. Structural Geology of Aconcagua Province and its Relationship to the Central Valley Graben, Chile. *Geological Society of America Bulletin* 76 (6), 651-664. [https://doi.org/10.1130/0016-7606\(1965\)76\[651:SGOAPA\]2.0.CO;2](https://doi.org/10.1130/0016-7606(1965)76[651:SGOAPA]2.0.CO;2)

Cembrano J., González G., Arancibia G., Ahumada I., Olivares V. & Herrera V. 2005. Fault zone development and strain partitioning in an extensional strike-slip duplex: A case study from the Mesozoic Atacama fault system, Northern Chile. *Tectonophysics* 400 (1-4), 105-125. <https://doi.org/10.1016/j.tecto.2005.02.012>

Cembrano J., Lavenu A., Yáñez G., Riquelme R., Garcia M., González G. & Héral G. 2007. Neotectonics. In: Moreno T. & Gibbons W. (Eds.), *The Geology of Chile*. Geological Society of London, 21-114. <https://doi.org/10.1144/GOCH.9>

Cembrano J. & Lara L. 2009. The link between volcanism and tectonics in the southern volcanic zone of the Chilean Andes: A review. *Tectonophysics* 471 (1-2). 96-113. <https://doi.org/10.1016/j.tecto.2009.02.038>

Chapman J.B., Carrapa B., DeCelles P., Wothington J., Mancin N., Cobianchi M., Stoica M., Wang X., Gadoev M. & Oimahmadov I. 2019. The Tajik Basin: A composite record of sedimentary basin evolution in response to tectonics in the Pamir. *Basin Research*, 1-21. <https://doi.org/10.1111/bre.12381>

Charrier R., Baeza O., Elgueta S., Flynn J.J., Gans P., Ka S.M., Muñoz N., Wyss A.R. & Zurita E. 2002. Evidence for Cenozoic extensional basin development and tectonic inversion south of the flat-slab segment, southern Central Andes, Chile (33°-36°S.L.). *Journal of South American Earth Sciences* 15 (1), 117-139. [https://doi.org/10.1016/S0895-9811\(02\)00009-3](https://doi.org/10.1016/S0895-9811(02)00009-3)

Charrier R., Pinto L. & Rodríguez M.P. 2007. Tectonostratigraphic evolution of the Andean Orogen in Chile. In: Moreno T. & Gibbons W. (Eds.), *The Geology of Chile*. Geological Society of London, 21-114. <https://doi.org/10.1144/GOCH.3>

- Choi J-H., Edwards P., Ko K. & Kim Y-S. 2016. Definition and classification of fault damage zones: A review and a new methodological approach. *Earth-Science Reviews* 152, 70-87.
<https://doi.org/10.1016/j.earscirev.2015.11.006>
- Clark I. 2015. Groundwater geochemistry and isotopes (1st ed.). CRC Press, 456 pp.
<https://doi.org/10.1201/b18347>
- Climent M.J., Coscollà C., López A., Barra R. & Urrutia R. 2019. Legacy and current-use pesticides (CUPs) in the atmosphere of a rural area in central Chile, using passive air samplers. *Science of The Total Environment* 662, 646-654. <https://doi.org/10.1016/j.scitotenv.2019.01.302>
- Cloutier V., Lefebvre R., Therrien R. & Savard M.M. 2008. Multivariate statistical analysis of geochemical data as indicative of the hydrogeochemical evolution of groundwater in a sedimentary rock aquifer system. *Journal of Hydrology* 353 (3-4), 294–313. <https://doi.org/10.1016/j.jhydrol.2008.02.015>
- Costumero R., Sánchez J., García-Pedrero A., Rivera D., Lillo M., Gonzalo-Martín C. & Menasalvas E. 2016. Geography of legal water disputes in Chile. *Journal of Maps* 13 (1), 7-13.
<https://doi.org/10.1080/17445647.2016.1252803>
- Coira B., Davidson J., Mpodozis C. & Ramos V. 1982. Tectonic and magmatic evolution of the Andes of northern Argentina and Chile. *Earth-Science Reviews* 18 (3-4), 303-332. [https://doi.org/10.1016/0012-8252\(82\)90042-3](https://doi.org/10.1016/0012-8252(82)90042-3)
- Cortés G., Vargas X. & McPhee J. 2011. Climatic sensitivity of streamflow timing in the extratropical western Andes Cordillera. *Journal of Hydrology* 405 (1-2), 93-109. <https://doi.org/10.1016/j.jhydrol.2011.05.013>
- Craig H. 1961. Isotopic Variations in Meteoric Waters. *Science* 133 (3465), 1702–1703.
<https://doi.org/10.1126/science.133.3465.1702>
- Custodio E. & Jódar J. 2016. Simple solutions for steady-state diffuse recharge evaluation in sloping homogeneous unconfined aquifers by means of atmospheric tracers. *Journal of Hydrology* 540, 287-305.
<https://doi.org/10.1016/j.jhydrol.2016.06.035>
- Darwin C. 1839. The voyage of the Beagle. Wordsworth, 733 pp.
- Daniele L., Cannatelli C., Buscher J.T. & Bonatici G. 2019. Chemical composition of Chilean bottled waters: Anomalous values and possible effects on human health. *Science of The Total Environment* 689, 526-533.
<https://doi.org/10.1016/j.scitotenv.2019.06.165>
- Darapsky L. 1890. Las aguas minerales en Chile. Imprenta del Universo de Guillermo Helfmann, 196 p.
- DeCelles P.G., Ducea M.N., Kapp P. & Zandt G. 2009. Cyclicity in Cordilleran orogenic systems. *Nature Geoscience* 2, 251-257. <https://doi.org/10.1038/ngeo469>
- Deckart K., Clark A.H., Aguilar A.C., Vargas R.R., Bertens A.N., Mortensen J.K. & Fanning M. 2005. Magmatic and hydrothermal chronology of the Giant Río Blanco porphyry copper deposit, central Chile: Implications of

an integrated U-Pb and 40Ar/ 39Ar database. Economic Geology 100, 905-934.
<https://doi.org/10.2113/gsecongeo.100.5.905>

Descloitres M., Chalikakis K., Legchenko A., Moussa A.M., Genton P., Favreau G., Le Coz M., Boucher M. & Oï M. 2013. Investigation of groundwater resources in the Komadugu Yobe Valley (Lake Chad Basin, Niger) using MRS and TDEM methods. Journal of African Earth Sciences 87, 71-85.
<https://doi.org/10.1016/j.jafrearsci.2013.07.006>

de Vries J.J. & Simmers I. 2002. Groundwater recharge: an overview of processes and challenges. Hydrogeology Journal 10 (1), 5-17. <https://doi.org/10.1007/s10040-001-0171-7>

DGA. 2015. Determinación de la Disponibilidad de Aguas Subterráneas en el Valle del Río Aconcagua. Dirección General de Aguas (DGA), Santiago, Chile.

DGA. 2016. Disponibilidad de Recursos Hídricos para el Otorgamiento de Derechos de Aprovechamiento de Aguas Subterráneas en el Valle del Aconcagua: Sectores hidrogeológicos de San Felipe, Putaendo, Panquehue, Catemu y Llay Llay. Dirección General de Aguas (DGA), Santiago, Chile.

DGA. 2019. Inventario Público de Información Hidrológica y Meteorológica. Dirección General de Aguas (DGA), Santiago, Chile. <http://snia.dga.cl/BNAConsultas/reportes>

Dimmen V., Rotevatn A., Peacock D.C.P., Nixon C.W. & Nærland K. 2017. Quantifying structural controls on fluid flow: Insights from carbonate-hosted fault damage zones on the Maltese Islands. Journal of Structural Geology 101, 43-57. <https://doi.org/10.1016/j.jsg.2017.05.012>

Elango L. & Kannan R. 2007. Rock–water interaction and its control on chemical composition of groundwater. In: Sarkar D., Datta R. & Hannigan R. (Eds.), Concepts and Applications in Environmental Geochemistry. Elsevier 5, 229–243. [https://doi.org/10.1016/S1474-8177\(07\)05011-5](https://doi.org/10.1016/S1474-8177(07)05011-5)

Farías M., Charrier R., Comte D., Martinod J. & Hérail G. 2005. Late Cenozoic deformation and uplift of the western flank of the Altiplano: Evidence from the depositional, tectonic, and geomorphologic evolution and shallow seismic activity (northern Chile at 19°30'S). Tectonics 24 (4), TC4001. <https://doi.org/10.1029/2004TC001667>

Farías M., Charrier R., Carretier S., Martinod J., Fock A., Campbell D., Cáceres J. & Comte D. 2008. Late Miocene high and rapid surface uplift and its erosional response in the Andes of central Chile (33°–35°S). Tectonics 27 (1), TC1005. <https://doi.org/10.1029/2006TC002046>

Farías M., Comte D., Charrier R., Martinod J., David C., Tassara A., Tapia F. & Fock A. 2010. Crustal-scale structural architecture in central Chile based on seismicity and surface geology: Implications for Andean mountain building. Tectonics 29 (3), TC3006. <https://doi.org/10.1029/2009TC002480>

Faulkner D.R., Jackson C.A.L., Lunn R.J., Schlische R.W., Shipton Z.K., Wibberley C.A.J. & Withjack M.O. 2010. A review of recent developments concerning the structure, mechanics and fluid flow properties of fault zones. Journal of Structural Geology 32 (11), 1557-1575. <https://doi.org/10.1016/j.jsg.2010.06.009>

- Faye G.D., Yamaji A., Yonezu K., Tindell T. & Watanabe K. 2018. Paleostress and fluid-pressure regimes inferred from the orientations of Hishikari low sulfidation epithermal gold veins in southern Japan. *Journal of Structural Geology* 110, 131-141. <https://doi.org/10.1016/j.jsg.2018.03.002>
- Fernández E., Grilli A., Alvarez D. & Aravena R. 2017. Evaluation of nitrate levels in groundwater under agricultural fields in two pilot areas in central Chile: A hydrogeological and geochemical approach. *Hydrological Processes* 31 (1), 1206-1224. <https://doi.org/10.1002/hyp.11103>
- Fick S.E. & Hijmans R.J. 2017. WorldClim 2: new 1-km spatial resolution climate surfaces for global land areas. *International Journal of Climatology* 37 (12), 4302-4315. <https://doi.org/10.1002/joc.5086>
- Figueroa R. 2020. Advances in the Western Andean Front aquifers characterization by gravimetric and electrical surveys (Central Chile-23°50'S) (MSc Thesis). Pontificia Universidad Católica de Chile, Santiago, Chile.
- Filzmoser P., Hron K. & Reimann C. 2009. Univariate statistical analysis of environmental (compositional) data: Problems and possibilities. *Science of The Total Environment* 407 (23), 6100-6108. <https://doi.org/10.1016/J.SCITOTENV.2009.08.008>
- Foks S.S., Stets E.G., Singha K. & Clow D.W. 2018. Influence of climate on alpine stream chemistry and water sources. *Hydrological Processes* 32 (13), 1993–2008. <https://doi.org/10.1002/hyp.13124>
- Frengstad B. & Banks D. 2007. Universal controls on the evolution of groundwater chemistry in shallow crystalline rock aquifers: the evidence from empirical and theoretical studies. In: Krásný J. & Sharp J.M. (Eds.), *Groundwater in Fractured Rocks: IAH Selected Paper Series*. CRC Press, 275–289.
- Fuentes F., Vergara M., Aguirre L. & Féraud G. 2002. Contact relationships of Tertiary volcanic units from the Andes of Central Chile (33°S): a reinterpretation based on $^{40}\text{Ar}/^{39}\text{Ar}$ dating. *Revista Geológica de Chile* 29 (2), 151-165.
- Fuentes F. 2004. Petrología y metamorfismo de muy bajo grado de unidades volcánicas oligoceno-miocenas en la ladera occidental de Los Andes de Chile Central (33°S) (PhD Thesis). Universidad de Chile, Santiago, Chile.
- Fuentes F., Aguirre L., Vergara M., Valdebenito L. & Fonseca E. 2004. Miocene fossil hydrothermal system associated with a volcanic complex in the Andes of central Chile. *Journal of Volcanology and Geothermal Research* 138 (1-2), 139-161. <https://doi.org/10.1016/j.jvolgeores.2004.07.001>
- Galaz V. 2007. Stealing from the poor? Game theory and the politics of water markets in Chile. *Environmental Politics* 13 (2), 414-437. <https://doi.org/10.1080/0964401042000209649>
- Gana P. & Wall R. 1997. Evidencias geocronológicas $^{40}\text{Ar}/^{39}\text{Ar}$ y K-Ar de un hiatus cretácico superior-eoceno en Chile central (33-33° 30'S). *Revista Geológica de Chile* 24 (2), 145–163.
- Garreaud R.D. 2009. The Andes climate and weather. *Advances in Geosciences* 22, 3–11. <https://doi.org/10.5194/adgeo-22-3-2009>

Garreaud R.D. 2013. Warm Winter Storms in Central Chile. *Journal of Hydrometeorology* 14, 1515-1534.

<https://doi.org/10.1175/JHM-D-12-0135.1>

Garreaud R.D., Lopez P., Minvielle M. & Rojas M. 2013. Large-Scale Control on the Patagonian Climate. *Journal of Climate* 26, 215-230. <https://doi.org/10.1175/JCLI-D-12-00001.1>

Garreaud R.D., Alvarez-Garreton C., Barichivich J., Boisier J.P., Christie D., Galleguillos M., LeQuesne C., McPhee J. & Zambrano-Bigiarini M. 2017. The 2010–2015 megadrought in central Chile: impacts on regional hydroclimate and vegetation. *Hydrology and Earth System Sciences* 21 (12), 6307–6327. <https://doi.org/10.5194/hess-21-6307-2017>

Garreaud R.D., Boisier J.P., Rondanelli R., Montecinos A., Sepúlveda H.H. & Veloso-Aguila D. 2019. The Central Chile Mega Drought (2010–2018): A climate dynamics perspective. *International Journal of Climatology*, 1-19. <https://doi.org/10.1002/joc.6219>

Giambiagi L.B., Ramos V.A., Godoy E., Alvarez P.P. & Orts S. 2003. Cenozoic deformation and tectonic style of the Andes, between 33° and 34° south latitude. *Tectonics* 22 (4), 1041. <https://doi.org/10.1029/2001TC001354>

Giménez-Forcada E., Vega-Alegre M. & Timón-Sánchez S. 2017. Characterization of regional cold-hydrothermal inflows enriched in arsenic and associated trace-elements in the southern part of the Duero Basin (Spain), by multivariate statistical analysis. *Science of The Total Environment* 593-594, 211-226. <https://doi.org/10.1016/j.scitotenv.2017.03.071>

Glas R. , Lautz L., McKenzie J., Moucha R., Chavez D., Mark B. & Lane Jr J.W. 2019. Hydrogeology of an alpine talus aquifer: Cordillera Blanca, Peru. *Hydrogeology Journal* 27 (6), 2137-2154. <https://doi.org/10.1007/s10040-019-01982-5>

Godoy E., Yañez G. & Vera E. 1999. Inversion of an Oligocene volcano-tectonic basin and uplifting of its superimposed Miocene magmatic arc in the Chilean Central Andes: first seismic and gravity evidences. *Tectonophysics* 306 (2), 217–236. [https://doi.org/10.1016/S0040-1951\(99\)00046-3](https://doi.org/10.1016/S0040-1951(99)00046-3)

Gudmundsson A. 2011. Rock fractures in geological processes. Cambridge University Press, 592. <https://doi.org/10.1017/CBO9780511975684>

Güler C., Thyne G.D., McCray J.E. & Turner A.K. 2002. Evaluation of graphical and multivariate statistical methods for classification of water chemistry data. *Hydrogeology Journal* 10 (4), 455–474. <https://doi.org/10.1007/s10040-002-0196-6>

Güngör H. & Elik A. 2007. Comparison of ultrasound-assisted leaching with conventional and acid bomb digestion for determination of metals in sediment samples. *Microchemical Journal* 86 (1), 65–70. <https://doi.org/10.1016/J.MICROC.2006.10.006>

Hauser A. 1997. Catastro y caracterización de las fuentes de aguas minerales y termales de Chile. Servicio Nacional de Geología y Minería (SERNAGEOMIN), Santiago, Chile.

- Healy R. 2010. Estimating Groundwater Recharge. Cambridge University Press, 256 pp.
<https://doi.org/10.1017/CBO9780511780745.002>
- Hoke G.D., Aranibar J.N., Viale M., Araneo D.C. & Llano C. 2013. Seasonal moisture sources and the isotopic composition of precipitation, rivers, and carbonates across the Andes at 32.5-35.5°S. *Geochemistry, Geophysics, Geosystems* 14 (4), 962–978. <https://doi.org/10.1002/ggge.20045>
- Horton B.K. 2018. Tectonic Regimes of the Central and Southern Andes: Responses to Variations in Plate Coupling During Subduction. *Tectonics* 37 (2), 402-429. <https://doi.org/10.1002/2017TC004624>
- Huggenberger P. & Aigner T. 1999. Introduction to the special issue on aquifer-sedimentology: problems, perspectives and modern approaches. *Sedimentary Geology* 129 (3-4), 179-186.
[https://doi.org/10.1016/S0037-0738\(99\)00101-3](https://doi.org/10.1016/S0037-0738(99)00101-3)
- IAEA/GNIP. 2014. Precipitation sampling guide.
- IAEA/WMO. 2019. Global Network of Isotopes in Precipitation. The GNIP Database.
<http://nucleus.iaea.org/wiser>
- Janke J.R., Ng S. & Bellisario A. 2017. An inventory and estimate of water stored in firn fields, glaciers, debris-covered glaciers, and rock glaciers in the Aconcagua River Basin, Chile. *Geomorphology* 296, 142-152.
<https://doi.org/10.1016/j.geomorph.2017.09.002>
- Jara P. & Charrier R. 2014. New stratigraphical and geochronological constraints for the Mezo-Cenozoic deposits in the High Andes of central Chile between 32° and 32°30'S: Structural and palaeogeographic implications. *Andean Geology* 41 (1), 174–209. <https://doi.org/10.5027/andgeoV41n1-a07>
- Jébrak M. 1997. Hydrothermal breccias in vein-type ore deposits: A review of mechanisms, morphology and size distribution. *Ore Geology Reviewes* 12 (3), 111-134. [https://doi.org/10.1016/S0169-1368\(97\)00009-7](https://doi.org/10.1016/S0169-1368(97)00009-7)
- Jing L. & Stephansson O. 1997. Network Topology and Homogenization of Fractured Rocks. In: Jamtveit B. & Yardley B.W.D. (Eds), *Fluid Flow and Transport in Rocks*. Springer, 191-202.
https://doi.org/10.1007/978-94-009-1533-6_11
- Jódar J., Cabrera J.A., Martos-Rosillo S., Ruiz-Constán A., González-Ramón A., Lambán L.J., Herrera C. & Custodio E. 2017. Groundwater discharge in high-mountain watersheds: A valuable resource for downstream semi-arid zones. The case of the Bérchules River in Sierra Nevada (Southern Spain). *Science of The Total Environment* 593–594, 760–772. <https://doi.org/10.1016/j.scitotenv.2017.03.190>
- Jolly R.J.H & Sanderson D.J. 1997. A Mohr circle construction for the opening of a pre-existing fracture. *Journal of Structural Geology* 19 (6), 887-892. [https://doi.org/10.1016/S0191-8141\(97\)00014-X](https://doi.org/10.1016/S0191-8141(97)00014-X)
- Jordan T.E., Isacks B., Allmendinger R., Brewer J., Ramos V. & Aando C. 1983. Andean tectonics related to geometry of subducted Nazca plate. *GSA Bulletin* 94 (3), 341–361. [https://doi.org/10.1130/0016-7606\(1983\)94<341:ATRTGO>2.0.CO;2](https://doi.org/10.1130/0016-7606(1983)94<341:ATRTGO>2.0.CO;2)
- Jordan T.E., Burns W.M., Veiga R., Pángaro F., Copeland P., Kelley S. & Mpodozis C. 2001. Extension and basin

- formation in the southern Andes caused by increased convergence rate: A mid-Cenozoic trigger for the Andes. *Tectonics* 20 (3), 308–324. <https://doi.org/10.1029/1999TC001181>
- Jordan T., Herrera C., Kirk-Lawlor N. & Godfrey L. 2015. Architecture of the aquifers of the Calama Basin, Loa catchment basin, northern Chile. *Geosphere* 11 (5), 1438–1474. <https://doi.org/10.1130/GES01176.1>
- Jorquera C.O., Oates C.J., Plant J.A., Kyser K., Ihlenfeld C. & Voulvoulis N. 2015. Regional hydrogeochemical mapping in Central Chile: natural and anthropogenic sources of elements and compounds. *Geochemistry: Exploration, Environment, Analysis* 15 (1), 72–96. <https://doi.org/10.1144/geochem2013-220>
- Kaasalainen H. & Stefánsson A. 2012. The chemistry of trace elements in surface geothermal waters and steam, Iceland. *Chemical Geology* 330–331, 60–85. <https://doi.org/10.1016/j.chemgeo.2012.08.019>
- Kamb W.B. 1959. Ice petrofabric observations from Blue Glacier, Washington, in relation to theory and experiment. *Journal of Geophysical research* 64 (11), 1891–1909. <https://doi.org/10.1029/JZ064i011p01891>
- Kay S.M., Godoy E. & Kurtz A. 2005. Episodic arc migration, crustal thickening, subduction erosion, and magmatism in the south-central Andes. *Bulletin of the Geological Society of America* 117 (1-2), 67–88. <https://doi.org/10.1130/B25431.1>
- Kayser H.F. 1960. The application of electronic computers to factor analysis. *Educational and Physchological Measurement* 20 (1), 141–151. <https://doi.org/10.1177/001316446002000116>
- Kebede S., Travi Y., Asrat A., Alemayehu T., Ayenew T. & Tessema Z. 2008. Groundwater water origin and flow along selected transects in Ethiopian rift volcanic aquifers. *Hydrogeology Journal* 16 (1), 55–73. <https://doi.org/10.1007/s10040-007-0210-0>
- Kim Y-S., Peacock D.C.P. & Sanderson D.J. 2004. Fault damage zones. *Journal of Structural Geology* 26 (3), 503–517. <https://doi.org/10.1016/j.jsg.2003.08.002>
- Kresic N. & Mikszewski A. 2012. Hydrogeological conceptual site models: Data analysis and visualization (1st ed.). CRC Press, 600 pp. <https://doi.org/10.1201/b12151>
- Laborde A., Barrier L., Simoes M., Li H., Coudroy T., Van der Woerd J. & Tapponnier P. 2019. Cenozoic deformation of the Tarim Basin and surrounding ranges (Xinjiang, China): A regional overview. *Earth-Science Reviews* 197, 102891. <https://doi.org/10.1016/j.earscirev.2019.102891>
- Lerman A. & Wu L. 2008. Kinetics of Global Geochemical Cycles. In: Brantley S., Kubicki J. & White A. (Eds.), *Kinetics of Water-Rock Interaction*. Springer, 655–736. https://doi.org/10.1007/978-0-387-73563-4_13
- Li L., Maher K., Navarrete-Sitcher A., Druhan J., Meile C., Lawrence C., Moore J., Perdrial J., Sullivan P., Thompson A., Jin L., Bolton E.W., Brantley S.L., Dietrich W.E., Mayer K.U., Steefel C.I., Valocchi A., Zachara J., Kocar B., McIntosh J., Tutolo B.M., Kumar M., Sonnenthal E., Bao C. & Beisman J. 2017. Expanding the role of reactive transport models in critical zone processes. *Earth-Science Reviews* 165, 280–301. <https://doi.org/10.1016/j.earscirev.2016.09.001>
- Maher K. & Mayer K.U. 2019. The art of reactive transport model building. *Elements* 15 (2), 117–118.

<https://doi.org/10.2138/gselements.15.2.117>

- Maillot J., Davy P., Le Goc R., Darcel C. & de Dreuzy J.R. 2016. Connectivity, permeability and channeling in randomly-distributed and kinematically-defined discrete fracture network models. *Water Resources Research* 613–615. <https://doi.org/10.1002/2016WR018973>
- Makel G.H. 2007. The modelling of fractured reservoirs: constraints and potential for fracture network geometry and hydraulics analysis. *Geological Society of London* 292, 375-403. <https://doi.org/10.1144/SP292.21>
- Manzocchi T. 2002. The connectivity of two-dimensional networks of spatially correlated fractures. *Water Resources Research* 38 (9), 1-1-1-20. <https://doi.org/10.1029/2000WR000180>
- Markovich K.H., Manning A.H., Condon L.E. & McIntosh J.C. 2019. Mountain-block Recharge: A review of Current Understanding. *Water Resources Research*, 55. <https://doi.org/10.1029/2019WR025676>
- Marret R. & Allmendinger R.W. 1990. Kinematic analysis of fault-slip data. *Journal of Structural Geology* 12 (8), 973-986. [https://doi.org/10.1016/0191-8141\(90\)90093-E](https://doi.org/10.1016/0191-8141(90)90093-E)
- Martínez F., Arriagada C., Peña M., Deckart K. & Charrier R. 2016. Tectonic styles and crustal shortening of the Central Andes “Pampean” flat-slab segment in northern Chile (27–29°S). *Tectonophysics* 667, 144-162. <https://doi.org/10.1016/j.tecto.2015.11.019>
- Martinod J., Husson L., Roperch P., Guillaume B. & Espurt N. 2010. Horizontal subduction zones, convergence velocity and the building of the Andes. *Earth and Planetary Science Letters* 299 (3-4), 299-309. <https://doi.org/10.1016/j.epsl.2010.09.010>
- Martos-Rosillo S., Ruiz-Constán A., González-Ramón A., Mediavilla R., Martín-Civantos J.M., Martínez-Moreno F.J., Jódar J., Marín-Lechado C., Medialdea A., Galindo-Zaldívar J., Pedrera A. & Durán J.J. 2019. The oldest managed aquifer recharge system in Europe: New insights from the Espino recharge channel (Sierra Nevada, southern Spain). *Journal of Hydrology* 578, 124047. <https://doi.org/10.1016/j.jhydrol.2019.124047>
- Matusiewicz H. 2003. Wet digestion methods. In: Mester Z.M. & Sturgeon R. (Eds.), *Sample Preparation for Trace Element Analysis*. Elsevier 41, 193–233. [https://doi.org/10.1016/S0166-526X\(03\)41006-4](https://doi.org/10.1016/S0166-526X(03)41006-4)
- Melnick D. & Echtler H.P. 2006. Morphotectonic and Geologic Digital Map Compilations of the South-Central Andes (36°–42°S). In: Oncken O., Chong G., Franz G., Giese P., Götze H-J., Ramos V.A., Strecker M.R. & Wigger P. (Eds.), *The Andes*. Springer, 565-568. https://doi.org/10.1007/978-3-540-48684-8_30
- Melosh B.L., Rowe C.D., Smit L., Groenewald C., Lambert C.W. & Macey P. 2014. Snap, Crackle, Pop: Dilational fault breccias record seismic slip below the brittle–plastic transition. *Earth and Planetary Science Letters* 403, 432-445. <https://doi.org/10.1016/j.epsl.2014.07.002>
- Mitchell T.M. & Faulkner D.R. 2012. Towards quantifying the matrix permeability of fault damage zones in low porosity rocks. *Earth and Planetary Science Letters* 339-340, 24-31. <https://doi.org/10.1016/j.epsl.2012.05.014>
- Moeck C., Radny D., Borer P., Rothardt J., Auckenthaler A., Berg M. & Schirmer M. 2016. Multicomponent

- statistical analysis to identify flow and transport processes in a highly-complex environment. *Journal of Hydrology* 542, 437–449. <https://doi.org/10.1016/j.jhydrol.2016.09.023>
- Montecinos A. & Aceituno P. 2003. Seasonality of the ENSO-related rainfall variability in central Chile and associated circulation anomalies. *Journal of Climate* 16, 281–296. [https://doi.org/10.1175/1520-0442\(2003\)016<0281:SOTERR>2.0.CO;2](https://doi.org/10.1175/1520-0442(2003)016<0281:SOTERR>2.0.CO;2)
- Moya C.E., Raiber M., Taulis M. & Cox M.E. 2015. Hydrochemical evolution and groundwater flow processes in the Galilee and Eromanga basins, Great Artesian Basin, Australia: A multivariate statistical approach. *Science of The Total Environment* 508, 411–426. <https://doi.org/10.1016/J.SCITOTENV.2014.11.099>
- Mpodozis C. & Ramos V. 1989. The Andes of Chile and Argentina. In: Erickson G.E., Cañas-Pinochet M.T. & Reinemund J. (Eds.), *Geology of the Andes and its relation to hydrocarbon and mineral resources*. Circum-Pacific Council for Energy and Mineral Resources, 59–90.
- Muñoz J.F., Fernández B. & Escauriaza C. 2003. Evaluation of groundwater availability and sustainable extraction rate for the Upper Santiago Valley Aquifer, Chile. *Hydrogeology Journal* 11 (6), 687–700. <https://doi.org/10.1007/s10040-003-0292-2>
- Muñoz M., Fuentes F., Vergara M., Aguirre L., Nyström J., Féraud G. & Demant A. 2006. Abanico East Formation: petrology and geochemistry of volcanic rocks behind the Cenozoic arc front in the Andean Cordillera, central Chile (33°50'S), *Revista Geológica de Chile* 33 (1), 109–140. <http://dx.doi.org/10.5027/andgeoV33n1-a05>
- Muñoz E., Arumí J.L., Wagener T., Oyarzún R. & Parra V. 2016. Unraveling complex hydrogeological processes in Andean basins in south-central Chile: An integrated assessment to understand hydrological dissimilarity. *Hydrological Processes* 30 (26), 4934–4943. <https://doi.org/10.1002/hyp.11032>
- Negri A., Daniele L., Aravena D., Muñoz M., Delgado A. & Morata D. 2018. Decoding fjord water contribution and geochemical processes in the Aysen thermal springs (Southern Patagonia, Chile). *Journal of Geochemical Exploration* 185, 1–13. <https://doi.org/10.1016/J.GEXPL.2017.10.026>
- NOAA/National Weather Service. 2019. El Niño Southern Oscillation (ENSO): Historical El Niño/La Niña episodes (1950-present). https://origin.cpc.ncep.noaa.gov/products/analysis_monitoring/ensostuff/ONI_v5.php
- Novoa V., Ahumada-Rudolph R., Rojas O., Sáez K., de la Barrera F. & Arumí J.L. 2019. Understanding agricultural water footprint variability to improve water management in Chile. *Science of The Total Environment* 670, 188–199. <https://doi.org/10.1016/j.scitotenv.2019.03.127>
- Nyberg B., Nixon C.W. & Sanderson D.J. 2018. NetworkGT: A GIS tool for geometric and topological analysis of two-dimensional fracture networks. *Geosphere* 14 (4), 1618–1634. <https://doi.org/10.1130/GES01595.1>
- Nyström J., Vergara M., Morata D. & Levi B. 2003. Tertiary volcanism during extension in the Andean foothills of central Chile (33°15'–33°45'S). *Geological Society of America Bulletin* 115 (12), 1523–1527. <https://doi.org/10.1130/B25099.1>

- Ochoa-Tocachi B.F., Bardales J.D., Antiporta J., Pérez K., Acosta L., Mao F., Zulkafli Z., Gil-Ríos J., Angulo O., Grainger S., Gammie G., De Bièvre B. & buytaert W. 2019. Potential contributions of pre-Inca infiltration infrastructure to Andean water security. *Nature Sustainability* 2, 584-593. <https://doi.org/10.1038/s41893-019-0307-1>
- Ogilvie S.R. & Glover P.W.J. 2001. The petrophysical properties of deformation bands in relation to their microstructure. *Earth and Planetary Science Letters* 139 (1-2), 129-142. [https://doi.org/10.1016/S0012-821X\(01\)00492-7](https://doi.org/10.1016/S0012-821X(01)00492-7)
- Ohlanders N., Rodriguez M. & McPhee J. 2013. Stable water isotope variation in a Central Andean watershed dominated by glacier and snowmelt. *Hydrology and Earth System Sciences* 17, 1035-1050. <https://doi.org/10.5194/hess-17-1035-2013>
- Oyarzún R., Barrera F., Salazar P., Maturana H., Oyarzún J., Aguirre E., Alvarez P., Jourde H. & Kretschmer N. 2014. Multi-method assessment of connectivity between surface water and shallow groundwater: the case of Limarí River basin, north-central Chile. *Hydrogeology Journal* 22 (8), 1857-1873. <https://doi.org/10.1007/s10040-014-1170-9>
- Oyarzún R., Zambra S., Maturana H., Oyarzún J., Aguirre E. & Kretschmer N. 2016. Chemical and isotopic assessment of surface water–shallow groundwater interaction in the arid Grande river basin, North-Central Chile. *Hydrological Sciences Journal* 61 (12), 2193-2204. <https://doi.org/10.1080/02626667.2015.1093635>
- Oyarzún R., Oyarzún J., Fairley J.P., Núñez J., Gómez N., Arumí J.L. & Maturana H. 2017. A simple approach for the analysis of the structural-geologic control of groundwater in an arid rural, mid-mountain, granitic and volcanic-sedimentary terrain: The case of the Coquimbo Region, North-Central Chile. *Journal of Arid Environments* 142, 31-35. <https://doi.org/10.1016/J.JARIDENV.2017.03.003>
- Padilla H. & Vergara M. 1985. Control estructural y alteración tipo campo geotérmico en los intrusivos subvolcánicos miocénicos del área Cuesta de Chacabuco-Baños El Corazón, Chile Central. *Revista Geológica de Chile* 24, 3-17.
- Parada M.A., Rivano S., Sepulveda P., Herve M., Herve F., Puig A., Munizaga F., Brook M., Pankhurst R. & Snelling N. 1988. Mesozoic and cenozoic plutonic development in the Andes of central Chile (30°30'-32°30'S). *Journal of South American Earth Sciences* 1 (3), 249-260. [https://doi.org/10.1016/0895-9811\(88\)90003-X](https://doi.org/10.1016/0895-9811(88)90003-X)
- Peacock D.C.P. & Sanderson D.J. 1992. Effects of layering and anisotropy on fault geometry. *Journal of the Geological Society* 149, 793-802. <https://doi.org/10.1144/gsjgs.149.5.0793>
- Peacock D.C.P. & Sanderson D.J. 1995. Pull-aparts, shear fractures and pressure solution. *Tectonophysics* 241 (1-2), 1-13. [https://doi.org/10.1016/0040-1951\(94\)00184-B](https://doi.org/10.1016/0040-1951(94)00184-B)
- Peacock D.C.P., Nixon C.W., Rotevatn A., Sanderson D.J. & Zuluaga L.F. 2016. Glossary of fault and other fracture networks. *Journal of Structural Geology* 92, 12-92. <https://doi.org/10.1016/j.jsg.2016.09.008>

- Peacock D.C.P., Nixon C.W., Rotevatn A., Sanderson D.J. & Zuluaga L.F. 2017. Interacting faults. *Journal of Structural Geology* 97, 1-22. <https://doi.org/10.1016/j.jsg.2017.02.008>
- Pérez-Flores P., Wang G., Mitchell T.M., Meredith P.G., Nara Y., Sarkar V. & Cembrano J. 2017b. The effect of offset on fracture permeability of rocks from the Southern Andes Volcanic Zone, Chile. *Journal of Structural Geology* 104, 142-158. <https://doi.org/10.1016/j.jsg.2017.09.015>
- Petit J.P. 1987. Criteria for the sense of movement on fault surfaces in brittle rocks. *Journal of Structural Geology* 9 (5-6), 597-608. [https://doi.org/10.1016/0191-8141\(87\)90145-3](https://doi.org/10.1016/0191-8141(87)90145-3)
- Piquer J., Berry R.F., Scott R.J. & Cooke D.R. 2016. Arc-oblique fault systems: their role in the Cenozoic structural evolution and metallogenesis of the Andes of central Chile. *Journal of Structural Geology* 89, 101-117. <https://doi.org/10.1016/j.jsg.2016.05.008>
- Piquer J., Hollings P., Rivera O., Cooke D.R., Baker M. & Testa F. 2017. Along-strike segmentation of the Abanico Basin, central Chile: New chronological, geochemical and structural constraints. *Lithos* 268-271, 174-197. <https://doi.org/10.1016/j.lithos.2016.10.025>
- Piquer J., Yañez G., Rivera O. & Cooke D.R. 2019. Long-lived crustal damage zones associated with fault intersections in the high Andes of Central Chile. *Andean Geology* 46, 223-239. <https://doi.org/10.5027/andgeoV46n2-3106>
- Platt J.P. & Vissers R.L.M. 1980. Extensional structures in anisotropic rocks. *Journal of Structural Geology* 2 (4), 397-410. [https://doi.org/10.1016/0191-8141\(80\)90002-4](https://doi.org/10.1016/0191-8141(80)90002-4)
- Poblete F., Roperch P., Hervé F., Diraison M., Espinoza M. & Arriagada C. 2014. The curved Magallanes fold and thrust belt: Tectonic insights from a paleomagnetic and anisotropy of magnetic susceptibility study. *Tectonics* 33 (12), 2526-2551. <https://doi.org/10.1002/2014TC003555>
- Pourrier J., Jourde H., Kinnard C., Gascoin S. & Monnier S. 2014. Glacier meltwater flow paths and storage in a geomorphologically complex glacial foreland: The case of the Tapado glacier, dry Andes of Chile (30°S). *Journal of Hydrology* 519 (Part A), 1068-1083. <https://doi.org/10.1016/j.jhydrol.2014.08.023>
- Pozo K., Oyola G., Estellano V.H., Harner T., Rudolph A., Prybilova P., Kukucka P., Audi O., Klánová J., Metzdorff A. & Focardi S. 2017. Persistent Organic Pollutants (POPs) in the atmosphere of three Chilean cities using passive air samplers. *Science of the Total Environment* 586, 107-114. <https://doi.org/10.1016/j.scitotenv.2016.11.054>
- Ramsay J. 1980. The crack-seal mechanism of rock deformation. *Nature* 284, 135-139. <https://doi.org/10.1038/284135a0>
- Rauld R. 2011. Deformación cortical y peligro sísmico asociado a la falla San Ramón en el frente cordillerano de Santiago, Chile Central (33°S) (PhD Thesis). Universidad de Chile, Santiago, Chile.
- Ribeiro L., Kretschmer N., Nascimento J., Buxo A., Rötting T., Soto G., Señoret M., Oyarzún J., Maturana H. & Oyarzún R. 2015. Evaluating piezometric trends using the Mann-Kendall test on the alluvial aquifers of the

Elqui River basin, Chile. Hydrological Sciences Journal 60 (10), 1840-1852.
<https://doi.org/10.1080/02626667.2014.945936>

Riesner M., Lacassin R., Simoes M., Armijo R., Rauld R. & Vargas G. 2017. Kinematics of the active West Andean fold-and-thrust belt (central Chile): Structure and long-term shortening rate. Tectonics 36 (2), 287-303.
<https://doi.org/10.1002/2016TC004269>

Riesner M., Lacassin R., Simoes M., Carrizo D. & Armijo R. 2018. Revisiting the Crustal Structure and Kinematics of the Central Andes at 33.5°S: Implications for the Mechanics of Andean Mountain Building. Tectonics 37 (5), 1347-1375. <https://doi.org/10.1002/2017TC004513>

Riesner M., Simoes M., Carrizo D. & Lacassin R. 2019. Early exhumation of the Frontal Cordillera (Southern Central Andes) and implications for Andean mountain-building at ~33.5°S. Scientific Reports 9, 7972. <https://doi.org/10.1038/s41598-019-44320-1>

Rivano S., Godoy E., Vergara M. & Villarroel R. 1990. Redefinición de la formación farellones en la Cordillera de los Andes de Chile central (32-34°S). Revista Geológica de Chile 17 (2), 205-214.

Rivano S., Sepúlveda P., Boric R. & Espiñeira D. 1993. Hojas Quillota y Portillo, Escala 1:250.000. Servicio Nacional de Geología y Minería (SERNAGEOMIN), Santiago, Chile.

Rivera D., Godoy-Faúndez A., Lillo M., Alvez A., Delgado V., Gonzalo-Martín C., Menasalvas E., Costumero R. & García-Pedrero A. 2016. Legal disputes as a proxy for regional conflicts over water rights in Chile. Journal of Hydrology 535, 36-45. <https://doi.org/10.1016/j.jhydrol.2016.01.057>

Rodriguez M., Ohlanders N., Pellicciotti F., Williams M.K. & McPhee J. 2016. Estimating runoff from a glacierized catchment using natural tracers in the semi-arid Andes cordillera. Hydrological Processes 30 (20), 3609-3626. <https://doi.org/10.1002/hyp.10973>

Rojas R. & Dassargues A. 2007. Groundwater flow modelling of the regional aquifer of the Pampa del Tamarugal, northern Chile. Hydrogeology Journal 15 (3), 537-551. <https://doi.org/10.1007/s10040-006-0084-6>

Ruiz-Pereira S.F. & Veetil B.K. 2019. Glacier decline in the Central Andes (33°S): Context and magnitude from satellite and historical data. Journal of South American Earth Sciences 94, 102249. <https://doi.org/10.1016/j.jsames.2019.102249>

Salas I., Herrera C., Luque J.A., Delgado J., Urrutia J. & Jordan T. 2016. Recent climatic events controlling the hydrological and the aquifer dynamics at arid areas: The case of Huasco River watershed, northern Chile. Science of The Total Environment 571, 178-194. <https://doi.org/10.1016/j.scitotenv.2016.07.132>

Salcher B.C., Meurers B., Smit J., Decker K., Hölzel M. & Wagreich M. 2012. Strike-slip tectonics and Quaternary basin formation along the Vienna Basin fault system inferred from Bouguer gravity derivatives. Tectonics 31 (3), TC3004. <https://doi.org/10.1029/2011TC002979>

Sánchez-Alfaro P., Pérez-Flores P., Arancibia G., Cembrano J. & Reich M. 2013. Crustal deformation effects on the chemical evolution of geothermal systems: the intra-arc Liquiñe–Ofqui fault system, Southern Andes.

- Sánchez-Murillo R., Aguirre-Dueñas E., Gallardo-Amestica M., Moya-Vega P., Birkel C., Esquivel-Hernández G. & Boll J. 2018. Isotopic characterization of waters across chile. In: Rivera D.A., Godoy-Faundez A. & Lillo-Saavedra M. (Eds.), Andean Hydrology. CRC Press, 205–230. <https://doi.org/10.1201/9781315155982-9>
- Sanderson D.J. & Nixon C.W. 2015. The use of topology in fracture network characterization. Journal of Structural Geology 72, 56-66. <https://doi.org/10.1016/j.jsg.2015.01.005>
- Sanderson D.J. & Nixon C.W. 2018. Topology, connectivity and percolation in fracture networks. Journal of Structural Geology 115, 167-177. <https://doi.org/10.1016/j.jsg.2018.07.011>
- Santibáñez I., Cembrano J., García-Pérez T., Costa C., Yáñez G., Marquardt C., Arancibia G. & González G. 2019. Crustal faults in the Chilean Andes: geological constraints and seismic potential. Andean Geology 46 (1), 32-65. <http://dx.doi.org/10.5027/andgeoV46n1-3067>
- Sarricolea P., Herrera-Ossandon M. & Meseguer-Ruiz Ó. 2016. Climatic regionalisation of continental Chile. Journal of Maps 13 (2), 66-73. <https://doi.org/10.1080/17445647.2016.1259592>
- Saylor J., DeCelles P., Gehrels G., Murphy M., Zhang R. & Kapp P. 2010. Basin formation in the High Himalaya by arc-parallel extension and tectonic damming: Zhada basin, southwestern Tibet. Tectonics 29 (1), TC1004. <https://doi.org/10.1029/2008TC002390>
- Scanlon B.R., Keese K.E., Flint A.L., Flint L.E., Gaye C.B., Edmunds W.M. & Simmers I. 2006. Global synthesis of groundwater recharge in semiarid and arid regions. Hydrological Processes 20 (15), 3335-3370. <https://doi.org/10.1002/hyp.6335>
- Schaffer N., MacDonell S., Réveillet S., Réveillet M., Yáñez E. & Valois R. 2019. Rock glaciers as a water resource in a changing climate in the semiarid Chilean Andes. Regional Environmental Change 19 (5), 1263-1279. <https://doi.org/10.1007/s10113-018-01459-3>
- Schellart W.P. 2017. Andean mountain building and magmatic arc migration driven by subduction- induced whole mantle flow. Nature Communications 8, 2010. <https://doi.org/10.1038/s41467-017-01847-z>
- SERNAGEOMIN. 2003. Mapa geológico de Chile 1:1,000,000. Servicio Nacional de Geología y Minería (SERNAGEOMIN), Santiago, Chile.
- Shah N., Nachabe M. & Ross M. 2007. Extinction Depth and Evapotranspiration from Ground Water under Selected Land Covers. Groundwater 45 (3), 329-338. <https://doi.org/10.1111/j.1745-6584.2007.00302.x>
- Sibson R.H. 1986. Brecciation processes in fault zones: Inferences from earthquake rupturing. Pure and Applied Geophysics 124 (1-2), 159-175. <https://doi.org/10.1007/BF00875724>
- Simmers I. 1997. Groundwater recharge principles, problems and developments. In: Simmers I. (Ed.), Recharge of phreatic aquifers in (semi-)arid areas. CRC Press, 1-18.
- Simmers I. 2003. Hydrological Processes and Water Resources Management. In: Simmers I. (Ed.), Understanding Water in a Dry Environment: Hydrological Processes in Arid and Semi-Arid Zones. CRC Press, 1-14.

- Staudinger M., Stoelzle M., Seeger S., Seibert J., Weiler M. & Stahl K. 2017. Catchment water storage variation with elevation. *Hydrological Processes* 31 (11), 2000–2015. <https://doi.org/10.1002/hyp.11158>
- Steefel C.I., DePaolo D.J. & Lichtner P.C. 2005. Reactive transport modeling: An essential tool and a new research approach for the Earth sciences. *Earth and Planetary Science Letters* 240 (3-4), 539-558. <https://doi.org/10.1016/j.epsl.2005.09.017>
- Steefel C.I., Appelo C.A.J., Arora B., Jacques D., Kalbacher T., Kolditz O., Lagneau V., Lichtner P.C., Mayer K.U., Meeussen J.C.L., Molins S., Moulton D., Shao H., Šimůnek J., Spycher N., Yabusaki S.B. & Yeh G.T. 2015. Reactive transport codes for subsurfaces environmental simulation. *Computational Geosciences* 19, 445-478. <https://doi.org/10.1007/s10596-014-9443-x>
- Stehr A. & Aguayo M. 2017. Snow cover dynamics in Andean watersheds of Chile (32.0–39.5° S) during the years 2000–2016. *Hydrology and Earth System Sciences* 21 (10), 5111-5126. <https://doi.org/10.5194/hess-21-5111-2017>
- Tamayo T. & Carmona A. 2019. El negocio del agua: cómo Chile se convirtió en tierra seca. Ediciones B, 232 pp.
- Tassara A., Götze H.J., Schmidt S. & Hackney R. 2006. Three-dimensional density model of the Nazca plate and the Andean continental margin. *Journal of Geophysical Research* 111 (B9), B09404. <https://doi.org/10.1029/2005JB003976>
- Taillefer A., Guillou-Frottier L., Soliva R., Magri F., Lopez S., Courrioux G., Millot R., Ladouce B. & Le Goff E. 2018. Topographic and Faults Control of Hydrothermal Circulation Along Dormant Faults in an Orogen. *Geochemistry, Geophysics, Geosystems* 19 (12), 4972-4995. <https://doi.org/10.1029/2018GC007965>
- Tardani D., Reich M., Roulleau E., Takahata N., Sano Y., Pérez-Flores P., Sánchez-Alfaro P., Cembrano J. & Arancibia G. 2016. Exploring the structural controls on helium, nitrogen and carbon isotope signatures in hydrothermal fluids along an intra-arc fault system. *Geochimica et Cosmochimica Acta* 184, 193-211. <https://doi.org/10.1016/j.gca.2016.04.031>
- Taucare M., Daniele L., Viguier B., Vallejos A & Arancibia G. 2020. Groundwater resources and recharge processes in the Western Andean Front of Central Chile. *Science of The Total Environment* 722, 137824. <https://doi.org/10.1016/j.scitotenv.2020.137824>
- Thomas H. 1958. Geología de la cordillera de la costa entre el Valle de La Ligua y la Cuesta de Barriga. Servicio Nacional de Geología y Minería (SERNAGEOMIN), Santiago, Chile.
- Urrutia J., Jódar J., Medina A., Herrera C., Chong G., Urqueta H. & Luque J.A. 2018. Hydrogeology and sustainable future groundwater abstraction from the Agua Verde aquifer in the Atacama Desert, northern Chile. *Hydrogeology Journal* 26 (6), 1989-2007. <https://doi.org/10.1007/s10040-018-1740-3>
- Valdés-Pineda R., Pizarro R., García-Chevesich P., Valdés J.B., Olivares C., Vera M., Balocchi F., Pérez F., Vallejos C., Fuentes R., Abarza A. & Helwig B. 2014. Water governance in Chile: Availability, management and climate change. *Journal of Hydrology* 519 (Part C), 2538-2567. <https://doi.org/10.1016/j.jhydrol.2014.04.016>

- Valois R., MacDonell S., Núñez J.H. & Maureira-Cortés H. 2020. Groundwater level trends and recharge event characterization using historical observed data in semi-arid Chile. *Hydrological Sciences Journal*, 20 pp. <https://doi.org/10.1080/02626667.2020.1711912>
- Vargas G., Klinger Y., Rockwell T.K., Forman S.L., Rebolledo S., Baize S., Lacassin R. & Armijo R. 2014. Probing large intraplate earthquakes at the west flank of the Andes. *Geology* 42 (12), 1083–1086. <https://doi.org/10.1130/G35741.1>
- Veloso E., Cembrano J., Arancibia G., Heuser G., Neira S., Siña A., Garrido I., Vermeesch P. & Selby D. 2017. Tectono-metallogenetic evolution of the Fe–Cu deposit of Dominga, northern Chile. *Mineralium Deposita* 52, 595–620. <https://doi.org/10.1007/s00126-016-0682-8>
- Veloso E., Tardani D., Elizalde D., Godoy B., Sánchez-Alfaro P., Aron F., Reich M. & Morata D. 2019. A review of the geodynamic constraints on the development and evolution of geothermal systems in the Central Andean Volcanic Zone (18–28°Lat.S). *International Geology Review*, 1-25. [10.1080/00206814.2019.1644678](https://doi.org/10.1080/00206814.2019.1644678)
- Vergara M., Charrier R., Munizaga F., Rivano S., Sepulveda P., Thiele R. & Drake R. 1988. Miocene volcanism in the central Chilean Andes (31°30'S–34°35'S). *Journal of South American Earth Sciences* 1 (2), 199-209. [https://doi.org/10.1016/0895-9811\(88\)90038-7](https://doi.org/10.1016/0895-9811(88)90038-7)
- Viale M. & Garreaud R.D. 2014. Summer Precipitation Events over the Western Slope of the Subtropical Andes. *Monthly Weather Review* 142, 1074-1092. <https://doi.org/10.1175/MWR-D-13-00259.1>
- Viguier B., Jourde H., Yáñez G., Lira E.S., Leonardi V., Moya C.E., García-Pérez T., Maringue J. & Lictevout E. 2018. Multidisciplinary study for the assessment of the geometry, boundaries and preferential recharge zones of an overexploited aquifer in the Atacama Desert (Pampa del Tamarugal, Northern Chile). *Journal of South American Earth Sciences* 86, 366-383. <https://doi.org/10.1016/J.JSAMES.2018.05.018>
- Viguier B., Daniele L., Jourde H., Leonardi V. & Yáñez G. 2019. Changes in the conceptual model of the Pampa del Tamarugal Aquifer: Implications for Central Depression water resources. *Journal of South American Earth Sciences* 94, 102217. <https://doi.org/10.1016/j.jsames.2019.102217>
- Viswanathan H.S., Hyman J.D., Karra S., O’Malley D., Srinivasan S., Hagberg A. & Srinivasan G. 2018. Advancing Graph-Based Algorithms for Predicting Flow and Transport in Fractured Rock. *Water Resources Research* 54 (9), 6085-6099. <https://doi.org/10.1029/2017WR022368>
- Wall R., Sellés D. & Gana P. 1999. Área Tilit-Santiago, región Metropolitana, Escala 1:100.000. Servicio Nacional de Geología y Minería (SERNAGEOMIN), Santiago, Chile.
- Walter B., Géraud Y., Hauteville Y., Diraison M. & Raisson F. 2019. Fluid Circulations at Structural Intersections through the Toro-Bunyoro Fault System (Albertine Rift, Uganda): A Multidisciplinary Study of a Composite Hydrogeological System. *Geofluids*, 20 pp. <https://doi.org/10.1155/2019/8161469>
- Wang P., Sun Z., Hu Y. & Cheng H. 2019. Leaching of heavy metals from abandoned mine tailings brought by precipitation and the associated environmental impact. *Science of The Total Environment* 695, 133893. <https://doi.org/10.1016/j.scitotenv.2019.133893>

- Waylen P.R. & Caviedes C.N. 1990. Annual and seasonal fluctuations of precipitation and streamflow in the Aconcagua River basin, Chile. *Journal of Hydrology* 120 (1-4), 79-102. [https://doi.org/10.1016/0022-1694\(90\)90143-L](https://doi.org/10.1016/0022-1694(90)90143-L)
- Wilson J.L. & Guan H. 2004. Mountain-block hydrology and mountain-front recharge. In: Hogan J.F., Phillips F.M. & Scanlon B.R. (Eds.), *Groundwater Recharge in a Desert Environment: The Southwestern United States*. American Geophysical Union 9, 113–137.
- Woodcock N.H. & Fischer M. 1986. Strike-slip duplexes. *Journal of Structural Geology* 8 (7), 725-735. [https://doi.org/10.1016/0191-8141\(86\)90021-0](https://doi.org/10.1016/0191-8141(86)90021-0)
- Woodcock N.H. & Mort K. 2008. Classification of fault breccias and related fault rocks. *Geological Magazine* 145 (3), 435-440. <https://doi.org/10.1017/S0016756808004883>
- Yamaji A. 2000. The multiple inverse method: a new technique to separate stresses from heterogeneous fault-slip data. *Journal of Structural Geology* 22 (4), 441-452. [https://doi.org/10.1016/S0191-8141\(99\)00163-7](https://doi.org/10.1016/S0191-8141(99)00163-7)
- Yamaji A. 2016. Genetic algorithm for fitting a mixed Bingham distribution to 3D orientations: a tool for the statistical and paleostress analyses of fracture orientations. *Island Arc* 25 (1), 72-83. <https://doi.org/10.1111/iar.12135>
- Yáñez G., Ranero C., von Huene R. & Díaz J. 2001. Magnetic anomaly interpretation across the southern central Andes (32°-34°S): The role of the Juan Fernandez Ridge in the late Tertiary evolution of the margin. *Journal of Geophysical Research* 106 (B4), 6325-6345. <https://doi.org/10.1029/2000JB900337>
- Yáñez G., Cembrano J., Pardo M., Ranero C. & Selles D. 2002. The Challenger–Juan Fernández–Maipo major tectonic transition of the Nazca–Andean subduction system at 33–34°S: geodynamic evidence and implications. *Journal of South American Earth Sciences* 15 (1), 23-38. [https://doi.org/10.1016/S0895-9811\(02\)00004-4](https://doi.org/10.1016/S0895-9811(02)00004-4)
- Yáñez G. & Cembrano J. 2004. Role of viscous plate coupling in the late Tertiary Andean tectonics. *Journal of Geophysical Research: Solid Earth* 109 (B2), B02407. <https://doi.org/10.1029/2003jb002494>
- Yáñez G., Muñoz M., Flores-Aqueveque V. & Bosch A. 2015. Gravity depth to basement in Santiago Basin, Chile: implications for its geological evolution, hydrogeology, low enthalpy geothermal, soil characterization and geo-hazards. *Andean Geology* 42 (2), 147–172. <https://doi.org/10.5027/andgeoV42n2-a01>
- Yáñez G. & Rivera O. 2019. Crustal dense blocks in the fore-arc and arc region of Chilean ranges and their role in the magma ascent and composition: Breaking paradigms in the Andean metallogeny. *Journal of South American Earth Sciences* 93, 51-66. <https://doi.org/10.1016/j.jsames.2019.04.006>

This page intentionally left blank

APPENDIX

APPENDIX

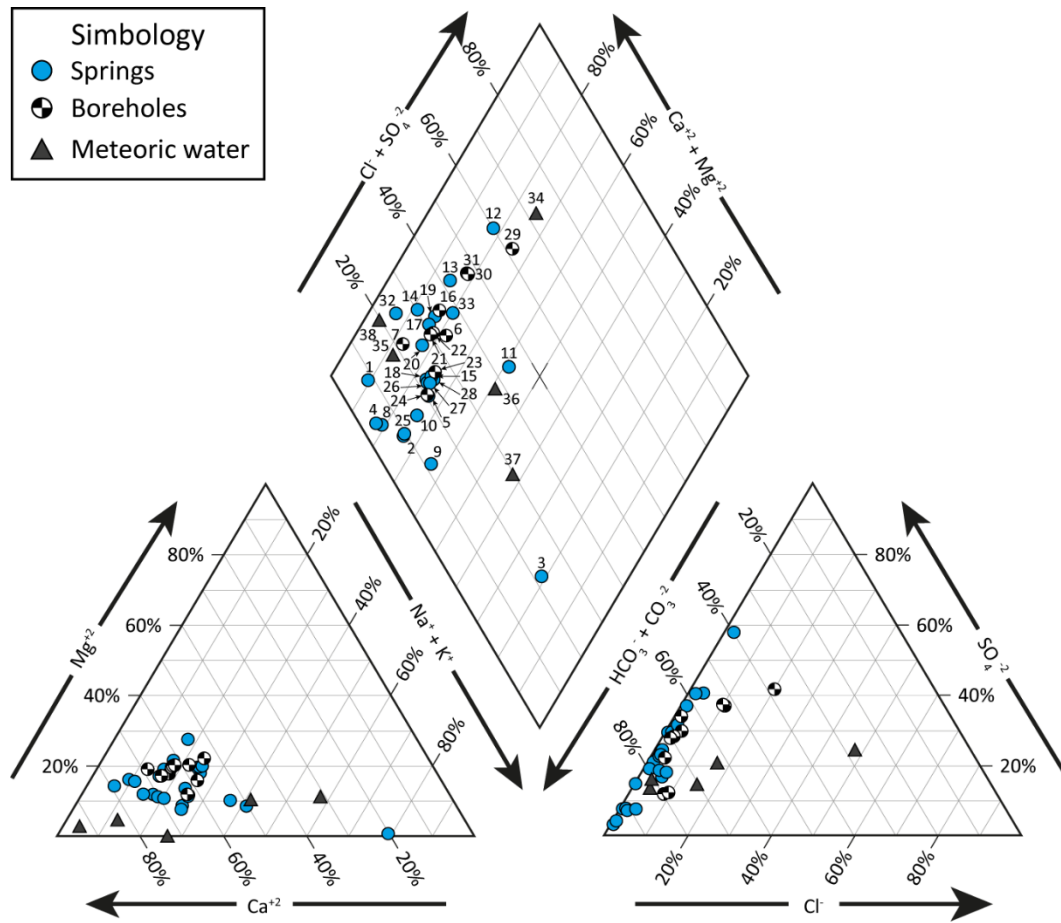
A

Water Samples

A.1. Location of sampling points (Datum: UTM WGS84-19S).

Sample Id	Source	Coordinate		Altitude (m asl)	Sampling date				
		mE	mN		jun-16	feb-17	feb-18	jun-18	sept-18
1	Spring	354541	6392408	2465		x			
2	Spring	351612	6391045	1933		x			x
3	Spring	350964	6389610	1562		x			x
4	Spring	350785	6389613	1515		x			x
5	Spring	350612	6386855	1246	x	x	x		x
6	Borehole	348818	6382377	910	x	x			x
7	Borehole	348441	6381600	902	x	x		x	x
8	Spring	355331	6387711	2380			x		x
9	Spring	353303	6389921	2301			x		x
10	Spring	353784	6388029	2085			x		x
11	Spring	357115	6383154	1784	x	x			
12	Spring	350555	6382668	1128		x	x		x
13	Spring	359178	6382221	2179		x			x
14	Spring	358070	6381330	1783		x			
15	Spring	357475	6379896	1490			x		
16	Borehole	356021	6378910	1283	x	x	x		x
17	Spring	355488	6378429	1239	x	x	x		x
18	Spring	355577	6377517	1157			x		
19	Spring	355027	6376911	1088	x	x	x		x
20	Spring	355104	6376532	1077	x	x	x		x
21	Borehole	354627	6375657	980			x		x
22	Borehole	354420	6375537	973			x		x
23	Borehole	354461	6374474	939			x		x
24	Borehole	357593	6367031	1146				x	
25	Spring	357343	6369566	1088	x	x		x	x
26	Spring	355574	6369980	993		x	x		x
27	Spring	355670	6370061	981	x	x	x		x
28	Spring	355519	6369994	976	x	x			x
29	Borehole	356032	6366676	919				x	
30	Borehole	354833	6370128	918			x	x	x
31	Borehole	354289	6370182	889				x	
32	Spring	361720	6378636	1701		x			
33	Spring	363164	6375307	1456	x				
34	Meteoric	361599	6386149	2715		x			
35	Meteoric	357982	6382180	1965		x			
36	Meteoric	357433	6369324	1132				x	
37	Meteoric	349350	6381770	970				x	
38	Meteoric	350993	6368689	830		x			

A.2. Piper diagram showing the hydrogeochemical facies of water samples.



APPENDIX

B

Structural Geology

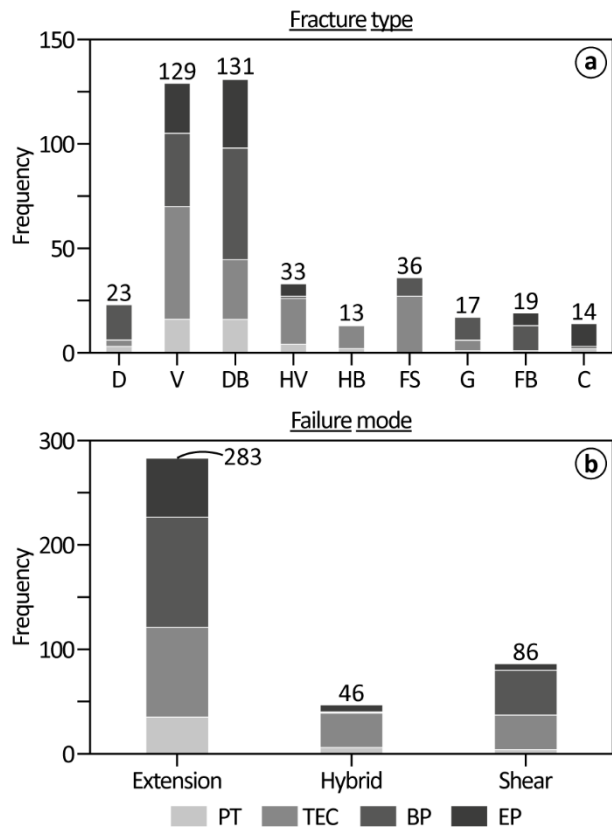
B.1. Location of the structural sites.

Structural site	Coordinate	
	mE	mN
Potrerillos	355000	6380250
Termas El Corazón	355500	6370000
Bypass	355500	6361000
Estero Pocuro	356500	6353000

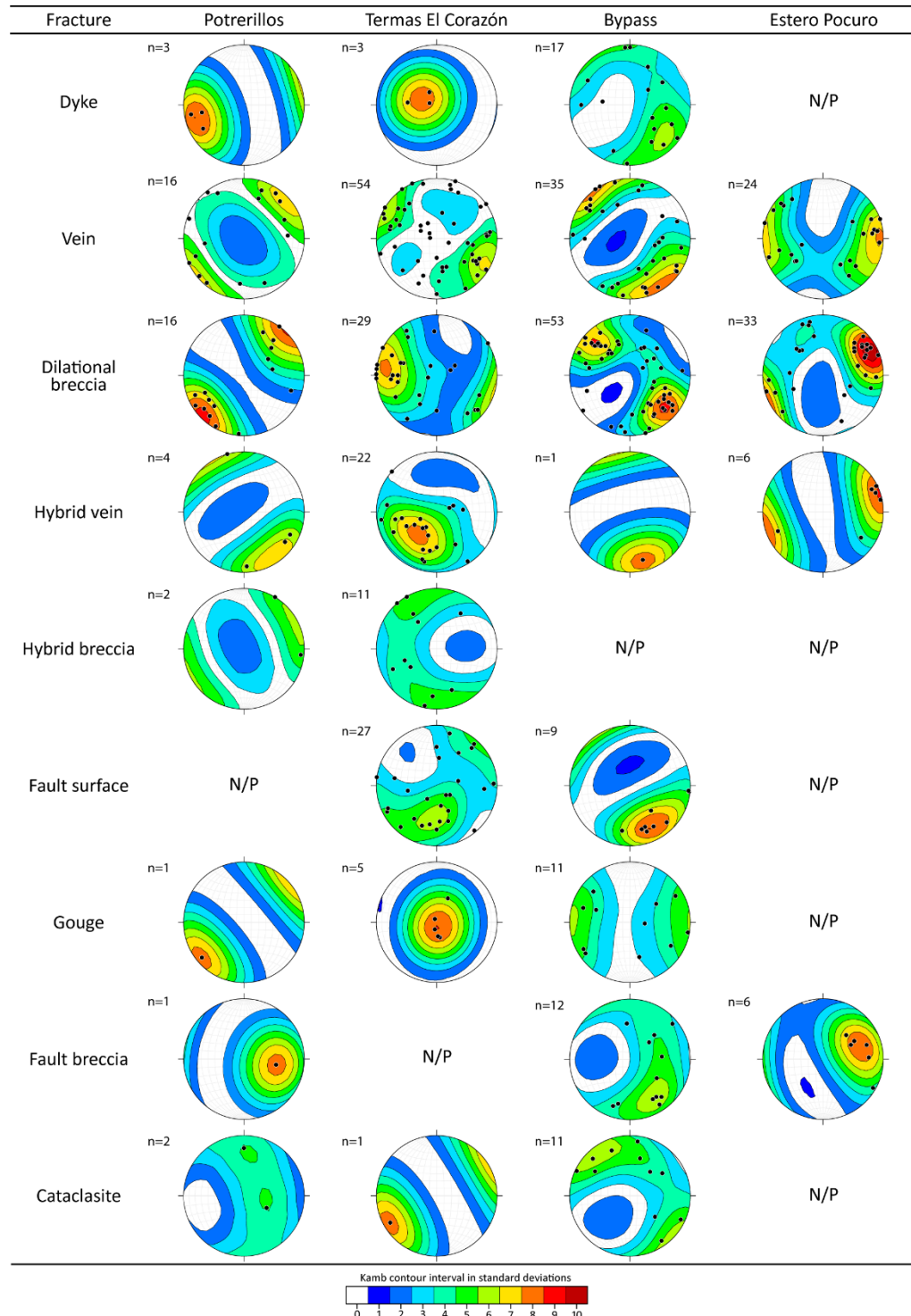
B.2. Measured fractures from each structural site within the Pocuro Fault Zone.

Failure mode	Fracture type	Structural site				Total
		Potrerillos	Termas El Corazón	Bypass	Estero Pocuro	
Extension	Dyke	3	3	17	0	23
	Vein	16	54	35	24	129
Hybrid	Dilatational breccia	16	29	53	33	131
	Hybrid vein	4	22	1	6	33
Shear	Hybrid breccia	2	11	0	0	13
	Fault surface	0	27	9	0	36
	Gouge	1	5	11	0	17
	Fault breccia	1	0	12	6	19
	Cataclasite	2	1	11	0	14
	Total	45	152	149	69	415

B.3. Histogram of measured fractures (D, dyke; V, vein; DB, dilational breccia; HV, hybrid vein; HB, hybrid breccia; FS, fault surface; G, gouge; FB, fault breccia; C, cataclasite) within the Pocuro Fault Zone at each structural site: BP, *Bypass*; EP, *Estero Pocuro*; PT, *Potrerillos*; TEC, *Termas El Corazón*.



B.4. Fractures orientations plotted in pole contour diagrams (Stereonet 10; Allmendinger *et al.* 2012^a) with Kamb Contour Interval as contouring procedures (Kamb, 1959^b). N/P: No present.



- a. Allmendinger R.W., Cardozo N.C. & Fisher D. 2012. Structural geology algorithms: Vectors & Tensors. Cambridge University Press, 302 pp. <https://doi.org/10.1017/CBO9780511920202>
- b. Kamb W.B. 1959. Ice petrofabric observations from Blue Glacier, Washington, in relation to theory and experiment. Journal of Geophysical research 64 (11), 1891-1909. <https://doi.org/10.1029/JZ064i011p01891>

B.5. Microstructural analysis

The fieldwork was complemented with microstructural analyses on 2 representative oriented thin sections (Fig. B.5) to refine the structural analysis and to constrain the tectonic processes involved during the paleo-fluid circulation.

In the *Bypass* structural site, a N70W-oriented quartz hybrid vein located within a sinistral duplex arrangement was sampled. The thin section shows a quartz crystalline aggregate with a sigmoid shape between two parallel N70W sinistral faults (Fig. B.5a). The vein is composed of a quartz granular mosaic with an average size of ~1.5 mm, surrounded by a subgrain wall of fine subangular quartz (<0.3 mm). EW-oriented cataclastic bands separate some quartz lens elongated in ~EW direction from the sigmoid vein. This arrangement is known as “isolated lenses” (Kim *et al.* 2004) and commonly occurs in the transfer zones between two faults in strike-slip duplexes (Woodcock and Fischer, 1986; Peacock and Sanderson, 1995). According to previous observations at regional and outcrop scale, the strike-slip duplex arrangement occurs at different scales in the NS-oriented normal-sinistral faults. In addition, several N65E-oriented parallel minor tensional veins filled by quartz are arranged at 45° from the faults (Fig. B.5b), consistent with the kinematic in terms of the “*petit criteria*” (Petit, 1987). Hence the narrow spatial relation between veins and faults highlights a strong genetic link between the paleo-fluid circulation and the duplex development.

In the *Estero Pocuro* structural site, two N15-22W-oriented composite veins were sampled (Fig. B.5c). The veins are composed of an aggregate of euhedral crystals of laumontite with calcite in the central part of the vein. A monomictic breccia occurs in the central part of the vein (Fig. B.5d). It is constituted by highly angular laumontite clasts surrounded by calcite cement. The clasts are rectangular in shape and the size is less than 0.5 mm. Also, a jigsaw puzzle pattern of the fragmentation with gently clasts rotation is observed (Fig. B.5d), a typical texture of mosaic breccias which generate by in-situ fragmentation during a fluid-assisted brecciation (Sibson, 1986; Jebrak, 1997; Woodcock and Mort, 2008; Melosh *et al.* 2014). Therefore, this texture confirms that at least two crack-seal episodes occurred (Ramsay, 1980) and further highlights that fluid which allow calcite precipitation utilized the previous fractures (laumontite-quartz fracture) for its circulation.

References

- Jébrak M. 1997. Hydrothermal breccias in vein-type ore deposits: A review of mechanisms, morphology and size distribution. *Ore Geology Review* 12 (3), 111-134. [https://doi.org/10.1016/S0169-1368\(97\)00009-7](https://doi.org/10.1016/S0169-1368(97)00009-7)
- Kim Y-S., Peacock D.C.P. & Sanderson D.J. 2004. Fault damage zones. *Journal of Structural Geology* 26 (3), 503-517. <https://doi.org/10.1016/j.jsg.2003.08.002>

- Melosh B.L., Rowe C.D., Smit L., Groenewald C., Lambert C.W. & Macey P. 2014. Snap, Crackle, Pop: Dilatational fault breccias record seismic slip below the brittle-plastic transition. *Earth and Planetary Science Letters* 403, 432-445. <https://doi.org/10.1016/j.epsl.2014.07.002>
- Peacock D.C.P. & Sanderson D.J. 1995. Pull-aparts, shear fractures and pressure solution. *Tectonophysics* 241 (1-2), 1-13. [https://doi.org/10.1016/0040-1951\(94\)00184-B](https://doi.org/10.1016/0040-1951(94)00184-B)
- Petit J.P. 1987. Criteria for the sense of movement on fault surfaces in brittle rocks. *Journal of Structural Geology* 9 (5-6), 597-608. [https://doi.org/10.1016/0191-8141\(87\)90145-3](https://doi.org/10.1016/0191-8141(87)90145-3)
- Ramsay J. 1980. The crack-seal mechanism of rock deformation. *Nature* 284, 135-139. <https://doi.org/10.1038/284135a0>
- Sibson R.H. 1986. Brecciation processes in fault zones: Inferences from earthquake rupturing. *Pure and Applied Geophysics* 124 (1-2), 159-175. <https://doi.org/10.1007/BF00875724>
- Woodcock N.H. & Fischer M. 1986. Strike-slip duplexes. *Journal of Structural Geology* 8 (7), 725-735. [https://doi.org/10.1016/0191-8141\(86\)90021-0](https://doi.org/10.1016/0191-8141(86)90021-0)
- Woodcock N.H. & Mort K. 2008. Classification of fault breccias and related fault rocks. *Geological Magazine* 145 (3), 435-440. <https://doi.org/10.1017/S0016756808004883>

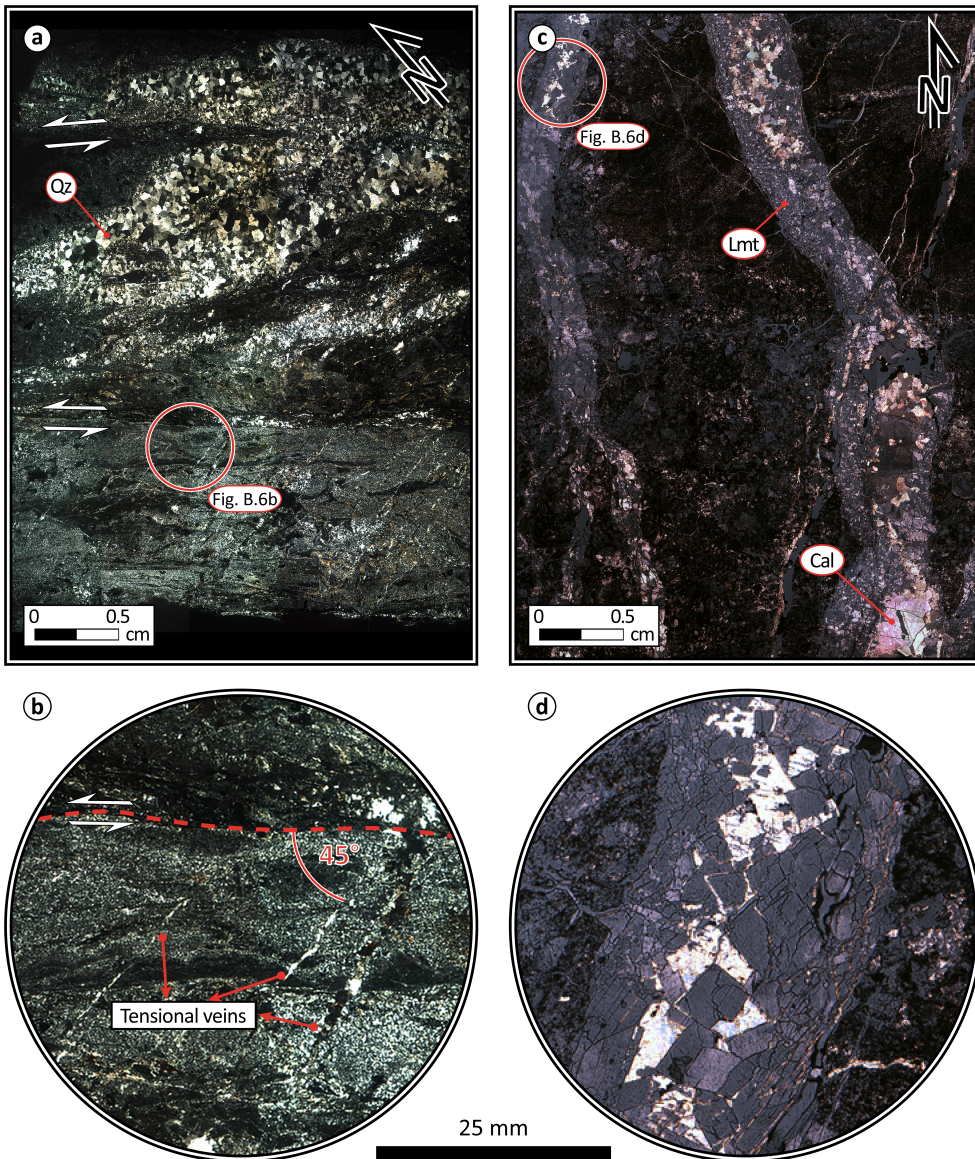
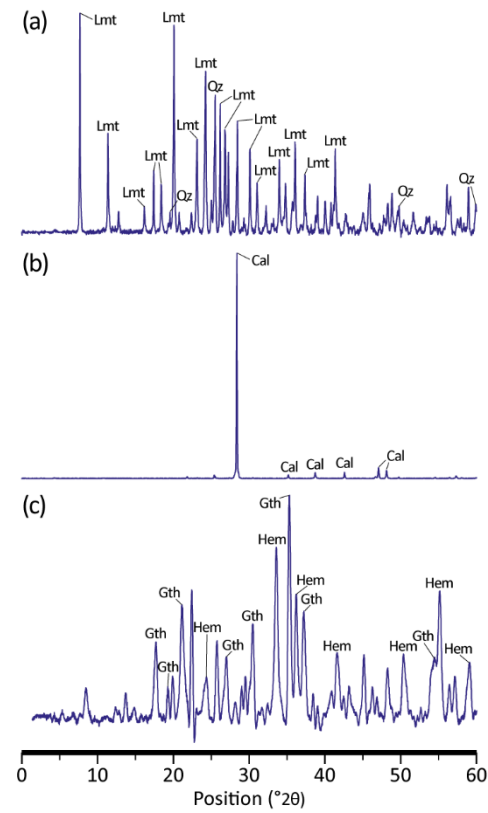


Fig. B.5: Oriented thin sections photo-mosaics in plan-view: a) N70W quartz-vein between two parallel sinistral faults and b) zoom showing quartz tensional veins. c) N15W and N22W composites veins and d) zoom showing a monomictic mosaic breccia in the middle of the vein. (Cal, calcite; Lmt, laumontite; Qz, quartz).

B.6. Interpreted diffractograms of the fractures minerals filling from x-ray diffraction: a) Lmt (laumontite), Qz (quartz); b) Cal (calcite); and, c) Gth (goethite), Hem (hematite).



B.7. Fracture data inversion

To establish the tectonic regime during the circulation of fluids, the open source software GArcmB (Yamaji, 2016) was used to estimates the orientations of the principal stress axes (*i.e.* σ_1 , σ_2 and σ_3). GArcmb is the software to calculate the stress field from randomly oriented tensional fractures data. Through a mixed Bingham distribution, the method calculates the most suitable axes for the minimum, intermediate and maximum concentrations of the fractures poles, which are parallel to σ_1 , σ_2 and σ_3 , respectively. Each axis is plotted with a 95% confidence ellipse. GArcmB can separate the stress fields resulting from a polyphasic deformation using the Bayesian Information Criterion (BIC). Usually, the optimum number of stress field solution is given by the minimum BIC value. In this research, the maximum number of possible solutions is tested (5 clusters); in this case, the appropriate dataset must contain at least 30 tensional fractures. Because the relationship between deformation and fluid circulation is studied, it solely employs veins data for the estimation of stress fields (without dykes data). Furthermore, GArcmB allows estimating the driving pressure index (DPI) as the representative non-dimensional fluid pressure (P_f) value for the fluids (Faye *et al.* 2018). Thus, fractures exhibiting $DPI \approx 0$ were formed from very weakly overpressured fluids, meaning that P_f is similar to σ_3 . Strongly overpressured fluids give rise to tensional fractures exhibiting $DPI \approx 1$, where P_f is similar to σ_1 . According to Jolly and Sanderson (1997), as P_f increases from σ_3 to σ_1 , the fractures will able to open as follow:

- $P_f \approx \sigma_3$ ($DPI \approx 0$), fractures will open only perpendicular to σ_3 .
- $P_f \approx \sigma_2$ ($0 < DPI < 1$), fractures will open in a wide range but perpendicular to σ_1 .
- $P_f \approx \sigma_1$ ($DPI \geq 1$), all orientations of fractures are able to open.

GArcmB calculates the σ_3 -axis accurately, but at a high value of stress ratio ($\phi = (\sigma_2 - \sigma_3)/(\sigma_1 - \sigma_3)$) it does not calculate accurately the position of σ_1 - and σ_2 -axes allowing the rotation of those axes at around σ_3 . Therefore, the Multiple Inverse Method (MIM; Yamaji, 2000) is also used to fit the position of σ_1 - and σ_2 -axes. MIM is a numerical technique to separate stress fields from heterogeneous fault slip data resulted from polyphase deformation (Yamaji, 2000). The method estimates the best fit stress field associated with a group of several faults. Then, the orientations of the calculated stress axes are plotted in two separate stereograms, one for σ_1 and another for σ_3 axes solutions. Each plotted axis is depicted by a “tadpole” symbol with head and tail, indicating the orientation of one of the principal axes with the head and pointing towards the orientation of the complementary axis with the tail (*i.e.* tail on σ_1 points towards the orientation of σ_3 and vice versa). For each tadpole, MIM calculates the stress ratio and paints them according to ϕ -values. Thus, clusters of tadpoles with similar colours and similar tail orientations represent the stress field solution for a group of faults. Also, a histogram of the ϕ -values is used to determine the representative range of ϕ -value for the faults. If the histogram shows a bimodal

distribution, one stress field solution for each range of representative ϕ -values is calculated. Finally, the stress field solution is calibrated by choosing the solution with a bigger number of faults related with misfit angles less than 30°.

After calculating the stress orientation, the kinematic analysis is performed to test the consistency with the strain axes. Thus, using a set of fault-slip data the maximum (shortening, P) and minimum (stretching, T) strain axes is calculated by means of the software Faultkin 8.1 (Marret and Allmendinger, 1990; Allmendinger *et al.* 2012). The main P- and T-axes are determined by clustering each fault axes according to a statistical Bingham distribution, assuming that all the faults result from one uniform strain field.

References

- Allmendinger R.W., Cardozo N.C. & Fisher D. 2012. Structural geology algorithms: Vectors & Tensors. Cambridge University Press, 302 pp. <https://doi.org/10.1017/CBO9780511920202>
- Faye G.D., Yamaji A., Yonezu K., Tindell T. & Watanabe K. 2018. Paleostress and fluid-pressure regimes inferred from the orientations of Hishikari low sulfidation epithermal gold veins in southern Japan. Journal of Structural Geology 110, 131-141. <https://doi.org/10.1016/j.jsg.2018.03.002>
- Jolly R.J.H & Sanderson D.J. 1997. A Mohr circle construction for the opening of a pre-existing fracture. Journal of Structural Geology 19 (6), 887-892. [https://doi.org/10.1016/S0191-8141\(97\)00014-X](https://doi.org/10.1016/S0191-8141(97)00014-X)
- Marret R. & Allmendinger R.W. 1990. Kinematic analysis of fault-slip data. Journal of Structural Geology 12 (8), 973-986. [https://doi.org/10.1016/0191-8141\(90\)90093-E](https://doi.org/10.1016/0191-8141(90)90093-E)
- Yamaji A. 2000. The multiple inverse method: a new technique to separate stresses from heterogeneous fault-slip data. Journal of Structural Geology 22 (4), 441-452. [https://doi.org/10.1016/S0191-8141\(99\)00163-7](https://doi.org/10.1016/S0191-8141(99)00163-7)
- Yamaji A. 2016. Genetic algorithm for fitting a mixed Bingham distribution to 3D orientations: a tool for the statistical and paleostress analyses of fracture orientations. Island Arc 25 (1), 72-83. <https://doi.org/10.1111/iar.12135>

B.8. Total of hydrothermal tensional fractures from each structural site within the Pocuro Fault Zone.

Structural site	Laumontite + Quartz	Calcite	Composite vein	Total
Potrerillos	32	0	0	32
Termas El Corazón	62	17	4	83
Bypass	63	23	2	88
Estero Pocuro	54	0	3	57
Total	211	40	9	260

B.9. Stress field estimation from veins data

Regarding the previous findings there are two types of veins in the study area: laumontite-quartz veins and calcite veins. In this section, the composite veins (laumontite-quartz edge and calcite centre) are considered as two different veins, *i.e.* one laumontite-quartz vein and one calcite vein.

As is evidenced by the crosscutting relationship these veins result from different deformation stages, then the data is grouped according to the mineral filling allowing the stress field estimation for each deformation stage. The stress field is estimated for the entire study area (regional scale) and each structural site (local scale) (Fig. B.9). Note that the regional scale data includes all the veins measured in the different structural sites. The condition of at least 30 veins to test all the possible solutions is satisfied for both events at a regional scale, while for each structural site such condition is solely satisfied by laumontite-quartz veins. Then, the minimum Bayesian Information Criterion (BIC) was reached for an optimal cluster value (K) equal to 1 in each inversion (Fig. B.9), meaning that a single stress condition explains all the veins orientations.

For the laumontite-quartz veins (Stage I) at the entire study area, a total of 220 veins were inverted (Fig. B.9a). The optimal stress field is an extensional regime with stress axes orientations σ_1 (308/87), σ_2 (197/01) and σ_3 (107/03), which is compatible with the NS-oriented normal-sinistral faults (Fig. B9a). The stress ratio (ϕ) is 0.50, indicating a triaxial regime. The driving pressure index (DPI) is 1.89; therefore, the laumontite-quartz veins were formed under strong overpressure fluids conditions. It is consistent with the random vein orientations observed in NS-oriented normal-sinistral faults, since at high DPI values the fractures open in any direction (Jolly and Sanderson, 1997).

The data from veins is also analysed by the structural site to distinguish a local scale stress field from the regional scale solution. The stress fields estimated from each structural site for the Stage I were conducted using 32 veins for *Potrerillos*, 66 veins for *Termas El Corazón*, 65 veins for *Bypass* and 57 for *Estero Pocuro*. Despite that different solutions are obtained for each structural site, in every site the σ_3 -axis is horizontal. In *Potrerillos* (Fig. B.9c) the stress field corresponds to an extensional regime with stress axes orientations σ_1 (233/87), σ_2 (137/00) and σ_3 (046/03). The stress ratio is 0.63 indicating that σ_2 is slightly similar to σ_1 , it means that σ_2 - and σ_1 -axes may potentially interchange around the σ_3 -axis as is observed in the stress solution confidence ellipse. The DPI is 0.75 allowing that fractures open in a wide range of orientations around the σ_1 -axis, which is consistent with the vein orientation in *Potrerillos* (N20-50W; Fig. B.9c). In *Termas El Corazón* (Fig. B.9d) the stress field is an obliquely oriented stress regime with stress axes orientations σ_1 (026/41), σ_2 (198/48) and σ_3 (293/04). The stress ratio is 0.39 indicating that σ_2 is slightly similar to σ_3 , it means that σ_2 - and σ_3 -axes may potentially interchange around the σ_1 -axis as, although the confidence ellipse of the stress solution shows well-defined stress axes. The DPI is

1.19, allowing that fractures open in any orientation, which is consistent with the vein orientation in *Termas El Corazón* (Fig. B.9d). In *Bypass* (Fig. B.9e) the stress field corresponds to a strike-slip regime with stress axes orientations σ_1 (230/23), σ_2 (047/67) and σ_3 (140/01). The stress ratio is 0.63 indicating that σ_2 is slightly similar to σ_1 , it means that σ_2 - and σ_1 -axes may potentially interchange around the σ_3 -axis as it is observed in the stress solution confidence ellipse. Also, this value represents a transtensional tectonic regime (*e.g.* Siame *et al.* 2005) that is compatible with sinistral arrangements observed in *Bypass* (Fig. B.9e). The DPI is 0.95 allowing fractures open in almost any orientations around the σ_1 -axis, which is consistent with the vein orientation in *Bypass* (N30-60E; Fig. B.9e). Finally, in *Estero Pocuro* (Fig. B.9f) the stress field corresponds to an extensional regime with stress axes orientations σ_1 (197/71), σ_2 (347/17) and σ_3 (080/09). The stress ratio is 0.79 indicating that σ_2 is quite similar to σ_1 , it means that is relatively easy for σ_2 - and σ_1 -axes to be rotated around the σ_3 -axis, as it is observed in the large confidence ellipse. Despite that the preferential orientation of the veins in *Estero Pocuro* is N10-30W (Fig. B.9f), the DPI value is 1.19 allowing that fractures open in any orientation.

For the calcite veins (Stage II) at the entire study area a total of 49 veins were inverted (Fig. B.9b). The optimal stress field is an obliquely oriented stress regime with stress axes orientations σ_1 (249/50), σ_2 (018/28) and σ_3 (123/26). The stress ratio is 0.63 indicating that σ_2 is slightly similar to σ_1 , it means that σ_2 - and σ_1 -axes may potentially interchange around the σ_3 -axis as it is observed in the stress solution confidence ellipse. The DPI is 1.50, therefore the calcite veins were formed under strong overpressure fluids conditions. Likely, the obliquity of the stress axes is due to that Stage II was developed in previously fractured rocks deformed by Stage I (a highly anisotropic rock). Thus, the rock did not fail under the classic and ideal failure model, where one of the principal stress axes is vertical, affecting the orientation of the stress field (Platt and Vissers, 1980; Peacock and Sanderson, 1992; Bons *et al.* 2012).

References

- Allmendinger R.W., Cardozo N.C. & Fisher D. 2012. Structural geology algorithms: Vectors & Tensors. Cambridge University Press, 302 pp. <https://doi.org/10.1017/CBO9780511920202>
- Bons P.D., Elburg M.A. & Gomez-Rivas E. 2012. A review of the formation of tectonic veins and their microstructures. Journal of Structural Geology 43, 33-62. <https://doi.org/10.1016/j.jsg.2012.07.005>
- Jolly R.J.H & Sanderson D.J. 1997. A Mohr circle construction for the opening of a pre-existing fracture. Journal of Structural Geology 19 (6), 887-892. [https://doi.org/10.1016/S0191-8141\(97\)00014-X](https://doi.org/10.1016/S0191-8141(97)00014-X)
- Kamb W.B. 1959. Ice petrofabric observations from Blue Glacier, Washington, in relation to theory and experiment. Journal of Geophysical research 64 (11), 1891-1909. <https://doi.org/10.1029/JZ064i011p01891>
- Peacock D.C.P. & Sanderson D.J. 1992. Effects of layering and anisotropy on fault geometry. Journal of the Geological Society 149, 793-802. <https://doi.org/10.1144/gsjgs.149.5.0793>
- Platt J.P. & Vissers R.L.M. 1980. Extensional structures in anisotropic rocks. Journal of Structural Geology 2 (4), 397-410. [https://doi.org/10.1016/0191-8141\(80\)90002-4](https://doi.org/10.1016/0191-8141(80)90002-4)
- Yamaji A. 2016. Genetic algorithm for fitting a mixed Bingham distribution to 3D orientations: a tool for the statistical and paleostress analyses of fracture orientations. Island Arc 25 (1), 72-83. <https://doi.org/10.1111/iar.12135>

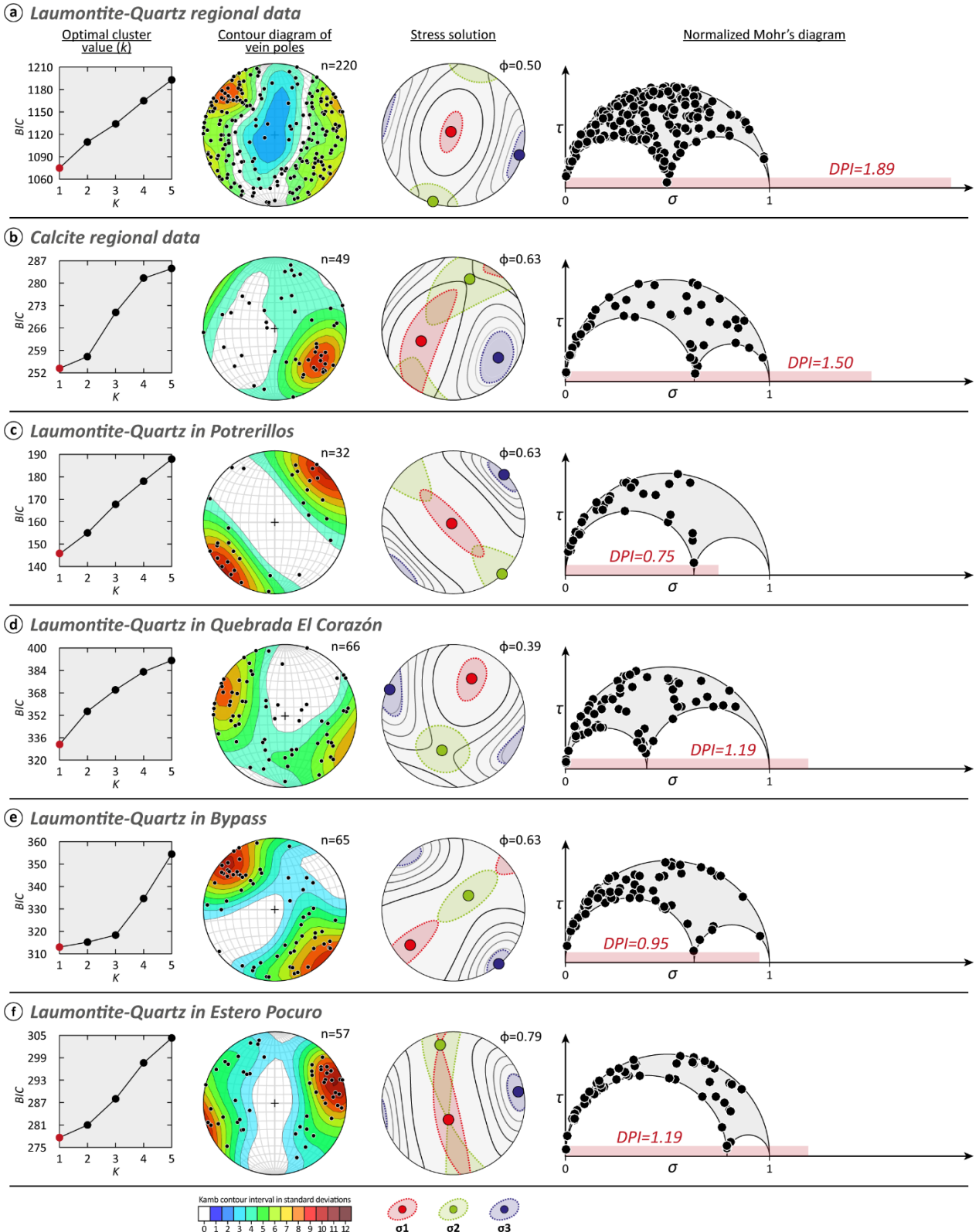


Fig. B.9: Results from the inversion of tensional fractures filled by hydrothermal mineral within PFZ using GArcmB (Yamaji, 2016): a)-b) for regional scale; c)-f) for each structural site. The pole contour diagrams were performed using the software Stereonet 10 (Allmendinger *et al.* 2012) with Kamb Contour Interval as contouring procedures (Kamb, 1959).

B.10. Stress and strain field estimation from fault slip data

The fault-slip data inversion was carried out using a total of 25 faults with complete datum collected along the study area (Fig. B.10). The Multiple Inverse Method (MIM) reveals a bimodal ϕ -value distribution with modes at 0.3 and at 0.7 with three main solutions explaining 18 faults (Fig. B.10a).

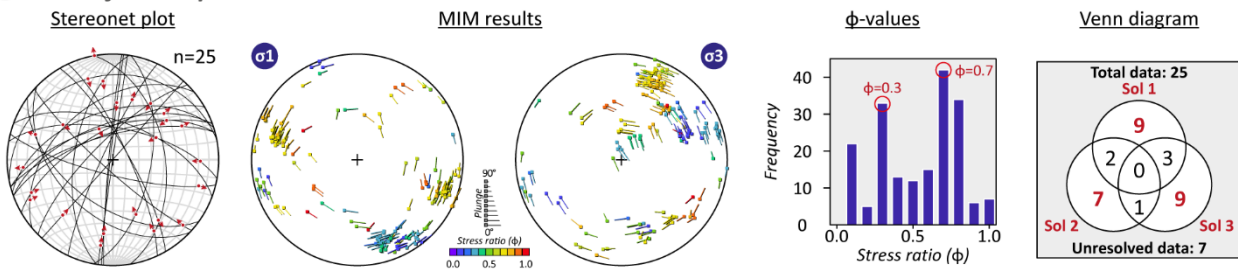
Solution 1 (Fig. B.10b), associated with a ϕ -value equal to 0.3, corresponds to a compressional regime with stress axes orientations σ_1 (165/00), σ_2 (256/00) and σ_3 (006/78), which is consistent with the principal strain axes solution that indicates a NE-oriented shortening. Solution 2 (Fig. B.10c), associated with a ϕ -value equal to 0.7, corresponds to a sinistral transtensional regime with stress axes orientations σ_1 (236/12), σ_2 (344/56) and σ_3 (139/31), which is consistent with the principal strain axes solution that indicates a NW-oriented shortening. Solution 3 (Fig. B.10d), associated with a ϕ -value equal to 0.7, corresponds to dextral transtensional regime with stress axes orientations σ_1 (115/15), σ_2 (246/67) and σ_3 (020/16), which is consistent with the principal strain axes solution that indicates a NE-oriented shortening. The solution 1 groups reverse faults related to both NS-oriented reverse faults and to the Oblique Basement Faults. Thus, both fault systems have resulted from a compressional stress field by two different tectonic events as demonstrated by the cross-cutting relationship (see Sect. 5.1.2).

Regarding solutions 2 and 3, both solutions group normal-sinistral and normal-dextral faults, which are spatially associated with the duplexes veins arrangements of NS-oriented normal-sinistral faults. When comparing both solutions with those resulting from the vein data inversion, the orientation of σ_3 -axis for solution 2 is almost the same that the calculated for *Termas El Corazón* and *Bypass* (Fig. B.9d and B.9e), while for solution 3 is almost the same as *Potrerillos* and *Estero Pocuro* (Fig. B.9c and B.9f). Considering high value of stress ratio calculated by GArcmB (Fig. B.9), the position of σ_1 - and σ_2 -axes is fixed by MIM inversion method. Thus, NS-oriented normal-sinistral faults result from an extensional regime with a local transtensional tectonic regime that promotes the development of normal-sinistral and normal-dextral faults.

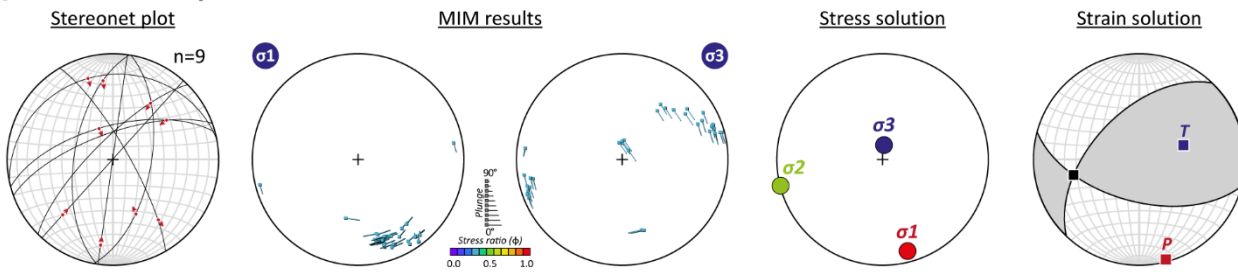
References

- Allmendinger R.W., Cardozo N.C. & Fisher D. 2012. Structural geology algorithms: Vectors & Tensors. Cambridge University Press, 302 pp. <https://doi.org/10.1017/CBO9780511920202>
- Yamaji A. 2000. The multiple inverse method: a new technique to separate stresses from heterogeneous fault-slip data. Journal of Structural Geology 22 (4), 441-452. [https://doi.org/10.1016/S0191-8141\(99\)00163-7](https://doi.org/10.1016/S0191-8141(99)00163-7)

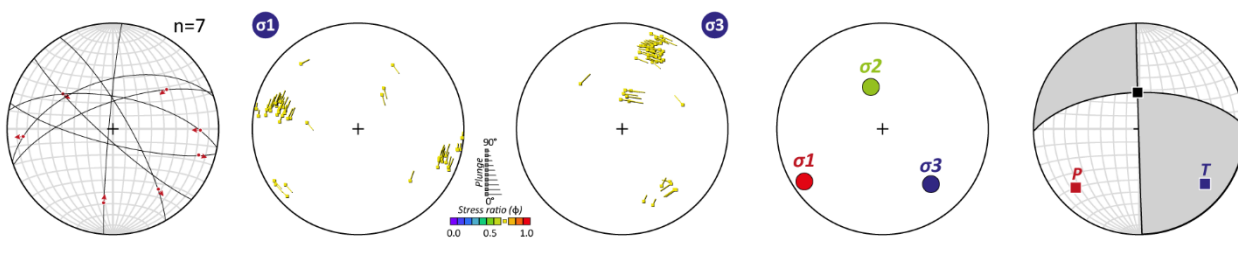
a) Entire fault-slip data



b) Solution 1 — $\phi=0.3$



c) Solution 2 — $\phi=0.7$



d) Solution 3 — $\phi=0.7$

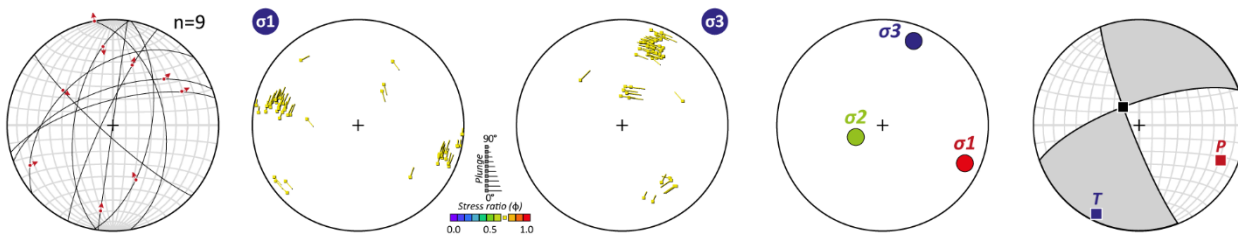


Fig. B.10: Results from the inversion of fault-slip data. Stress and strain solutions were performed with MIM (Yamaji, 2000) and Faultkin (Allmendinger *et al.* 2012), respectively.

B.11. Cartoon diagrams summarizing the crosscutting relationship with the detailed structural map performed at each structural site. Each map is compared with the tectonic stress solution and the strain axes (red arrows: shortening; blue arrows: stretching).

